TRANSITION METAL CARBONYL COMPLEXES FOR BIOMEDICAL APPLICATIONS

CALVIN POH HWA TIONG

NATIONAL UNIVERSITY OF SINGAPORE

2016

TRANSITION METAL CARBONYL COMPLEXES FOR BIOMEDICAL APPLICATIONS

CALVIN POH HWA TIONG

(B.Sc. (HONS), NUS)

A THESIS SUBMITTED

FOR THE DEGREE OF DOCTOR OF PHILOSOPHY

DEPARTMENT OF CHEMISTRY

NATIONAL UNIVERSITY OF SINGAPORE

2016

Declaration

I hereby declare that this thesis is my original work and it has been written by me in its entirety, under the supervision of Associate Professor Fan Wai Yip in the laboratory of Associate Professor Fan Wai Yip, Chemistry Department, National University of Singapore between 8th January 2012 to 8th January 2016.

I have duly acknowledged all the sources of information which have been used in the thesis.

This thesis has not been submitted for any degree in any university previously.

CALVIN POH HWA TIONG		
Name	**Signature**	**Date**

Acknowledgement

The completion of this thesis marks a major milestone in my life and I would like to extend my deepest gratitude to the following important people for their continuous support and belief in me throughout the four years of my doctorate.

First and foremost, I would like to thank my supervisor and mentor, Associate Professor Fan Wai Yip for his invaluable guidance through the year. He has conveyed a spirit of adventure in regard to research and exploration and also an excitement in regard to teaching.

I would also like to extend my heartfelt gratitude for all the help and support rendered by my lab group, and most importantly the fun and laughter they have brought to my lab experience throughout these years.

This thesis would not have come to fruition without the technical expertise of the CMMAC staff, notably, Miss Tan Geok Kheng, Mdm. Han Yanhui and Mdm. Wong Lai Kwai respectively. My deepest appreciation goes to them for sharing their expertise and deep knowledge on the instruments with me.

I would also like to thank my family and friends for their unwavering support these 4 years, especially during the period when the thesis was being written.

Last but not least I wish to thank the National University of Singapore for awarding me the prestigious President Graduate Fellowship and thus granting me the opportunity to pursue my degree.

"There are sadistic scientists who hurry to hunt down errors instead of establishing the truth." – Marie Curie

Table of Contents

Summary

Organometallic complexes have long been employed as therapeutic agents in the diverse field of biomedical sciences. In this thesis, the use of organometallic complexes as anti-cancer drugs, as cell signaling molecules and as thiol sensors are explored. In Chapter 1, a brief introduction to the chemistry of organometallic and transition metal complexes along with the objectives of this work are described. The variable oxidation states exhibited by transition metals allows for a huge myriad of derivatives to be synthesized and used for the different biomedical applications listed above. In addition, the presence of carbonyl ligands in the molecule facilitates the characterization of the newly synthesized complexes. Representative examples of transition metal complexes well-studied in the field of anti-cancer, cell signaling and thiol sensing are then listed and their pros and cons discussed.

In Chapter 2, the synthesis and use of $CpFe(CO)_2X$ as possible cytotoxic agents towards breast (MDA-MB-231) and HeLa adenocarcinoma cells were investigated. The MTT assays have shown that these $CpFe(CO)_2X$ class of complexes are effective against both the breast and HeLa cell lines with $CpFe(CO)_2I$ performing the best with IC_{50} of 3.7 μM. Confocal and flow cytometry data also support the data obtained from cytotoxicity assays. Previous studies have shown that organic isothiocyanates such as sulforaphane, benzyl isothiocyanate and phenethyl isothiocyanate inhibit the growth of breast cancer cells, but have undesirable effects on normal mammary cells. It was hoped that by introducing a benign metal such as iron, in the form of

cyclopentadienyl iron dicarbonyl [$CpFe(CO)_2$] complexes, the toxicity towards normal cells can be mitigated.

Chapter 3 investigates the cytotoxic properties of other metals complexes such as those of manganese and cobalt in the treatment of breast and cervical cancer. The results are not as promising as the CpFe derivatives with the cobalt complexes inactive towards the breast cancer cells. The manganese complexes on the other hand were too toxic towards the normal mammary cells to be of any practical use. The effectiveness of other iron-containing complexes without the cyclopentadienyl (Cp) ring on causing cell death in both breast and cervical adenocarcinoma was also evaluated, compared and discussed with reference to the cytotoxicity data obtained from Chapter 2. In addition, the potency and efficacy of organic isothiocyanates as anti-carcinogenic agents from initial studies will be discussed as well.

Chapter 4 discusses the role of gasotransmitters such as H_2S and CO in our body. First of all, an iron carbonyl complex carrying a thiocarboyxlic acid ligand was synthesized. The resulting complex is water soluble, and air and light stable. Not only that, irradiation under UV-vis radiation released the CO within an hour. H_2S release was achieved from a series of Group 6 transition metal carbonyl hydrosulfides. These release H_2S slowly over an hour upon hydrolysis in water. Cytotoxicity tests performed on these releasing molecules have shown that they are benign towards normal mammary cells. The ability to release these gaseous small molecules from metal carbonyl complexes allows them to find applications in diverse conditions involving blood vessel dysfunction and inflammation.

Besides anti-cancer treatment and gas release, organometallic complexes can also be used in the sensing of thiols, an important class of naturally occurring organic molecules whose levels in the body have been shown to be implicated in a variety of ailments such as Alzheimer's cancer and cardiovascular disease. This will be discussed in Chapter 5, where an investigative study of using $CpMn(CO)_2$ radical that can function as a thiol sensing molecule was carried out. Aromatic and aliphatic thiols induce different colour changes which were characterized by UV-vis and infrared spectroscopy. Further functionalization by CO substitution was also performed which enable the differentiation between glutathione and cysteine, both naturally occurring thiols.

List of Tables

List of Figures

List of Schemes

List of Publications

1. H.T. Poh, B.T. Sim, T.S. Chwee, W.K. Leong, W.Y. Fan, The Dithiolate-Bridged Diiron Hexacarbonyl Complex Na2[(μ-SCH_2CH_2COO)$Fe(CO)_3$]$_2$ as a Water-Soluble PhotoCORM, Organometallics, 33 (2014) 959-963.

2. H.T. Poh, A.A. Bengali, W.Y. Fan, Group VI transition metal carbonyl hydrosulfides Na[$M(CO)_5$(SH)] (M = Cr, Mo, W) as water-soluble H2S-releasing agents, RSC Advances, 5 (2015) 10703-10706.

3. H.T. Poh, J.W. Kee, T.S. Chwee, W.Y. Fan, A persistent manganese carbonyl radical with infrared absorption and fluorescence modality, Journal of Organometallic Chemistry, 759 (2014) 11-14.

4. H.T. Poh, T.S. Chwee, W.Y. Fan, Stable manganese carbonyl radicals as a rapid colorimetric thiol and hydrazine sensor, RSC Advances, 5 (2015) 15159-15163.

5. H.T. Poh, P.C. Ho and W.Y. Fan, Cyclopentadienyl iron dicarbonyl ($CpFe(CO)_2$) derivatives as apoptosis-inducing agents, RSC Advances, 6 (2016) 18814.

Chapter 1

Introduction

The first use of organometallic complexes in the study of biological systems began in 1985 and it saw the birth of the term ‘bioorganometallic chemistry’ [1, 2]. This idea of bringing together two different disciplines – chemistry and biology – has of course been proposed before by many researchers, each opening up a new field of bioorganometallic research. This multidisciplinary nature of this new area has subsequently led to the development of organometallic complexes for a broad variety of biomedical applications.

Some of the biomedical applications arising from the advancement of bioorganometallic chemistry research are anti-cancer [3-5], radiopharmaceuticals [6, 7], gasotransmitters releasing molecules [8-14], bioprobes [15-17], organometallic tracers in non-isotopic immunoassay [18-

20], genosensors [21-23], models for bioorganometallic reaction centres [24-28] and supramolecular host processes [29, 30]. For the scope of this thesis, we shall focus on three areas, namely, anti-cancer to be discussed in Chapter 2 and 3, CO- and H_2S- releasing molecules in Chapter 4 and in Chapter 5 we will examine how a manganese based complex can be used as a probe for sensing of biomolecules molecules.

1.1 Organometallic Compounds as Anti-Cancer Agents

One of the first carcinogens discovered and identified in 1930 is a class of compounds known as polycyclic aromatic hydrocarbons [31] and thereafter it sparked off a multi-million dollar research industry whose mission is to identify the cause and to develop strategies for the prevention, diagnosis and treatment of cancer. Today, even though that goal has remained the same, cancer is no longer regarded as a single disease but rather a collection of more than 200 types of ailments that can affect potentially every single organ in the human body [32]. Due to this diverse cancer typing, survival rates are highly variable and are dependent upon the type and stage of the tumour growth. For instance, patients with testicular cancer, prostate cancer, melanoma and Hodgkin lymphoma typically have a 10-year survival rate of 80% but for patients suffering from pancreas, lung, stomach, oesophagus and brain cancer, the 10-year survival rate plummets to a dismal 15% [33]. Evidently, while we have achieved numerous breakthroughs in cancer biology over the last five decades, this molecular knowledge and new information have not led to a significant improvement in cancer mortality. This is in part due to the fact that of all the potential drug candidates that research churns out, only a depressing 5% of them eventually made it into the commercial market. In contrast, nearly

20% of cardiovascular drugs that have undergone clinical trials are now commercially available [34]. Not only that, the huge diversity of cancer types has made it perplexing to translate the new research knowledge into cures. Cancer research thus must press on so that these new discoveries can be made that improve the way we prevent, diagnose and treat cancer.

1.1.1 Use of Carbonyl Complexes in Treatment of Cancer

Currently, chemotherapy remains the most common type of treatment that cancer patients undergo although it is usually in combination with surgery and/or radiotherapy. While cytotoxic platinum drugs (cisplatin, carboplatin and oxaliplatin) are still used in more than 50% of the treatment regimens during chemotherapy [35], there is still a need to sought out alternative drugs that can effectively curb the proliferation of cancer tumours due to the emergence of platinum resistance and severe side effects associated with current platinum-based therapeutics such as neuro-, hepato- and nephrotoxicity [36]. Such limitations imposed by platinum-based drugs (**Figure 1.1**) have prompted chemists to look to the use of other transition metals in the development of anti-cancer drugs. In particular, organometallic complexes (compounds containing at least a single metal-carbon bond) containing ruthenium and osmium have shown to be extremely promising drug candidates and hence are among the most widely studied non-platinum drugs for anti-cancer therapy [37-41]. Other popular organometallic complexes (**Figure 1.2**) that have also demonstrated inhibitory properties towards cancer cells proliferation include organic compounds with organometallic modifications such as ferrocifen [42-44] and paullones [45-47]. Metallocenes

[48-52] and metallocenyls [53] have also been documented to show *in vitro* metal-based anticancer activity.

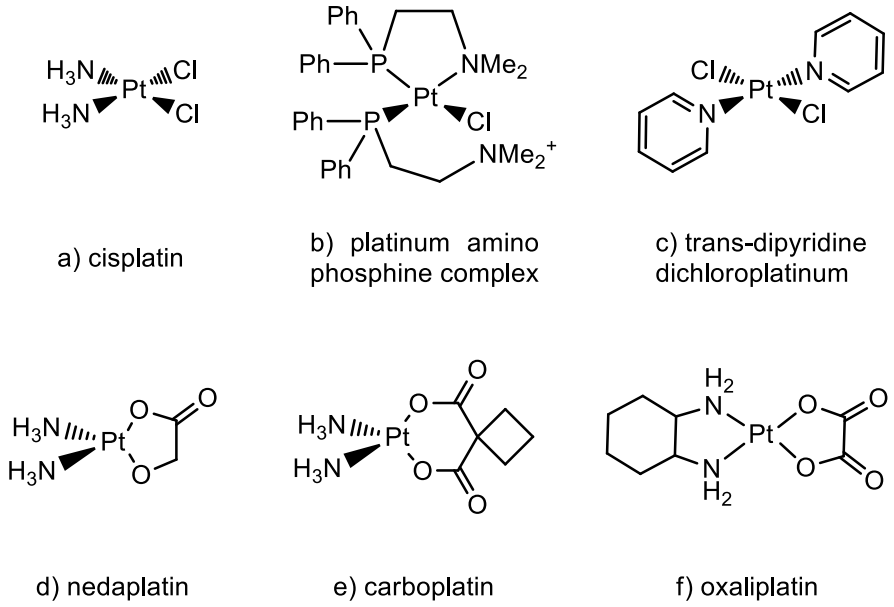

Figure 1.1 Selected examples of platinum based drugs commonly used in chemotherapy.

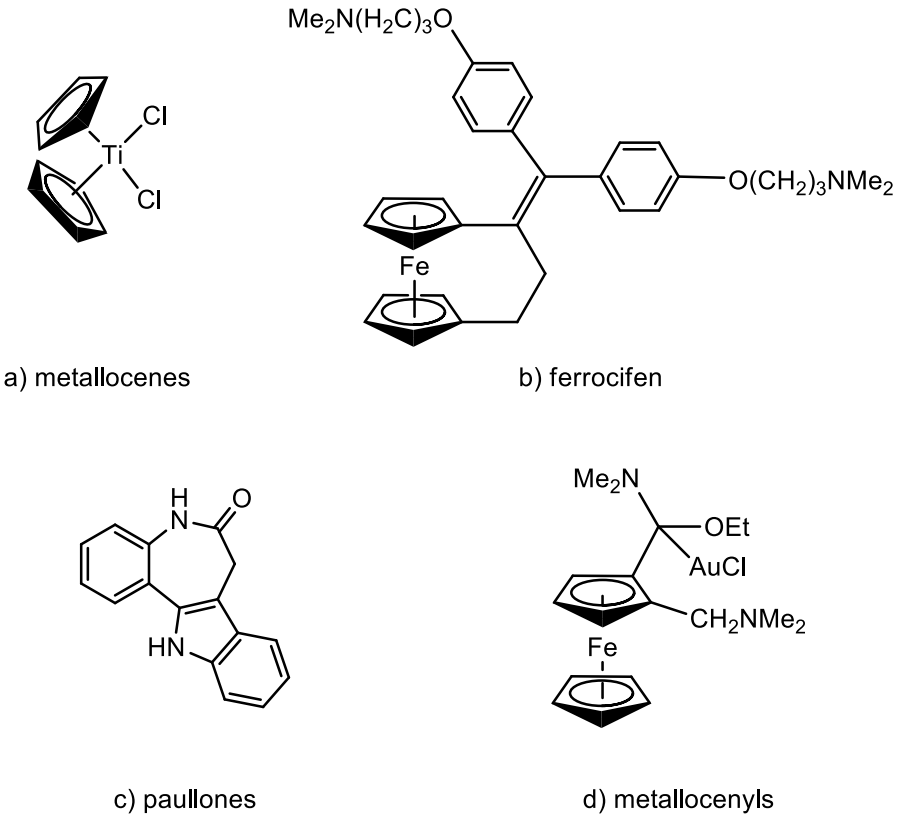

Figure 1.2 Classes of organometallic complexes with anticancer properties.

Organometallic complexes offers many unique properties not found in classical organic compounds. Structurally, they can adopt a huge variety of shapes ranging from linear to octahedral and even beyond. This structural assortment allows chemists ample opportunities to easily modify the stereochemistry of an organometallic complex. For example, a carbon atom with four different substituents can only exist as two different stereoisomers. In contrast, a metal ion surrounded by 6 different ligands has a total of 30 stereoisomers! Not only that, because of the d-orbitals possessed by metal ions, they can adopt a variety of geometries whereas carbon can adopt only planar and tetrahedral geometries (**Figure 1.3**). These unique properties of metal complexes, coupled with rational ligand design, allow chemists to come up with novel ways to circumvent the limitations of current cancer treatment methodology.

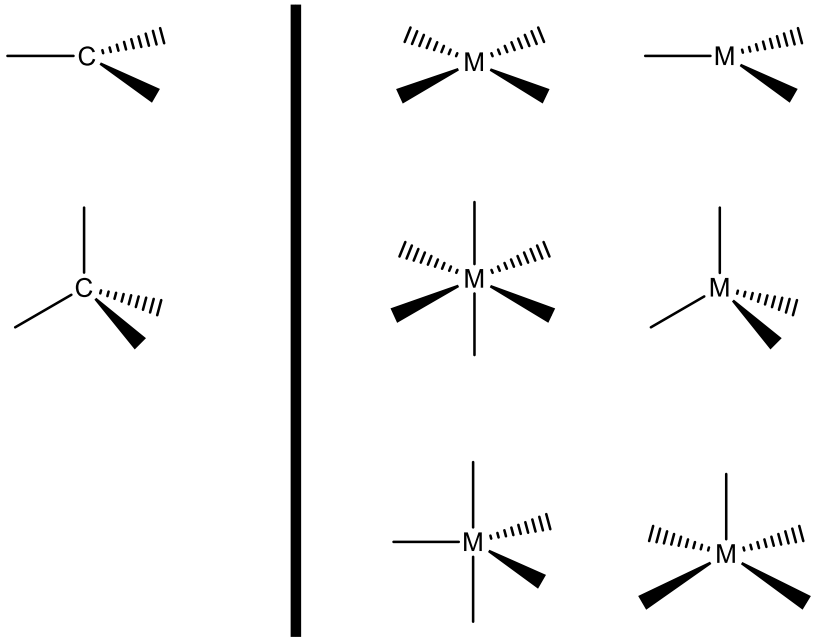

Figure 1.3 Possible geometries adopted by a carbon atom and a metal ion

As of today, osmium and ruthenium complexes have been extensively researched and their cytotoxic and biological properties are now well-documented [3-5, 45, 46, 54-58]. However, the use of transition metal carbonyl complexes in the pursuit of alternative anti-cancer drugs have not received as much attention as only a few transition metal carbonyl complexes can be found in literature (**Figure 1.4**), and even fewer have reasonably low IC_{50} values. [54, 56, 57].

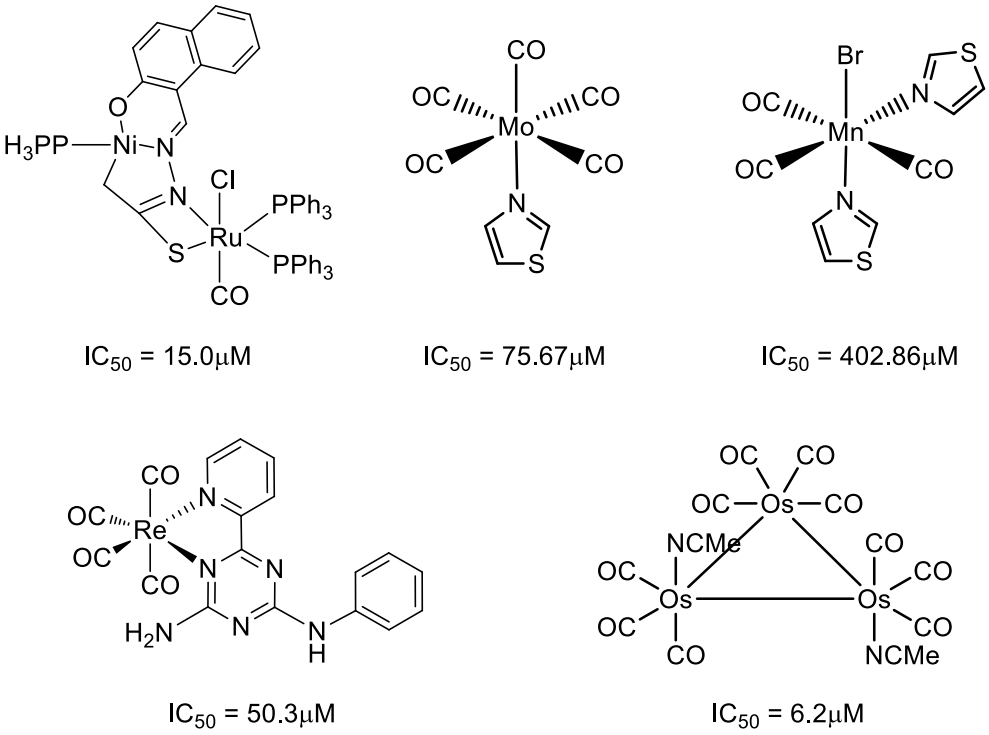

Figure 1.4 Examples of transition metal carbonyl complexes with cytotoxic activity.

There are two main advantages in incorporating carbonyl ligands in the development of anti-cancer therapeutics. One is that the fate of the metal complex in the cell can be easily monitored via infrared spectroscopy since the carbonyl functionality is known to produce a relatively strong IR signal in the 1900 cm^{-1} – 2100 cm^{-1} region. Secondly, carbonyl ligands are labile enough to

allow for diverse substitutions using a large variety of ligands such as phosphines, alkenes, pyridines, amines and thiols. This opens up endless possibilities for tweaking the cytotoxic properties of the resulting metal complex, limited only by the number of ligands available.

1.1.2 The Role of Iron in Carcinogenesis

Iron is an abundant element occurring naturally in living organisms and is best known for its role in the formation of the oxygen carrier haemoglobin. However, besides this well-known function, iron is also involved in a wide range of biological processes such as metabolism, cell replication and detoxification [59]. Chemically, iron exists in solution as the hydrated Fe^{2+} and Fe^{3+} cations, and these species undergo facile electron transfer and acid-base reactions. This redox capability allows iron to partake in enzymatic reaction, but at the same time also enables it to participate in potentially deleterious biological events such as free radicals generation. The simplest of such events is the Fenton reaction which generates two reactive oxygen species – superoxide ($O_2^{-\bullet}$) and hydroxyl ($OH^{\bullet}$) radical. The Fenton's reaction pathway is outlined in **Scheme 1.1**. The hydrogen peroxide in the scheme is the by-product of aerobic respiration.

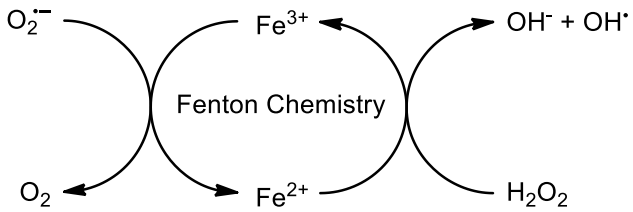

Scheme 1.1 Fenton Chemistry and generation of Reactive Oxygen Species (ROS)

The superoxide and hydroxyl radicals, collectively termed reactive oxygen species (ROS) generated via the Fenton's reaction are highly reactive and destructive. They can potentially damage lipids (fatty acids) and proteins (amino acids side chains with reactive groups) which are important constituents of organelles such as the mitochondria and nucleus in a living cell. In addition, iron in the +3 oxidation state is highly oxidising and can damage DNA via strand breakages and base modifications. Therefore, iron in biological organisms is considered as both essential and toxic.

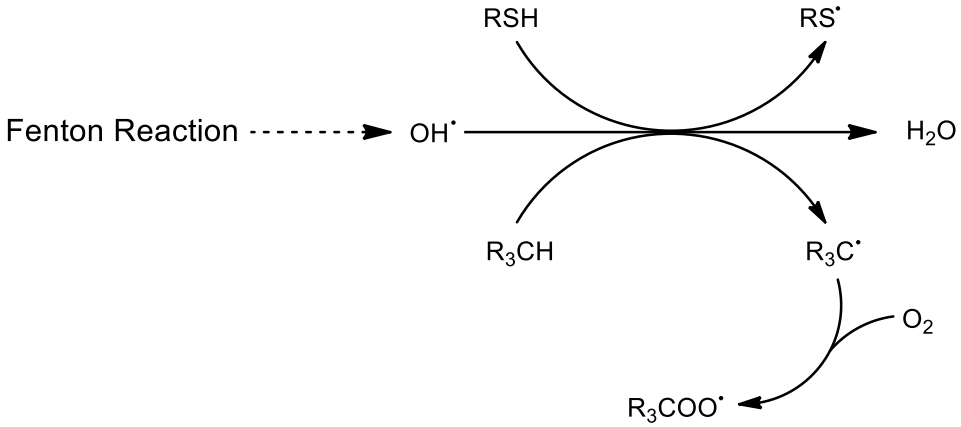

Scheme 1.2 Potential deleterious pathways taken by the hydroxyl radical generated from the Fenton Reaction

The essential yet toxic dual property of iron necessitates a deeper understanding of how iron works in a biological system. The recent discovery of new proteins that are involved in iron metabolism [60] have now greatly facilitated our comprehension of the dual traits of iron in our body. For example, newly identified iron efflux pumps [61], iron regulators, oxidases and reductases [62-64] have offered scientists a new look at how tumour cells influence and impact normal iron metabolism. These studies not only provide

valuable knowledge on the relationship between iron and cancer, they have also opened up the possibility of a new class of iron-based therapeutics.

Unfortunately, iron-based complexes exhibiting cytotoxic properties are far and few between, with the most classical example being organic derivatives of ferrocene as exemplified in **Figure 1.4**. While encouraging results have emerged from the use of iron chelators such as deferasirox and ciclopirox (**Figure 1.5**) as anti-cancer agents, none of them have yet to clear clinical trials.

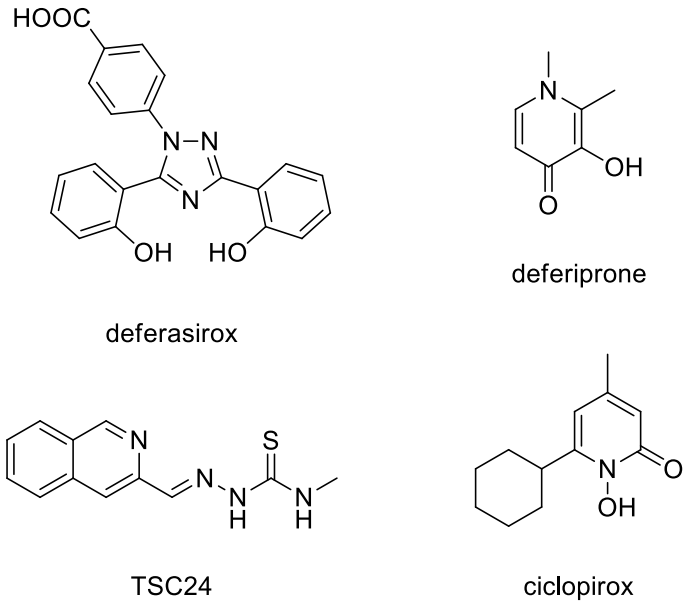

Figure 1.5 Examples of iron chelators undergoing evaluation as anti-cancer agents

1.1.3 Comparative Studies with Organic Isothiocyanates

The anti-cancer activity of modern drugs does not always involve a metal. In fact, more often than not; simple organic molecules can be used to trigger cell death. For example, the three common chemotherapy drugs deoxcytidine, gemcitabine and decitabine (**Figure 1.6**) are really just simple derivatives of the nucleoside cytidine [65]. Thus, in Chapter 3 of this thesis we will

investigate and compare the effects of organic isothiocyanates on cell proliferation versus that of the organometallic $CpFe(CO)_2X$ class of metal carbonyl complexes.

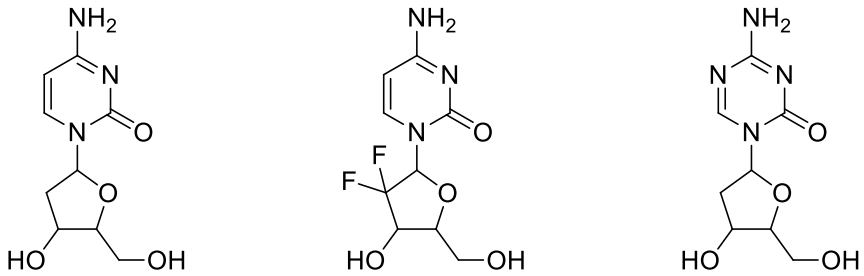

Figure 1.6 Some nucleosides derivatives used in chemotherapy

This comparative study was motivated by literature data that showed a positive correlation between the consumption of cruciferous vegetables such as broccoli, cauliflower and cabbage plants and a reduction in the risk of developing cancer [66-68]. This apparent link between the consumption and reduction in cancer risk was further verified when Professor Talalay's group first isolated and elucidated the structure of the key molecule [69], now known as sulforaphane, that is responsible for the protection against chemical carcinogenesis [70-74].

The discovery that an isothiocyanate as simple as sulforaphane have anti-proliferative properties paved the way for the development of other aryl and arylalkyl isothiocyanates (**Figure 1.7**) as an alternative to sulforaphane. This is needed because while sulforaphane has reasonably low IC_{50} value against a variety of carcinoma, it is a little too toxic towards normal cell lines (IC_{50} of 14 μM against human retinal pigment epithelial cells ARPE-19 [73]). Hence the synthesis of a variety of organic isothiocyanates that are structurally

different from sulforaphane was carried out in the hope that these new compounds would have reduced toxicity while at the same time preserved the potency of sulforaphane. The efficacy and potency of these compounds will also be discussed in Chapter 3.

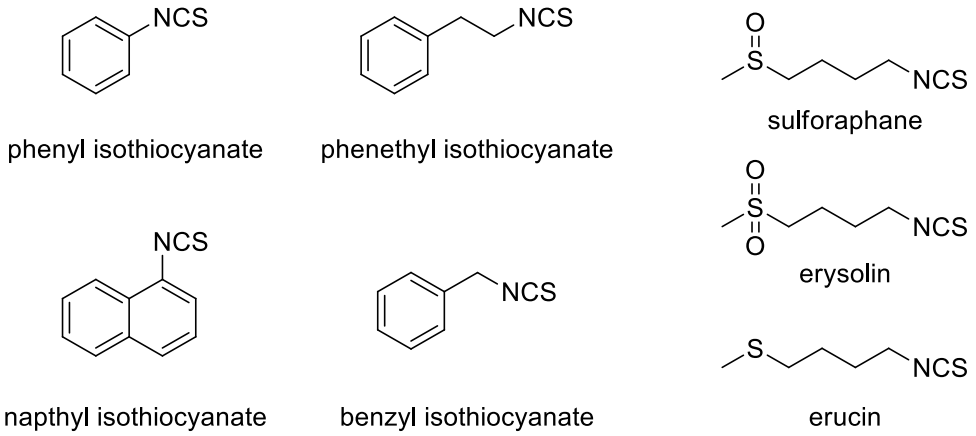

Figure 1.7 Organic isothiocyanates with anti-carcinogenic properties

1.2 Organometallic Complexes as Cell Signalling Agents

In a living cell, the transmission of information is essential for it to respond to its changes in its cellular environment. The cell hence must be able to receive and process signals that are outside of its immediate environment. As such, cells must function either as transmitters or receivers or both. The mechanism of such signalling processes is often facilitated by many different molecules ranging from simple gases like nitric oxide, carbon monoxide, hydrogen sulfide [75, 76] to small molecules such as steroids to huge proteins exemplified by cytokines and hormones (**Figure 1.8**). These molecules bind reversibly to their target receptor under normal physiological conditions and exert their effect over short distances (neuronal transmissions across a synapse). Other signalling molecules however, have to travel a longer distance

to reach its target receptor. An example of such a signalling molecule is the follicle stimulating hormone which has to travel via the blood stream from the mammalian brain to the ovaries to exert its effect. In Chapter 4, we will synthesize water soluble transition metal carbonyl complexes and use them as H_2S and CO releasing molecules.

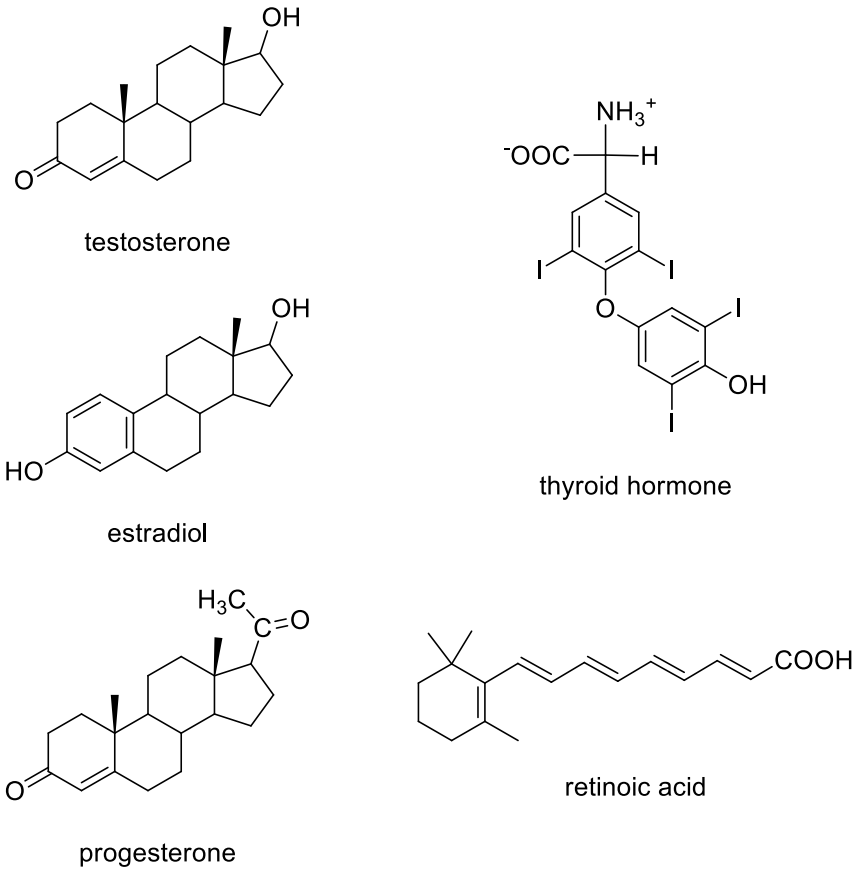

Figure 1.8 Naturally occurring signaling molecules in the human body

1.2.1 NO Releasing Molecules

Of the three small signalling molecules, the role of nitric oxide (NO) in biological systems and its mechanism of action of the various processes it mediates has already been researched extensively and is, at present, used routinely to treat infants suffering from pulmonary hypertension [77]. Nitric oxide is a soluble endogenously produced messenger gas molecule with a half-

life of between 6-30 seconds and being a small, uncharged molecule, it can diffuse freely across cell membranes. This molecule is known for its diverse range of functions in physiological systems both as a toxin and as a messenger molcule. First of all, it is known to regulate vasodilation and certain gastrointestinal and urinary functions [78]. NO also supports the immune system when it comes under attack from tumours, viruses or other invading microorganisms by contributing to the destructive action mediated by the macrophages against these foreign bodies [79]. The cardiovascular system is maintained by a series of NO regulated processes which include vasodilation, inhibition of platelet aggregation [80], and modulation of leukocyte adhesion to the endothelium [81]. Different classes of NO releasing molecules are exemplified in Figure 1.9 and a summary of the role of NO both as a toxin and as a messenger molecule is tabulated in **Table 1.1** [82]

Table 1.1 Physiological and Pathophysiological Roles of Nitric Oxide

Tissue	Messenger	Toxin
Heart	Coronary perfusion, negative inotropic ischemia	Myocardial “stunning,” septic shock, reperfusion
Lung	Ventilation-perfusion matching	Immune complex-induced alveolitis
Kidney	Glomerular perfusion, renin secretion	Acute kidney failure, glomerulonephritis
Immune System	Antimicrobial, antitumor	Antiallograft, graft versus host disease, inflammation
Gastrointestinal	Blood flow, peristalsis, exocrine secretion	Mutagenesis, mucosal damage

These critical roles of nitric oxide have driven the research and development of a myriad of NO-releasing molecules (NO-RMs) over the past decade. Now, moving beyond just molecules with a single function, scientists are diverting their attention to the synthesis of multi-functional NO-RMs such as NO-NSAID and NO-steroids [14] (**Figure 1.9**). Due to the diverse research attention on NO as an important biological messenger molecule, we shall focus on the other two gasotransmitters, CO and H_2S, in Chapter 4, and hence NO releasing molecules will only be touched briefly upon.

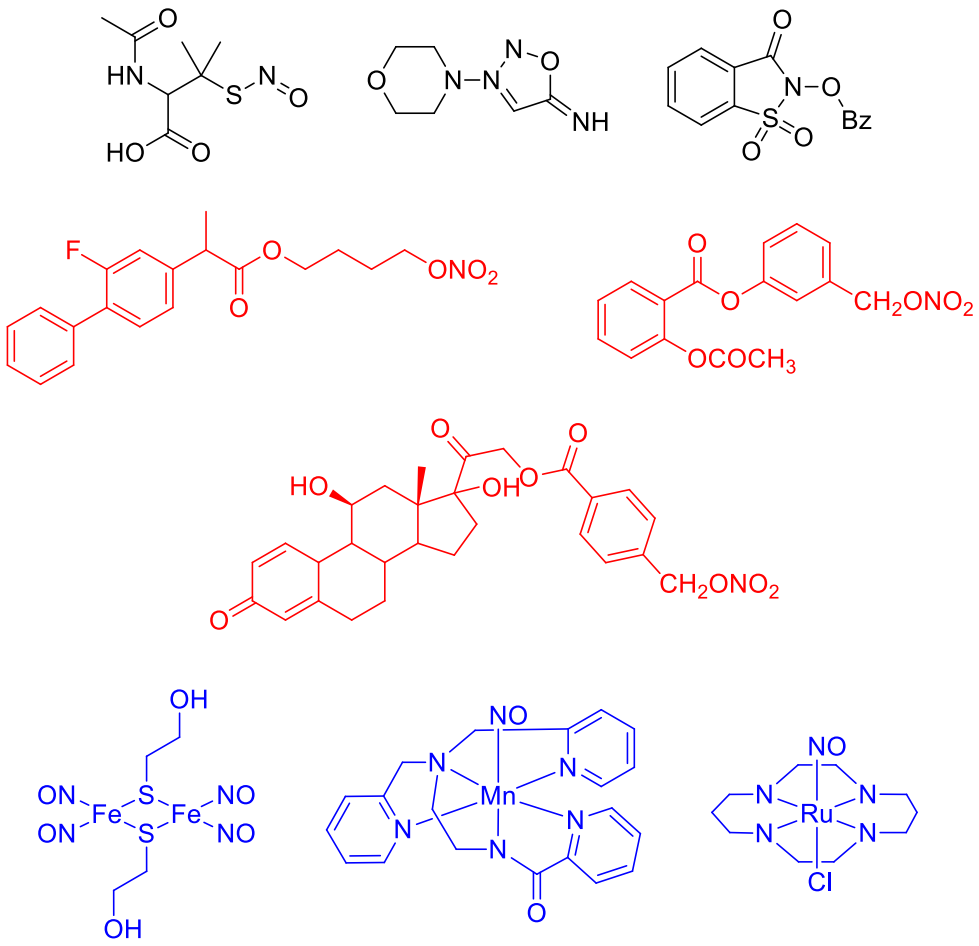

Figure 1.9 Examples of NO releasing molecules derived from organic nitrites (black), NSAIDs and steroids (red) and metal complexes (blue).

1.2.2 H_2S Releasing Molecules

While the effects of nitric oxide on pathological and physiological processes are well-documented, that cannot be said for the other two gasotransmitters hydrogen sulfide (H_2S) and carbon monoxide (CO). This has caused the development of H_2S and CO releasing molecules into pharmaceutical agents to be slow and sluggish [83]. Therefore the focus of Chapter 5 would be on both CO and H_2S releasing molecules. Both these gases have similar properties – they are both toxic air pollutants but are formed at sufficient levels in cellular systems to induce physiological and pathological changes without triggering cell death. Thankfully, with increasingly more research studies focusing on the elucidation of H_2S synthetic and metabolic pathways, this gas is gradually being recognized as important signalling molecule. The understanding of how H_2S is made and the mechanisms of action *in vivo* would shed some light on its role in many pathological and physiological processes [84], thus potentially leading to an increased rate in developing drugs that can release H_2S in a controllable and safe manner. In fact, animal studies using H_2S releasing agents have shown promise in treating H_2S related ailments and several of such drugs (**Figure 1.10**) has reached clinical trials.

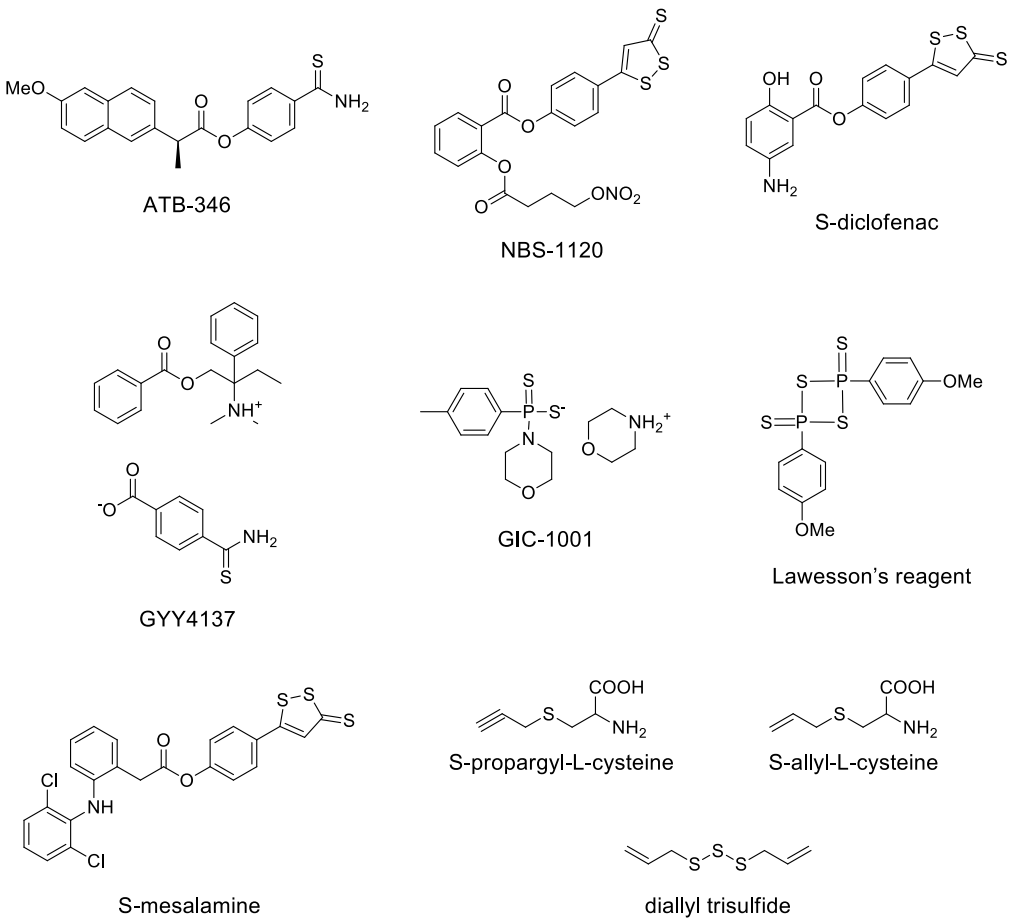

Figure 1.10 H_2S releasing molecules currently in clinical trials

Modern era of H_2S research probably began when it was discovered that H_2S generated from sodium hydrosulfide (NaSH), the simplest H_2S releasing compound, dilates the blood vessels in mouse models in both *in vitro* and *in vivo* studies [85, 86]. Following this finding, other researchers have reported that H_2S also dilates rat aorta, gastric artery, and portal vein [85, 87-89], along with the mesenteric [90, 91], cavernosal [92], and hepatic vascular beds [93]. On top of that, administration of NaSH in live mouse models led to a significant drop in blood pressure. Putting together these data and observations, H_2S clearly has a role to play in maintaining cardiovascular health, and thus the demand for newer and more efficient H_2S donors is constantly growing.

The molecules in **Figure 1.10** have clearly shown that existing H_2S releasing molecules does not involve organometallic complexes. Inorganic molecules such as NaSH and Na_2S are commonly used for H_2S research. However these inorganic salts have no therapeutic value because they release H_2S too rapidly upon hydrolysis in water. Synthetic H_2S donors like those illustrated in **Figure 1.10** are thus predominately the main H_2S releasing drugs used in research where controlled and sustained H_2S release is required. Nonetheless, these organic molecules do suffer from certain drawbacks that will constrain the progress of H_2S research. For instance, these organic H_2S donors have been found to function only *in vitro* and not *in vivo*. Compounds that can release H_2S in both circumstances have not been found [12]. Furthermore, there is an accompanying difficulty in quantifying the concentration of H_2S released under physiological conditions when such H_2S donors are used for research studies.

Hence, Chapter 4 will examine the use of organometallic complexes that act as H_2S donors. These complexes will carry with them carbonyl ligands as well that enables tracking and monitoring via infrared spectroscopy. The distinct infrared absorption spectra of the different intermediates before and after H_2S release makes quantification of the H_2S concentration easier. More importantly, these organometallic complexes are also water soluble which is advantageous for biological experiments and as will be discussed, the compounds have minimal cytotoxicity towards normal cells.

1.2.3 CO Releasing Molecules

Carbon monoxide has for a long while not been regarded as a molecule that can provide beneficial and therapeutic benefits thanks to its reputation as a

'silent killer'. This belief is changing as research on carbon monoxide as a viable therapeutic agent have garnered increasing interest over the last few years [94]. Indeed, present data not only demonstrates the protective properties of CO during preclinical trials, it also showed no undesirable effects during safety assessments and toxicology tests in healthy volunteers [95]. In addition, unlike NO and H_2S, CO only reacts with transition metals of a specific redox state, like iron or manganese, making the development of CO-based drugs more versatile and flexible. Hence metal carbonyl complexes present a good starting point for the synthesis of complexes carrying varying number CO ligands. These organometallic carbonyl complexes that can release CO upon photo or thermal activation are termed CO releasing molecules (CO-RMs). **Figure 1.11** illustrates some metal carbonyl complexes that can behave as CO-RMs.

The development of CO-RMs started in 2000 when Roberto Motterlini first tested $Fe(CO)_5$, $Mn_2(CO)_{10}$ and $[Ru(CO)_3Cl_2]_2$ and found that they are biologically active [10]. Unfortunately these metal carbonyls are not water soluble which presents a problem when dealing with biological systems – that the bioavailability of the complex might be insufficient for any therapeutic effect to occur. Eventually though, collaboration with Brian Mann saw the synthesis of the first water soluble CO-RM, $Ru(CO)_3Cl$(glycinate) [8], which was given the designation **CORM-3** (**Figure 1.12**). **CORM-3** was tested both *in vitro* and *in vivo* in mouse models and was found to release CO rapidly (half - life of under 1 min) under physiological conditions.

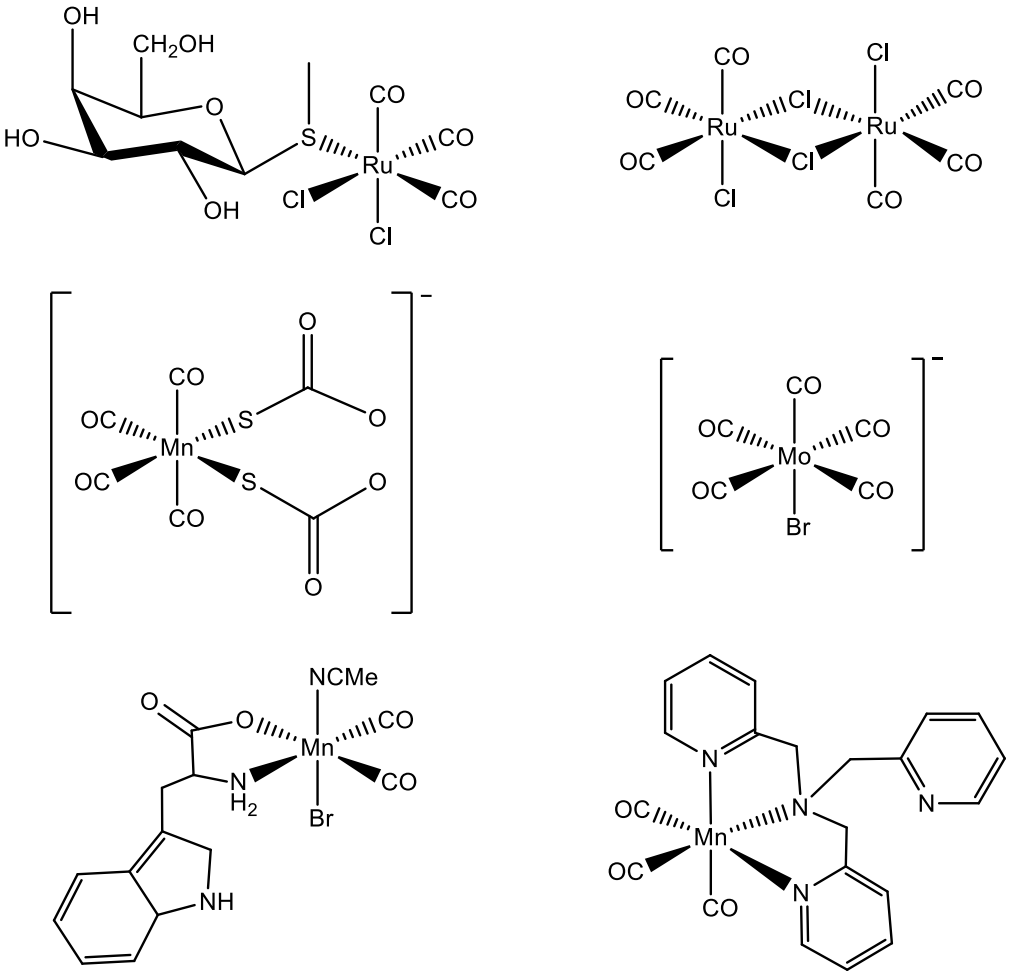

Figure 1.11 CO-RMs based on transition metal carbonyl complexes

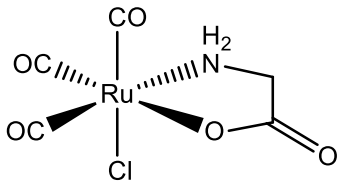

Figure 1.12 Chemical structure of $Ru(CO)_3Cl(glycinate)$ **CORM-3**, the first water soluble CO-RM.

The complexes listed in **Figure 1.11** are of course, by no means exhaustive. The chemistry of transition metal carbonyl complexes is known to be highly versatile and varied as can be seen from the facile substitution of the carbonyl functionality with a huge diversity of ligands. This is advantageous as it enables chemists to fine-tune the kinetics of the CO gas release, allowing for

controlled release of the gasotransmitter only when required and only in therapeutic doses. In addition, the CO-RMs in **Figure 1.11** suggests that there is not a transition metal that is preferred over the others in the synthesis of CO-RMs. Indeed, CO-RMs containing ruthenium, molybdenum, iron, manganese, cobalt are currently being synthesized and evaluated for their suitability as CO-RMs [96].

The growing interest in the physiological role of CO in biological systems requires that new CO-RMs be made available quickly. It can be challenging to synthesize new CO-RMs as they require several ideal chemical and bioactive properties such as:

- Non-toxicity
- Water solubility
- Controlled release
- Sufficient stability for administration under physiological conditions

In addition, fast and easy methods to quantify the amount of CO release in biological systems also need to be developed to allow real time monitoring *in vivo*. Current approaches of CO quantification either use myoglobin to determine CO content spectrophotometrically or by using a CO electrode to make electrochemical measurements. In Chapter 4, we introduce an alternative method of CO quantification by means of infrared spectroscopy.

1.3 Organometallic Complexes as Optical Sensors

Traditionally, there are two broad categories of optical sensors, those that use transmitted or reflected light for sensing and those that rely on fluorescent, phosphorescent and emitted light as an indicator for the presence or absence of

an analyte. Current progress in the field of optical sensors focus more on the design of fluorescent and phosphorescent probes with little research emphasis on the development of transition metal based sensors [97-100] that works via the use of transmitted light, particularly the visible region of the electromagnetic spectrum.

These phosphorescent and fluorescent probes are typically based on mid- to late-transition metals in low oxidation states. Rhenium, iridium and ruthenium metal complexes (**Figure 1.13**) are the most commonly studied examples of optical probes used for cell imaging purposes. It is only in the recent years that platinum and gold metal complexes started to garner interest in lieu of the fact that both platinum [101] and gold [102, 103] are also used as anti-cancer drugs, and so this combined imaging and therapeutic application become particularly interesting.

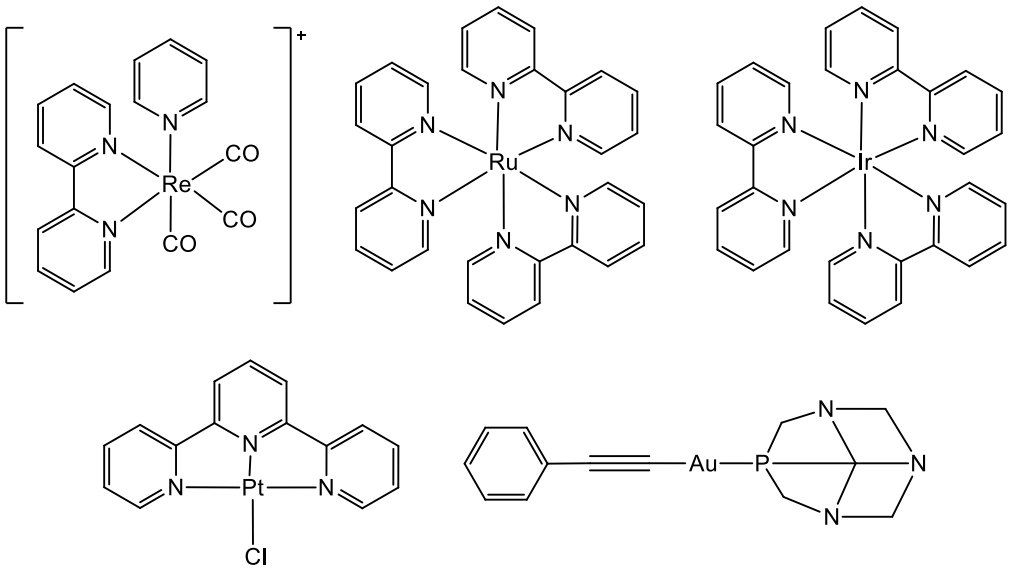

Figure 1.13 Representative Re, Ru, Ir, Pt and Au optical probes

With all the hype surrounding luminescent molecules, it is not surprising that the development of transition metal carbonyl complexes as molecular sensors has been neglected. In literature, transition metal carbonyl complexes that can be used as potential sensing agents are far and few between even though carbonyl complexes are very versatile reagents with the carbonyl ligand playing an additional role as a probe for vibrational microscopy. The CO ligand absorbs at between 1900 cm^{-1} to 2100 cm^{-1}, a region free from potential absorptions from background biological materials. Such a property provides for a high signal to noise ratio which can be exploited when used as a probe for infrared microscopy.

1.3.1 Organometallic Complexes for Thiol Sensing

Thiols are biologically important molecules which regulate a variety of biological processes in an organism. Of particular importance are those that are involved in maintaining redox homeostasis such as glutathione (GSH), cysteine (Cys) and homocysteine (HCys). In addition to maintaining redox balance, thiols are also known to play a functional role in enzymes catalytic sites and metabolic pathways [104]. Indeed, researches have suggested that thiols levels, especially that of homocysteine, are linked to a number of diseases including Alzheimer's, cancer and cardiovascular diseases [105-107]. Plasma thiol concentrations have also been linked to the oxidative stress levels associated with the development of some of these conditions [108-111].

In view of the biological importance of thiols, it is not surprising that there already exist some analytical methodologies for the detection and quantification of thiols. Some well-known instrumental methods include HPLC [112-114], capillary electrophoresis [115, 116], mass spectrometry [117,

118] and electrochemical methods [119, 120]. However, these methods have their own drawbacks, for example, high equipment costs, complexity, sample processing and run times which make them impractical to be used for studying sensitive biological systems and for field applications.

Compared to instrumental techniques, fluorescence and optical sensing present a more viable and attractive option for the detection of thiols. This can be seen from the increased research efforts devoted to the development of optical and fluorescent sensors for thiols [121, 122] over the last decade. Such optical and fluorescent probes have the advantage of sensitivity, simplicity and most importantly, potential for *in vivo* bioimaging which is becoming increasingly important in the field of biomedical science [123-125]. **Figure 1.14** lists some examples of current fluorophores that is used for small molecules sensing. These optical probes function via a variety of reaction mechanisms ranging from Michael additions [126, 127], cyclization with aldehydes [128, 129], cleavages of sulfonamides and sulfonate esters [130-132], cleavage of selenium-nitrogen bonds [133-135], redox processes in metal complexes [136-138], cleavages of disulfides bonds [139-141] to the use of nanoparticles in the form of quantum dots [142-146]. Remarkably, metal carbonyls as optical probes have not received much attention even though they form highly coloured complexes which change colour easily depending on its chemical environment. The CO ligand in such metal carbonyl complexes can function both as a probe for vibrational spectroscopy and also indirectly act as an optical probe by influencing the ligand field of the complex, thereby altering the photo-physical properties of the said metal carbonyl complex.

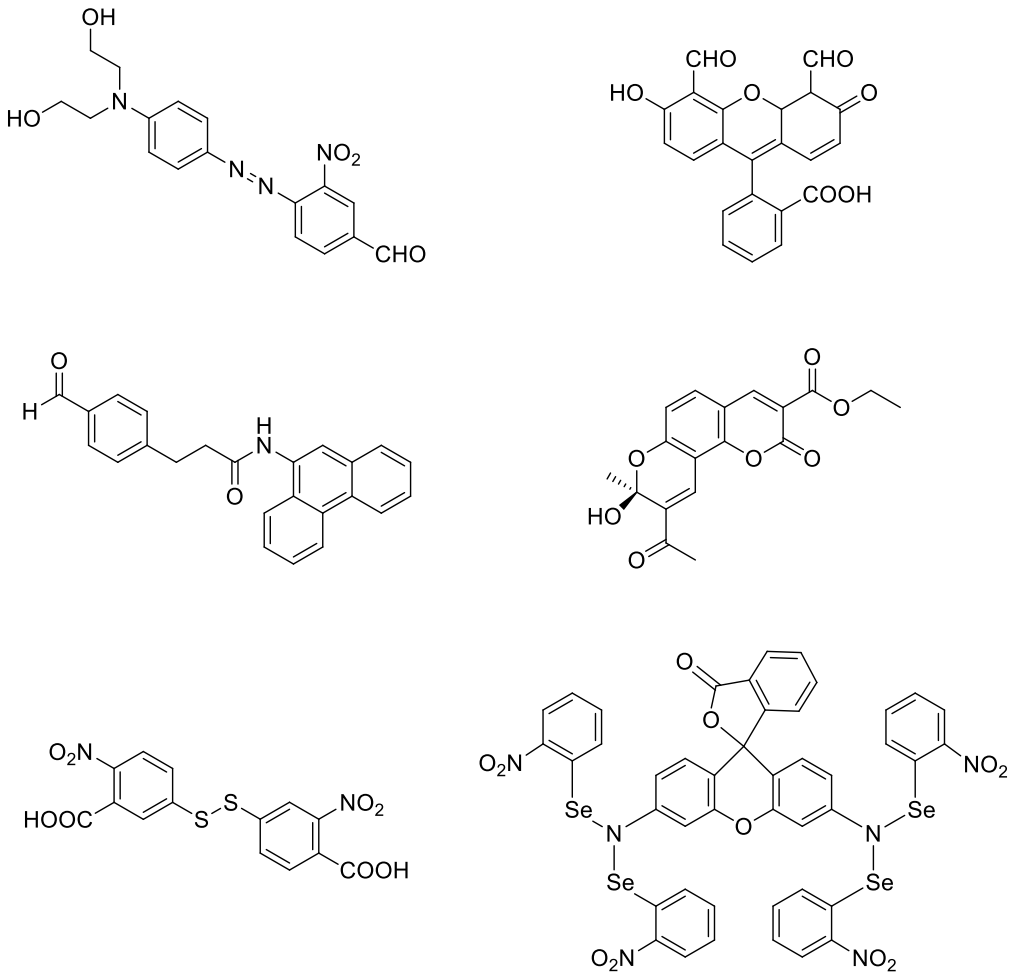

Figure 1.14 Common fluorophores selective for thiols

In Chapter 5 we will discuss the utility of a functional radical probe containing a manganese carbonyl scaffold. Not only does this probe exhibits different absorbance in the visible light region depending on its redox state, the preparation of such a radical complex may also serve as a dual probe in infrared and fluorescent imaging studies in chemical biology, especially in radical-rich environments involving NO and ROS. Interestingly, it also has the ability to distinguish between different biological thiols such as between glutathione and cysteine!

1.3.2 Organometallic Complexes for Hydrazine Sensing

Chapter 5 of this thesis will also include a section describing the application of the manganese carbonyl radical in the detection of hydrazine, N_2H_4. Hydrazine has long been established as a highly toxic small molecule and has shown to induce cancer of the liver and the nervous system in laboratory animals [147]. Because of its molecular size and ease of dispersal, it can be easily absorbed into the human body through skin, oral or inhalation routes of exposure. Despite the toxicity, however, hydrazine has been, and still is, used extensively as a fuel in rocket and missile propulsion systems [148] and is also found as a common reactant in fuel cells [149]. A simple molecule possessing both reducing and basic properties, hydrazine is widely used in the chemical industry for the manufacture of pharmaceuticals, pesticides, dyes and emulsions [150, 151]. Due to its ubiquitous yet toxic nature, there is a need for reliable and sensitive methods to detect hydrazine and its derivatives.

Current analytical techniques for the detection of hydrazine include, but are not limited to, spectroscopic [152-154], potentiometric [155, 156], chemiluminescence [157] and chromatographic [158]. These techniques although well established, are often not easy to apply and may require expensive instrumentation which would not be ideal for real time monitoring and field applications. An inexpensive and convenient method that has been used to detect a variety of ionic and neutral analytes is the use of chromogenic probes that changes colour in the presence of the molecule of interest. Strangely, even though several of such optical probes have already been developed for the detection of a variety of cations, anions and neutral molecules [159, 160] (**Figure 1.15**), there have been very few reports of

optical probes for hydrazine. Therefore, a section in Chapter 5 will examine the use of a manganese carbonyl probe to detect and quantify hydrazine.

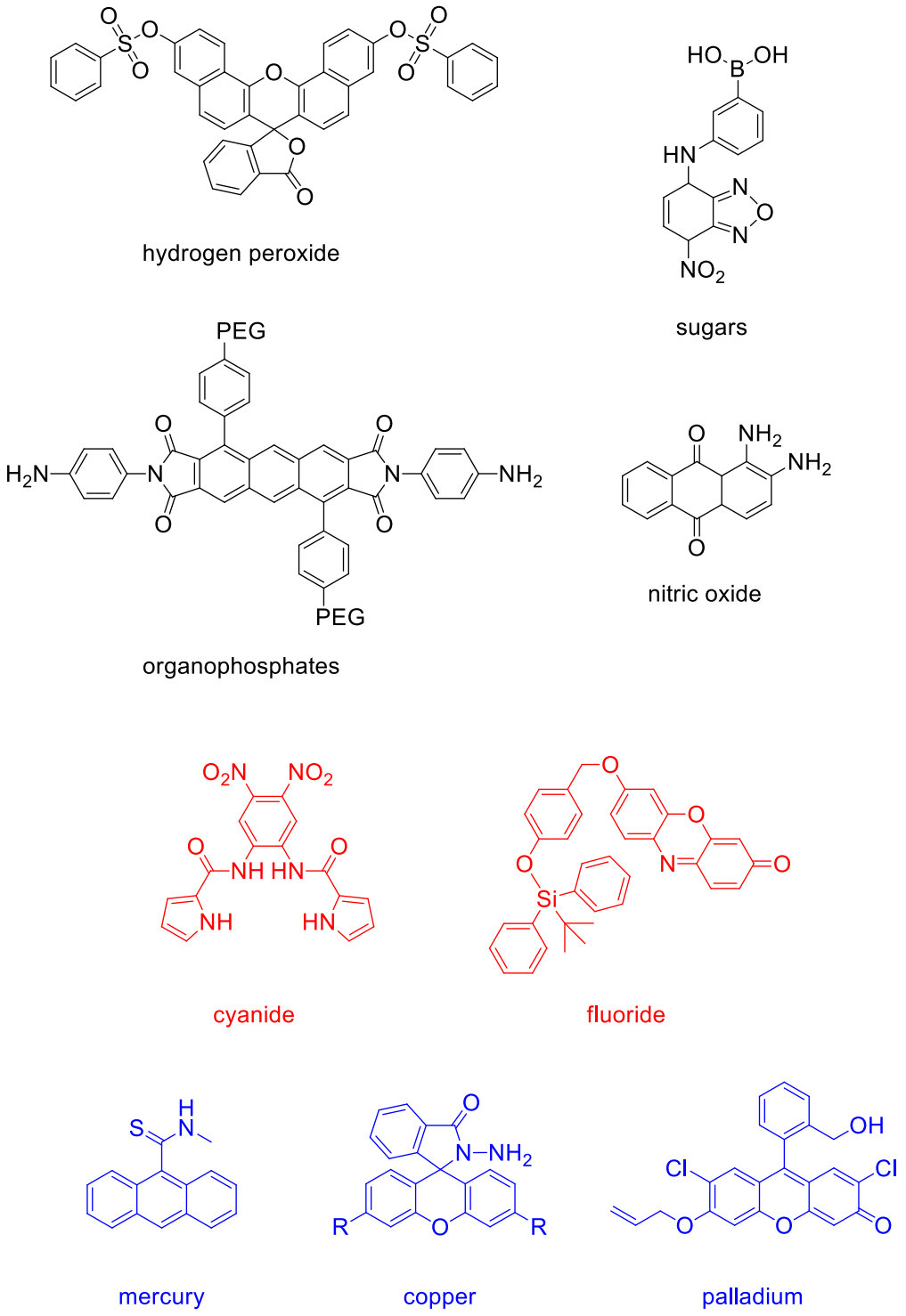

Figure 1.15 Chemical probes used for the detection of various neutral (black), cationic (blue) and anionic (red) analytes

1.4 Project Focus and Thesis Organization

Transition metal carbonyl complexes have provided chemists a means to monitor the fate of the complex via infrared spectroscopy. This has allowed many catalytic mechanisms to be elucidated and hence transition metal catalysis is still widely researched in many laboratories. The use of transition metal carbonyl complexes in the area of biomedical applications is still in its infancy and much more can certainly be done to bring newer and more efficient drugs, sensors and signalling molecules into the commercial market.

The focus of this thesis is therefore to search for new metal carbonyl complexes that have potential applications in the biomedical industry.

Chapter 2 will touch upon the potential anti-cancer activity of an iron-based carbonyl complex with a half sandwich scaffold – $CpFe(CO)_2$. Similar to ruthenium and osmium half sandwich complexes, the iron analogue also retards cancer cell proliferation via apoptosis, without the accompanying cytotoxic effects towards normal cell lines. The use of a metal complex with a carbonyl ligand can provide us an alternative means to monitor via infrared spectroscopy the fate of the complex upon entering a biological system. A total of seven Fp complexes were synthesized using published methods and their cytotoxic properties were evaluated against three different cell lines (ER– breast carcinoma MDA-MB-231, ER+ breast carcinoma MCF-7 and HeLa cell line). These cytotoxicity data were then compared with normal cell lines MCF-10A (normal mammalian breast cells), TAMH (Transforming growth factor alpha mouse hepatocyte) and HL-1 (Mouse cardiomyocyte derived from AT-1 mouse atrial cardiomyocyte tumor lineage).

In Chapter 3, we begin to explore the efficacy of organic isothiocyanates as a metal-free anti-cancer therapeutics. This study arose because it has been reported that sulforaphane (an isothiocyanate) was found to exhibit chemo-protective properties to a variety of cancer cell lines. Work then began to synthesize organic molecules carrying the isothiocyanate moiety which was then evaluated against the breast cancer cell line. Chapter 3 also discusses the differences in the cell viability assays between an organic isothiocyanate versus a metal-bearing isothiocyanate in order to establish whether the presence of a redox active metal increases or decreases the anti-proliferative activity of the molecule. In addition, several modifications to the $CpFe(CO)_2$ core such as the modification of the cyclopentadienyl ring and changing the metal centre, was also carried out and the effect of the change was then evaluated against the cancer cell lines.

Chapter 4 moves away from anti-cancer complexes and being to discuss the utility of transition metal carbonyl complexes as CO and H_2S releasing molecules, both of which are important gasotransmitters in a biological system. In this chapter, water soluble complexes were synthesized and subjected to different conditions to induce the release of the respective gasotransmitters. Different analytical methods were used to track and quantify the amount of gases released during the course of the reaction.

In Chapter 5, a manganese based carbonyl complex was developed and used to detect and distinguish between different thiols, which are crucial and ubiquitous molecules occurring in the amino acid cysteine and the antioxidant glutathione. These thiols have important roles in mammals and therefore it is crucial that we can monitor and determine the quantity of such biological

thiols at any time during *in vitro* or *in vivo* experiments. The reaction of different thiols with the manganese complex induces a change in the UV-vis absorption spectrum over time. These changes can be easily monitored with a UV spectrometer after which Beer's Law can then be applied to calculate the concentration of the analyte present.

Chapter 2

Transition Metal Carbonyl Complexes as Anti-Cancer Agents

2.1 Introduction

The success of cisplatin in testicular cancer treatment has led to much research interest in the discovery of organometallic anti-cancer compounds [39, 40, 161] such as arene ruthenium [3, 4, 37, 162, 163], ferrocene derivatives [164-166] (which was also discussed in an excellent review paper [167]) and metal carbene complexes [168-170]. Although not as prevalent, transition metal carbonyl complexes have also been featured as anti-cancer compounds since the first demonstration of cytotoxicity by alkyne hexacarbonyldicobalt species [171-174]. An iron carbonyl diene nucleoside complex has been shown to induce apoptosis in cancer cells [175, 176] while rhenium carbonyl tamoxifen

complexes bind strongly to estradiol receptor sites in breast cancer cells [177, 178]. Osmium carbonyl clusters [57] have been used as a new class of apoptosis-inducing agents while an iron dithiocarbamate carbonyl complex used as a CO-releasing molecule (CORM) has exhibited anti-cancer activity [179]. Manganese carbonyl N-heterocycles have demonstrated photo-induced cytotoxicity [180-182] and half-sandwich cymantrene peptides conjugates synthesized by Schatzschneider group have also demonstrated potential in anticancer chemotherapy [183-185].

Our motivation in using inexpensive iron carbonyls as anti-cancer agents came during in vitro testing of organic and inorganic isothiocyanates on ER- breast carcinoma cancer cells (MDA-MB-231). We discovered that cyclopentadienyl iron dicarbonyl isothiocyanate $CpFe(CO)_2NCS$ demonstrated more potent cytotoxicity towards these cells, compared to sulforaphane, an organic isothiocyanate found in cruciferous vegetables [70, 74]. Interestingly, the normal cells are unharmed by the iron complexes. This promising result initiated a series of experiments to evaluate the cytotoxicity of $CpFe(CO)_2X$ class of complexes on MDA-MB-231 cells as well as the more widely researched HeLa cell-line. Indeed, our results have suggested that even without the isothiocyanate functionality, these metal complexes are still cytotoxic, and may have triggered cancer cell death via a different mechanism.

2.2 Results

2.2.1 Chemistry of Cyclopentadienyl Iron Dicarbonyl Complexes

Seven iron complexes of formula $CpFe(CO)_2X$ (**1** to **7**, Scheme 2.1) and for comparison purposes, three metal carbonyl dimers $[CpMo(CO)_3]_2$ (8),

$Re_2(CO)_{10}$ (**9**) and $Mn_2(CO)_{10}$ (**10**), were tested for cytotoxicity against MDA-MB-231 breast cancer cells and HeLa cervical cancer cells. Complexes **1**, **2**, **4**, **5** and **6** were prepared according to slightly-modified literature methods [186, 187] while **3**, **7**, **8**, **9** and **10** were commercially available.

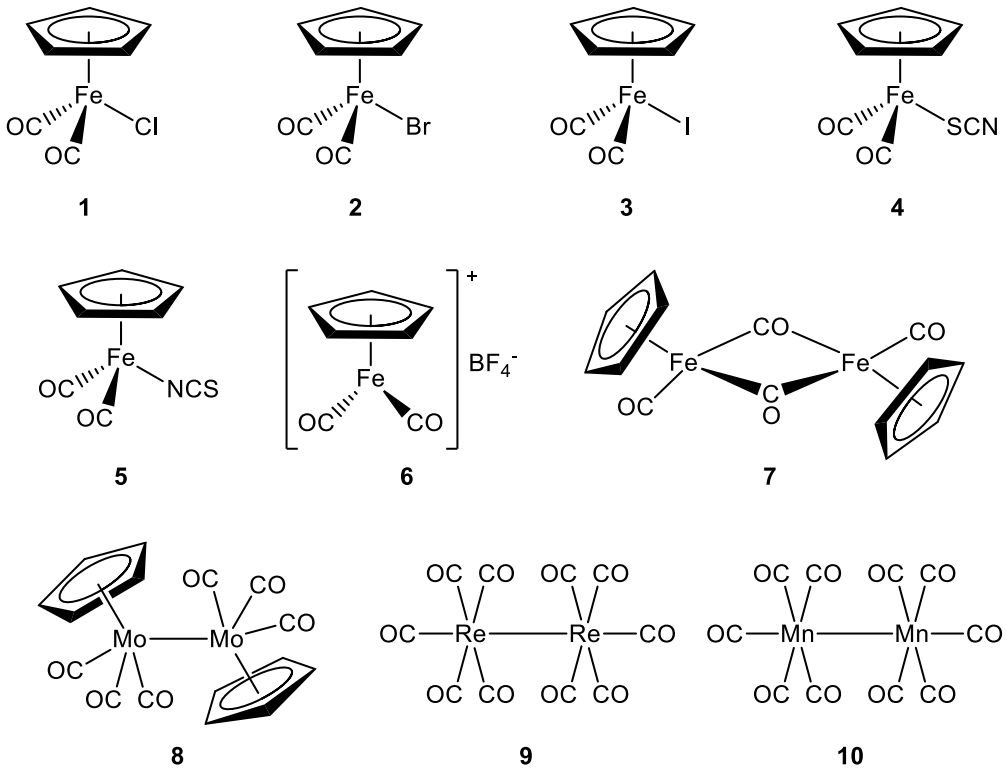

Scheme 2.1 Chemical structure of the 10 metal carbonyl complexes evaluated for anti-cancer activity

To complete the structural characterization of the complexes in **Scheme 2.1**, the X-ray single crystal structures of red $CpFe(CO)_2SCN$ **4**, (**Figure 2.1**) and its yellow isomer, $CpFe(CO)_2NCS$, **5**, were obtained (Figure 2.2). The Fe-N-C-S moiety in **5** is close to linearity with a bond angle of 178.90(3)° and the short N≡C bond of 1.159(5)Å adopting triple bond character. A bent Fe-S-CN angle of 100.96(17)° due to lone pair repulsion is determined in **4** as predicted by the VSEPR theory together with a C ≡ N bond length of

1.163(7)Å. The C≡N bond lengths in both isomers are similar to those found in organic thiocyanates and isothiocyanates. The more efficient π–backbonding from the NCS functionality to the iron center in the linear Fe-NCS fragment of **5** also leads to slightly higher υCO values.

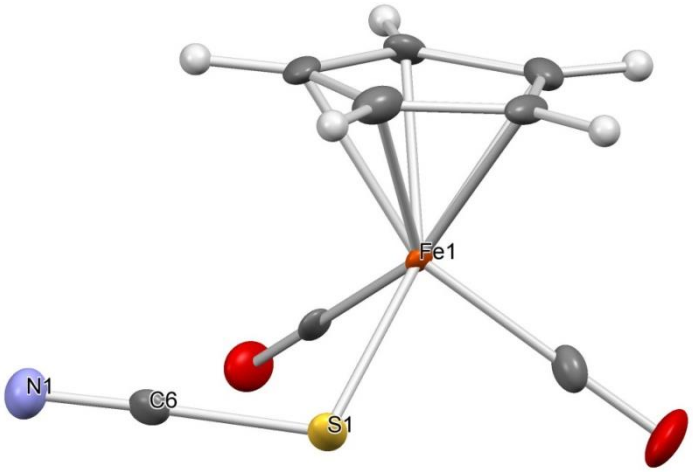

Figure 2.1 X-ray crystal structure of **4** with thermal ellipsoids at 50% probability

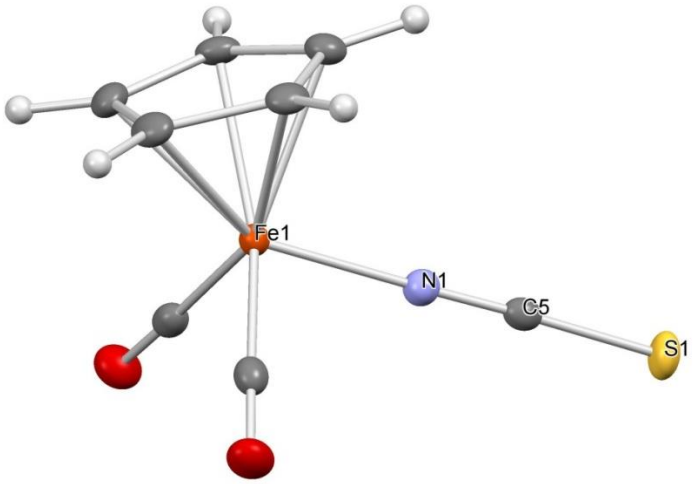

Figure 2.2 X-ray crystal structure of **5** with thermal ellipsoids at 50% probability

2.2.2 Biological Evaluation

The IC_{50} values for **1** to **10** evaluated against ER- breast carcinoma cancer cells (MDA-MB-231) and HeLa cervical cancer cell line in DMSO solvent are shown below in Table 2.1. The values were obtained after 24 hour incubation

Table 2.1 IC_{50} values of Fp derivatives versus the commercially known metal dimers.

		[IC_{50}] / μM	
Class of Complex	Complex	MDA-MB-231	HeLa
$CpFe(CO)_2X$	1	17.3 ± 1.3	18.3 ± 1.2
	2	10.5 ± 1.2	13.7 ± 1.2
	3	3.0 ± 1.1	6.7 ± 1.1
	4	3.4 ± 1.1	7.0 ± 1.1
	5	3.8 ± 1.1	8.0 ± 1.2
	6	8.7 ± 1.1	9.0 ± 1.0
	7	13.6 ± 1.2	15.5 ± 1.2
Transition Metal Carbonyl Dimers	8	>200	>200
	9	>200	>200
	10	>200	>200

All the iron complexes **1** to **7** showed cytotoxicity towards the cancer cells with IC_{50} values ranging from 3.0 μM to 17.3 μM, with **3** being the most potent over a 24-hour incubation period. The presence of the SCN/NCS group in **4** and **5** does not appear to impart additional cytotoxicity as compared to the rest of the $CpFe(CO)_2$ derivatives. In contrast, dimers **8, 9** and **10** do not show appreciable cytotoxicity. Remarkably, all the complexes are not cytotoxic towards the corresponding normal mammary epithelial cells MCF-10A and two other normal cell lines, TAMH (Transforming growth factor- alpha mouse hepatocyte) and HL-1(Mouse cardiomyocyte derived from AT-1 mouse atrial

cardiomyocyte tumor lineage) [188]. IC_{50} values could not be determined since the normal cell viabilities over the tested concentration range remains close to 100%. Although the IC_{50} values for cancer cell cytotoxicity are not in the nM (nanomolar) range, the iron complexes induce only cancer cell death while leaving normal cells intact.

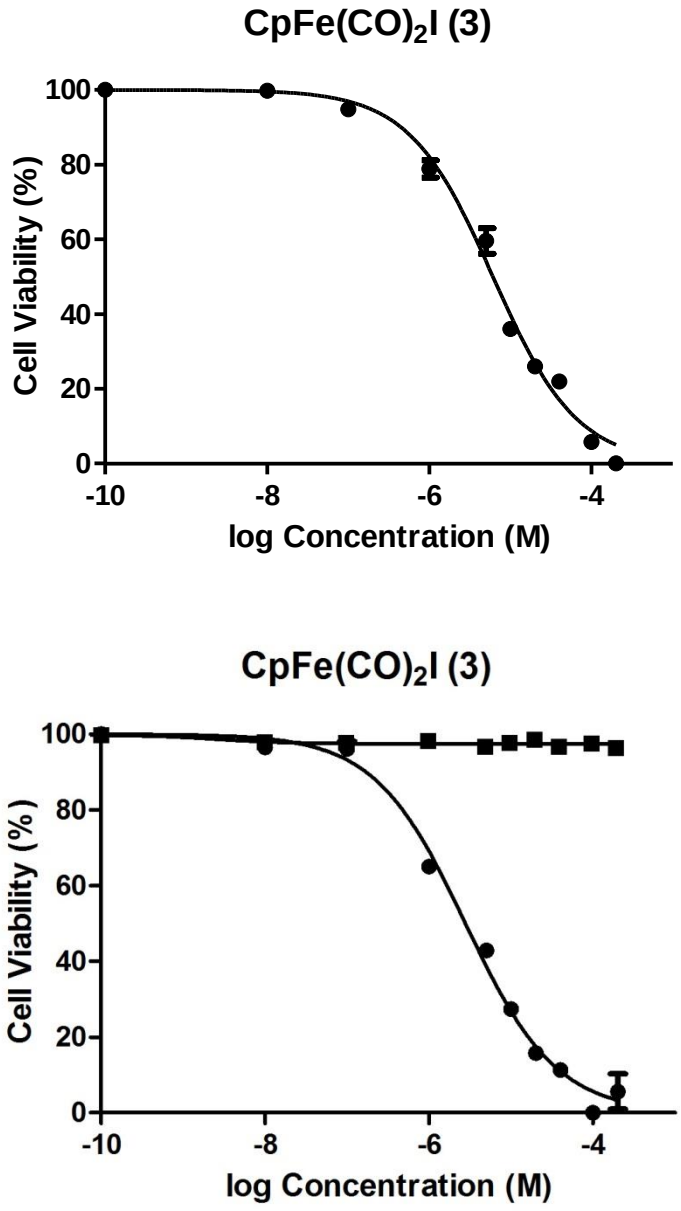

Figure 2.3 Dose-response curves of complex **3** for HeLa (top) and MDA-MB-231 (•, bottom) cell line. The normal cell line MCF-10A (■, bottom) has been co-plotted together on the MDA-MB-231 IC_{50} curve.

The effect of the iron complexes on the cancer cells can be observed by light microscopy (**Figure 2.4**). The cancer cells are initially of regular shape with the cellular membranes clearly visible and defined. The cells are round in shape as they have been trypsinized prior to imaging. After treatment with complex **3** for 24 hours, the cells become irregularly-shaped because of the decoupling of the cytoskeleton from the plasma membrane followed by eventual loss of cytoplasmic material. The nuclei are now not as clearly visible and the cytoplasmic membranes are no longer well-defined. This blebbing process is widely believed [189-191] to be an indicator of apoptosis. This observation is consistent with the flow cytometry and confocal data (**Figure 2.5** and **2.6**) which indicates that the cells treated with 5 μM of **3** undergo early apoptosis (AV^+/PI^-). Increasing the dosage to 10 μM causes a larger proportion of the cells to proceed to late apoptosis phase (AV^+/PI^+).

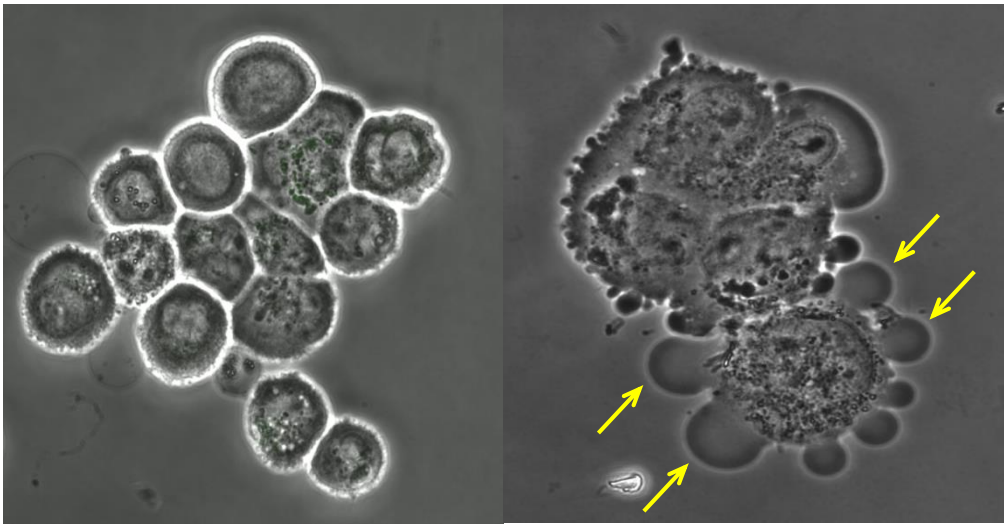

Figure 2.4 Bright field image at 400× magnification of MDA-MB-231 mammary cancer cells before (left) and after (right) treatment with **3**. Both images were obtained after treatment with 40 μM of complex **3** for 24 hours at 37°C. The cells in the left image have been trypsinized and show the presence of an intact cell membrane. The right image shows multiple blebs (indicated by arrows) on a cell which is characteristic of apoptosis.

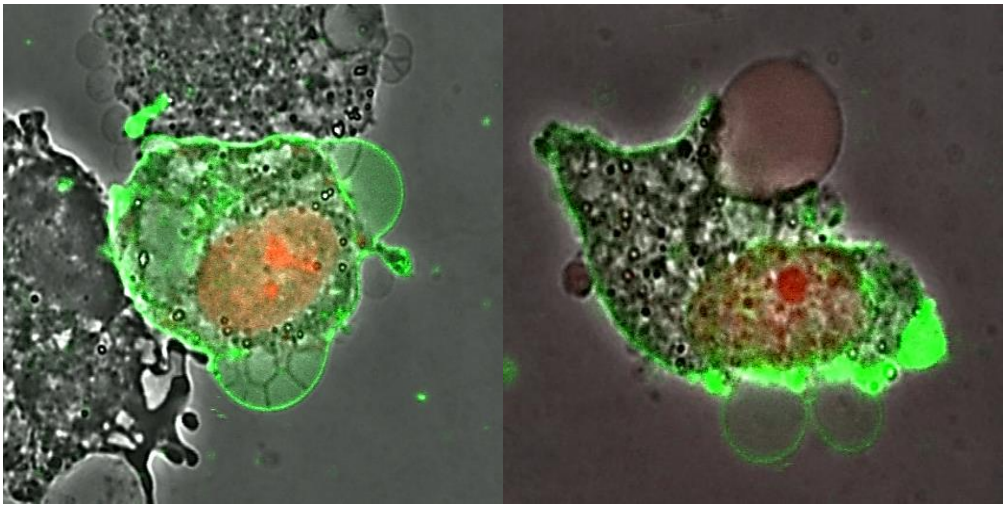

Figure 2.5. Confocal image of MDA-MB-231 cells after treatment with 40 μM of **3** (left) and **7** (right).Both images are doubly stained with Annexin V Alexa Fluor 488 and PI and taken at 600× magnification. The nucleus (red) is observed to be swollen together with the presence of blebbing (green) suggests that the cell is undergoing late apoptosis. Blebbing is again observed together with a large swollen nucleus for the right image after treatment with **7.**

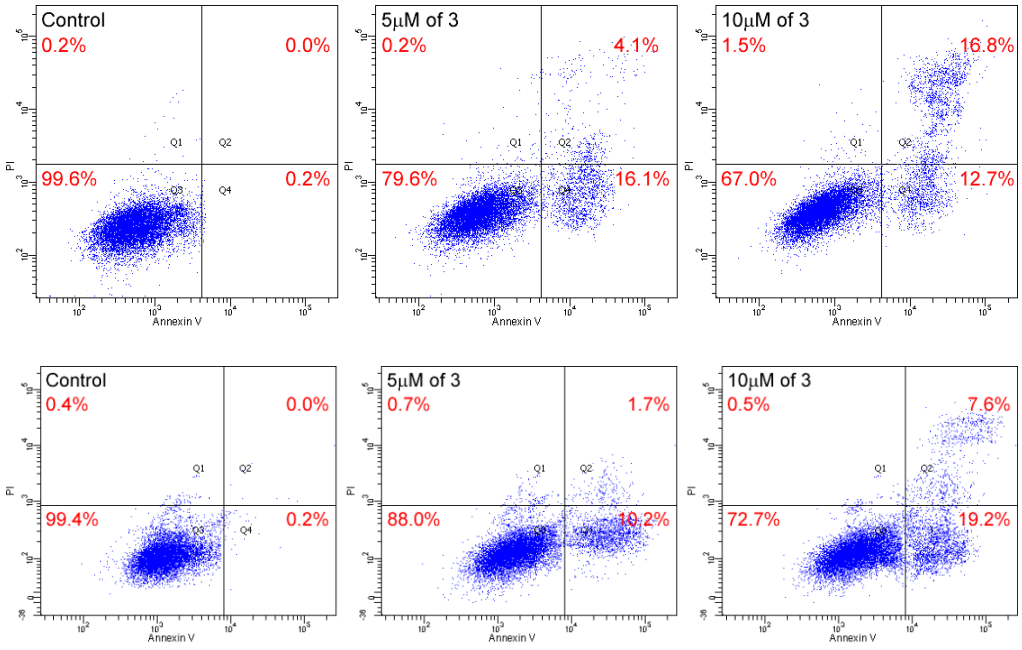

Figure 2.6 Flow cytometry data of HeLa (top) and MDA-MB-231 (bottom) cells treated with 0 μM, 5 μM and 10 μM of **3** at 37°C over 24 hours.

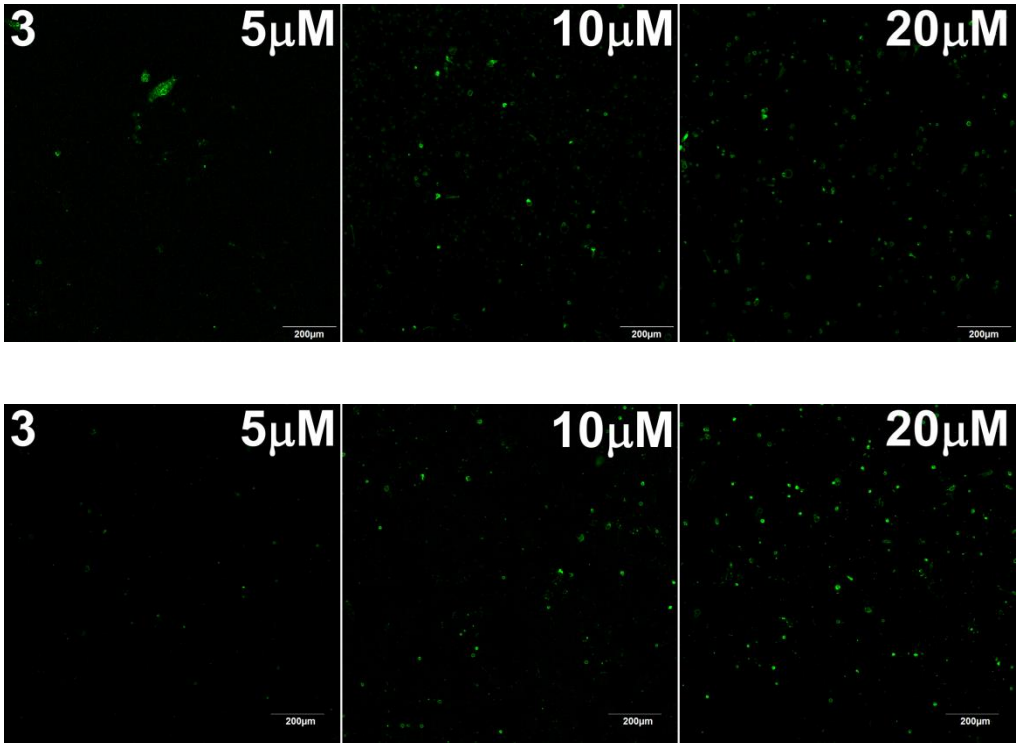

Figure 2.7 Confocal image acquired at 10× magnification of MDA-MB-231 (top) and HeLa (bottom) cells. The cells were treated with 5 μM, 10 μM and 20 μM of **3** for 24 hours at 37°C and stained with Annexin V and PI.

In order to shed more insight into the mode of action of the iron complexes towards cancer cells, **3** and **7** have been chosen for further study. Studies into their water-solubility, permeability across a membrane, metabolic stability and cytotoxicity towards other normal cells were carried out. The respective solubility of **3** and **7** in water have been determined to be 141 ± 20 μM and 31 ± 2 μM. These values were determined by first dissolving weighed amounts of **3** and **7** with stirring in a known volume of deionized water until the first sign of excess solids were seen at the bottom of the cuvette. The UV-vis absorbance was then monitored until it reaches a constant value for at least an hour. The UV-vis spectra of the complexes in water and in hexane also appeared similar hence **3** and **7** should still be structurally intact without undergoing extensive dissociation or hydrolysis in water.

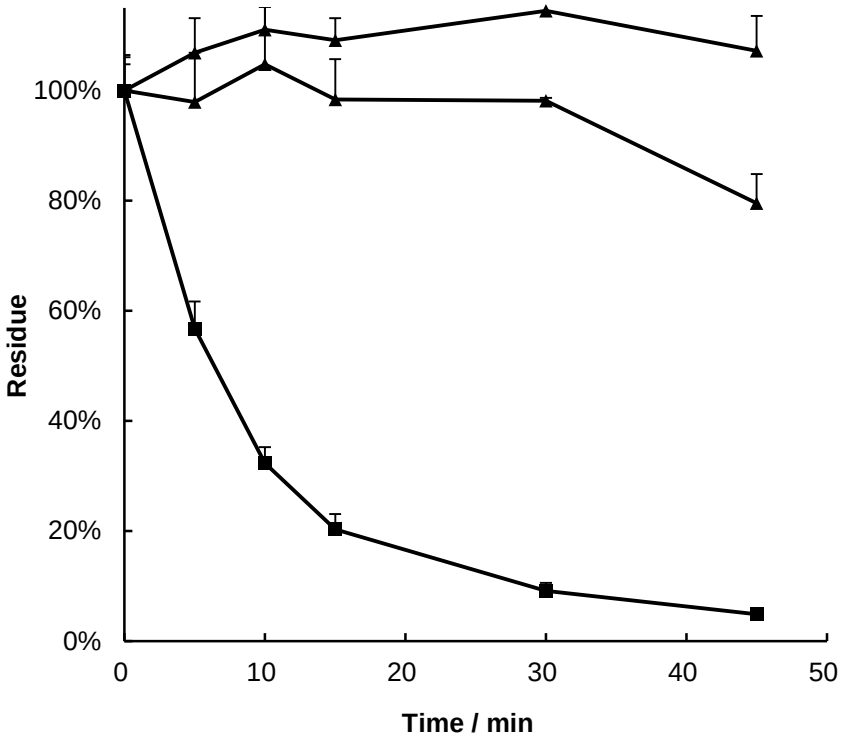

Figure 2.8 Metabolic stability studies of complex **3** in both MRLM (▲) and FRLM (•) versus a positive control, midazolam (■).

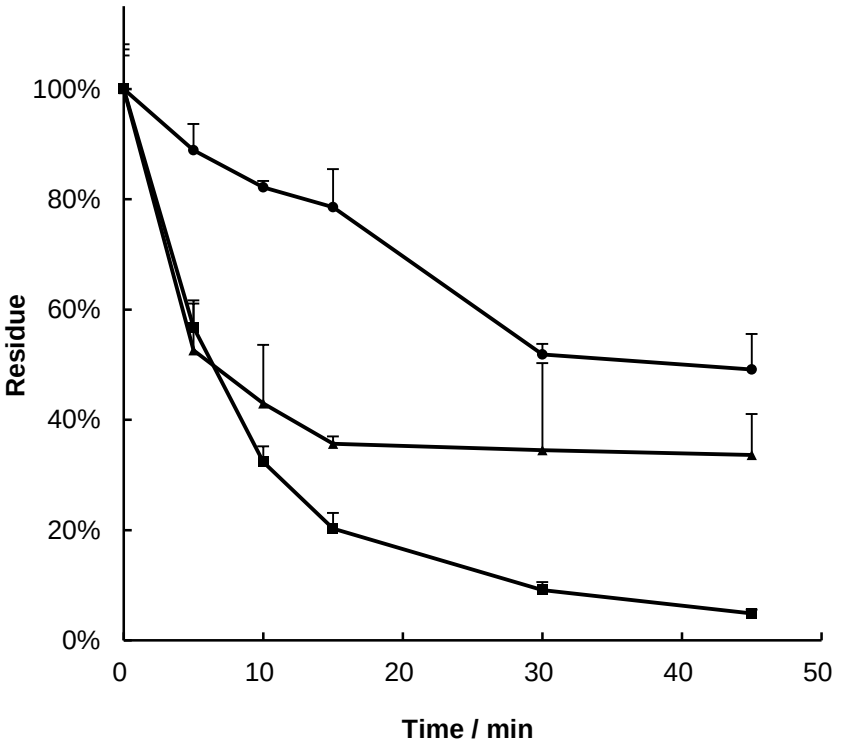

Figure 2.9 Metabolic stability studies of complex **7** in both MRLM (▲) and FRLM (•) versus a positive control, midazolam (■).

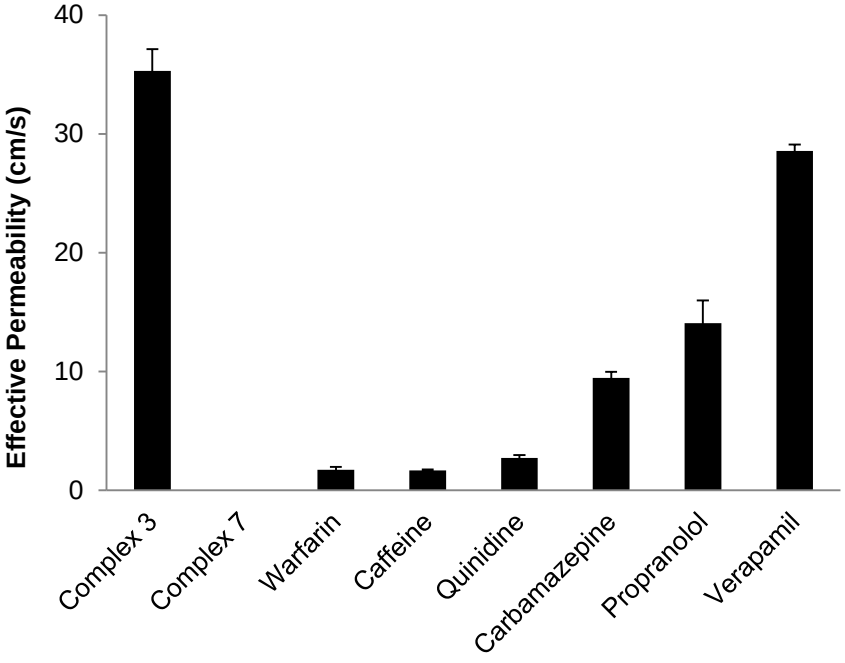

Figure 2.10 Permeability studies of complexes **3** and **7** using lecithin as the barrier, as compared against some established drugs after 6 hours of incubation.

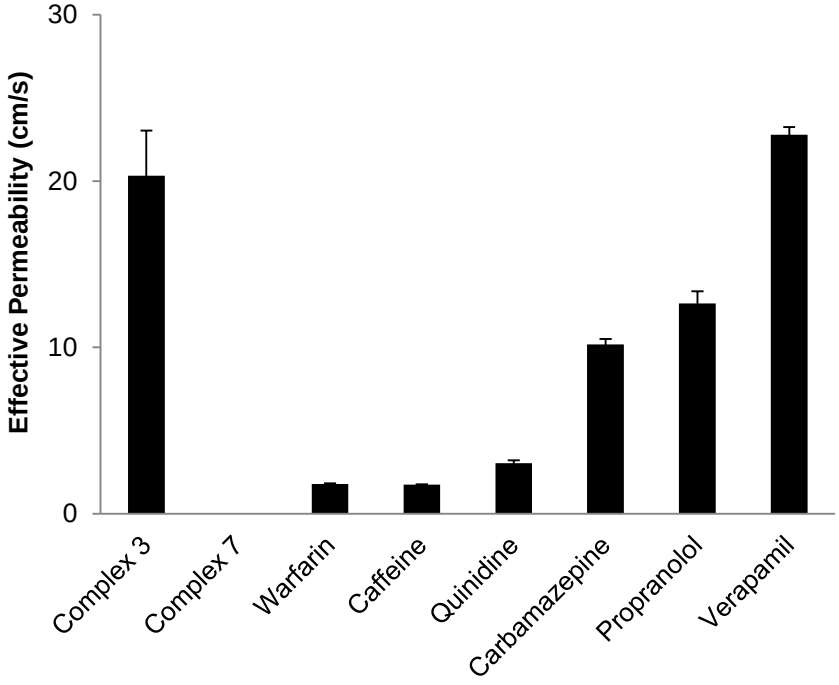

Figure 2.11 Permeability studies of complexes **3** and **7** using lecithin as the barrier, as compared against some established drugs after 16 hours of incubation.

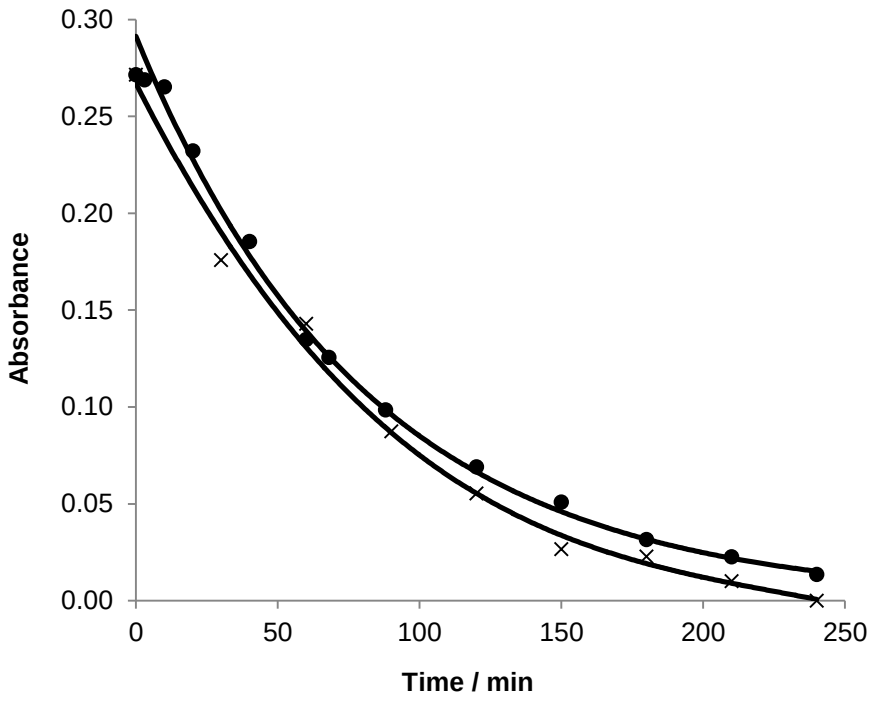

Figure 2.12 Decay of carbonyl stretching frequency of **3 (×)** and **7 (•)** upon reaction with 30% hydrogen peroxide.

The *in vitro* metabolic stability of **3** and **7** was studied by assessing the percentage loss of the complexes over time in the presence of pooled rat liver microsomes (MRLM) [192] (**Figure 2.8 and Figure 2.9**). An estimate of the *in vitro* degradation half-life ($t_{1/2}$) and intrinsic clearance (CL_{int}) can then be determined. Compare to midazolam, a compound which is rapidly metabolized, complex **3** is shown to be very slowly metabolized in rat liver microsomes and hence is regarded as metabolic-stable. However **7** is only moderately stable under the same conditions.

The effective permeability of these two complexes was determined by the parallel artificial membrane permeation assay (PAMPA) which is widely employed in the pharmaceutical industry to predict oral absorption potential of early drug candidates (**Figure 2.10 and Figure 2.11**) [193-195] The PAMPA assay indicates that **3** has good permeability across lecithin as a lipid barrier

after 16 hours of incubation. In fact the effective permeability of **3** is even higher than verapamil, a drug which already exhibits high permeability for the period of testing. In contrast, **7** does not show measurable permeability across lecithin.

Chemical reactivity studies carried out on **3** and **7** showed that they do not react with natural amino acids such as glycine (control), lysine (amine), tyrosine (phenol), histidine (imidazole), serine (aliphatic alcohol), methionine (sulfide) and cysteine (thiol) at 35^{o}C to 40^{o}C over a period of 12 hours. This conclusion was derived from the monitoring of the CO infrared stretching signals of **3** and **7** after the addition of the respective amino acids in DMSO. In particular, this inactivity towards cysteine suggests that these iron complexes operate via a different mode of action in cellular growth inhibition contrary to organic isothiocyanates which target cysteine residues on the Keap1 protein [72, 73, 196] Radical-mediated cell apoptosis pathways have also been considered, since the dimers **7** to **10** are well-known precursors to reactive mononuclear metal-centered radicals upon thermal or photochemical excitation [197]. The presence of such radicals in a cell environment could disrupt radical-dependent cell cycles. However the lack of cytotoxicity exhibited by **8**, **9** and **10** lends little support to a direct radical-mediated cell death. In addition, the role of **3** and **7** as CORMs is also unlikely. If CO release triggers cell death directly, all the tested metal carbonyls would have shown similar cytotoxicity effects.

The IC_{50} values listed in **Table 2.1** suggests that cell death is brought about by the presence of the $CpFe(CO)_2$ moiety. Studies [198-200] have shown that there is an abundance of highly-oxidizing reactive oxygen species (ROS) in

cancer cells, which promotes the Fenton reaction in which Fe^{2+} is oxidized to Fe^{3+}. The feasibility of this reaction was tested using hydrogen peroxide to represent an ROS. Indeed, the υ_{CO} IR absorbance of **3** and **7** showed a decrease against time, albeit at a much lower decomposition rate compare to $FeSO_4$, a typical iron salt used in the Fenton test (**Figure 2.11**). Upon completion of the reaction, a further chemical test with potassium thiocyanate turns the solution mixture red, indicating the presence of Fe^{3+}. Complexes **3** and **7** therefore are possible Fenton-type catalysts which might have disrupted ROS-mediated cell cycles leading to premature cancer cell death [201]. In contrast, the much lower ROS concentration present in normal cells may have mitigated the impact caused by the iron complexes.

2.3 Conclusion

In conclusion, we have shown that cyclopentadienyl iron carbonyl complexes are cytotoxic towards breast cancer cells but not normal cells with IC_{50} values of ranging from 3.0 μM to 17.3 μM. These complexes are structurally similar, each containing a $CpFe(CO)_2$ core with a differing functional group directly bonded to the iron center. With other metal carbonyls dimers, no significant cytotoxicity on the cancer cells was observed. As such, it is inferred that it is the $CpFe(CO)_2$ moiety that is largely responsible for the cytotoxic observations. The functional group on the iron does not appear to influence the cytotoxic properties of the complex as exemplified by the isothiocyanate complex **5**. These half-sandwich iron complexes are inexpensive, either commercially available or easily prepared. In particular, **3** is metabolic-stable and demonstrates good permeability across a lipid barrier and could be a potential candidate for future *in-vivo* studies. While the mechanism of action

remains to be elucidated, it is believed that the pathway to cellular death may be associated with Fenton-like reactions caused by the $[CpFe(CO)_2]^+$ species.

2.4 Experimental

2.4.1 Materials

Cyclopentadienyl iron dicarbonyl dimer $[CpFe(CO)_2]_2$, cyclopentadienyl dicarbonyl iodide $[CpFe(CO)_2I]$, cyclopentadienyl molybdenum tricarbonyl, $[CpMo(CO)_3]_2$, rhenium carbonyl $[Re_2(CO)_{10}]$, manganese carbonyl $[Mn_2(CO)_{10}]$, tetrachloromethane, dichloromethane, bromine, potassium thiocyanate, silver (I) tetrafluoroborate, ethanol, hexane and chloroform were purchased from Sigma-Aldrich. Penicillin-Streptomycin was obtained from GIBCO laboratories. Thiazolyl blue (MTT) was obtained from Promega. 10× Phosphate Buffered Saline (PBS) pH 7.4, Dulbecco's Modified Eagle's Medium (DMEM) Fetal Bovine Serum (FBS) were purchased from Thermo Fisher Scientific Inc. (Logan, UT, USA). Ultrapure water used was purified by a Milli-Q UV purification system (Sartorius Stedim Biotech SA, Aubagne Cedex, France). Annexin V/PI cell viability assay stains were purchased from Life Technologies. The HeLa, MDA-MB-231, MCF-7, MCF-10A cell lines were received with appreciation from Professor Paul Ho from the Department of Pharmacy, National University of Singapore and Professor Leong from School of Physical and Chemical Sciences, National Technological University. The TAMH and HL-1 cell line were cultured in Professor Brian Dymock laboratory. All chemicals were used without further purification.

2.4.2 Instrumentation and General Methods

All manipulations for chemical synthesis were carried out using standard Schlenk techniques under a nitrogen atmosphere. Photochemical experiments were conducted with a Legrand broadband lamp (350 – 800 nm, 11 W). All infrared spectra were obtained with Shimadzu IR Prestige - 21 Fourier – transformed infrared spectrometer (1000 – 4000 cm^{-1}, 1 cm^{-1} resolution, 16 scans co–added for spectra averaging) using a 0.05 mm path – length CaF_2 cell for liquid samples. Electrospray ionisation (ESI) was conducted using a Finnigan MAT LCQ spectrometer. ^{1}H and ^{13}C NMR spectra were recorded using Bruker AMX 300 Fourier Transform Spectrometer operating at 300 MHz for proton and 75 MHz for carbon nuclei at room temperature, using $CDCl_3$ as solvent unless otherwise stated. The chemical shifts were referenced to tetramethylsilane and are reported in ppm.

2.4.3 Solid State Structural Determination

Single crystal X-ray structural studies were performed on Bruker-AXS Smart Apex CCD Single-Crystal Diffractometers by CMMAC, National University of Singapore. Data were collected at 100(2) K using graphite-monochromated Mo K_α radiation (λ = 0.71073 Å). Data collection was evaluated using SMART CCD system and processed for Lorentz and polarisation effects using SAINT software and for absorption effects using SADABS software. Structural solution and refinement were then carried out using SHELXTL suite of programs. The structure was solved by direct methods. All H atoms were put at calculated positions using the riding model.

2.4.4 Syntheses of 1, $CpFe(CO)_2Cl$ and 2, $CpFe(CO)_2Br$

$CpFe(CO)_2Cl$, $CpFe(CO)_2Br$ and $CpFe(CO)_2^+BF_4^-$ were synthesized according to literature methods [187]. Briefly, 1 molar equivalent of $[CpFe(CO)_2]_2$ was dissolved in tetrachloromethane and refluxed until the bridging CO peak of the dimer starting reactant has completely disappear. The product was then passed through a silica column and the orange product eluted using 100% ethyl acetate. $CpFe(CO)_2Br$ was synthesized in a similar way except that the dimer was refluxed with bromine in hexane. Yield **1**: 90%, **2**: 88%. IR $CpFe(CO)_2Cl$ (chloroform, υ_{max}, cm^{-1}): 2012s, 2057s (C=O). IR $CpFe(CO)_2Br$ (ethyl acetate, υ_{max}, cm^{-1}): 1999s, 2045s (C=O).

2.4.5 Syntheses of 4, $CpFe(CO)_2SCN$ and 5, $CpFe(CO)_2NCS$

Both isomers, $CpFe(CO)_2NCS$ and $CpFe(CO)_2SCN$, were obtained via a modified method [186]. Briefly, 1 molar equivalent of $[CpFe(CO)_2]_2$ dimer was dissolved in absolute ethanol. 3 molar equivalents of potassium thiocyanate and 0.6 ml of tetrafluoroboric acid were added under ambient conditions with vigorous agitation. The solvent was then removed under reduced pressure after 1 hour and the two isomers separated via column chromatography using silica as stationary phase and dichloromethane as the mobile phase. IR absorption bands conform to the data published previously [202]. Crystals suitable for x-ray analysis were grown from hexane. Yield **4**: 54%, **5**: 33%. IR $CpFe(CO)_2NCS$ (dichloromethane, υ_{max}, cm^{-1}): 2023s, 2067s (C=O), 2118m (C=N). IR $CpFe(CO)_2SCN$ (dichloromethane, υ_{max}, cm^{-1}): 2008s, 2052s (C=O), 2116m (C=N).

2.4.6 Synthesis of 6, $CpFe(CO)_2^+BF_4^-$

The synthesis of **6** was accomplished via a modified literature method [187]. 1 molar equivalent of $CpFe(CO)_2I$ was dissolved in dichloromethane and 1.1 molar equivalents of silver tetrafluoroborate was added. The mixture was stirred for 2 hours under nitrogen at room temperature. An orange solution of the cation was obtained after the filtration of yellow silver iodide. IR $CpFe(CO)_2^+BF_4^-$ (dichloromethane, υ_{max}, cm^{-1}): 2001, 2046 (C=O).

2.4.7 Reactions of 3 and 7 with H_2O_2

4 mg of **3** (13 μmol) was dissolved in 2 ml of THF. 5 molar equivalents of aqueous hydrogen peroxide (30%) were then added swiftly and the mixture stirred vigorously under nitrogen. The changes in carbonyl absorption intensity of **3** at 2042 cm^{-1} were recorded at every 30 minutes interval until the signal becomes indistinguishable from background noise. The same procedure was carried out for the reaction between **7** (10 μM, ν_{CO} band at 1790 cm^{-1}) and hydrogen peroxide in the same solvent.

2.4.8 Cell Culture and Drug Treatment

The cells were maintained in Dulbecco's modified Eagle's medium (DMEM, Grand Island, NY, USA) supplemented with 10% fetal bovine serum (FBS), 1% l-glutamate (GIBCO Laboratories), and 1% penicillin/streptomycin (GIBCO Laboratories) at 37°C in 5% CO_2 atmosphere. Compounds **1** to **10** were dissolved in DMSO and serially diluted until the final concentration used for incubation were 0.01 μM, 0.1 μM, 1 μM, 5 μM, 10 μM, 20 μM, 40 μM, 100 μM and 200 μM. The treatment of the cells was performed by seeding the cells in DMEM growth medium at the same initial density. They were

incubated for 24 hours to allow adhesion and growth before treatment (80% confluence). The media was then removed and the cells washed once with PBS and then treated with the various concentrations of the compounds in DMEM only. Control cells were treated with 0.1% DMSO. All 4 cell lines were treated in the same manner. All final DMSO concentrations are at 0.1%.

2.4.9 Annexin V and PI Staining for Flow Cytometry

The percentage of cells actively undergoing apoptosis was determined using Annexin-V Alexa Fluor 488 based immunofluorescence, as described previously [203]. Briefly, cells were plated onto a 24-well dish and allowed to reach 80% confluence. The cells were then treated with a positive control, negative control and **5** μM and 10 μM of **3** and **7** separately. **Figure 2.13** shows the plate distribution of the drug and the various controls. After 24 hours, the cells were trypsinized, centrifuged at 150 RCF and double-stained with 2.5 μL of Annexin-V and 0.5 μL of propidium iodide (PI). An incubation time of 15 minutes were allowed after addition of the antibody and PI stain prior to flow analysis. The cells were then analyzed using BD LSRFortessa instrument running BD FACSDiva software. All experiments were performed in triplicates and two independent experiments were performed.

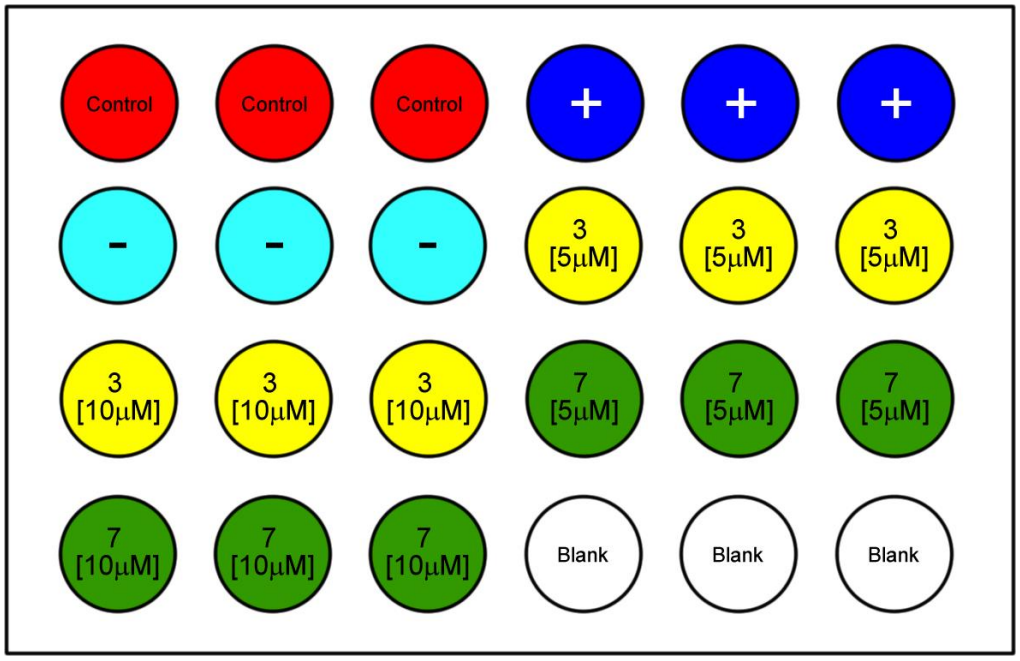

Figure 2.13 Distribution of blank (white), DMSO control (red), positive control of *cis*-platin (blue), negative control (cyan) and cells treated with **3** (yellow) and **7** (green) on a 24 well plate.

2.4.10 Confocal Microscopy

High resolution images were obtained using Olympus Fluoview FV300 confocal laser scanning microscope at 400× and 600×. Cells were seeded on coverslips at a density of 1×10^5 cells per well in DMEM growth medium supplemented with 10% FBS and 1% penicillin/streptomycin and allowed to reach 80% confluence over 24 h. They were then treated with 5 μM, 10 μM and 20 μM of **3** for 24 h. After treatment, the cells were washed with PBS, and stained with Annexin V and PI, then washed again with PBS and subsequently mounted onto a glass slide, examined and photographed. Apoptotic cells were defined based on the distribution of the Annexin V and PI stains. Early apoptotic cells were defined by Annexin V positive, PI negative (AV^+/PI^-). Necrotic and late apoptotic cells were defined by Annexin V and PI positive (AV^+/PI^+). Healthy cells were defined by Annexin V and PI negative (AV^-/PI^-).

2.4.11 MTT Proliferation Assay

The anti-proliferation activity of the $CpFe(CO)_2X$ complexes were determined using MTT assay. Approximately 10,000 cells per well were seeded in a 96-well plate and allowed to adhere for approximately 24 hours at 37°C. The cells were then treated with varying concentrations of the complexes in media for another 24 hours and then left to incubate in a 37°C incubator with 5% CO_2. The final concentration of DMSO in the medium was 0.1% (v/v). Following treatment, the media was removed and each well washed with 100 μL of PBS, followed by 100 μL of MTT, (0.5mg/mL) in media and incubated for an additional 2 hours. After the incubation period, the MTT was removed and 100 μL of DMSO was added to dissolve the formazan crystals. The absorbance intensities at 470 nm were then measured and cell viabilities relative to the control (DMSO) were calculated. The IC_{50} values, which is defined as the concentration necessary to inhibit the growth of 50% of the cell population were then determined using Graphpad Prism version 5.0 by fitting the values on a dose-response curve (Cell viability vs log drug concentration). The experiments were performed in triplicates for each concentration and three independent experiments were performed.

2.4.12 Light Microscopy

10,000 cells were each seeded onto a glass cover slips placed in a 6-well dish and allowed to reach 80% confluence in DMEM media. The cells were then treated with **20** μM and **40** μM of **3**. After 24 hours, the media was removed and the cells washed twice with PBS. The cover slips were then mounted onto glass slides and imaged under a light microscope.

2.4.13 Determination of the *In Vitro* Metabolic Stability of 3 and 7

Pooled male and female rat liver microsomes were obtained from BD Gentest Corp. (Woburn, MA, USA). Milli-Q water (Millipore Corp., Milford, MA, USA) was used throughout the experiment. All other chemicals and reagents were of analytical grade and solvents were of HPLC grade. An Agilent 1100 series high performance-liquid chromatography system with diode array detector (Agilent Technologies, Waldbronn, Germany) was employed for chemical analysis.

Chromatographic separation was performed on an Zorbax Eclipse Plus C18 column (2.1 × 100 mm, i.d., 3.5 μm, Agilent Technologies, Palo Alto, CA, USA) with a Security Guard Cartridge (3.0 × 4 mm, Agilent Technologies, Palo Alto, CA, USA) on isocratic elution using a mobile phase consisting of methanol–water (45:55, v/v) at a flow rate of 1.2 mL/min with UV detection at 262 nm. For sample analysis, a 20 μL sample injection was used. Phosphate buffer (100 mM, pH 7.4) containing 1 mM EDTA was prepared from 400 mM mono- and dibasic potassium phosphate stock solution. NADPH stock solutions (10 mM) in phosphate buffer were freshly prepared daily.

Liver microsomal incubations were conducted in triplicate. Incubation mixtures consisted of 7.5 μL of 20 mg/mL FRLM and MRLM (final: 0.3 mg microsome protein/mL), 2.5 μL of 600 μM of complexes **3** or **7** in acetonitrile (final: 3 μM), 440 μL of 0.1 M phosphate buffer (pH 7.4). The mixture was first shaken for 5 min for pre-incubation in a shaking water bath at 37°C. Reaction was initiated by adding 50 μL of 10 mM NADPH to obtain a final concentration of 1mM NADPH in the mixture. The total volume of the

reaction mixture was 500 µL. For metabolic stability studies, aliquots of 50 µL of the incubation sample mixture were collected at 0, 5, 10, 15, 30, and 45 min. After collection of samples, the reaction was terminated with 100 µL of chilled acetonitrile. The mixture was then centrifuged at 10,000 g to remove the protein and the supernatant was subsequently applied to LC analysis.

Positive control (PC) samples were prepared as described above, except the test compound was replaced with the known P450 substrate (Midazolam, 3 µM). The samples were assayed for the degradation of midazolam to evaluate the adequacy of the experimental conditions for drug metabolism study. Negative control samples were also prepared as described above but without NADPH.

In the determination of the *in vitro* half-life ($T_{1/2}$), the peak areas of drug were converted to parent remaining percentages using the t = 0 peak area values as 100%. The remaining percentages of the candidate were plotted against the microsomal incubation time. Data points were determined from the average of three measurements with standard deviations as the error bars. The *in vitro* $T_{1/2}$ (in units of min) was calculated from the slope of the linear regression (k) of the natural logarithm of the parent remaining percentage versus incubation time according to the following formulae.

Equations:

$T_{1/2} = 0.693/k$ (min)

V (µL/mg) = Volume of incubation / amount of microsomal protein in the incubation (µl/mg)

$CL_{int,\ in\ vitro}$ = V x 0.693 / $T_{1/2}$ (µL/min/mg protein)

$CL_{int,\ app}$ = CL_{int} (45 mg microsomal protein/g of liver) (45 g of liver*/kg body weight) *20 and 45 g of liver/kg of body weight were used for human and rat, respectively.

2.4.14 Determination of the Permeability of Complexes 3 and 7

The effective permeabilities (P_e) of **3** and **7** were determined by the parallel artificial membrane permeation assay (PAMPA) which is widely employed in the pharmaceutical industry to predict oral absorption potential of early drug candidates. Permeability was assessed at pH 7.4 over 2 different permeation time, 6h and 16h, at ambient temperature. Caffeine, quinidine, verapamil, carbamazepine, warfarin, (±)-propranolol hydrochloride, L-α-phosphatidylcholine (lecithin) (Lyophilized powder from egg yolk) and **t**he phosphate buffer saline (PBS) solution were also obtained from Sigma Aldrich.

12 mM stock solution for each of the complexes **3** and **7** was prepared in DMSO. Calibrators were made in 1× PBS solution and diluted to give solutions of 120 µM, 60 µM, 30 µM, 15 µM, 7.5 µM, 3.75 µM, 1.875 µM, and 0.9375 µM. 250 µL of each calibrator solution was transferred to HPLC PP vials and analysed by HPLC-UV (254 nm). 50mM stock solution of each of the standards (caffeine, carbamazepine, quinidine, verapamil, propranolol, warfarin) was prepared in DMSO and diluted with 1× PBS to give standard calibrator solutions of 500 µM, 250 µM, 125 µM, 62.5 µM, 31.25 µM and 15.62 µM. The concentration of DMSO in each solution was kept at 1% (v/v). 250 µL of each standard calibrator solution was transferred to separate wells

in a 96-well plate. The UV/Vis absorbance of each well was read at λ_{max} of the standard compound to give its calibration curve.

A 1% solution (w/v) of lecithin in dodecane was prepared and 5 µL of this 1% lecithin/dodecane solution was pipetted into the well of the donor plate. 12 mM stock solution of **3** was prepared in DMSO. 10 µL of the 12 mM stock solution was diluted with 990 µL of 1× PBS buffer to give a 120 µM solution. The final concentration of DMSO in the solution is 1% (v/v). 300 µL of this solution was added to the well in the donor plate (with lecithin). 300 µL of 1× PBS buffer (containing 1% v/v DMSO) was added into the corresponding well in the acceptor plate. The donor plate was placed on top of the acceptor plate. The underside of the membrane in the donor plate must be in contact with the buffer in the acceptor well. The donor/acceptor plate unit was covered, placed in an air-tight container and agitated in an incubator (250 rpm, 6 hours) at temperature of 30.0°C (± 2.5 °C). After this time, 250 µL per well of the donor and acceptor plates were transferred to separate HPLC PP vials. The concentration of analyte present in each sample were analyse by HPLC-UV (254 nm). The assay was repeated using a 2nd stock solution (12 mM) of **3**. The Effective Permeability P_e was calculated from the equation below [195].

$$P_e = -2.303 \times \frac{V_A V_D}{V_A + V_D \times A \times t} \times \log\{1 - \frac{V_A + V_D}{V_D \times S} \times \frac{C_{A(t)}}{C_{D(0)}}$$

$$S = \left[\frac{V_A}{V_D} \times \frac{C_{A(t)}}{C_{D(0)}}\right] + \frac{C_{D(t)}}{C_{D(0)}}$$

where:

(i) C_A = concentration of test compound in acceptor well after period of incubation (6 h or 16 h).

(ii) $C_{D\,(0)}$ = concentrations of test compound at time 0

(iii) $C_{D\,(t)}$ = concentrations of test compound in donor wells after period of incubation (6 h or 16 h).

(iv) V_A= volume of acceptor well (0.3 cm^3)

(v) V_D = volume of donor well (0.3 cm^3)

(vi) A = filter area

(vii) t = permeation time (21600 s or 57600 s)

(viii) S = fraction of the sample remaining in the donor and the acceptor wells after permeation time

2.4.15 Chemical Reactivity Studies

The reaction of **3** and **7** with various amino acid substrates were evaluated as follow. 10 mg of **3** was first dissolved in 50 mL of DMSO. The initial infrared spectrum was obtained. Following that, 1 mole equivalent of the various amino acids was added separately to the solution of **3** and the solution warmed and maintained using a water bath at a temperature of 40°C. The IR bands were then monitored over 12 hours and conclusions were inferred from the changes to the infrared absorptions bands. The same procedure was also applied to **7** to evaluate its chemical reactivity.

2.4.16 Water Solubility and Stability Experiment

0.100 mg portions of **3** and **7** was each separately added with stirring to 50 mL volume of deionized water until the first sign of excess solids were seen at the bottom of the cuvette. The experiment was then repeated three times to get an average value for the mass. The UV-vis absorbance was then subsequently

monitored until it reached a constant value for at least an hour to evaluate the stability of the complex in aqueous medium.

Chapter 3

Structural Modification Studies of ‘Hit’ Complexes

3.1 Introduction

In Chapter 2, we have identified $CpFe(CO)_2X$ carbonyl complexes as potential anti-cancer agents and found that they have indeed anti-proliferative properties with reasonably low IC_{50} values, so termed ‘hit’ complexes. In this chapter, modifications to the structure of the ‘hit’ complexes are performed to assess whether these ‘hit’ complexes identified in Chapter 2 can be made more potent.

One of the ‘hit’ complex of particular interest is $CpFe(CO)_2NCS$. This complex is interesting because the isothiocyanate functional group which it carries has been shown to be responsible for the chemo-protective effects

observed in organic isothiocyanates [69-74]. These organic isothiocyanates destroy cancer cells by strongly inducing the expression of phase II genes. These genes when switched on, code for enzymes that are responsible for the metabolism of xenobiotics and carcinogens and are termed phase II enzymes. A simplified schematic of the mechanism of phase II enzyme induction is shown in **Figure 3.1**. In this sense, organic isothiocyanates trigger cancer cell death via a different mechanism as compared to their organometallic counterpart, which induces apoptosis via a Fenton-type reaction. The question now is to establish whether the presence of a metal would have altered the mechanism of action in inducing cellular death. Hence a series of different organic isothiocyanates were synthesized for the purpose of the comparison with the metal-based analogues.

To further verify that the $CpFe(CO)_2$ moiety is essential for its anti-proliferative properties and also for comparison purposes, several other structural and chemical modifications were made to the $CpFe(CO)_2$ scaffold. With each newly modified complex, their cytotoxicity profile was investigated and compared against the 'hit' complexes identified in the previous chapter.

3.2 Results and Discussion

To compare the effect of the various organic isothiocyanates on the cancer cell lines, we started off by synthesizing a series of different isothiocyanates using a variety of literature methods. These experimental procedures and final synthesized compounds are outlined in **Scheme 3.1** to **Scheme 3.3**.

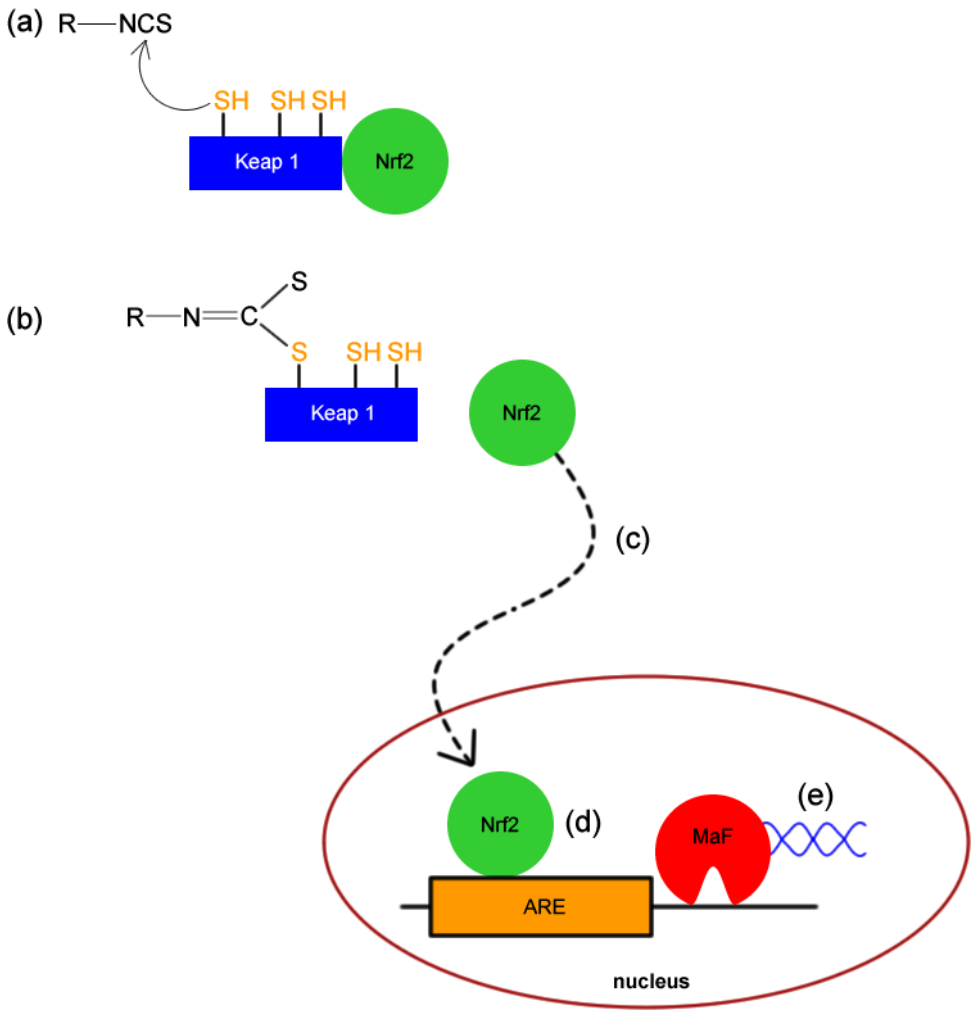

Figure 3.1 The phase II enzyme induction system. (a) An isothiocyanate acts as an inducer by covalently modifying cysteine residues on the KEAP1 protein. This causes (b) the signalling molecule Nrf2 to dissociate and (c) translocate into the nucleus. In the nucleus, it associates (d) with the antioxidant response element (ARE) to (e) initiate production of phase II enzymes.

3.2.1 Chemistry of Isothiocyanates

As illustrated in **Schemes 3.1** to **3.3**, there are several methods to synthesize isothiocyanates starting from different precursors. In **Scheme 3.1** a carboxylic acid is first converted to the acid chloride intermediate via a DMF catalysed halogenation reaction with oxalyl chloride. Subsequent reaction with solid potassium thiocyanate yields the final acyl isothiocyanate. This method also generates exclusively the isothiocyanate as supported by the infrared spectrum

data of the IR-active NCS functionality. Typically an isothiocyanate functional group produces a broader infrared absorption band and at lower frequency as compared to the thiocyanate functional group which appears as a sharp band (**Figure 3.2**). The broader infrared band commonly observed with the isothiocyanate functional group is due to the overlapping of the C=N stretch and the first overtone of the C=N stretch. This gives the appearance of a broad band which may also sometimes appear as a shoulder.

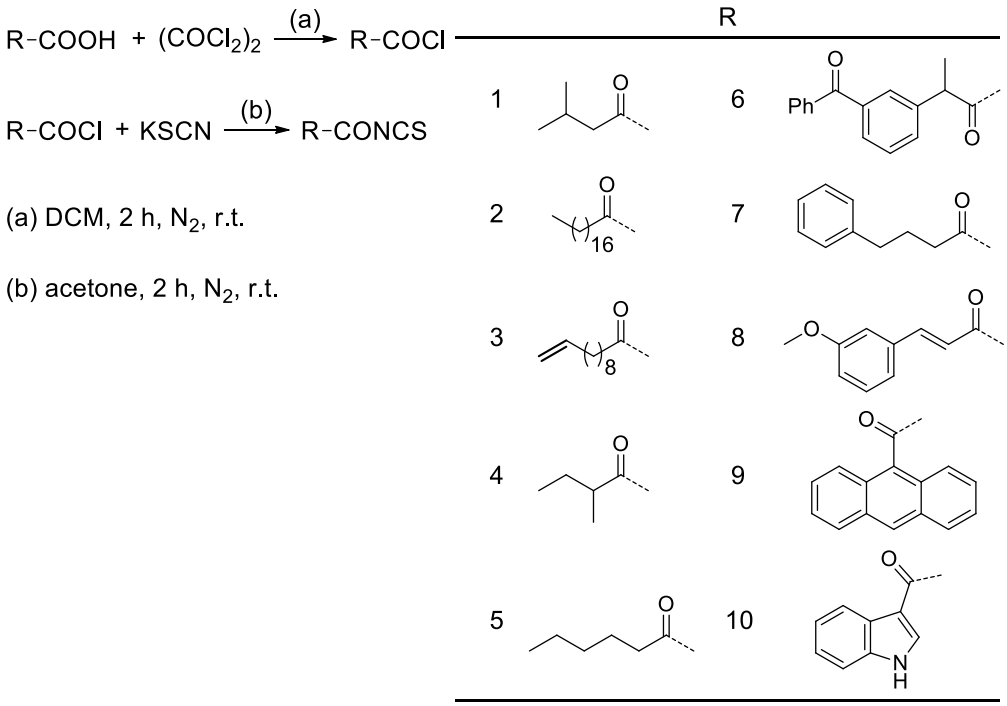

Scheme 3.1 Synthetic route for synthesising acyl isothiocyanates

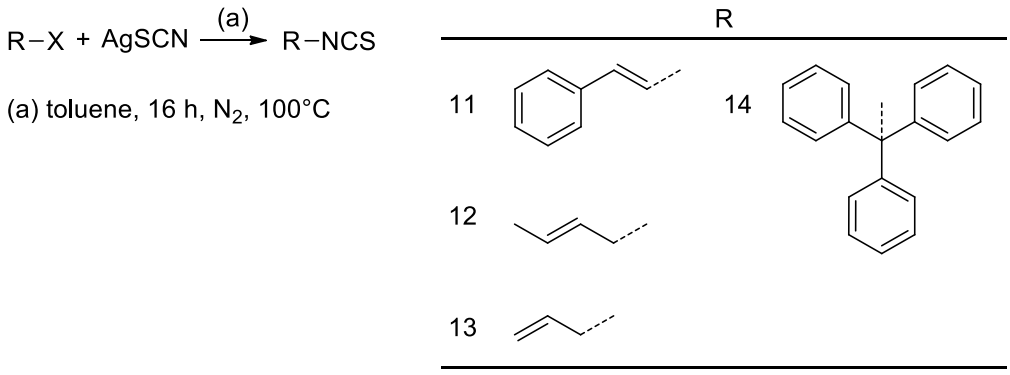

Scheme 3.2 Synthetic route for synthesising allylic isothiocyanates

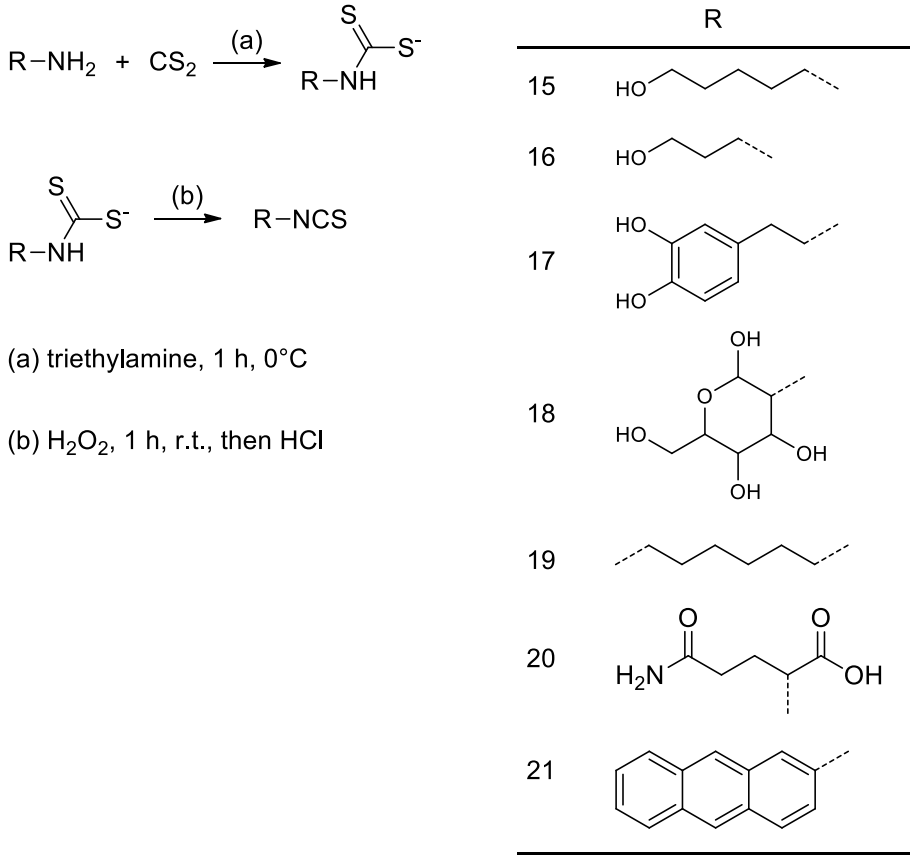

Scheme 3.3 Synthetic route for synthesising aliphatic isothiocyanates

The method employed in **Scheme 3.2** involves the nucleophilic displacement of an allylic or tertiary alkyl halide using silver thiocyanate in a non-polar solvent. This method yields exclusively the isothiocyanate isomer as the use of the AgSCN favours the attack from the nitrogen rather than the sulfur due to strong association of the soft silver with the sulfur atom. This exposes the nitrogen atom and allows an N-attack on the electrophile, leading to the formation of only the isothiocyanate isomer. To confirm this hypothesis, experiments were performed with potassium thiocyanate (KSCN) and it was observed that only the thiocyanate isomer was obtained exclusively as indicated by the infrared spectrum and comparison to literature value.

The third method of synthesising isothiocyanates (**Scheme 3.3**) employs a direct nucleophilic attack of a primary or secondary amine on the electrophilic carbon disulfide, CS_2, under low temperatures in the presence of an organic base such as triethylamine as a catalyst. Subsequent decomposition of the dithiocarbamate salt using hydrogen peroxide yields the isothiocyanate in good yields after purification through a silica column.

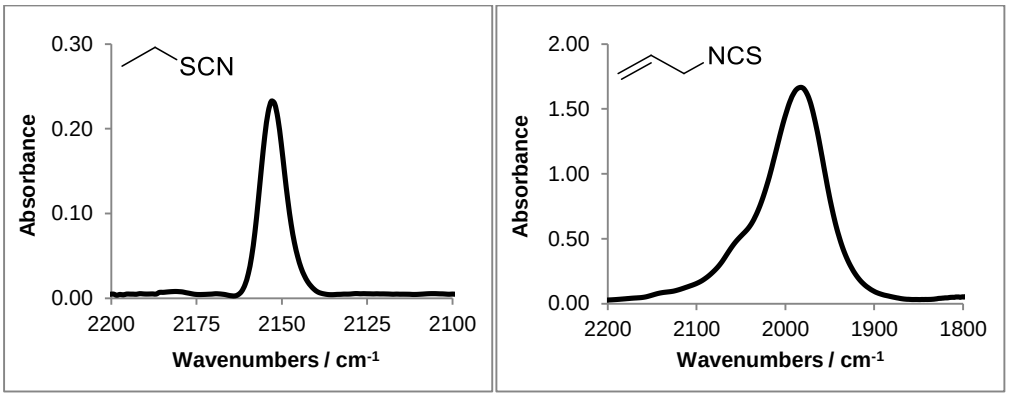

Figure 3.2 Comparison of the shape and infrared absorption frequency of the ethyl thiocyanate (left) and allyl isothiocyanate (right) functionality

The chemical structure of some of the isothiocyanates was confirmed via X-ray single crystal diffraction of the thiourea derivatives (**Figure 3.3**). The X-ray structure of the acyl isothiocyanate derivative has shown that the acid chloride intermediate undergoes an attack by the nitrogen of the NCS nucleophile and not the sulfur atom. The crystal structure of the sterically hindered triphenyl isothiocyanate also shows the presence of a C-N bonding and no C-S bonding was observed.

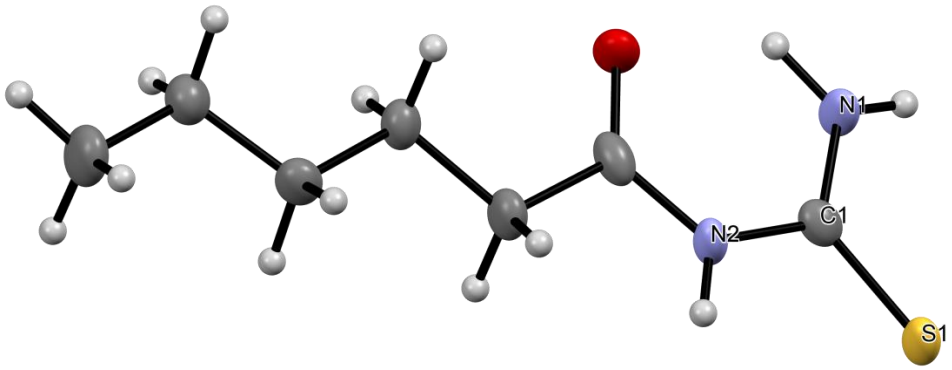

Figure 3.3 X-ray crystal structure of thiourea derivative of hexanoyl isothiocyanate with thermal ellipsoids at 50% probability

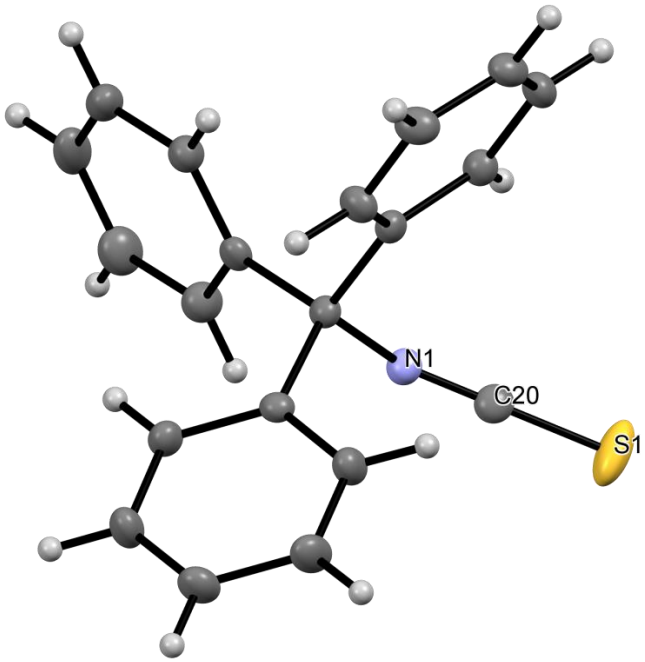

Figure 3.4 X-ray crystal structure of triphenyl isothiocyanate with thermal ellipsoids at 50% probability

3.2.2 Biological Studies of Organic Isothiocyanates

The *in vitro* anti-cancer activity of the 21 organic isothiocyanates was evaluated against the human ER– breast carcinoma (MDA-MB-231) and normal breast epithelial cell line (MCF-10A) using the MTT [3-[4,5-dimethylthiazol-2-yl]-2,5- diphenyltetrazolium bromide or thiazolyl blue] assay. The cell viabilities are normalized against that of DMSO which acts as

the control in the experiment. The MTT assay results of the 19 isothiocyanates are tabulated in **Figure 3.5**.

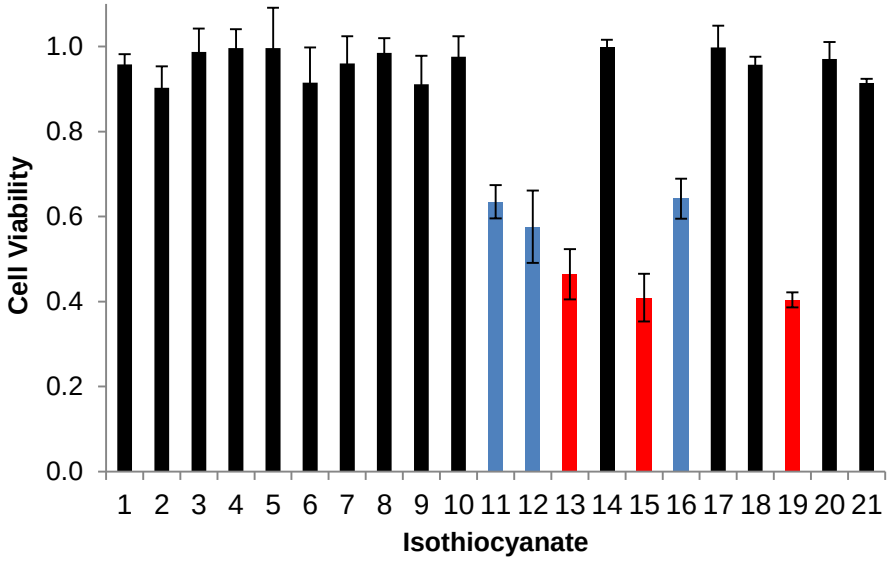

Figure 3.5 Effect of 40 μM of isothiocyanate 1-21 on cell viability for the MDA-MB-231 cell line as determined by the MTT assay. Six isothiocyanates have been identified to possess anti-proliferative properties towards the breast carcinoma and are sorted into two groups according to their efficacy - blue (moderate activity) and red (good activity). Values have been normalized to DMSO treated cells.

The MTT assay results in **Figure 3.5** suggest that the 10 acyl isothiocyanates were ineffective as phase II enzymes inducers since the breast carcinoma were still viable after 24 hours incubation. However, replacing the carbonyl moiety by a methylene group increased the potency against the cell line, as exemplified by compounds **11-13**, **15**, **16**, and **19**. The difference in potency can be attributed to the increased reactivity of the isothiocyanate as a result of the neighbouring electron withdrawing carbonyl moiety. The increased electrophilic character of the central carbon in the isothiocyanate (N=C=S) moiety would favour addition reaction with any nucleophilic amines or thiols present in the cytosol, effectively degrading the active isothiocyanate into a

thiocarbamate and rendering it inefficient at phase II enzyme induction. Hence, by moving this electron withdrawing group away, an increase in the potency of the isothiocyanate towards the carcinoma cells is to be expected. This observation is supported by prior studies [71, 73] that have concluded that a polar group such as sulfoxide or ketone group about four carbons away (regardless of orientation) would be ideal for the isothiocyanate to exhibit good potency towards cancer cells.

For isothiocyanates **14** and **21**, it is postulated that the steric bulk of the multiple phenyl substituents is hindering the interaction of the isothiocyanate functionality with the protein of interest, in this case the KEAP1 protein **(Figure 3.1**). This results in the isothiocyanate unable to induce the production of phase II enzymes, and hence little of no cell death was observed.

Isothiocyanates **17**, **18** and **20** share a common property. They all possess reasonably good water solubility since they are derived from dopamine, glucosamine and glutamine respectively. This increased solubility in aqueous media might have led to unwanted hydrolytic reactions that can render the isothiocyanate functional group inactive during the cell treatment, thereby explaining the lack of cytotoxicity towards the MDA-MB-231 cell line.

The six organic isothiocyanates with moderate to good (blue and red in **Figure 3.5**) anti-cancer activity identified from the MTT assay is then evaluated against the normal mammary cell line MCF-10A. The results from the MTT assay indicates that only the allyl isothiocyanates **11-13** (which are found naturally in broccolis) are relatively benign towards the normal breast cells. The remaining three compounds are deemed too toxic towards the normal

cells, killing more than half of the cell population at 40 μM concentration (**Figure 3.6**).

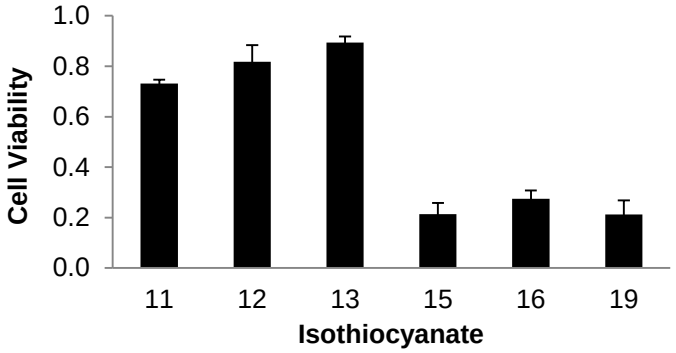

Figure 3.6 Effect of 40 μM of the six potential isothiocyanates on cell viability for the MCF-10A normal mammary cell line as determined by the MTT assay. Values have been normalized to DMSO.

Evidently, the organic isothiocyanates **15**, **16** and **19** do not appear to be good candidates as potential anti-cancer agents. In addition, compounds **11**-**13** have already been extensively studied by Professor Talalay's group and hence their effects on cancer and normal cells are already well-known and hence were used in the study as positive controls to allow for comparison of the potency of the newly synthesized isothiocyanates.

Comparing with the $CpFe(CO)_2X$ class of transition metal carbonyl complexes in Chapter 2, these organic isothiocyanates anti-cancer activity are certainly on par with their transition metal analogues. However, further studies with these organic isothiocyanates on normal mammary cell lines showed that they have considerable toxicity which is not a characteristic of an ideal drug (**Figure 3.7**).

The IC_{50} values against the normal mammary cells range is 18 μM for **15** and 21 μM for **16** which is even more toxic as compared to the natural

isothiocyanate sulforaphane (IC_{50} = 40 μM against MCF-12A [204]). Therefore, it can be concluded that even though these organic isothiocyanates are sufficiently potent against breast cancer cell line, they unfortunately are not as benign as the transition metal analogues.

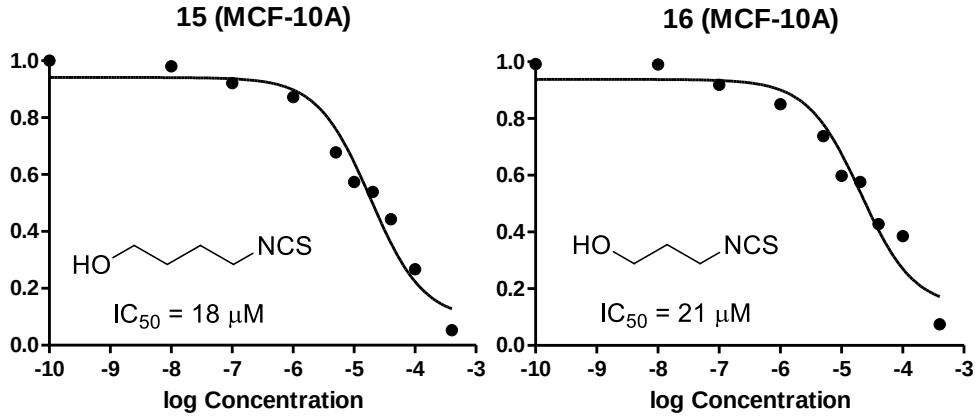

Figure 3.7 Dose response curve of isothiocyanate **15** and **16** on MCF-10A normal cell line

3.2.3 Structural Modifications to the $CpFe(CO)_2$ Moiety

To further validate the importance of the $CpFe(CO)_2$ moiety in imparting the transition metal carbonyl with anti-cancer properties, the structure of the $CpFe(CO)_2$ were modified in parts and the resulting complex evaluated again against the MDA-MB-231 cell line.

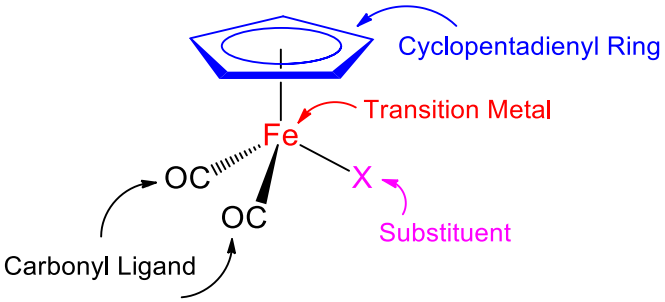

Figure 3.8 Possible chemical modifications made to the $CpFe(CO)_2$ moiety. Each part of the complex is modified one at a time to generate new complexes.

From **Figure 3.8**, it is possible to render four different types of chemical modifications to the $CpFe(CO)_2$ moiety to achieve a new set of transition metal complexes. In the case of substituent X, the effect of these changes have been discussed in Chapter 2 and hence would not be considered in this section. These chemical changes are outlined in the table below.

Table 3.1 Chemical modifications to $CpFe(CO)_2$ moiety

Type of Modification		Structure of Complex
Cyclopentadienyl → Allyl	**22**	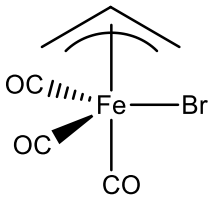
Iron → Manganese	**23**	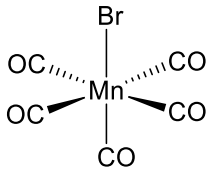
	24	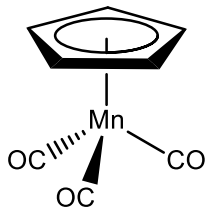
Iron → Cobalt	**25-31**	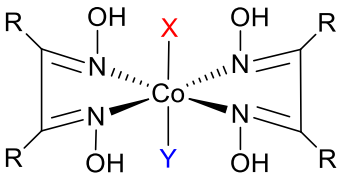
Carbonyl → Amine	**32**	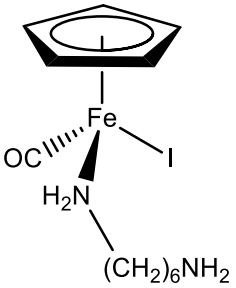

For complexes **25-31**, the various combinations of the axial ligands are tabulated below in **Table 3.2**.

Table 3.2 Axial ligands and R groups on cobalt based complexes.dmgH = dimethylglyoxime; dpgH = diphenylglyoxime.

Complex	X	Y	R
25	Cl	Cl	dmgH
26	CH_3COO	CH_3COO	dmgH
27	SCN	SCN	dmgH
28	Cl	Pyridine	dpgH
29	Cl	Aniline	dmgH
30	SCN	Pyridine	dpgH
31	SCN	Pyridine	dmgH

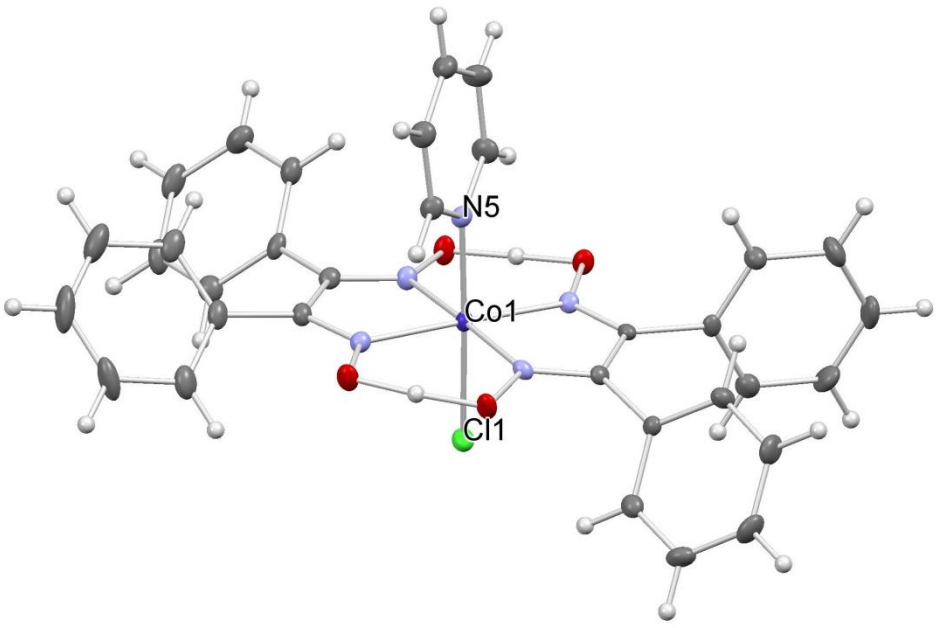

Figure 3.9 X-ray Crystal Structure of Co(dpgH)(pyridine)Cl, **28**, with thermal ellipsoids shown at 50% probability. dpgH = diphenylglyoxime.

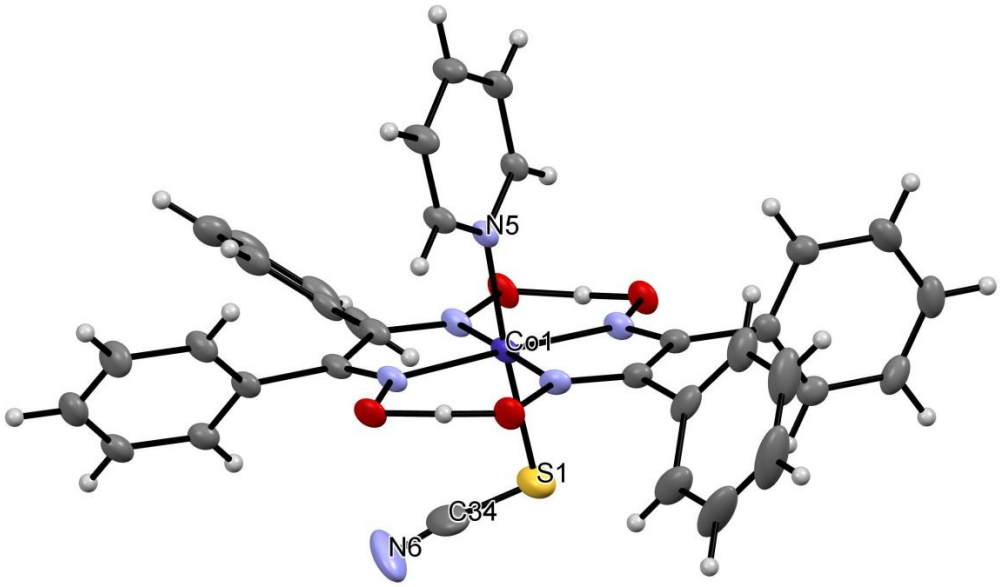

Figure 3.10 X-ray Crystal Structure of Co(dpgH)(pyridine)SCN, **30**, with thermal ellipsoids shown at 50% probability.

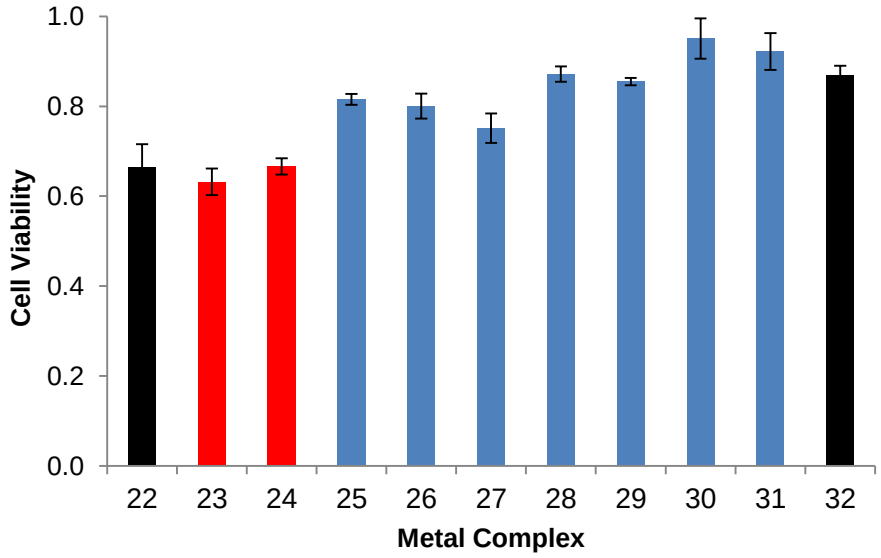

Figure 3.11 Cell viability study of the modified $CpFe(CO)_2$ transition metal complexes **22-27** on MDA-MB-231 cell line. The cells were treated with the 40 μM of complexes for 24 hours at 37°C and assayed using MTT. Red: Manganese complexes. Blue: Cobalt complexes. Black: Iron complexes

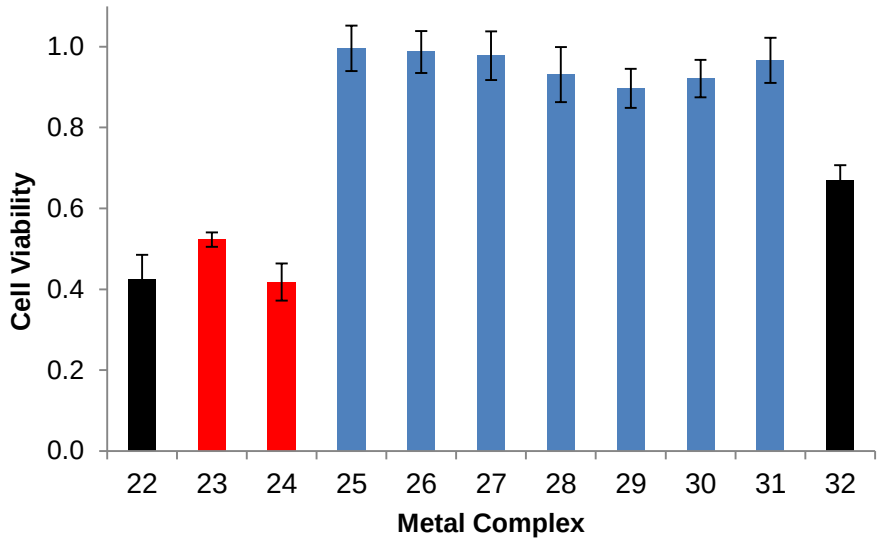

Figure 3.12 Cell viability study of modified $CpFe(CO)_2$ transition metal complexes **22-27** on MCF-10A cell line. The cells were treated with the 40 μM of complexes for 24 hours at 37°C and assayed using MTT. Red: Manganese complexes. Blue: Cobalt complexes. Black: Iron complexes

3.2.4 Biological Analysis of the New Complexes after Modification

The initial modifications were made and selected based on stability of the synthesized complex and the ease of synthesis. In addition, a few of the tested complexes were already commercially available and were used as the first step towards investigating the effect of changing the structure of the 'hit' compounds in Chapter 2 on the potency of the complex. Hence, if a transition metal complex performs poorly during cytotoxic evaluation, it would not be subjected to further biological analysis such as confocal microscopy and flow cytometry. The initial MTT data summarized in **Figure 3.11** and **3.12** allows the following conclusions to be derived:

1. As illustrated by complex **22**, replacing the cyclopentadienyl ring with an allyl ligand does not considerably improve the potency against the cancer cell line MDA-MB-231. Despite this, an increased cytotoxic effect was observed for the normal breast cells MCF-10A.

2. Changing the metal to manganese (**23** and **24**) also does not appear to grant additional cytotoxicity towards the cancer cells but instead increases the cytotoxicity towards the normal mammary cell line.
3. The cobalt based complexes **25-31** (which structurally resembles that of the vitamin B_{12} cobalamin) are not significantly cytotoxic towards cancer cells and also hardly kills the normal mammary cells at 40 μM concentrations regardless of which axial ligands were used. Furthermore, a change of the planar dimethylglyoxime bidendate ligand to the sterically bulky diphenylglyoxime did not confer additional chemical toxicity towards both the normal and cancer cell lines.
4. At first glance, **32** looks structurally similar to that of the 'hit' compound $CpFe(CO)_2I$ minus one carbonyl ligand. This modification however, reduces the toxicity of the complex based on the MTT assay data (a rise in cell viability from 56% to 90%) even though it left the normal cell line unscathed. This difference is hypothesized to be attributed to the long amine chain which might interfere with the Fenton redox reactions by sterically preventing incoming radicals from interacting with the iron centre.

3.3 Conclusion

To sum up, structurally altering the $CpFe(CO)_2$ have led to unpredictable changes to the cytotoxicity of the resulting complexes. Clearly without elucidating the mechanism of action of the 'hit' complexes in Chapter 2, it is difficult to make an informed decision on what type of chemical modification is required for an increase in potency towards the cancer cells and at the same

time maintain or even reduce the cytotoxic nature on the normal cell lines. Nonetheless, what is clear is that we do have several complexes such as the manganese based complexes **23** and **24** that appear to be promising (killing off nearly a third of the cancer cells) and could potentially be further researched and modified upon.

3.4 Experimental

3.4.1 Materials

Cyclopentadienyl manganese tricarbonyl, manganese pentacarbonyl bromide, cobalt (II) acetate, cobalt (II) chloride, 1,6-diaminohexane, potassium thiocyanate, silver thiocyanate, triphenyl methanol, 5-amino-1-pentanol, 4-amino-1-butanol 1-aminoanthracene, 8-hydroxyquinoline, pyridine, histidine, allyl bromide, cinnamyl bromide, crotyl bromide, isovaleric acid, undecanoic acid, 4-phenylbutyric acid, 6-phenylhexanoic acid, 2-methylbutyric acid, ketoprofen, 9-anthracenecarboxylic acid, indole acetic acid, 3-pyridinecarbaldehyde, triethylamine, toluene, methanol, ethanol, hexane and chloroform were purchased from Sigma-Aldrich. glucosamine hydrochloride, glutamine hydrochloride, dopamine hydrochloride, carbon disulfide, hydrogen peroxide, sodium hydroxide and 3-methoxycinnamic acid were purchased from Alfa Aesar. DMSO-d_6, acetone-d_6, methanol-d_4, D_2O, $CDCl_3$ was purchased from Cambridge Isotopes. Penicillin-Streptomycin was obtained from GIBCO laboratories. Thiazolyl blue (MTT) was obtained from Promega. 10× Phosphate Buffered Saline (PBS) pH 7.4, Dulbecco's Modified Eagle's Medium (DMEM) Fetal Bovine Serum (FBS) were purchased from Thermo Fisher Scientific Inc. (Logan, UT, USA). Ultrapure water used was purified by

a Milli-Q UV purification system (Sartorius Stedim Biotech SA, Aubagne Cedex, France). Annexin V/PI cell viability assay stains were purchased from Life Technologies. The MDA-MB-231 and MCF-10A cell lines were received with appreciation from Professor Paul Ho from the Department of Pharmacy, National University of Singapore and Professor Leong from School of Physical and Chemical Sciences, National Technological University. All chemicals were used without further purification.

3.4.2 Solid State Structural Determination

Single crystal X-ray structural studies were performed on Bruker-AXS Smart Apex CCD Single-Crystal Diffractometers by CMMAC, National University of Singapore. Data were collected at 100(2) K using graphite-monochromated Mo K_α radiation (λ = 0.71073 Å). Data collection was evaluated using SMART CCD system and processed for Lorentz and polarisation effects using SAINT software and for absorption effects using SADABS software. Structural solution and refinement were then carried out using SHELXTL suite of programs. The structure was solved by direct methods. All H atoms were put at calculated positions using the riding model.

3.4.3 Instrumentation and General Methods

All manipulations for chemical synthesis were carried out using standard Schlenk techniques under a nitrogen atmosphere. Photochemical experiments were conducted with a Legrand broadband lamp (350 – 800 nm, 11 W). All infrared spectra were obtained with Shimadzu IR Prestige - 21 Fourier – transformed infrared spectrometer (1000 – 4000 cm^{-1}, 1 cm^{-1} resolution, 16 scans co–added for spectra averaging) using a 0.05 mm path – length CaF_2 cell for liquid samples. Electrospray ionisation (ESI) was conducted using a

Finnigan MAT LCQ spectrometer. ^{1}H and ^{13}C NMR spectra were recorded using Bruker AMX 300 Fourier Transform Spectrometer operating at 300 MHz for both proton and carbon nuclei at room temperature, using $CDCl_3$ as solvent unless otherwise stated. The chemical shifts were referenced to tetramethylsilane and are reported in ppm.

3.4.4 Cell Culture and Drug Treatment

Both MDA-MB-231 and MCF-10A cell lines were maintained in Dulbecco's modified Eagle's medium (DMEM, Grand Island, NY, USA) supplemented with 10% fetal bovine serum (FBS), 1% l-glutamate (GIBCO Laboratories), and 1% penicillin/streptomycin (GIBCO Laboratories) at 37°C in 5% CO_2 atmosphere. Compounds **1**-**32** were dissolved in DMSO and diluted until the final concentration used for incubation were 40 μM. The treatment of the cells was performed by seeding the cells in DMEM growth medium at the same initial density. They were incubated for 24 hours to allow adhesion and growth before treatment (80% confluence). The cells were washed once with PBS and then treated with 40 μM of the compounds **1**-**32** in DMEM. Control cells were treated with 0.1% DMSO. All cell lines were treated in the same manner. All final DMSO concentrations are at 0.1%.

3.4.5 MTT Proliferation Assay

The anti-proliferation activity of the various organic isothiocyanates and metal complexes were determined using MTT assay. Approximately 10,000 cells per well were seeded in a 96-well plate and allowed to adhere for approximately 24 hours at 37°C. The cells were then treated with 40 μM of the compounds in media for another 24 hours and then left to incubate in a 37°C incubator with 5%

CO_2. The final concentration of DMSO in the medium was 0.1% (v/v). Following treatment, the media was removed and each well washed with 100 μL of PBS, followed by 100 μL of MTT, (0.5mg/mL) in media and incubated for an additional 2 hours. After the incubation period, the MTT was removed and 100 μL of DMSO was added to dissolve the formazan crystals. The absorbance intensities at 470 nm were then measured and cell viabilities relative to the control (DMSO) were calculated. The experiments were performed in triplicates for each concentration and three independent experiments were performed.

3.4.6 Synthesis of Acyl Isothiocyanates 1-10

1 mole equivalent of both the carboxylic acid and oxalyl chloride was dissolved in dichloromethane and the solution stirred under an atmosphere of nitrogen at room temperature. 2 drops of DMF as a catalyst was added after the addition of both the reactants. Upon addition of the catalytic DMF, brisk effervescence was observed and the reaction mixture turned yellow. The reaction was monitored by TLC and is typically completed within two hours or when evolution of the gaseous by-products has ceased. The product is then used immediately in the next step.

Potassium thiocyanate (1 mole equivalent based on the carboxylic acid) was dissolved in 5 mL of acetone. This was then added dropwise to the freshly prepared acid chloride in the previous step. The mixture was then warmed gently for 2 hours during which a white precipitate of potassium chloride is observed. The salt was then was filtered after the reaction is completed and the filtrate was extracted with diethyl ether, and the solvent removed via rotary

evaporation followed by drying in a high vacuum. The acyl isothiocyanates were then analysed via infrared spectroscopy (for the presence of the NCS functional group) and ^{1}H NMR.

1: The product was obtained as a light yellow liquid after vacuum drying. ^{1}H NMR ($CDCl_3$, ppm): 2.35-2.46 (m, 1H, ^{3}J = 6 Hz), 1.64-1.79 (m, 1H, ^{3}J = 6 Hz), 1.38-1.57 (m, 1H, ^{3}J = 6 Hz), 1.18 (d, 3H, ^{3}J = 6 Hz), 0.95 (t, 3H, ^{3}J = 6 Hz). IR (acetone, υ_{max}, cm^{-1}): 1977 (SC=N).

2: The product was obtained as a light yellow liquid after vacuum drying. Yield: 76%. ^{1}H NMR ($CDCl_3$, ppm): 5.83-5.96 (m, 1H), 5.09-5.17 (m, 2H), 2.27-2.32 (m, 2H), 2.07-2.09 (m, 2H), 1.02-1.39 (m, 12H). IR (hexane, υ_{max}, cm^{-1}): 1972 (SC=N), 1741 (C=O).

3: The product was obtained as an oily liquid. Yield: 70%. ^{1}H NMR ($CDCl_3$, ppm): 5.83-5.96 (m, 1H, ^{3}J = 6 Hz), 5.09-5.17 (t, 2H, ^{3}J = 15 Hz), 2.29 (t, 2H ^{3}J = 7.5 Hz), 2.09 (t, 2H, ^{3}J = 6 Hz), 1.02-1.39 (m, 12H). IR (acetone, υ_{max}, cm^{-1}): 1981 (SC=N),

4: The product was obtained as a light yellow liquid after vacuum drying. Yield: 54%. ^{1}H NMR (benzene-d_6, ppm): 2.07 (t, 2H, ^{3}J = 7.5 Hz), 1.15-1.49 (m, 29H), 0.91 (t, 3H, ^{3}J = 6Hz). (IR (hexane, υ_{max}, cm^{-1}): 1979 (SC=N). 1740 (C=O).

5: The product was obtained as a light yellow liquid after vacuum drying. Yield: 60%. ^{1}H NMR (CD_2Cl_2, ppm): 2.86-2.90 (t, 2H), 1.68-1.71 (m, 2H), 1.28-1.33 (m, 2H), 0.86-0.91 (m, 3H). (IR (acetone, υ_{max}, cm^{-1}): 1984 (SC=N).

6: The product was obtained as deep yellow oil after rotary evaporation. Yield: 52%. ^{1}H NMR ($CDCl_3$, ppm): 7.53-7.81 (m, 9H), 4.02-4.09 (q, 1H), 2.51-2.53 (d, 3H). IR (acetone, υ_{max}, cm^{-1}): 1970 (SC=N).

7: The product was obtained as a light yellow liquid after vacuum drying. Yield: 66%. ^{1}H NMR ($CDCl_3$, ppm): 7.17-7.32 (m, 5H, ^{3}J = 7.5 Hz), 2.68 (t, 2H, ^{3}J = 9 Hz), 2.38 (t, 2H, ^{3}J = 7.5 Hz), 1.97 (m, 2H, ^{3}J = 7.5 Hz). IR (ethyl acetate, υ_{max}, cm^{-1}): 1977 (SC=N).

8: The product was obtained as a light yellow liquid after vacuum drying. Yield: 86%. ^{1}H NMR ($CDCl_3$, ppm): 7.73-7.79 (d, 1H, ^{3}J = 18 Hz), 7.32 (t, 1H, ^{3}J = 7.5 Hz), 7.15 (d, 1H, ^{3}J = 6 Hz), 7.07 (t, 1H, ^{3}J = 6 Hz), 6.98 (dd, 1H, ^{3}J = 6 Hz), 6.42-6.47 (d, 1H, ^{3}J = 15 Hz), 3.85 (s, 3H). IR (acetone, υ_{max}, cm^{-1}): 1967 (C=N).

9: The product was obtained as a light yellow viscous liquid after vacuum drying. Yield: 67%. IR (acetone, υ_{max}, cm^{-1}): 1976 (SC=N).

10: The product was obtained as a light yellow liquid after vacuum drying. Yield: 62%. ^{1}H NMR (CD_3CN, ppm): 6.92-.6.94 (d, 1H), 6.77-6.8-0 (d, 1H), 6.66 (d, 1H), 6.39-6.53 (dt, 2H), 3.07 (s, 2H). IR (acetone, υ_{max}, cm^{-1}): 1977 (SC=N).

3.4.7 Synthesis of Isothiocyanates 11-14

1 equivalent of the organic allylic or alkyl halide is dissolved in toluene and 2 equivalents of silver thiocyanate were added as a suspension in toluene. The reaction mixture was refluxed at 100°C under a nitrogen atmosphere for 16

hours to yield exclusively the isothiocyanate isomer as confirmed via infrared spectroscopy. The thiocyanate linkage isomer was not obtained.

11: The compound was obtained as a yellow viscous liquid and is sufficiently pure as ascertained from TLC and NMR without the need for purification. Yield: 92%. ^{1}H NMR (toluene-d_8, ppm): 7.34-7.37 (m, 5H), 6.64-6.73 (m, 1H), 6.14-6.35 (m, 1H), 4.30-4.32 (m, 1H), 3.76-3.78 (m, 1H). IR (toluene, υ_{max}, cm^{-1}): 2086 br (SC=N).

12: The compound was obtained as a yellow viscous liquid and is sufficiently pure as ascertained from TLC and NMR without the need for purification. Yield: 88%. ^{1}H NMR ($CDCl_3$, ppm): 5.83-5.94 (m, 2H), 5.31-5.39 (m, 1H), 3.52-3.55 (d, 3H, ^{3}J = 9 Hz). IR (toluene, υ_{max}, cm^{-1}): 2058, 2093 (SC=N).

13: The compound was obtained as a yellow viscous liquid and is sufficiently pure as ascertained from TLC and NMR without the need for purification. Yield: 75%. ^{1}H NMR (toluene-d_8, ppm): 5.04-5.15 (m, 1H), 4.74-4.95 (m, 2H), 3.05-3.08 (dt, 2H). IR (toluene, υ_{max}, cm^{-1}): 2097, 2164 (SC=N).

14: The compound was obtained as colourless crystals upon recrystallization from acetone. Yield: 93%. IR (acetone, υ_{max}, cm^{-1}): 2059, 2125, 2551 (SC=N).

3.4.8 Synthesis of Isothiocyanates 15-21

1 equivalent of amine in THF was mixed with 5 equivalents of triethylamine and cooled in an ice bath. Five equivalent of carbon disulfide was added dropwise into the mixture with stirring. The reaction flask was removed from the ice bath after addition of the carbon disulfide is completed and allowed to stir for 1 hour at room temperature. Decomposition of the resulting

thiocarbamate salt was then effected via the addition of two equivalent of hydrogen peroxide. The resulting mixture was then stirred for another 30 minutes before adding concentrated hydrochloric acid to remove the excess trimethylamine. The isothiocyanate was then extracted twice using ethyl acetate after which the solvent was removed under vacuum and the resulting solution extracted with ethyl acetate. The crude product was then purified via column chromatography using 1:1 ethyl acetate-hexane as eluent.

15: The compound was obtained as a light yellow liquid and is sufficiently pure as ascertained from TLC and NMR without the need for purification. Yield: 64%. ^{1}H NMR ($CDCl_3$, ppm): 3.66 (t, 2H, ^{3}J = 7.5 Hz), 3.53 (t, 2H, ^{3}J = 7.5 Hz), 1.46-1.75 (m, 6H, ^{3}J = 6 Hz). IR (ethyl acetate, υ_{max}, cm^{-1}): 2106, 2186 (SC=N)

16: The compound was obtained as a light yellow viscous liquid and is sufficiently pure as ascertained from TLC and NMR without the need for purification. Yield: 71%. ^{1}H NMR ($CDCl_3$, ppm): 3.48 (t, 2H, ^{3}J = 6 Hz), 2.65 (t, 2H, ^{3}J = 7.5 Hz), 1.46 (m, 2H, ^{3}J = 7.5 Hz) IR (ethyl acetate, υ_{max}, cm^{-1}): 2107, 2184 (SC=N).

17: The compound was obtained as a colourless liquid and is sufficiently pure as ascertained from TLC and NMR without the need for purification. Yield: 66%. ^{1}H NMR (CD_3OD, ppm): 6.72-6.79 (dd, 2H, ^{3}J = 9 Hz), 6.60-6.63 (dd, 1H, ^{3}J = 6 Hz) 3.14 (t, 2H, ^{3}J = 6 Hz), 2.83 (t, 2H, ^{3}J = 6 Hz). IR (ethanol, υ_{max}, cm^{-1}): 2100, 2183 (SC=N).

18: The compound was obtained as a colourless viscous liquid and is sufficiently pure as ascertained from TLC and NMR without the need for

purification. Yield: 56%. ^{1}H NMR (D_2O, ppm): 5.44-5.45 (d 1H, ^{3}J = 3 Hz), 3.79-3.93 (m, 4H), 3.48 (t, 1H, ^{3}J = 9 Hz), 3.27-3.32 (dd, 1H, ^{3}J = 10.5 Hz). IR (THF, ν_{max}, cm^{-1}): 2159, 2171 (SC=N).

19: The compound was obtained as a light yellow viscous liquid and is sufficiently pure as ascertained from TLC and NMR without the need for purification. Yield: 64%. ^{1}H NMR ($CDCl_3$, ppm): 2.67 (t, 4H, ^{3}J = 7.5 Hz), 1.29-1.45 (m, 8H, ^{3}J = 6 Hz). IR (ethyl acetate, υ_{max}, cm^{-1}): 2105, 2177 (SC=N).

20: The compound was obtained as a pale yellow liquid and is sufficiently pure as ascertained from TLC and NMR without the need for purification. Yield: 52%. ^{1}H NMR (D_2O, ppm): 3.86 (t, 1H, ^{3}J = 6 Hz), 2.52-2.57 (dt, 2H, ^{3}J = 7.5 Hz), 2.19-2.26 (q, 2H, ^{3}J = 7.5 Hz). IR (THF, υ_{max}, cm^{-1}): 2156, 2167 (SC=N).

21: The compound was obtained as yellow oil and is sufficiently pure as ascertained from TLC and NMR without the need for purification. Yield: 76%. IR (ethyl acetate, υ_{max}, cm^{-1}): 2093, 2121 (SC=N).

3.4.9 Synthesis of 22, η^3-$C_3H_5Fe(CO)_3Br$

Three molar equivalents of allyl bromide were mixed with 1 molar equivalent of iron carbonyl in hexane. The hexane solution was then refluxed under nitrogen and the reaction monitored via infrared spectroscopy until the starting material carbonyl absorption bands completely disappeared. The reaction mixture was then purified via column chromatography using 1:1 hexane:ethyl acetate as eluent. The yellow brown fraction was collected and dried under a

vacuum in a desiccator. Yield: 58%. IR (hexane, υ_{max}, cm^{-1}): 2016, 2047, 2090 (C=O).

3.4.10 Synthesis of 25, $Co(dmgH)_2Cl_2$

2.2 mole equivalent of dimethylglyoxime was added to a stirred solution of 1 mole equivalent cobalt (II) chloride hydrate in 10 mL of acetone. A gentle stream of air was passed into the solution from which a green solid was slowly deposited. The reaction was then allowed to continue to stir over 1 hour. Subsequently, the reaction mixture was chilled on ice, filtered, and washed with 2 x 10 mL of cold acetone. The green crystalline product was then collected and dried under vacuum in a desiccator. Yield: 70%.

3.4.11 Synthesis of 26, $Co(dmgH)_2(CH_3COO)_2$

2.2 mole equivalent of dimethylglyoxime was added to a stirred solution of 1 mole equivalent cobalt (II) acetate hydrate in 10 mL of acetone. A gentle stream of air was then passed into the solution from which a green solid was slowly deposited. The reaction was then allowed to continue to stir over 1 hour. Subsequently, the reaction mixture was chilled on ice, filtered, and washed with 2 × 10 mL of cold acetone. The green crystalline product was then collected and dried under vacuum in a desiccator. Yield: 80%.

3.4.12 Synthesis of 27, $Co(dmgH)_2(SCN)_2$

1 mole equivalent of potassium thiocyanate was dissolved in acetone and 1 mole equivalent of cobalt chloride was added. The blue solution was stirred at room temperature for 2 h, and filtered to remove the white potassium chloride precipitate. The filtrate was then removed via rotary evaporation to obtain the

product, $Co(NCS)_2$. Yield: 65%. IR (dimethylformamide, υ_{max}, cm^{-1}): 2075 (SC=N).

1 mole equivalent of the cobalt (II) thiocyanate salt from the previous step was dissolved in 10 mL of acetone and then added to 2.2 mole equivalent of dimethylglyoxime. The reaction mixture was stirred at room temperature for 3.5 hours in the presence of air. A brown solid slowly deposited and is collected via suction filtration at the end of the 3.5 hours. The solid was washed with 2 × 10 mL cold acetone and dried under vacuum in a desiccator. Yield: 67%.IR (dimethylformamide, υ_{max}, cm^{-1}): 2109 (SC=N).

3.4.13 Synthesis of 28, $Co(dpgH)_2$(pyridine)Cl

2.2 mole equivalent of diphenylglyoxime was added to a stirred solution of 1 mole equivalent cobalt (II) chloride hydrate in 10 mL of acetone. A gentle stream of air was passed into the solution from which a green solid was slowly deposited. The reaction was then allowed to continue to stir over 1 hour. Subsequently, the reaction mixture was chilled on ice, filtered, and washed with 2 x 10 mL of cold acetone. The green crystalline product was then collected and dried under vacuum in a desiccator. Yield: 70%.

1 mole equivalent of the above $Co(dpgH)_2Cl_2$ is suspended in 10 mL of methanol. 2.2 mole equivalents of pyridine were then added with stirring. The agitation was continued until the green solid disappears and is replaced by a brown crystalline solid over about 20 to 30 minutes. 20 mL of deionised water was then added with stirring and the brown suspension was then cooled in ice for about 10 minutes. The product was then collected by suction filtration and

wash with 3 × 10 mL of 2:1 water/methanol and 2 × 10 mL of diethyl ether. Yield: 68%.

3.4.14 Synthesis of 29, $Co(dmgH)_2(NH_2Ph)Cl$

1 mole equivalent of complex **25** was suspended in 10 mL of methanol and aniline slowly added with stirring in air at room temperature for 1 h. The initial yellow solution turned red upon aniline addition. The crude product was filtered to remove insoluble solids and the filtrate was column chromatographed on silica gel eluting with 100% ethyl acetate. Yield: 63%. ES-MS (+ve mode): m/z = 416.0 $[M-H]^-$. Anal. calcd. for C14H21ClCoN5O4: (%): C 40.25, H 5.07, N 16.77; found: C 44.36, H 5.21, N 14.81.

3.4.15 Synthesis of 30, $Co(dpgH)_2$(pyridine)(SCN)

1 molar equivalent of potassium thiocyanate was dissolved in acetone and 1 mole equivalent of cobalt chloride was added. The blue solution was stirred at room temperature for 2 h, and filtered to remove the white potassium chloride precipitate. The filtrate was then removed via rotary evaporation to obtain the product, $Co(NCS)_2$. Yield: 77%. IR (dimethylformamide, υ_{max}, cm^{-1}): 2075 (SC=N).

1 mole equivalent of the cobalt (II) thiocyanate salt from the previous step was dissolved in 10 mL of acetone and then added to 2.2 mole equivalent of diphenylglyoxime. The reaction mixture was stirred at room temperature for 3.5 hours in the presence of air. A brown solid slowly deposited and is collected via suction filtration at the end of the 3.5 hours. The solid was washed with 2 × 10 mL cold acetone and dried under vacuum in a desiccator. Yield: 64%. IR (dimethylformamide, υ_{max}, cm^{-1}): 2110 (SC=N).

1 molar equivalent of the product from the previous step was then suspended in 25 mL of methanol and 2 equivalents of pyridine were added. The mixture was stirred at room temperature for 1 hour. Subsequently, 25 mL of water was added and the entire reaction mixture cooled in an ice bath for 10 minutes. A dark orange solid precipitated and was collected via suction filtration. The solid was washed with 2:1 water/methanol, followed by diethyl ether, and air dried to give the titled product. Yield: 52%. IR (dimethylformamide, υ_{max}, cm^{-1}): 2114 (SC=N).

3.4.16 Synthesis of 31, $Co(dmgH)_2$(pyridine)(NCS)

1 mole equivalent of the **27** was dissolved in 10 mL of acetone and then added to 2 equivalents of pyridine. The reaction mixture was stirred at room temperature for 1 hour. 40 mL of water was then added with stirring, and the suspension was cooled in an ice bath for 10 min. The precipitated product was collected via suction filtration, washed with 2:1 water/methanol, followed by diethyl ether, and air dried to give an orange product. Yield: 54%. IR (dimethylformamide, υ_{max}, cm^{-1}): 2113 (SC=N). ESI-MS (m/z): 424.7 $[M-H]^-$. Anal. calcd. for C14H19CoN6O4S: (%): C 39.44, H 4.49, N 19.71, S 7.52; found: C 39.84, H 4.88, N 16.91, S 6.23

3.4.17 Synthesis of 32, $CpFe(CO)(NH_2(CH_2)_6(NH_2)I$

1 equivalent of $CpFe(CO)_2I$ was dissolved in DMSO and 2 molar equivalent of 1,6-diaminohexane was added. The mixture was stirred for 24 hours under nitrogen at room temperature to obtain a yellowish-orange solution containing **32**. The DMSO was distilled off and an orange solid was obtained. Yield: 71%. IR (DMSO, υ_{max}, cm^{-1}): 1933 (C=O).

Chapter 4

Transition Metal Carbonyls as CO- and H_2S- Releasing Molecules

4.1 Introduction

Carbon monoxide, CO has been shown to play a vital role as a low concentration cell-signalling molecule in living organisms [10, 94, 205]. In the body, it has been identified that the endogenous CO is produced by the gene HO1 via the catalysis of haem, with the production rate estimated at 0.006 mL per hour per kg of body weight. However as many factors can alter the production rate of CO, a reliable estimation of its physiological concentration is not possible. Nonetheless, experiments performed using known quantities of CO have put the therapeutic dosage in the nanomolar range [206]. In the past decade, it has been found that individuals with reduced expression of the HO1

gene are more prone to diabetes, atherosclerosis, chronic obstructive pulmonary disease and arthritis [207-210] indicating that CO have indeed an essential role to play. These physiological properties of CO have been well–studied and in the last decade, carbon monoxide-releasing molecules known as CORMs have been used to release CO [211, 212]. The molecules used are mainly transition metal carbonyls such as $Mn_2(CO)_{10}$, $[Ru(CO)_3Cl_2]_2$ and $Ru(CO)_3Cl$(glycinate) [10, 213]. The CO release can be activated or triggered photochemically or thermally. The $Ru(CO)_3Cl$(glycinate) complex, one of the first water soluble CO-RM to be synthesized, readily loses CO at room temperature and hence is not a reliable source of CO since the release cannot be controlled. An iron dienylphosphate tricarbonyl complex is also known to release CO upon interaction with an enzyme [214].

If light has been used to trigger CO release from a molecule, the molecule is known as a photoCORM [215, 216]. While many metal carbonyl complexes which release CO upon UV irradiation are known, it is only recently that efficient visible light-initiated photoCORMs are described in literature, such as manganese carbonyl scorpionates [217] and iron carbonyls containing cysteamine ligands [218, 219].

A suitable photoCORM for use in biological systems has to satisfy many criteria such as water solubility, molecular stability, ability to release CO quickly upon mild visible-light irradiation and able to form water-soluble final products to prevent clogging the arteries. In this chapter, a water-soluble dithiolate-bridged diiron complex using 3-mercaptopropanoate as the bridging thiolate, $Na_2[(\mu\text{-}SCH_2CH_2COO)Fe(CO)_3]_2$, has been synthesized. While

analogous diiron complexes have already been extensively studied as [Fe-Fe] hydrogenase model compounds in reducing protons to dihydrogen [220, 221], this complex can also act as an efficient photoCORM by releasing CO within 30 minutes of broadband visible light irradiation. Instead of monitoring the changes in UV of myoglobin for CO quantification, the concentration of CO released into the headspace of the photolytic mixture is determined directly using gas-phase FTIR spectroscopy.

Another gasotransmitter that has become an area of research interest is the noxious gas, hydrogen sulfide (H_2S). Commonly formed by commensal bacteria, research has shown that the gas is a biologically important signalling molecule involving in a myriad of cellular processes such as muscle relaxation [222], neuromodulation [13, 223, 224], blood pressure regulation and insulin release [225, 226]. H2S has also been found to exhibit anti-cancer effects in both *in vivo* and *in vitro* studies. In mammalian tissues, H_2S is synthesized from L-cysteine via cystathionine-β-synthase (CBS) and cystathionine-γ-lyase (CSE) enzymes. The role of hydrogen sulfide as a small messenger molecule mirrors that of NO as both transmit information via the modification of sulfhydryl groups on the cysteine residues of their respective target proteins. In the case of H_2S, this modification is termed protein sulfhydration.

To date, however, H_2S-releasing molecules have been limited to light-activated organic dithiolate compounds such as *N*-(benzoylthio)benzamide and persulfide-based derivatives **[227]**, simple organic sulfides such as diallyl disulfide and diallyl trisulfide **[228]** or inorganic salts, such as sodium hydrosulfide (NaSH). For example NaSH releases H_2S in an uncontrolled

manner under aqueous conditions while endogenous H_2S is produced at a much slower rate and at a lower concentration of less than 500 nM [229]. Hence, NaSH does not accurately mimic the effects of naturally-produced endogenous H_2S. Not only that, research progress with H_2S is impeded by the reactivity of free gaseous H_2S with atmospheric oxygen forming different oxidative products and rendering the storage, manipulation and production of the gas particularly challenging. In addition, inhalation as a delivery option is also not viable. If H_2S is not suitably administered, the gas causes not only nausea and irritation of the mucus lining but is also potentially lethal [230]. To circumvent this problem, the search for water-soluble molecules that can release free hydrogen sulfide gas in a controlled fashion continues to be actively pursued by many research groups [11]. In this chapter, we will also report the synthesis and characterisation of a series of water-soluble Group VI transition metal carbonyl hydrosulfides capable of releasing free H_2S in a controlled manner upon hydrolysis.

Together, these CO- and H_2S-releasing molecules make up a class of water soluble gasotransmitters releasing molecules that is non-toxic to living cells and has good bioavailability in terms of controlled release of the signalling molecules.

4.2 Results and Discussion

4.2.1 Chemistry of CO Releasing Molecules

The orange diiron carbonyl complex containing 3-mercaptopropionic acid (MPA) as the bridging thiolate ligand, $(\mu\text{-MPA})_2[Fe(CO)_3]_2$ (**1**) was prepared by heating $Fe_3(CO)_{12}$ and three equivalents of MPA in toluene. The IR bands

obtained for (μ-MPA)$_2$[Fe(CO)$_3$]$_2$ in toluene as shown in **Figure 4.1** are in excellent agreement with reported values for similar diiron dithiolato complexes [220]. ESI mass spectrometry carried out on the complex in ethanol shows an intense signal at m/z = 488.40 corresponding to its molecular ion peak. The UV-vis spectrum (**Figure 4.1**) recorded for the complex in acetone shows an intense band at λ_{max} = 330 nm and a weaker band at $\lambda_{max} \approx$ 460 nm. The absorption of the complex tails off at about 600 nm in the visible region.

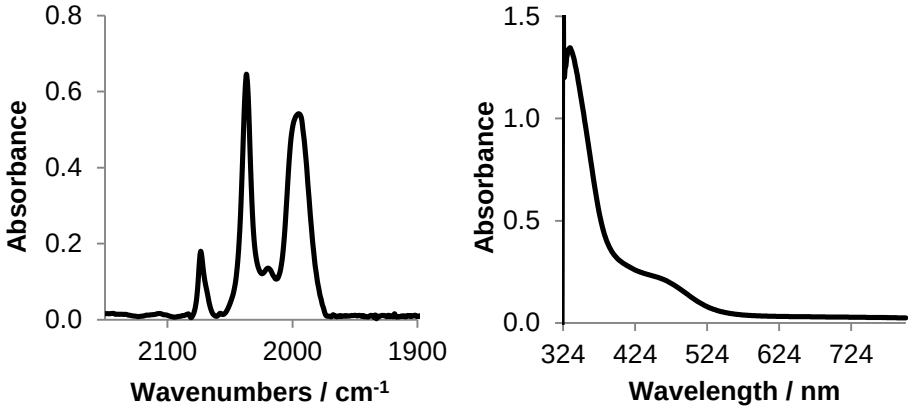

Figure 4.1 Infrared absorption (left) and UV-vis absorption spectrum of **1** taken in toluene and acetone respectively.

Single crystals of **1** obtained by slow evaporation of toluene were subjected to X-ray diffraction studies for structural determination (**Figure 4.2**). The complex crystallizes in the monoclinic space group P2(1)/n, with unit cell dimensions a = 7.794 Å, b = 25.126 Å, c = 9.179 Å, β = 97.415º. The overall structure resembles other previously-characterized thiolate-bridged diiron complexes [220]. The Fe(I) centre is coordinated to the sulfur end of MPA, thus freeing the carboxylic acid for further functionalization. In our case, a simple deprotonation of the acid groups is sufficient to render the complex water-soluble. The Fe–Fe distance is 2.51 Å, indicating the formation of a

single Fe – Fe bond. The Fe-CO bonds almost parallel to the Fe-Fe bond are slightly longer (1.805 Å) than the other four Fe-CO bonds (1.794 Å).

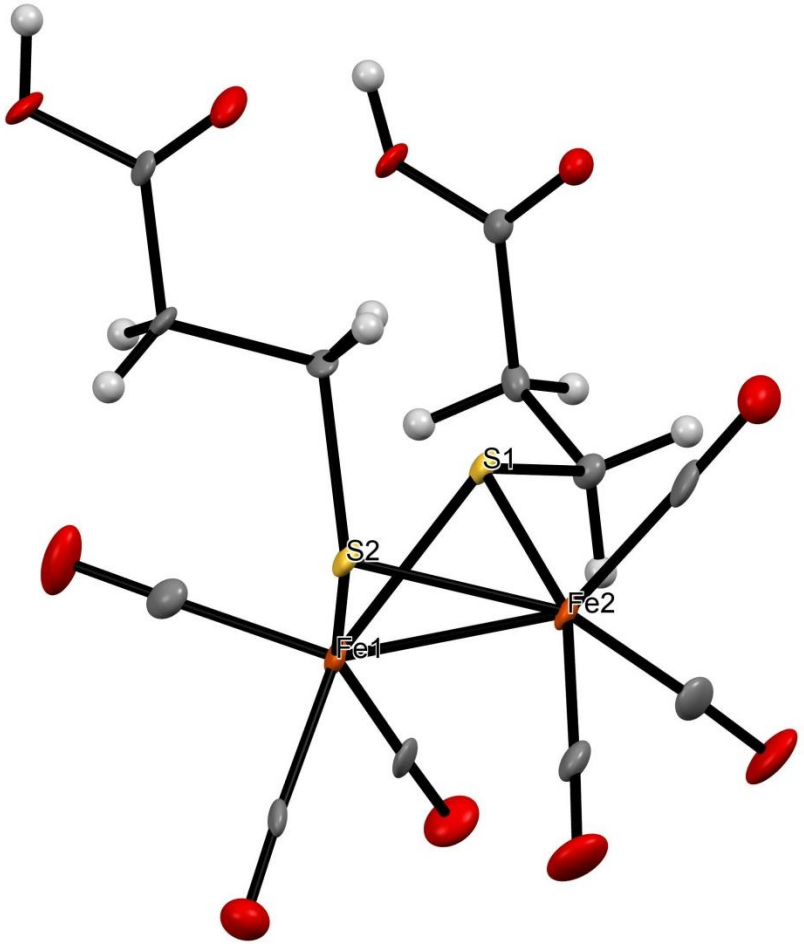

Figure 4.2 X-ray Crystal Structure of $(\mu\text{-MPA})_2[Fe(CO)_3]_2$, **1**, with thermal ellipsoids shown at 50% probability. MPA = 3-mercaptopropionic acid.

The diiron complex is stable in the dark and can be made to dissolve completely in water upon deprotonation by sodium carbonate. The complex remains intact in water as a carboxylate salt $Na_2[(\mu\text{-}SCH_2CH_2COO)Fe(CO)_3]_2$, **1·Na** since the UV-vis spectrum of the complex recorded in water has the same appearance as the parent molecule in toluene.

4.2.2 Quantification of CO Release from 1

Although diiron complexes with bridging thiolate ligands have been known to release CO upon nucleophilic substitution, the reaction is slow at room temperature unless strong donors such as PMe_3 are used [231]. Hence **1·Na** has been subjected to broadband visible light irradiation in order to release the CO ligand. In previous studies, the quantification of CO was mostly carried out by measuring the conversion of deoxymyoglobin to CO-bound myoglobin via their respective UV-vis absorbance. This presents some problems during UV-vis measurements. One, the presence of coloured complexes caused a background that hinders UV-vis detection. Two, in the myoglobin assay, a strong reducing agent such as dithionite is required and in some cases, the dithionite interferes with the CO release from metal carbonyls [232]. Finally, the binding constant of CO to myoglobin needs to be larger than that to the CO-RM to ensure an accurate quantification. Therefore, another method of measuring the CO concentration in the absence of myoglobin would be useful since any CO release can easily be traced to the photo-dissociation of the complex and thus confirms its role as a photoCORM.

The quantification of CO release is done by monitoring its gas-phase rovibrational spectrum in the headspace above the aqueous solution [233]. The headspace was directly connected to a 15cm-long gas cell equipped with CaF_2 windows for IR transmission. Since the solubility of CO in water is very low, most of the CO would be released into the headspace and gas cell hence minimising the error in determining its concentration. An added advantage is the CO quantification can be carried out *in situ*, without removing aliquots of the solution for sampling. Furthermore, as the CO pressures are in the range of

tens of Torr, pressure broadening effects are small and hence do not affect the peak absorbances significantly. As the line strength of each rovibrational line has been determined accurately, the concentration of CO can be calculated directly using the following equation [234]:

$$A^t(v) = \frac{S(m) \cdot C \cdot L}{\pi \cdot \gamma(\mathrm{m}) \cdot \ln(10)}$$

where $A^t(v)$ is the experimental absorbance, $S(m)$ is the line strength (cm^{-2} atm^{-1}), C is the concentration (atm), L is the path length (cm), and $\gamma(m)$ is the half-width of the line (cm^{-1}). In this work, L = 15 cm and a few P (m = $-J''$) and R branch ($m = J'' + 1$) lines have been used to determine the average concentration of CO. For example, the S values for the intense P(7) and P(8) rovibrational lines are 11.367 and 11.241 cm^{-2} atm^{-1}, respectively.

In the experiments, the release of the CO was performed by irradiation of an aqueous solution containing **1·Na** at room temperature. The gas-phase infrared absorption spectrum of CO is then monitored in the gas cell. By applying the equation, we found that each **1·Na** releases all six CO ligands within 30 to 40 minutes of broadband irradiation (**Figure 4.3**). In fact, CO signals can already be observed within a few minutes of irradiation. The release of the CO ligands from the complex is explained by the excitation of *d* electrons (t_{2g}) from the metal to the π* anti-bonding orbitals (t_{2u}) in the CO ligand, leading to cleavage of the M-C bond. The UV-vis absorbance of the complex at λ_{max} = 330 nm was also monitored and found to decrease rapidly also within the same period. The period of irradiation for which all CO are released depends on the easily adjusted distance of the lamp from the reaction mixture. For accuracy of CO

quantification, the irradiation was fixed at a distance such that sufficient data points can be collected and repeated. The same results were obtained in both aerated and deaerated aqueous solutions, indicating that air or oxygen does not affect the CO release.

The quantum yield of the initial photo-dissociation of **1·Na** at 390 nm was estimated to be 0.4 ± 0.1 by comparison to $CpMn(CO)_3$ photo-dissociation, which has a known quantum yield of near unity [235]. The wavelength of 390 nm was chosen, as both complexes have moderate absorbances in this region. While the quantum yield may not be very high, the photo-dissociation of the diiron thiolate can still proceed equally efficiently in air or under vacuum.

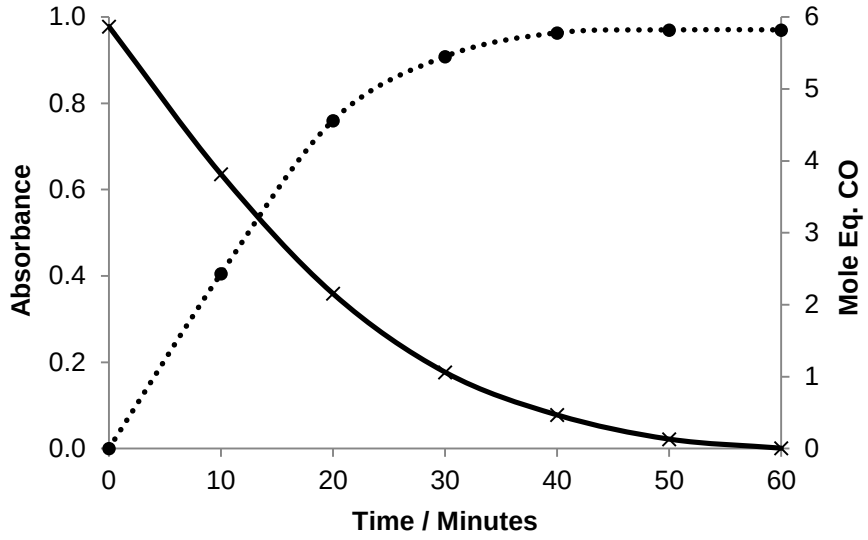

Figure 4.3 Change in the gas-phase CO quantity and UV-vis absorbance. The CO quantity is expressed as mole equivalent of **1·Na** with respect to the period of irradiation detected using FTIR spectroscopy (dotted line). The change in the UV-vis absorbance of **1·Na** against the irradiation period is shown as a dashed line

We are unable to detect any intermediates during irradiation although stepwise release of CO from the complex is expected. Thiolate-bridge diiron complex is known to lose two CO molecules upon nucleophilic substitution and becomes

a diiron tetracarbonyl species [236]. However in the absence of strong donors or nucleophiles, the intermediate complex or complexes most likely decompose quickly to release the remaining CO molecules. At the end of photolysis, the aqueous solution turns red without any observable deposits. The UV-vis spectrum of the red solution shows a small absorption band at λ_{max} = 475 nm while the ESI spectrum taken of the solution in methanol shows a signal at m/e = 407 (negative mode) tentatively assigned to a $Na_3[Fe^{III}(SCH_2CH_2COO)_3]$-methanol adduct.

4.2.3 Biological and Cytotoxicity Studies of 1

We have also carried out preliminary studies on the cytotoxicity of **1·Na** towards mammary epithelial cells MCF-10A (**Figure 4.4**). Treatment of the cells using a range of diiron complex concentration from 1 to 40 μM did not lead to any observable cytotoxicity within 24 hours, as determined via the MTT assay. In fact, we were unable to determine an IC_{50} value, since hardly any cell deaths occur over this range of concentration and time. Hence, even if the CO photo release period takes place in 1 hour, the diiron complex is expected to have minimal undesirable effect on the cells.

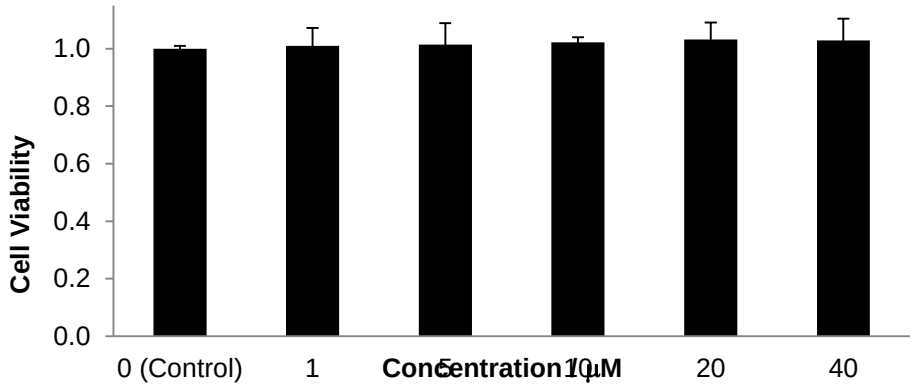

Figure 4.4 Viability of mammary epithelial cells MCF-10A after 24 hours incubation with **1·Na**, as determined by the MTT assay.Cell viabilities have been normalized to DMSO control.

4.2.4 Chemistry of H_2S-Releasing Molecules

The Group 6 transition metal carbonyl hydrosulfide anionic complexes $[M(CO)_5SH]^-$ (M = Cr, Mo, W; **Scheme 4.1**) were prepared by a modification of a previously published procedure [237]. Briefly, a methanol solution containing the transition metal hexacarbonyl, $M(CO)_6$ with sodium hydrosulfide (NaSH) was irradiated under a broadband UV source. The carbonyl infrared absorption bands obtained for the resulting complex suggests a pattern typical of C_4v symmetry, albeit being red-shifted due to the negative charge on the metal complex (**Figure 4.5**). The UV-vis spectra of the complexes show broad absorption down to 600-700 nm. ESI mass spectrometry carried out on all three complexes shows the characteristic molecular ion signal, M^- along with several signals corresponding to CO loss species. All three anions are also water-soluble.

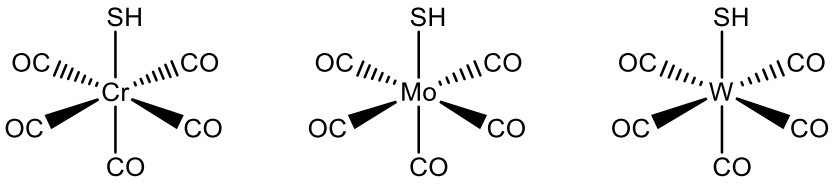

Scheme 4.1 Structures of the three Group 6 transition metal hydrosulfides anions

Comparing the three metal hydrosulfides, the molybdenum complex $Na[Mo(CO)_5SH]$ appears to be most stable as a solid in air, hence it is chosen for more detailed studies. When dissolved in water or wet methanol, the complex slowly hydrolyses at room temperature, although the hydrolysis can be accelerated by the addition of strong acids. Regardless of the acid strength, $Mo(CO)_5(MeOH)$ is found to be the major product in methanol solvent, as

characterised by its IR (**Figure 4.5**) and UV-vis (**Figure 4.6**) absorption spectra. Although the IR spectra of the product could not be obtained in water, comparison of the UV-vis spectrum of $Mo(CO)_5(MeOH)$ spectrum in methanol with that of the species formed after acidification suggests that $Mo(CO)_5(H_2O)$ is the most likely product in aqueous solution [238].

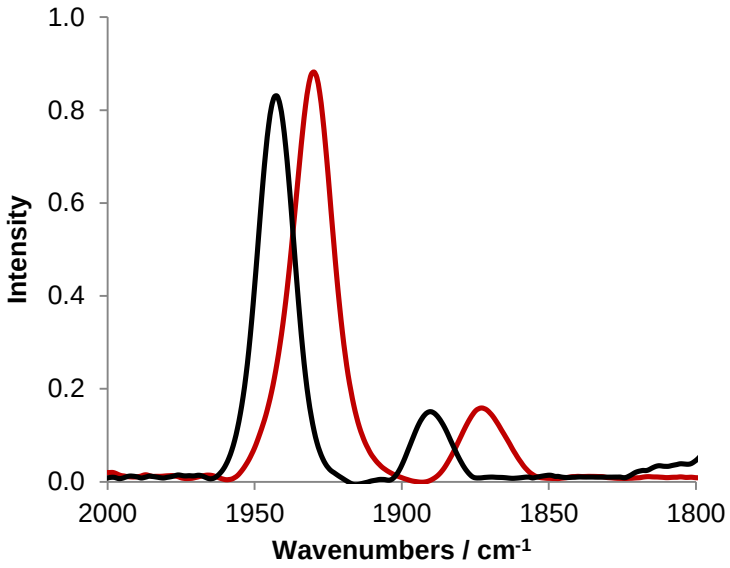

Figure 4.5 (left) Infrared spectrum of $[Mo(CO)_5SH]^-$ (red) and $[Mo(CO)_5(MeOH)]$ (black) taken in methanol.

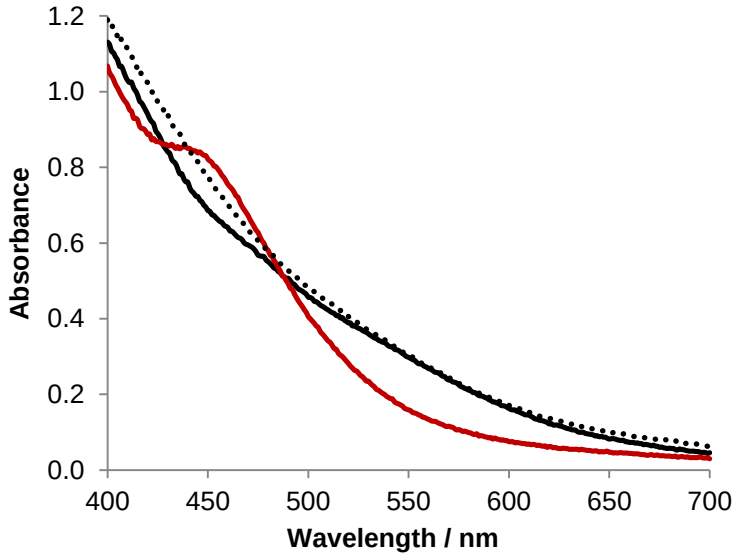

Figure 4.6 UV-vis spectrum of $[Mo(CO)_5SH]^-$ (red), $[Mo(CO)_5(MeOH)]^-$ (black) in methanol and $[Mo(CO)_5(H_2O)]^-$ (black dotted) in water.

4.2.5 Quantification Studies on the Hydrosulfides

We have also used the changes in pH of an aqueous solution of NaSH as an indicator of H_2S gas formation since pH is expected to increase due to the concomitant formation of sodium hydroxide;

$$NaSH + H_2O \rightleftharpoons NaOH + H_2S$$

The anion HS^- is a very weak base as inferred from its pKa value of 7. Hence it readily hydrolyses in water to yield the conjugate acid. Evolution of the H_2S, aided by the low solubility in aqueous medium further shifts the position of the equilibrium to the right in accordance with Le Chatelier's Principle. Indeed, the pH of the solution was determined to be around 11 only a few minutes after NaSH hydrolysis in deionised water. The contribution of the sparingly-soluble H_2S gas to pH changes in water can be considered to be negligible due to its low solubility [239]. By inference metal hydrosulfides are expected to undergo a similar reaction with water;

$$Na[Mo(CO)_5SH] + H_2O \rightleftharpoons NaOH + Mo(CO)_5(H_2O) + H_2S$$

However the pH increase is much slower and reaching similar pH values only after 1 hour (**Figure 4.8**).

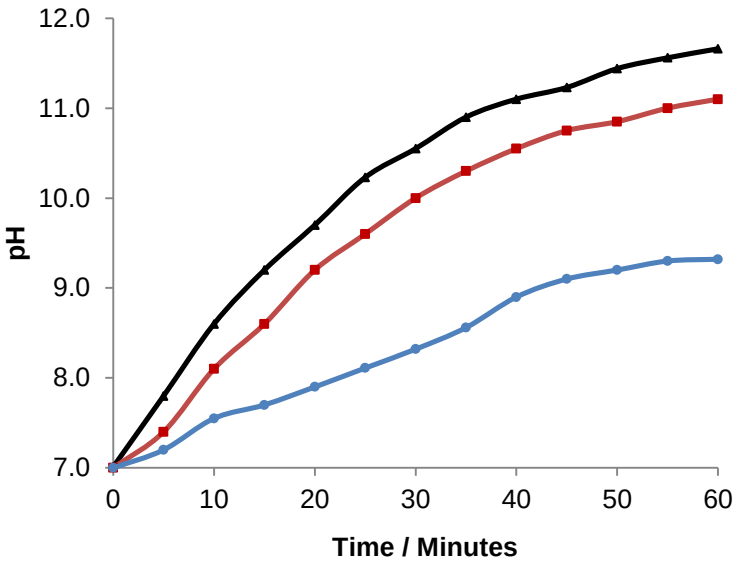

Figure 4.7 Changes in pH upon hydrolysis of the Cr (black), Mo (red) and W (blue) hydrosulfides as monitored using pH meter over a period of one hour.

The release of hydrogen sulfide gas from $[Mo(CO)_5SH]^-$ has been detected quantitatively via gas-phase infrared spectroscopy by monitoring its intense bending vibrational mode centred at 1180 cm^{-1} in the headspace above the aqueous solution. For the IR measurements, the headspace was directly connected to a 15cm-long gas cell equipped with CaF_2 windows for IR transmission. Since the solubility of H_2S in water is very low [239], most of the gas would be released into the headspace hence minimising the error in determining its concentration. This method also allows continuous monitoring of the gas *in situ* without the need to remove aliquots from the solution. The absorbance of the band is first calibrated by using a standard pressure of H_2S generated stoichiometrically from the reaction of a strong acid on a known quantity of solid NaSH. Care is taken such that the absorbance is proportional to the concentration according to Beer's law [9].

As seen in **Figure 4.8**, the release of H_2S occurs gradually over a period of 40 minutes for $Mo(CO)_5SH^-$ in a pH 6.5 phosphate buffer solution. The rate of

H_2S production reaches a plateau close to one mole equivalent of the amount of $Na[Mo(CO)_5SH]$ present initially in the aqueous solution. Interestingly, no CO peak (ν = 2143 cm^{-1}) was detected which indicates that the acidification process only affects the SH^- ligand. This result is also consistent with $Mo(CO)_5(H_2O)$ being the major product since both reactant and product contain the same number of CO ligands. Thus $Mo(CO)_5SH^-$ acts purely as a H_2S-releasing molecule and not as a CORM (CO-releasing molecule).

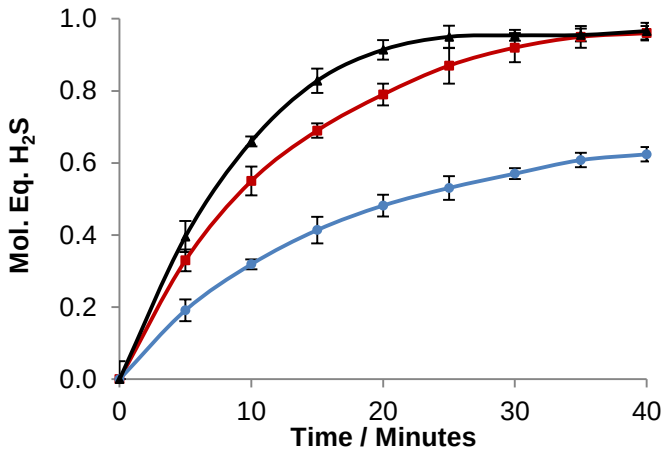

Figure 4.8 Changes in IR absorbance of H_2S release of Mo (red), Cr (black) and W (blue) vs time in a pH 6.5 phosphate buffer solution containing 0.005M of $Na[M(CO)_5SH]$.

From the results obtained via infrared and pH measurements, it can be proposed that the release of H_2S from the three metal hydrosulfides follow the order Cr > Mo > W. According to rate of evolution of H_2S as monitored via IR spectroscopy in **Figure 4.8**, the chromium complex releases H_2S fully in 25 minutes; the molybdenum complex requires 40 minutes and tungsten complex took more than an hour. The pH measurements in **Figure 4.7** lend further support to the proposed trend in the rate of hydrolysis of the metal hydrosulfides.

4.2.6 Biological and Cytotoxicity Studies on the Metal Hydrosulfides

If these metal complexes were to be used as H_2S releasing agents in biological systems, then their cytotoxic profile have to be first established. Hence the anti-cancer and cytotoxic properties of $Na[Mo(CO)_5SH]$ towards MCF-10A mammary epithelial cells and well as MDA-MB-231 breast adenocarcinoma cells were next evaluated. Treatment of the cells with concentrations ranging from 1 μM to 40 μM of the molybdenum hydrosulfide on the normal mammary cells did not lead to any observable cytotoxicity over a period of 24 hours, as concluded from the MTT assay (**Figure 4.9**). Interestingly, $Na[Mo(CO)_5SH]$ exhibited anti-proliferative properties towards the cancer cells, as deduced from the full IC_{50} analysis **(Figure 4.10**) although the established IC_{50} value is relatively high at around 66 μM. Nonetheless, it is believed that these metal hydrosulfides would have minimal undesirable effect on the cells during the duration of H_2S release in the cell based on our preliminary data. More importantly, the effect of the product as exemplified by $Mo(CO)_5(MeOH)$ on MCF-10A normal cells was also tested and found to be non-toxic over the concentration range and conditions (**Figure 4.9**).

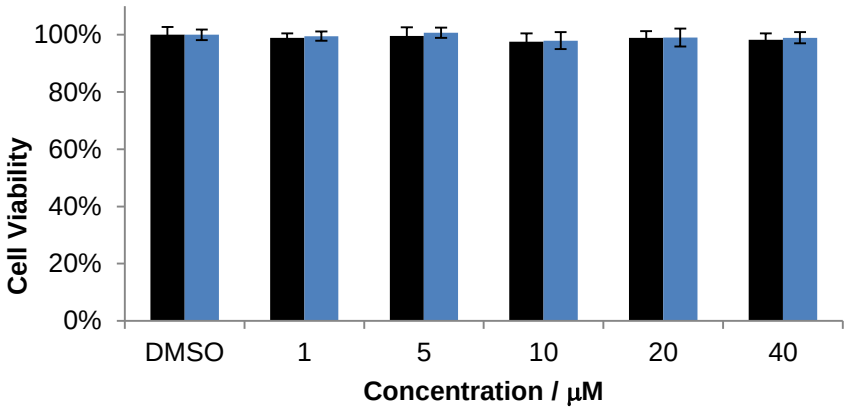

Figure 4.9 Viability of mammary epithelial cells MCF-10A after 24 h incubation with $Na[Mo(CO)_5SH]$ (black) and $[Mo(CO)_5(MeOH)]$ (blue) as determined by the MTS assay.Cell viabilities have been normalized with DMSO as a control.

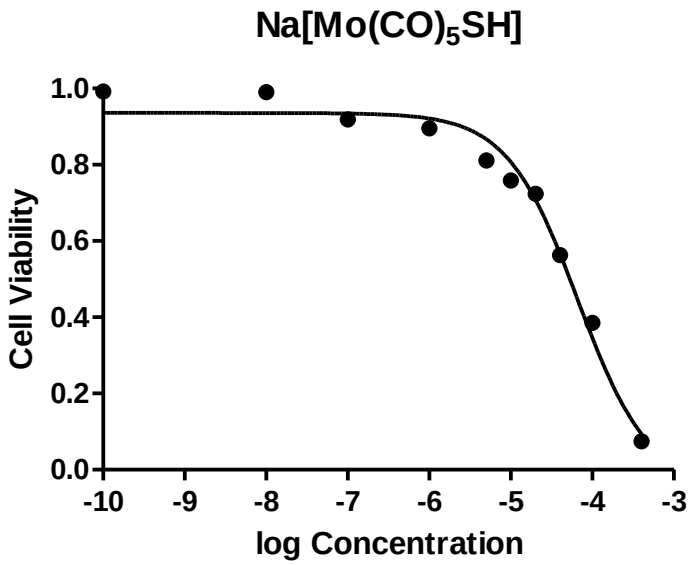

Figure 4.10 Dose-response curves for $Na[Mo(CO)_5SH]$ on the MDA-MB-231 cell line.

In conclusion, a class of Group 6 metal hydrosulfides that is capable of releasing hydrogen sulfide gas in a controlled manner has been synthesized and characterized. These complexes are stable in the solid state, are water-soluble, and do not exhibit cytotoxicity towards mammary epithelial cells. In addition, they do not release their CO ligands under the conditions employed for the release of H_2S. These complexes can indeed serve as selective hydrogen- sulfide releasing molecules. Infrared, UV-vis and pH measurements were employed to monitor the hydrogen sulfide release and all three methods placed the rates of H_2S release in the order Cr > Mo > W. This trend is consistent with the stability of the metal hydrosulfides with respect to the M-S bond strength. The more diffused *d* orbitals of the tungsten atom is better able to overlap with the hydrosulfide HOMO and hence a stronger interaction as compared to the smaller spatial extent of the chromium *d* orbitals.

4.3 Conclusions

In this chapter, we have discussed the preparation and characterisation of a several transition metal carbonyl complexes which function as gasotransmitters releasing agents. These complexes have been found to be stable, water-soluble, do not exhibit cytotoxicity and can release their respective gasotransmitters in a controlled manner. These are some of the more important criteria expected of a gasotransmitter releasing agent. For the case of the H_2S releasing molecules, it was found that the CO ligands do not dissociate under the experimental conditions, hence conferring some selectivity character to the metal complex. The quantification studies utilize a simple method based on infrared spectroscopy to measure the concentration of gases release hence circumventing the need for expensive instruments and elaborate setups. pH and UV-vis measurements were also employed in the case of the H_2S releasing studies to monitor the hydrogen sulfide release and both methods, along with the infrared data, placed the rates of H_2S release in the order Cr > Mo > W.

4.4 Experimental

4.4.1 Materials

Iron dodecarbonyl (95%) was purchased from Strem Chemicals. Deuterated chloroform (99.8%), stabilised with 0.5 wt% Ag, 0.03% TMS was purchased from Cambridge Isotope Laboratories. 3-mercaptopropionic acid (99%), sodium carbonate, ethanol, toluene, sodium hydrosulfide (99%), acetone, methanol and N,N-dimethylformamide were purchased from Sigma Aldrich. Group 6 metal carbonyls (98%) were purchased from Alfa Aesar. All solvents and reagents were used without further purification.

4.4.2 Instrumentation and General Methods

All manipulations for chemical synthesis were carried out using standard Schlenk techniques under a nitrogen atmosphere. Photochemical experiments were conducted with a Legrand broadband lamp (350 – 800nm, 11W). All IR spectra were obtained with Shimadzu IR Prestige - 21 Fourier – transformed infrared spectrometer (1000 – 4000 cm^{-1}, 1 cm^{-1} resolution, 16 scans co–added for spectra averaging) using a 0.05 mm path – length CaF_2 cell for liquid samples, and a 15 cm path – length CaF_2 gas cell for gas samples. The IR instrument was calibrated using standard CO gas from a CO cylinder prior to measurement. The IR instrument was calibrated using a H_2S generated from a known quantity of NaSH upon acidification. ^1H NMR spectra were recorded in $CDCl_3$, unless otherwise stated, on Bruker AC300 Fourier–transformed spectrometers operating at 300 MHz at room temperature. All UV-vis absorption spectra were obtained with a Shimadzu UV-2550 spectrophotometer. Electrospray ionisation (ESI) was conducted using a Finnigan MAT LCQ spectrometer.

4.4.3 Solid State Structural Determination

Single crystal X-ray structural studies were performed on Bruker-AXS Smart Apex CCD Single-Crystal Diffractometers by CMMAC, National University of Singapore. Data were collected at 100(2) K using graphite-monochromated Mo K_α radiation (λ = 0.71073 Å). Data collection was evaluated using SMART CCD system and processed for Lorentz and polarisation effects using SAINT software and for absorption effects using SADABS software. Structural solution and refinement were then carried out using SHELXTL

suite of programs. The structure was solved by direct methods. All H atoms were put at calculated positions using the riding model.

4.4.4 Preparation of 1 and 1·Na

1 molar equivalent of $Fe_3(CO)_{12}$ and 3 molar equivalents of 3-mercaptopropionic acid were dissolved in toluene and refluxed under N_2 atmosphere until a colour change from green to orange was observed. The excess MPA and toluene were removed by distillation leaving behind an orange solid. The solid was purified by recrystallization in toluene. Single crystals of **1** suitable for X-ray crystallography were obtained by slow vaporisation of toluene. Yield: 47%. IR (toluene, υ_{max}, cm^{-1}): 2073, 2037, 1997. ESI-MS (+ve mode): m/z = 480.4 $[M^+]$, m/z = 452 $[M\text{-}CO]^+$. ^{1}H NMR (C_6D_6, ppm): 2.04-2.08, (t, J = 6.2 Hz, 2H, C*H*$_2$S), 2.15-2.20 (t, J = 7.3 Hz 2H, *CH*$_2$COOH).

An aqueous solution containing Na_2CO_3 was added to a toluene solution containing **1**. The toluene layer became light yellow. The aqueous layer turned orange, indicating the formation of **1·Na**. ^{1}H NMR (D_2O, ppm): 2.57-2.62, (t, J = 7.0 Hz, 2H, C*H*$_2$S), 2.89-2.94 (t, J = 7.0 Hz, 2H, *CH*$_2$$COO^-$).

4.4.5 CO Quantification

The quantification of CO present can be determined from its CO rovibrational line strength. As tabulated by Medvecz [234], the equation used is as follow:

$$A^t(v) = \frac{S(m) \cdot C \cdot L}{\pi \cdot \gamma(\mathrm{m}) \cdot \ln(10)}$$

where $A^t(v)$ is the experimental absorbance, $S(m)$ is the line strength (cm^{-2} atm^{-1}), C is the concentration (atm), L is the path length (cm), and $\gamma(m)$ is the half-width of the line (cm^{-1}).

A sample of 2.0 mg of **1·Na** in 0.5mL deaerated water was subjected to visible light irradiation at room temperature for one hour at a fixed distance (10 cm). The reaction flask was equipped with a 15 cm long gas cell connected to the headspace above the aqueous solution. The FTIR spectrum of the fundamental band of CO was scanned over 60 minutes. The absorbance values of a few rovibrational P and R-branch lines were recorded and an average value obtained and converted into CO pressure using the equation. The ideal gas equation ($PV = nRT$ where V = volume of the gas cell and headspace) then converts the pressure to the number of moles of CO. The experiment was repeated using the same compound dissolved in aerated water. Identical data was obtained, indicating that oxygen does not interfere with the photochemistry to a significant extent.

4.4.6 Cell Culture and Cytotoxicity Studies

Experimental culture of the mammary epithelial cells MCF-10A and MDA-MB-231 were obtained from the American Type Culture Collection (ATCC) and cultured in tissue culture dishes (Nunc Inc., Naperville, IL, USA). The cells were maintained in Dulbecco's modified Eagle's medium (DMEM, Grand Island, NY, USA) supplemented with 10% fetal bovine serum (FBS) and 1% penicillin/streptomycin (GIBCO Laboratories) at 37°C in 5% CO_2 atmosphere. Cell cultures were maintained in an antibiotic-free condition during cell growth and experiments. Phosphate buffered saline (PBS) was

obtained from 1st Base. Concentrations ranging from 1 to 40 μM of **1·Na** was used for incubation with the cells for 24 hours.

4.4.7 Thermal Stability Measurements

Separate samples of **1** and its sodium salt, **1·Na** were dissolved in toluene and water respectively. These are then maintained at a temperature of 40°C to simulate a physiological temperature for 24 hours under atmospheric conditions in the dark to determine their thermal stability in solution. The samples were then analysed via IR and NMR respectively after a day. The spectroscopic data obtained indicates no appreciable degree of degradation compared to that for the pure sample.

4.4.8 Preparation of $[M(CO)_5(SH)]^-$ (M = Cr, W)

1 molar equivalent of $Mo(CO)_6$ and 10 molar equivalents of NaSH were dissolved in 2mL of acetone and placed inside a quartz tube. The tube was subsequently evacuated by means of a vacuum and then subjected to UV photolysis for 3 hours. The crude product was purified by precipitating the excess NaSH using a solvent mixture of methanol and diethyl ether (1:5 ratio). The volume was subsequently reduced and hexane was added to induce precipitation of the yellow $Na[Cr(CO)_5(SH)]$. Yield: 76%. IR (acetone, υ_{max}, cm^{-1}): 2046, 1939, 1887. ESI-MS (-ve mode): m/z = 224.7 $[M]^-$ and 196.8 $[M-CO]^-$. UV (methanol, $\lambda_{max,}$ nm): 388. Anal. calcd. for NaCrC5HO5S (%): C 26.68, S 14.24; found: C 26.59, S 14.21. The same procedure was applied to $W(CO)_6$ using the same ratio of starting materials and the orange $Na[W(CO)_5(SH)]$ was obtained. Yield: 85%. IR (acetone, υ_{max}, cm^{-1}): 2076, 1932, 1885. ES-MS (-ve mode): m/z = 356.7 $[M]^-$ m/z = 328.9 $[M-CO]^-$. UV

(methanol, $\lambda_{max,}$ nm): 463. Anal. calcd. for NaWC5HO5S: C 16.82, S 8.98; found: C 16.72, S 8.92.

4.4.9 Preparation of $[M(CO)_5(SH)]^-$ (M = Mo)

For the molybdenum derivative, instead of UV irradiation, a 355 nm pulsed laser was used for the synthesis. Irradiation of the starting materials in acetone for 2 hours formed the brown product. Yield: 79%. IR (acetone, υ_{max}, cm^{-1}): 2054, 1943, 1872. ESI-MS (-ve mode): m/z = 270.6 $[M]^-$, m/z = 242.8 $[M-CO]^-$. UV (methanol, $\lambda_{max,}$ nm): 439. Anal. calcd. for NaMoC5HO5S: C 22.32, S 11.92; found: C 22.47, S 11.97.

4.4.10 Measurement of Hydrogen Sulfide Release

A 5 mM methanol solution of the respective metal hydrosulfide was prepared by the addition of the appropriate mass into 10 ml of methanol. This solution was then subjected to hydrogen sulfide release by adding in either 10 ml of phosphate buffer at pH 6.5 or 4% aqueous HBF_4. HBF_4 was chosen because the anion is non-coordinating and hence would have minimal interference with the release. The release of hydrogen sulfide was then monitored directly or indirectly by three methods. (a) Infrared spectroscopy (b) UV-vis spectroscopy (c) pH measurements

4.4.11 Infrared Measurements

A 0.01 M solution of NaSH in deionised water was prepared for calibration purposes. The round bottom flask was then attached to a 15 cm long gas cell connected to the headspace above the solution. 15 mL of 1 M hydrochloric acid was then added and the release of H_2S was then monitored until there were no further changes to the infrared absorbance obtained. A calibration

curve was then plotted and subsequently used to determine the total gas concentration in the hydrolysis of the metal hydrosulfide. A separate solution containing 0.5 mM of the respective metal hydrosulfide was then added to an equivalent volume of pH 6.5 phosphate buffer. The reaction flask was equipped with the same 15 cm long gas cell connected to the headspace above the aqueous solution. The FTIR spectrum of the fundamental band of H_2S was obtained every 5 minutes for a total duration of 40 minutes. The concentration every 5 minutes were then calculated from the calibration curve and plotted against time.

4.4.12 UV-vis Measurements

To a solution containing 0.5 mM of metal hydrosulfide, an initial UV spectrum was taken at time t = 0. 0.2 ml of 4% aqueous HBF4 was then added to the solution of metal hydrosulfide in a quartz cuvette and an UV spectrum was obtained every 5 minutes over a period of 1 hour. The absorbance of the metal hydrosulfides starting material were used as an indicator of hydrogen sulfide release as the final product bands were too broad to be of any use.

4.4.13 pH Measurements

To a 0.01 M solution containing the metal hydrosulfide, the pH of the initial solution was measured using a pH meter. The pH was monitored every 5 minutes for a total duration of 1 hour

4.4.14 Cell Culture (H_2S)

Experimental cultures of the mammary epithelial cells MCF-10A and MDA-MB-231 were obtained from the American Type Culture Collection (ATCC) and cultured in tissue culture dishes (Nunc Inc., Naperville, IL, USA). The

cells were maintained in Dulbecco's modified Eagle's medium (DMEM, Grand Island, NY, USA) supplemented with 10% fetal bovine serum (FBS) and 1% penicillin/streptomycin (GIBCO Laboratories) at 37°C under a 5% CO_2 atmosphere. Cell cultures were maintained in an antibiotic-free condition during cell growth and experiments. Phosphate buffered saline (PBS) was obtained from 1st Base.

4.4.15 Evaluation of Cytotoxicity and Anti-Proliferative Properties

Approximately 10,000 cells per well were seeded in a 96-well plate and allowed to adhere for approximately 24 hours at 37°C. 40 μM of $Na[Mo(CO)_5SH]$ and $Mo(CO)_5(MeOH)$ in DMSO was separately prepared and serially diluted using DMEM media to obtain concentrations of 20 μM, 10 μM, 5 μM and 1 μM. 100 μL of each concentrations were then added to the cells in triplicates and incubated at 37°C and 5% CO_2 for 24 hours. The final concentration of DMSO in the medium was 0.1% (v/v).

4.4.16 MTT Proliferation Assay

The anti-proliferation activity of $Na[Mo(CO)_5SH]$ and $Mo(CO)_5(MeOH)$ were then determined using the MTT assay. Following treatment, the media was removed and each well washed with 100 μL of PBS, followed by 100 μL of MTT, (0.5mg/mL) in media and incubated for an additional 2 hours. After the incubation period, the MTT was removed and 100 μL of DMSO was added to dissolve the formazan crystals. The absorbance intensities at 470 nm were then measured and cell viabilities relative to the control (DMSO) were calculated. In the case for the treatment of $Na[Mo(CO)_5SH]$ on MDA-MB-231 cell line, the IC_{50} values, which is defined as the concentration necessary to inhibit the

growth of 50% of the cell population were determined using Graphpad Prism version 5.0 by fitting the values on a dose-response curve (Cell viability vs log drug concentration). The experiments were performed in triplicates for each concentration and two independent experiments were performed.

Chapter 5

Transition Metal Carbonyls as Thiol and Hydrazine Sensors

5.1 Introduction

Organometallic radicals have found many important uses such as in polymerisation, light-driven processes and heterogeneous catalysis [240-244]. Previously it has been reported that a class of stable manganese-based radicals containing either N or S ligands has been synthesized [245, 246]. Notably, the colours of the radical complex were highly dependent on the type of ligand. While S ligands produce a red colouration, a deep blue-green colouration was observed with N ligands. These new class of radicals were found to be stable and has an intense UV-vis absorption in the visible region. These unique

properties are thus exploited and used successfully in the detection of biological thiols and hydrazines.

Thiols are biologically important molecules which regulate a variety of biological process in an organism. Of particular importance are those that are involved in maintaining redox homeostasis such as glutathione (GSH), cysteine (Cys) and homocysteine (HCys). In addition to maintaining redox balance, thiols are also known to play a functional role in enzymes catalytic sites and metabolic pathways [104]. Indeed, research has suggested that thiols levels, especially that of homocysteine, are linked to a number of diseases including Alzheimer's, cancer and cardiovascular diseases [105, 107, 247]. Plasma thiol concentrations have also been linked to the oxidative stress levels associated with the development of some of these conditions [108-111].

In view of the biological importance of thiols, it is not surprising that there already exist some analytical methodologies for the detection and quantification of thiols. While instrumentation techniques are well established, fluorescence and optical techniques presents a more viable and attractive option for the detection of thiols as shown by the effort devoted to the development of optical and fluorescent sensors for thiols over the last decade [121, 122]. Such optical and fluorescent probes have the advantage of sensitivity, simplicity and most importantly, potential for in vivo bioimaging which is becoming increasingly important in the field of biomedical science [123-125]. These optical probes function via a variety of reaction mechanisms ranging from Michael additions [126, 127], cyclization with aldehydes [128, 129], cleavages of sulfonamides and sulfonate esters [130, 132, 135], cleavage of selenium-nitrogen bonds [131, 133], redox processes in metal complexes

[136-138], cleavage of disulfide bonds [139-141] to the use of nanoparticles [146, 248].

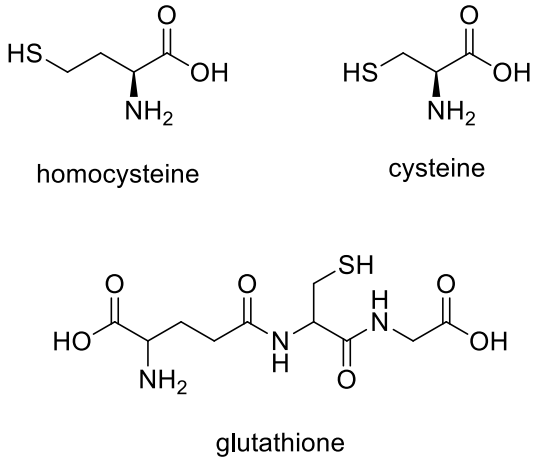

Scheme 5.1 Structure of the three most common biological thiols

Another class of compounds of detection interest are the hydrazines. Hydrazines are a source of pollution globally and can seriously affect human health. It is an explosive fuel that is widely used in missile propulsion systems **[148, 249]** and being a strong base, it is often found as a key reactant in the synthesis of dyes, pesticides, chemicals and pharmaceuticals **[147, 151].** The widespread use of hydrazines can potentially degrade the environment should its transportation, production and use not be carefully regulated and monitored. Existing techniques rely on expensive instrumentation such as HPLC **[250]**, GC **[251]** and capillary electrophoresis **[252]** which can be cumbersome to be employed for use in the field. Hence it is desirable that a simple and rapid sensor be developed for the detection of hydrazines.

The probe we are using contains a cyclopentadienyl manganese carbonyl ($CpMn(CO)_2$) scaffold. The unique properties of this probe is that it exhibits different absorbances in the visible light region depending on its redox state

and being a radical itself can serve as a dual probe in infrared and fluorescent imaging studies in chemical biology, especially in radical-rich environments involving reactive nitrogen (RNS) and oxygen (ROS) species such as those found in active cancer cells.

This radical complex was originally synthesized in the hope that in the presence of a fluorophore, the fluorescence would change significantly to allow us to use the radical for bioimaging purposes. However, for reasons that would be discussed in Section 5.2.1, the complex was not used for fluorescence works but rather adapted for use as a thiol and hydrazine sensor.

5.2 Results and Discussion

5.2.1 Fluorescence Studies with $CpMn(CO)_2$(2-aminoanthracene)

The titled radical complex was prepared via $CpMn(CO)_3$. The 355 nm UC-laser photolysis of $CpMn(CO)_3$ in THF generates the red $CpMn(CO)_2(THF)$ complex which then reacts with 2-aminoanthracene to form the orange $CpMn(CO)_2$(2-aminoanthracene) complex. Exposure to air or addition of H_2O_2 turns the solution a deep green, signifying the formation of the $CpMn(CO)_2$(2-aminoanthracenyl) radical (**Figure 5.1**). The IR frequencies are very similar to previously-reported $CpMn(CO)_2(ArNH)$ (Ar = arene) radical analogues [253, 254]. The green radical complex can be purified by passing the reaction mixture through a silica column using ethyl acetate as the eluant. By monitoring its ν_{CO} bands in the IR spectrum, we found that $CpMn(CO)_2$(2-aminoanthracenyl) radical is remarkably air-stable in THF at room temperature for more than a week. The radical is also soluble in many polar

and non-polar solvents such as DMSO, ethanol, acetone, diethyl ether and dichloromethane.

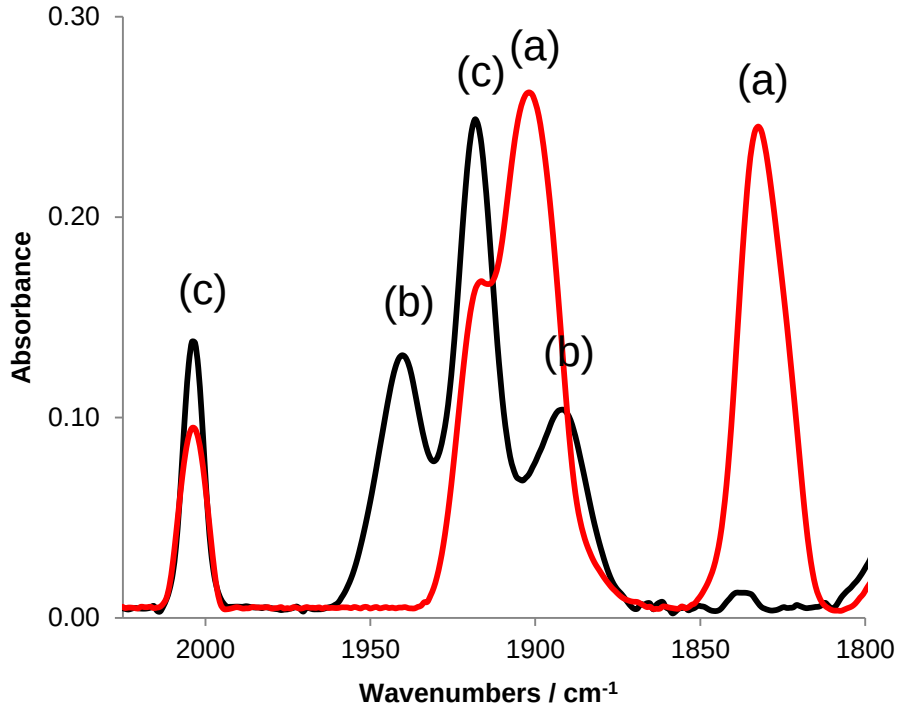

Figure 5.1 IR absorption spectra of various $CpMn(CO)_2$ species in THF. (a) $CpMn(CO)_2$(2-aminoanthracene), (b) CpMn(CO) (2-aminoanthracenyl) radical and (c) $CpMn(CO)_3$. Red: before O_2 exposure, Black: after O_2 exposure.

The ESR spectrum of $CpMn(CO)_2$(2-aminoanthracenyl) radical in THF (**Figure 5.2**) shows a sextet of lines with a g-factor centered at 2.005 ± 0.003 and coupling constants a(^{55}Mn) of 9.45 ± 0.30mT. The data are consistent with the spin being more localized on the Mn center (nuclear spin I_{Mn} = 5/2), which is previously observed for $CpMn(CO)_2$(anilinyl) analogues [255].

Two other sets of lines were recorded in the ESR spectrum. We believe that they correspond to decomposition products such as the manganese oxides, MnO and MnO_2 for which such multiplets were also previously observed [256].

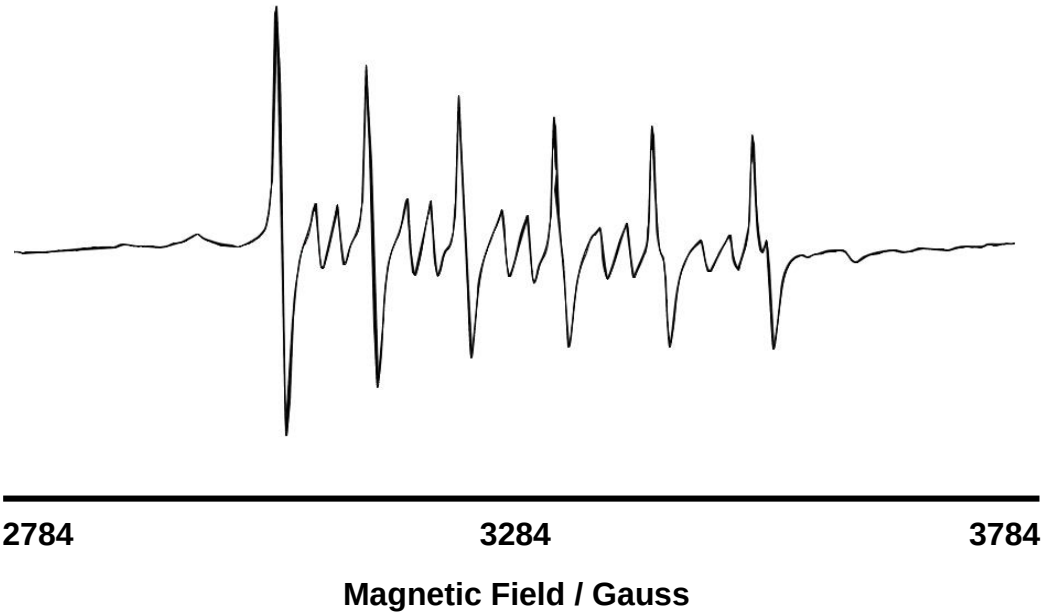

Figure 5.2 ESR spectrum of the $CpMn(CO)_2$ radical. (a) $CpMn(CO)_2$(2-aminoanthracenyl) radical in THF. The minor peaks (b) are assigned to MnO and MnO_2.

The UV-vis spectrum recorded for $CpMn(CO)_2$(2-aminoanthracenyl) in THF shows that the vibronic features of 2-aminoanthracene between 300 to 450 nm are retained even upon coordination to the metal (**Figure 5.3**). A broad emission band (λ_{max} at 480 nm) obtained for $CpMn(CO)_2$(2-aminoanthracenyl) upon 350 nm excitation, also resembles that of free 2-aminoanthracene. From time-resolved spectroscopy (Fig. 3), similar fluorescence $t_{1/2}$ of 6.4 ns and 7.6 ns have been recorded for $CpMn(CO)_2$(2-aminoanthracenyl) and 2-aminoanthracene in THF respectively. The quantum yield determined for the Mn-centered radical is 0.6, which is essentially the same as the corresponding value for free 2-aminoanthracene. The similarity in the spectral properties suggests that the $CpMn(CO)_2$ moiety couples weakly with the anthracene fluorophore and hence enables equally high quantum yield to be exhibited by $CpMn(CO)_2$(2-aminoanthracenyl) as well.

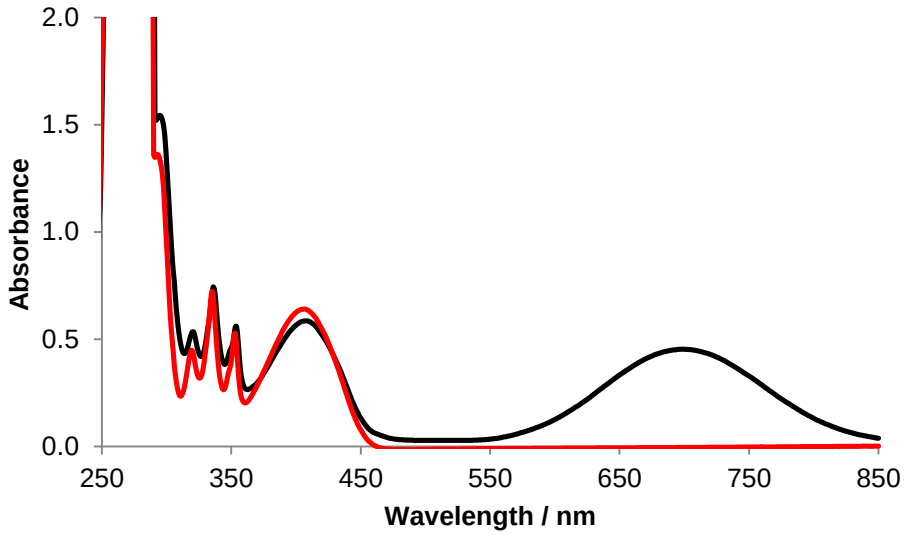

Figure 5.3 UV-vis absorption spectra of $CpMn(CO)_2$(2-aminoanthracenyl) radical (black) and 2-aminoanthracene (red) in THF

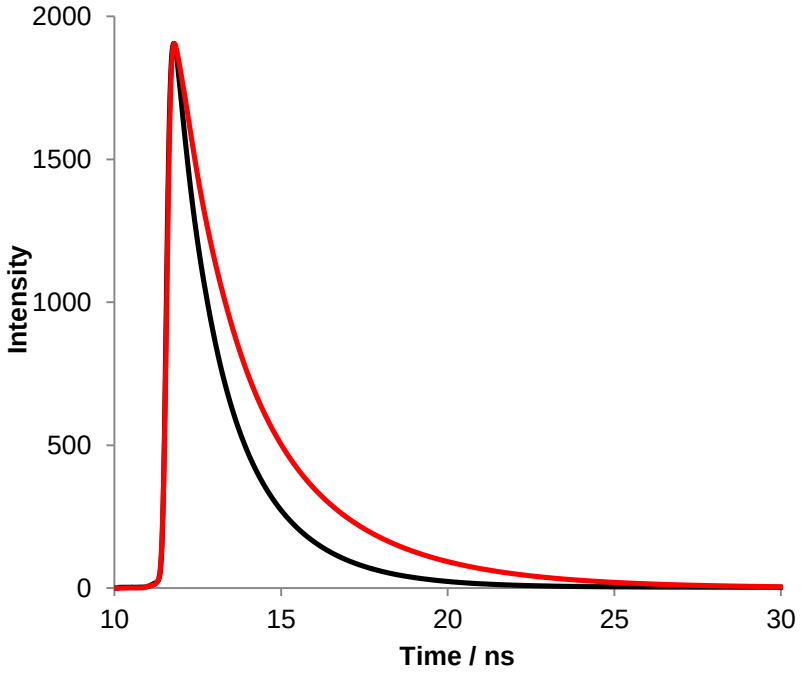

Figure 5.4 Time-resolved emission (λ_{exc} = 350 nm) spectra of $CpMn(CO)_2$(2-aminoanthracenyl) radical (black) and 2-aminoanthracene (red) in THF

5.2.2 Sensing of Thiols

The metal complex is easily made by a modification of a previously reported method **[254]**. Briefly, a diglyme solution of cyclopentadienyl manganese tricarbonyl ($CpMn(CO)_3$) was irradiated with an equimolar volume of aniline. The resulting orange carbonyl complex after photolysis is rapidly oxidized when exposed to air, forming an intense blue-green solution containing the metal radical probe. The reaction scheme is outlined in **Figure 5.5**.

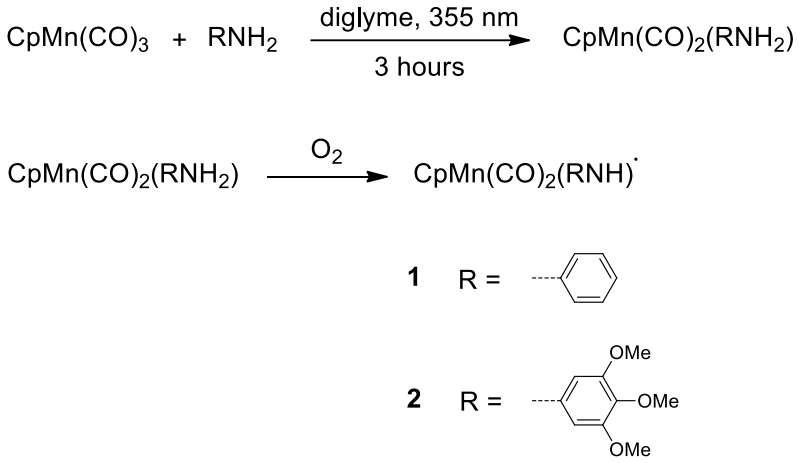

Figure 5.5 Reaction scheme for the synthesis of the radical probe, **1** and **2**

The sensitivity of **1** towards aliphatic thiols is first evaluated. The UV-vis spectrum (**Figure 5.6**) shows a broad absorption in the visible region with λ_{max} centered at 672 nm. This absorption has previously been described as a ligand-to-metal charge transfer (LMCT) transition from the anilinyl ring onto the Mn center **[245]**. The addition of an aliphatic thiol rapidly turns the solution dark red and produces a new absorption peak at 510 nm due to the formation of the $CpMn(CO)_2$(-SR) radical complex**[246]**. As the reaction progresses, a near isosbestic point at approximately 555 nm is observed indicating the clean conversion of **1** to the red complex. The visual colour changes are displayed in **Figure 5.7 a–b**.

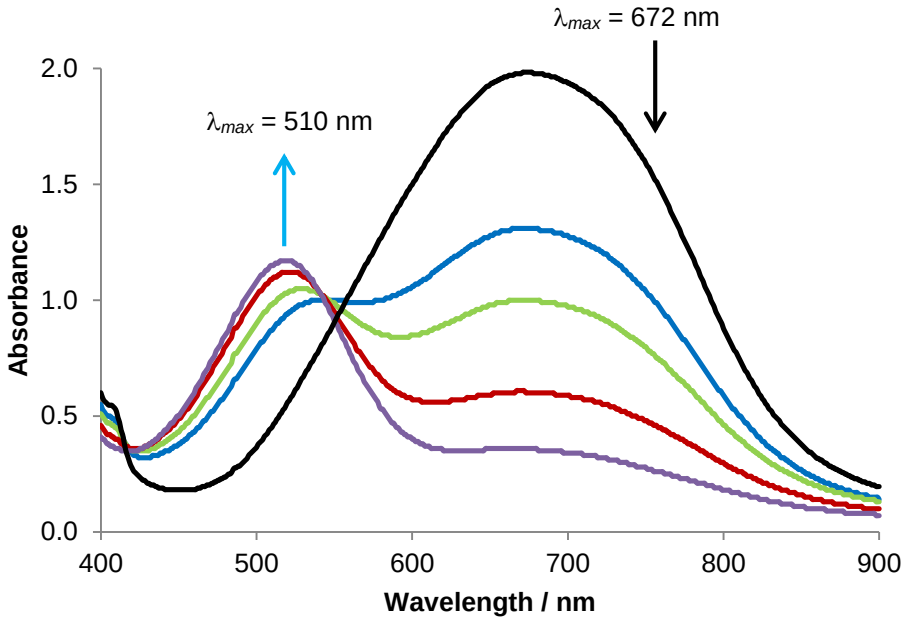

Figure 5.6 Changes in UV-vis spectrum upon addition of 0.50 mM of 1-octanethiol to 0.80 mM of 1 in diglyme monitored over 20 minutes at 1-minute interval.The black line represents the initial absorbance of **1**.

The detection of biological thiols such as cysteine, homocysteine and glutathione is also attempted by adding a drop of the blue diglyme solution containing **1** into an aqueous solution containing the thiol. As diglyme and water are miscible, a resultant homogeneous red solution is observed for both cysteine and homocysteine (**Figure 5.7**, **a–d)**. However, there is no colour change associated with glutathione, which could be a result of steric bulk hindering the formation of the thiol complex and subsequently, the radical (**Figure 5.7**, **a–e**). Nevertheless the negative result may be useful for distinguishing between glutathione and either cysteine or homocysteine.

Figure 5.7 Colour changes to the $CpMn(CO)_2$(anilinyl) radical **1** (0.50 mM) observed upon addition of 0.5 mM of the molecule to be detected. (a) **1** only (b) 1-octanethiol (c) *p*-thiocresol (d) cysteine (e) glutathione (f) phenylhydrazine.

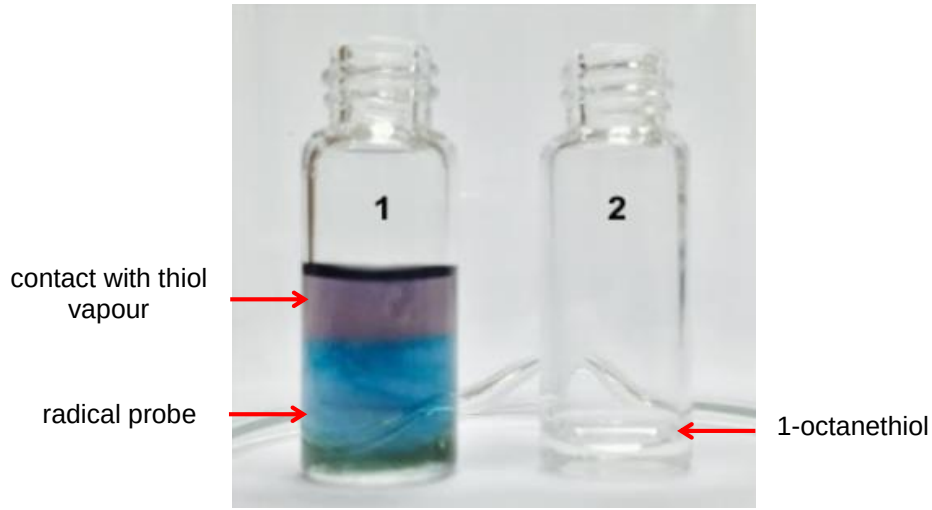

Figure 5.8 Colour change of **1** (vial 1) when exposed to vapours diffusing out of vial 2 containing 1-octanethiol. The purple colouration observed is the result of a colour combination of the red $CpMn(CO)_2(SR)$ radical and the blue complex **1**.

The addition of an aromatic thiol, *p*-thiocresol, to a solution containing 1 produces a darker blue coloration (**Figure 5.7c**). If the thiol concentration is very low, it becomes difficult to ascertain whether a reaction has indeed taken place due to the same shade of blue being produced. In this case, we have used

the lighter blue radical complex **2** as the sensor so that the difference in the colours is more pronounced. Compared to 1, the λ_{max} of the absorption of complex **2** is red-shifted to 714 nm. Upon the addition of *p*-thiocresol, the UV-vis spectrum rapidly changes and shows the appearance of two peaks at 614 nm and 480 nm which are assigned to $CpMn(CO)_2(-SC_6H_4CH_3)$, in agreement with previously published data **[246]**. An isosbestic point is also observed close to 600 nm indicating the clean conversion of **2** to $CpMn(CO)_2(-SC_6H_4CH_3)$ (**Figure 5.5**).

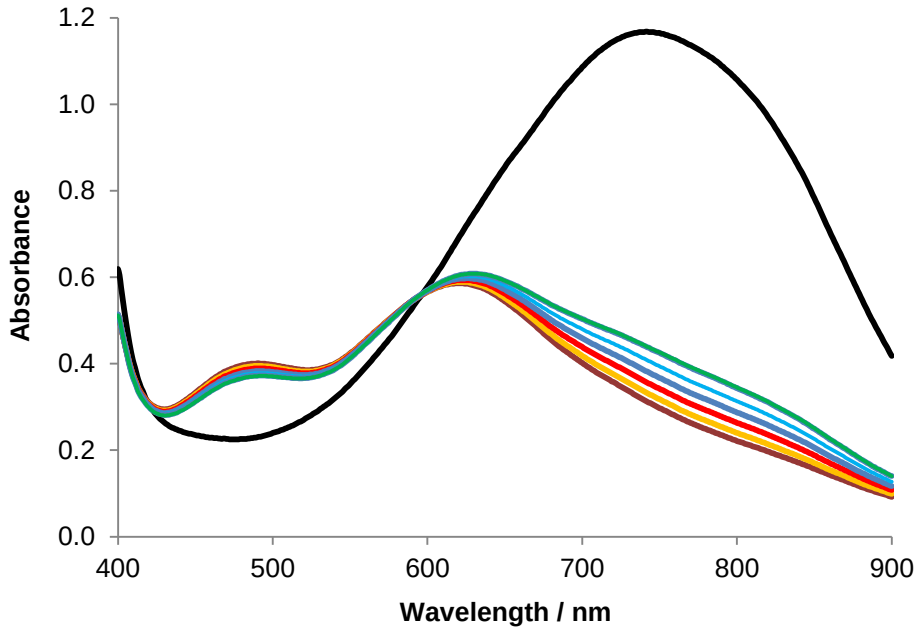

Figure 5.9 Changes in UV-vis spectrum upon addition of 0.20 mM of *p*-thiocresol to 0.50 mM of **2** in diglyme monitored over 10 minutes at 1-minute interval. The black line represents the initial absorbance of **2**.

5.2.3 Sensing of Hydrazines

Both **1** and **2** do not respond to the presence of aliphatic amines. However a test with hydrazine or phenylhydrazine gives a colour change from blue to orange-red, suggesting that **1** or **2** is selective towards hydrazines and not

amines (**Figure 5.7f**). Similar to the thiol case, an isosbestic point is observed near 550 nm in the UV-vis absorption spectrum showing a clean conversion of **1** to the $CpMn(CO)_2(NHNHPh)$ radical complex which absorbs at λ_{max} = 498 nm (**Figure 5.10**).

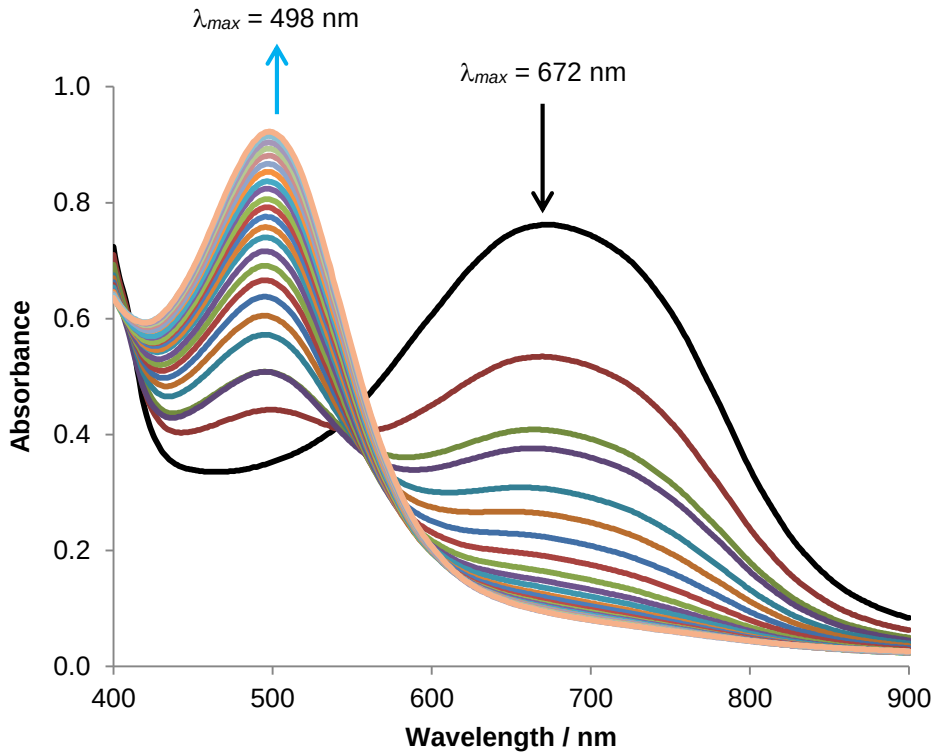

Figure 5.10 Changes in UV-vis spectrum upon addition of 0.35 mM of phenylhydrazine to 0.30 mM of **1** in diglyme monitored over 2 hours at 5-minute interval. The black line represents the initial absorbance of **1**.

5.2.4 Determination of Limits of Detection

The detection limit of **1** or **2** towards thiol detection is then assessed via visual inspection and UV-vis absorption spectroscopy. We have found that it is possible to observe the colour change from blue to red with the addition of only 0.1 mM (~15 ppm) of 1-octanethiol, with **1** in a slight excess. Furthermore, a solution of 1 changes colour when exposed to the vapour emitted by a solution of 1-octanethiol (**Figure 5.8**). Thus **1** can even be exploited as a visual thiol vapour detector. However, a more quantitative

determination of the detection limit has been carried out where the spectral absorbances of the generated radical complexes are measured (**Figure 5.11**).

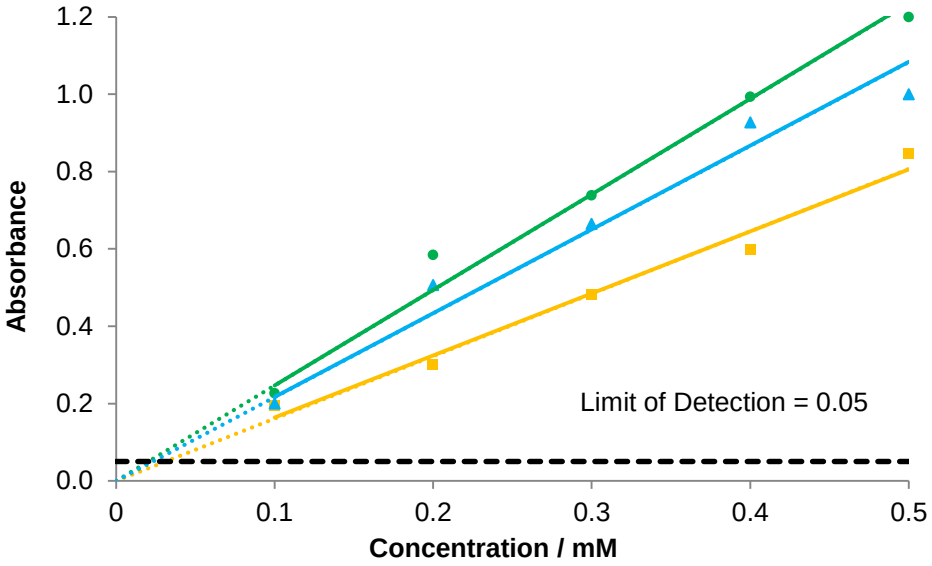

Figure 5.11 Absorbance vs concentration plot for 1-octanethiol (green), *p*-thiocresol (blue) and phenylhydrazine (orange). **1** is used for 1-octanethiol and phenylhydrazine sensing while **2** is used for *p*-thiocresol sensing. UV measurements were made under room temperature conditions using varying concentrations of the analyte.

The detection limits for 1-octanethiol, *p*-thiocresol (an aromatic thiol) and phenylhydrazine, have been determined to be 3.0 ppm, 2.9 ppm and 3.4 ppm respectively (**Figure 5.11**). As the absorption band of the complex is broad, the value chosen for estimation of the detection limits cannot be too low as it will introduce a small background contributed by the tailing end of the absorption band. Hence, a value of 0.05 absorbance units was chosen to maintain a good signal to noise ratio as well as to minimize signal contribution from the radical probe.

5.2.5 Computational Analysis of 1 with Thiols and Hydrazines

Although related radical complexes of **1** and **2** have been prepared and structurally characterised, their reactivities towards organic molecules have not been investigated before [245, 246]. Using the reaction of **1** with a thiol as an example (**Scheme 5.2**), we believe that the first step of the reaction is a hydrogen atom (of the S-H bond) abstraction by **1**. This regenerates the N-H bond of the aniline ligand which is subsequently displaced by the incoming thio radical. For the reaction to proceed spontaneously, the S-H bond has to be weaker than the aniline N-H bond. Similarly, the differences in the reactivity of **1** with other molecules can be traced mainly to the difference in the strength of the N-H bond of aniline and the corresponding bond of the other molecule.

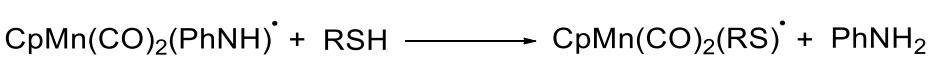

Scheme 5.2 The displacement of the anilinyl moiety of **1** with a thiol.

In order to better understand how **1** and **2** are able to sense thiols and hydrazines through reactions, the enthalpy and free energy changes of these reactions have been computed using density functional method in **Table 5.1** courtesy of Associate Professor Fan Wai Yip. To reduce computational time, the aliphatic thiol, aromatic thiol and hydrazine molecules are represented by their simplest members which are methanethiol, benzenethiol and hydrazine. Complex **1** is used to represent the sensor. To reduce computation time, the molecular structures are first optimized using the smaller basis set at b3lyp/lanl2dz level before single-point energy calculations are carried out using a larger basis set 6-311+g(d,p) in the Gaussian 09 suite of programs. The larger basis set was used after optimization has been completed since

subsequent calculations were only based on a single optimized structure. More importantly, as we are only interested in the trend rather than absolute values of the thermodynamic parameters, the use of two different basis sets would have little implications on the eventual conclusion.

Table 5.1 Enthalpies and free energies of reactions. The values are calculated using b3lyp/lanl2dz (structure optimization) followed by b3lyp/6-311+g** (single point energy). [Mn] = $CpMn(CO)_2$ moiety.

	ΔH $kJmol^{-1}$	ΔG $kJmol^{-1}$
[Mn]-NHPh + CH_3SH → [Mn]-SCH_3 + NH_2Ph	-73.2	-78.2
[Mn]-NHPh + N_2H_4 → [Mn]-$NHNH_2$ + NH_2Ph	-21.7	-30.6
[Mn]-NHPh + PhSH → [Mn]-SPh + NH_2Ph	-73.1	-72.2

Table 5.1 shows that the three substitution reactions have been calculated to be exothermic and exergonic as well, with the thiol reactions more spontaneous than the hydrazine counterpart. The aliphatic and aromatic S-H and hydrazine N-H bond energies are indeed low enough for 1 to act as a thiol and hydrazine sensor. The calculations are also in agreement with typical experimental dissociation energies (BDE) of the X-H bond (where X = S or N) which are in the order; aromatic N-H 380 $kJmol^{-1}$ > aliphatic S-H 350 $kJmol^{-1}$ > aromatic S-H 345 $kJmol^{-1}$ > hydrazine N-H 303 $kJmol^{-1}$ [151]. However, attempts at locating the transition state of the reaction are unsuccessful; hence we are unable to obtain values for the activation barriers.

5.3 Conclusion

In conclusion, a dark blue cyclopentadienyl manganese dicarbonyl anilinyl radical complex has been developed as a rapid and sensitive colorimetric thiol

and hydrazine sensor with sensitivity limits approaching 3 ppm. This complex is stable and easily prepared and can distinguish between the amino acid cysteine and the tripeptide glutathione, both biological thiols present in mammals. It has also be demonstrated that the probe can also be used to distinguish between hydrazine and amines, which is important considering that hydrazine are ubiquitous in our environment and is considered a toxic air pollutant. The measurements for the limits of detection for the thiols and hydrazine have been made via UV-vis spectroscopy and have shown to be in the low ppm region, suggesting that this probe is highly sensitive towards the presence of the respective analytes.

5.4 Experimental

5.4.1 Materials

Cyclopentadienyl manganese tricarbonyl ($CpMn(CO)_3$, 98%) was purchased from Alfa Aesar. 1-octanethiol, *p*-thiocresol, glycine, phenylhydrazine, aniline, 3,4,5-trimethoxyaniline, homocysteine, cysteine, reduced glutathione were purchased from Sigma Aldrich. Diethylene glycol dimethyl ether (diglyme) was purchased from Merck. All solvents and reagents were used without further purification.

5.4.2 Instrumentation and Methods

Photochemical experiments were conducted with Nd-YAG pulsed laser system (Quantel Brilliant B, 10ns pulse, 355 nm). All infrared (IR) absorption spectra were obtained on a Shimadzu IR Prestige-21 spectrometer, using a 0.1 mm path length CaF_2 cell for liquid samples. UV-vis absorption spectroscopy was carried out using a Shimadzu UV-1600 Series spectrometer with a 1 cm

path length quartz cell. Fluorescence spectroscopy was carried out with a Perkin Elmer LS-55 Luminescence Spectrometer while time-resolved fluorescence spectroscopy was carried out with a Horiba Jobin Yvon Fluorolog spectrometer. Continuous wave X-band ESR spectra in THF were obtained in a silica flat cell with a Bruker ELEXSYS E500 spectrometer using a variable-temperature Bruker liquid nitrogen cryostat.

5.4.3 Preparation of $CpMn(CO)_2$(2-aminoanthracenyl) radical

1 mole equivalent of $CpMn(CO)_3$ was dissolved in 2 ml of THF and irradiated at 355 nm for 10 minutes, affording a red solution. 3 mole equivalent of 2-aminoanthracene was then added, and the solution turned orange-yellow. The solution was either exposed to air or treated with 30% H_2O_2 (1 ml) and its colour gradually became green. The reaction mixture was further purified with column chromatography with silica as the stationary phase and ethyl acetate as the mobile phase. The green solid was collected and dried in air. IR (THF, υ_{max}, cm^{-1}): 1892, 1940. Anal. calcd. for C21H16MnNO2: (%): C 68.30, H 4.37, N 3.79, Mn 14.88; found: C 69.8, H 7.0, N 3.5, Mn 12.8.

5.4.4 Preparation of $CpMn(CO)_2(NHR)$ radicals (R=C_6H_5 (1) and $C_6H_2(OMe)_3$ (2))

All reactions were carried out using standard vacuum line and Schlenk techniques unless otherwise stated. 15 mg of $CpMn(CO)_3$ was dissolved in 4 ml of diglyme. Two molar equivalent of $PhNH_2$ (aniline) was then added before the flask was evacuated. The reaction mixture was then subjected to laser photolysis at 355 nm for 120 minutes upon which an orange solution of $CpMn(CO)_2(PhNH_2)$ was obtained. IR (diglyme, υ_{max}, cm^{-1}): 1916, 1842.

Oxidation of the complex to the $CpMn(CO)_2(NHPh)$ was performed by breaking the vacuum and allowing passage of air into the flask. A colour change from the orange to an intense dark blue solution was immediately observed. IR (diglyme, υ_{max}, cm^{-1}): 1959, 1904. The same method was applied to the preparation of the $CpMn(CO)_2$(trimethoxyanilinyl) radical. IR (diglyme, υ_{max}, cm^{-1}): 1949, 1894.

5.4.5 Stability Studies of 1 and 2

Stability of the radical was determined by monitoring the UV-vis spectrum over 5 days under atmospheric conditions. Briefly, a 0.1 mM solution of both sensors was prepared in diglyme and placed in an isolated fume cabinet not used for the handling of thiols and hydrazines. Their respective UV-spectrum was then obtained at the same time of the day over a period of 7 days. No significant changes to the colour or their UV-spectrum were observed.

5.4.6 UV-vis Absorption Measurements

An initial UV-vis absorption spectrum was recorded for a solution containing 0.80 mM of **1** in 4 ml of diglyme. Following that, 0.50 mM of 1-octanethiol was added and the solution was thoroughly mixed before recording the change in the spectrum. Subsequent measurements were taken at 1-minute interval for 20 minutes. The time period was chosen such that the final spectrum showed very little or no change in the band intensities. A similar procedure was repeated to acquire the UV-vis spectrum in the case of *p*-thiocresol with complex **2** and phenylhydrazine with complex **1** over the appropriate time interval and period. For the detection of water soluble thiols and hydrazines such as cysteine, glutathione and hydrazine hydrate, a 0.1mM solution of the

respective analyte was prepared and subjected to detection by the sensor. In all cases, the detection was performed under atmospheric conditions using the same concentration of complex **1** or **2**. Even though the kinetics of detection varies among the different analytes, the detection limit does not depend on the reaction time because the final product is stable for more than 24 hours to allow detection via UV-vis spectrophotometry.

5.4.7 Sensitivity Limit Calibration

Differing concentrations (0.1 mM to 0.5 mM) of 1-octanethiol in 5 cm^3 of diglyme were prepared in separate flasks. A 0.5 cm^3 diglyme solution containing complex **1** was then added to each flask such that the thiol was reacted completely. Only a slight excess of **1** was used in each case in order to minimize background contribution from the absorbance of **1** itself. The UV-vis spectrum of the product was then recorded to detect and measure the $CpMn(CO)_2(SR)$ peak absorbance at 510nm. A graph showing the absorbance vs thiol concentration was plotted, as shown in Figure 5. The same procedure was carried out to obtain the calibration plots for phenylhydrazine and *p*-thiocresol. Calculations of the detection limit were performed as follow: First, the equation for the calibration curve was obtained via linear regression. The equation is then equated to a *y*-value of 0.02 as the detection limit. From there, solving the equation for *x* gives the minimum concentration of the analyte that can be detected. The concentration is then converted to units of ppm. For *p*-thiocresol, complex **2** was used as the colorimetric sensor. An example of the calculation is shown below.

For phenylhydrazine, the equation of the curve obtained is $y = 1.6132x$ where *y* is the absorbance and *x* is the concentration in millimolar. A detection limit

of y = 0.05 is chosen because this minimizes contributions from the background as well as any residual absorbance presented from the sensor itself.

Thus, the calculations for determining the limit of detection is done by setting y = 0.05 in the above equation. Therefore,

$0.05 = 1.6132x$

Solving for x yields x = 0.03099 mM.

The molar mass of phenylhydrazine is 108.14 g mol^{-1}.

Mass of phenylhydrazine in 1 dm^3 = $0.03099 \times 10^{-3} \times 108.14 =$ **3.35×10^{-3} g**

We define the unit of ppm as 1 mg of solute in 1 liter of solution; therefore the detection limit for phenylhydrazine is thus 3.35 ppm ≈ 3.4ppm.

The same method is used to calculate the detection limit for 1-octanethiol and *p*-thiocresol.

5.4.8 Real Time Monitoring

A vial of 0.1 mL 1-octanethiol to simulate the presence atmospheric thiols is placed at an arbitrary distance of 1.5 meter away from another vial containing 0.1 mM of sensor **1**. The time taken for the sensor to change colour is monitored and the absorbance measured with a UV-vis spectrometer.

Chapter 6

Conclusions and Future Work

In conclusion, we have demonstrated that organometallic complexes can be used in the field of anti-cancer, in thiol sensing, and as CO and H_2S releasing agents. In the area of anti-cancer drug discovery, a class of iron containing cyclopentadienyl complex was found to exhibit low micromolar cytotoxicity towards both the breast cancer cell line MDA-MB-231 and cervical cancer cell line HeLa. Flow cytometry and confocal microscopy investigations have strongly suggested that cell death occurs by apoptosis and not necrosis. The complex with the lowest IC_{50} value, designated as the lead complex, was selected for membrane permeability and metabolic stability studies. The results were promising as they indicate that the lead complex is highly stable *in vitro* and very permeable across a lecithin barrier.

This class of cytotoxic iron complexes was then further modified by changing a part of the molecule one at a time to ascertain the effect of the substitution on the efficacy of the complex as an anti-cancer drug molecule. Interestingly, changing the metal to manganese reduces the cytotoxicity properties of the molecule but switching iron to cobalt completely shuts down the anti-proliferative properties. Modifications to the carbonyl and cyclopentadienyl ligands also resulted in the loss of the anti-proliferation property. It is also noteworthy that upon changing the metal to manganese, the complexes are no longer as selective as the iron based complexes towards normal cell lines.

Nonetheless, exactly how the iron complexes induce apoptosis while leaving normal cells unharmed is still a question to be answered. Even though a Fenton type mechanism was postulated, this theory was not verified with ROS assays. Further, the manganese complexes have shown to exhibit appreciable cytotoxicity but do not possess the selectivity of the iron complexes. Is it possible then when both metals are combined in a single complex as part of the future work, will it lead to increased selectivity and potency? These are some questions that can be answered by further synthetic and biological experiments.

The second area where organometallic carbonyl complexes can be employed is in their capabilities as CO and H_2S releasing molecules. On their own, transition metal carbonyl complexes are well known to release CO upon UV irradiation. By modifying the ligands around the metal center, we have designed several molecules that can release both CO and H_2S separately under different conditions. In addition, these complexes are water soluble and do not exhibit cytotoxicity towards normal mammary cells, suggesting that these

complexes may be appropriate for use *in vivo* studies. However, while these complexes possess such desirable properties, they are regrettably not as air stable as existing H_2S and CO releasing molecules. In addition, the effectiveness of these compounds as CO and H_2S releasing agents has not been validated. Nonetheless, as the research on these gasotransmitters is still relatively new compared to studies on their nitric oxide counterpart, there exist many possibilities for further investigations and studies in the development of novel, stable and non-toxic organometallic carbonyl complexes as CO and H_2S releasing agents.

Lastly, organometallic carbonyl complexes were then applied to the area of thiol sensing. Employing UV-vis techniques for qualitative and quantitative measurements, we are able to distinguish between two different naturally occurring thiols in a mammalian system – cysteine and glutathione. The complex used for the sensing experiments was then subsequently applied in the detection of hydrazine. Unfortunately, the probe failed to distinguish between aliphatic and aromatic hydrazines but only indicates the presence of hydrazines in general. Further studies would be required to fine tune the selectivity of the probe towards aliphatic and aromatic hydrazines.

Bibliography

[1] G. Jaouen, A. Vessieres, in: Pure Appl. Chem., 1985, pp. 1865.
[2] S. Top, G. Jaouen, A. Vessieres, J.P. Abjean, D. Davoust, C.A. Rodger, B.G. Sayer, M.J. McGlinchey, Chromium tricarbonyl complexes of estradiol derivatives: differentiation of .alpha.- and .beta.-diastereoisomers using 1- and 2-dimensional NMR spectroscopy at 500 MHz, Organometallics, 4 (1985) 2143-2150.
[3] E.S. Antonarakis, A. Emadi, Ruthenium-based chemotherapeutics: are they ready for prime time?, Cancer Chemother. Pharmacol., 66 (2010) 1-9.
[4] A. Bergamo, G. Sava, Ruthenium anticancer compounds: myths and realities of the emerging metal-based drugs, Dalton Trans., 40 (2011) 7817-7823.
[5] S.J. Dougan, A. Habtemariam, S.E. McHale, S. Parsons, P.J. Sadler, Catalytic organometallic anticancer complexes, Proc. Natl. Acad. Sci. U. S. A., 105 (2008) 11628-11633.
[6] M.J. Abrams, A. Davison, A.G. Jones, C.E. Costello, H. Pang, Synthesis and characterization of hexakis(alkyl isocyanide) and hexakis(aryl isocyanide) complexes of technetium(I), Inorg. Chem., 22 (1983) 2798-2800.
[7] G. Jaouen, S. Top, A. Vessières, R. Alberto, New paradigms for synthetic pathways inspired by bioorganometallic chemistry, J. Organomet. Chem., 600 (2000) 23-36.
[8] J.E. Clark, P. Naughton, S. Shurey, C.J. Green, T.R. Johnson, B.E. Mann, R. Foresti, R. Motterlini, Cardioprotective Actions by a Water-Soluble Carbon Monoxide–Releasing Molecule, Circ. Res., 93 (2003) e2-e8.
[9] H.T. Poh, B.T. Sim, T.S. Chwee, W.K. Leong, W.Y. Fan, The Dithiolate-Bridged Diiron Hexacarbonyl Complex Na2[(μ-SCH2CH2COO)Fe(CO)3]2 as a Water-Soluble PhotoCORM, Organometallics, 33 (2014) 959-963.
[10] R. Motterlini, J.E. Clark, R. Foresti, P. Sarathchandra, B.E. Mann, C.J. Green, Carbon Monoxide-Releasing Molecules: Characterization of Biochemical and Vascular Activities, Circ. Res., 90 (2002) e17-e24.
[11] L. Li, M. Whiteman, Y.Y. Guan, K.L. Neo, Y. Cheng, S.W. Lee, Y. Zhao, R. Baskar, C.H. Tan, P.K. Moore, Characterization of a novel, water-soluble hydrogen sulfide-releasing molecule (GYY4137): new insights into the biology of hydrogen sulfide, Circulation, 117 (2008) 2351-2360.
[12] W. Guo, Z.-y. Cheng, Y.-z. Zhu, Hydrogen sulfide and translational medicine, Acta pharmacologica Sinica, 34 (2013) 1284-1291.
[13] H. Kimura, Hydrogen sulfide as a neuromodulator, Mol. Neurobiol., 26 (2002) 13-19.
[14] J.L. Burgaud, J.P. Riffaud, P. Soldato, Nitric-Oxide Releasing Molecules : A New Class of Drugs with Several Major Indications, Curr. Pharm. Des., 8 (2002) 201-213.
[15] C.E. Anson, T.J. Baldwin, C.S. Creaser, M.A. Fey, G.R. Stephenson, IR-Active Organometallic pH Probes, Organometallics, 15 (1996) 1451-1456.
[16] C.S. Creaser, W.E. Hutchinson, R.G. Stephenson, Molecular Sensing via an Immobilized Organometalcarbonyl Probe Group, Appl. Spectrosc., 54 (2000) 1624-1628.
[17] C.S. Creaser, W.E. Hutchinson, G.R. Stephenson, An attenuated total reflectance optrode sensor incorporating infrared-active carbonylmetal probe groups, SENSORS AND ACTUATORS B, 82 (2002) 150-157.

[18] M. Cais, S. Dani, Y. Eden, O. Gandolfi, M. Horn, E.E. Isaacs, Y. Josephy, Y. Saar, E. Slovin, L. Snarsky, Metalloimmunoassay, Nature, 270 (1977) 534-535.
[19] R.S. Yalow, S.A. Berson, IMMUNOASSAY OF ENDOGENOUS PLASMA INSULIN IN MAN, The Journal of clinical investigation, 39 (1960) 1157-1175.
[20] R.S. Yalow, S.A. Berson, Assay of Plasma Insulin in Human Subjects by Immunological Methods, Nature, 184 (1959) 1648-1649.
[21] E. Palek, M. Fojta, Peer Reviewed: Detecting DNA Hybridization and Damage, Analytical chemistry, 73 (2001) 74 A-83 A.
[22] I. Willner, Biomaterials for Sensors, Fuel Cells, and Circuitry, Science, 298 (2002) 2407-2408.
[23] T.G. Drummond, M.G. Hill, J.K. Barton, Electrochemical DNA sensors, Nat Biotech, 21 (2003) 1192-1199.
[24] E.J. Lyon, S. Shima, G. Buurman, S. Chowdhuri, A. Batschauer, K. Steinbach, R.K. Thauer, UV-A/blue-light inactivation of the 'metal-free' hydrogenase (Hmd) from methanogenic archaea, European Journal of Biochemistry, 271 (2004) 195-204.
[25] J. Hirsch, S. DeBeer George, E.I. Solomon, B. Hedman, K.O. Hodgson, J.N. Burstyn, Raman and Extended X-ray Absorption Fine Structure Characterization of a Sulfur-Ligated Cu(I) Ethylene Complex: Modeling the Proposed Ethylene Binding Site of Arabidopsis thaliana ETR1, Inorganic chemistry, 40 (2001) 2439-2441.
[26] A.B. Bleecker, H. Kende, Ethylene: A Gaseous Signal Molecule in Plants, Annual Review of Cell and Developmental Biology, 16 (2000) 1-18.
[27] P.C. Dos Santos, D.R. Dean, Y. Hu, M.W. Ribbe, Formation and Insertion of the Nitrogenase Iron−Molybdenum Cofactor, Chemical reviews, 104 (2004) 1159-1174.
[28] S.C. Lee, R.H. Holm, The Clusters of Nitrogenase: Synthetic Methodology in the Construction of Weak-Field Clusters, Chemical reviews, 104 (2004) 1135-1158.
[29] D. Cram, The design of molecular hosts, guests, and their complexes, Science, 240 (1988) 760-767.
[30] A.V. Eliseev, H.-J. Schneider, Molecular Recognition of Nucleotides, Nucleosides, and Sugars by Aminocyclodextrins, Journal of the American Chemical Society, 116 (1994) 6081-6088.
[31] L.A. Loeb, C.C. Harris, Advances in Chemical Carcinogenesis: A Historical Review and Prospective, Cancer Res., 68 (2008) 6863-6872.
[32] A. Perez-Diez, A. Morgun, N. Shulzhenko, Microarrays for Cancer Diagnosis and Classification, Austin (TX): Landes Bioscience, Madame Curie Bioscience Database [Internet], 2000.
[33] A. Leonidova, G. Gasser, Underestimated Potential of Organometallic Rhenium Complexes as Anticancer Agents, ACS Chem. Biol., 9 (2014) 2180-2193.
[34] E.J. Emanuel, (2015, September 9), The Solution to Drug Prices, The New York Times, p. A31
[35] P.G. Corrie, Cytotoxic chemotherapy: clinical aspects, Medicine, 36 (2008) 24-28.
[36] Y. Jung, S.J. Lippard, Direct Cellular Responses to Platinum-Induced DNA Damage, Chem. Rev., 107 (2007) 1387-1407.

[37] P.J. Dyson, G. Sava, Metal-based antitumour drugs in the post genomic era, Dalton Trans., (2006) 1929-1933.
[38] C.G. Hartinger, N. Metzler-Nolte, P.J. Dyson, Challenges and Opportunities in the Development of Organometallic Anticancer Drugs, Organometallics, 31 (2012) 5677-5685.
[39] G. Gasser, I. Ott, N. Metzler-Nolte, Organometallic Anticancer Compounds, J. Med. Chem., 54 (2011) 3-25.
[40] G. Gasser, N. Metzler-Nolte, The potential of organometallic complexes in medicinal chemistry, Curr. Opin. Chem. Biol., 16 (2012) 84-91.
[41] M. Patra, G. Gasser, Organometallic compounds: an opportunity for chemical biology?, ChemBioChem, 13 (2012) 1232-1252.
[42] E. Hillard, A. Vessieres, L. Thouin, G. Jaouen, C. Amatore, Ferrocene-mediated proton-coupled electron transfer in a series of ferrocifen-type breast-cancer drug candidates, Angew Chem Int Ed Engl, 45 (2005) 285-290.
[43] Y. Wang, P. Pigeon, S. Top, M.J. McGlinchey, G. Jaouen, Organometallic Antitumor Compounds: Ferrocifens as Precursors to Quinone Methides, Angewandte Chemie International Edition, (2015) n/a-n/a.
[44] J.d.J. Cazares-Marinero, S. Top, A. Vessieres, G. Jaouen, Synthesis and antiproliferative activity of hydroxyferrocifen hybrids against triple-negative breast cancer cells, Dalton Trans., 43 (2014) 817-830.
[45] W.F. Schmid, R.O. John, V.B. Arion, M.A. Jakupec, B.K. Keppler, Highly Antiproliferative Ruthenium(II) and Osmium(II) Arene Complexes with Paullone-Derived Ligands, Organometallics, 26 (2007) 6643-6652.
[46] G. Mühlgassner, C. Bartel, W.F. Schmid, M.A. Jakupec, V.B. Arion, B.K. Keppler, Biological activity of ruthenium and osmium arene complexes with modified paullones in human cancer cells, J. Inorg. Biochem., 116 (2012) 180-187.
[47] L.K. Filak, S. Göschl, P. Heffeter, K. Ghannadzadeh Samper, A.E. Egger, M.A. Jakupec, B.K. Keppler, W. Berger, V.B. Arion, Metal–Arene Complexes with Indolo[3,2-c]-quinolines: Effects of Ruthenium vs Osmium and Modifications of the Lactam Unit on Intermolecular Interactions, Anticancer Activity, Cell Cycle, and Cellular Accumulation, Organometallics, 32 (2013) 903-914.
[48] D. Osella, H. Mahboobi, D. Colangelo, G. Cavigiolio, A. Vessières, G. Jaouen, FACS analysis of oxidative stress induced on tumour cells by SERMs, Inorg. Chim. Acta, 358 (2005) 1993-1998.
[49] S. Top, A. Vessières, G. Leclercq, J. Quivy, J. Tang, J. Vaissermann, M. Huché, G. Jaouen, Synthesis, Biochemical Properties and Molecular Modelling Studies of Organometallic Specific Estrogen Receptor Modulators (SERMs), the Ferrocifens and Hydroxyferrocifens: Evidence for an Antiproliferative Effect of Hydroxyferrocifens on both Hormone-Dependent and Hormone-Independent Breast Cancer Cell Lines, Chemistry – A European Journal, 9 (2003) 5223-5236.
[50] M. Domínguez-García, C. Ortega-Zúñiga, E. Meléndez, New tungstenocenes containing 3-hydroxy-4-pyrone ligands: antiproliferative activity on HT-29 and MCF-7 cell lines and binding to human serum albumin studied by fluorescence spectroscopy and molecular modeling methods, Journal of biological inorganic chemistry : JBIC : a publication of the Society of Biological Inorganic Chemistry, 18 (2013) 195-209.

[51] J. Fernández-Gallardo, B.T. Elie, F.J. Sulzmaier, M. Sanaú, J.W. Ramos, M. Contel, Organometallic Titanocene–Gold Compounds as Potential Chemotherapeutics in Renal Cancer. Study of their Protein Kinase Inhibitory Properties, Organometallics, 33 (2014) 6669-6681.
[52] P.M. Abeysinghe, M.M. Harding, Antitumour bis(cyclopentadienyl) metal complexes: titanocene and molybdocene dichloride and derivatives, Dalton Trans., 0 (2007) 3474-3482.
[53] A.J. Salmon, M.L. Williams, A. Innocenti, D. Vullo, C.T. Supuran, S.-A. Poulsen, Inhibition of carbonic anhydrase isozymes I, II and IX with benzenesulfonamides containing an organometallic moiety, Bioorg. Med. Chem. Lett., 17 (2007) 5032-5035.
[54] P. Kalaivani, R. Prabhakaran, F. Dallemer, K. Natarajan, Photophysical properties and in vitro cytotoxicity studies of new Ru(ii) carbonyl complexes and mixed geometrical Ru(ii)-Ni(ii) complex in HS-DNA/BSA protein and human lung (A549) and liver (HepG2) cells, RSC Advances, 4 (2014) 51850-51864.
[55] A. Mishra, H. Jung, J.W. Park, H.K. Kim, H. Kim, P.J. Stang, K.W. Chi, Anticancer Activity of Self-Assembled Molecular Rectangles via Arene-Ruthenium Acceptors and a New Unsymmetrical Amide Ligand, Organometallics, 31 (2012) 3519-3526.
[56] D.-L. Ma, C.-M. Che, F.-M. Siu, M. Yang, K.-Y. Wong, DNA Binding and Cytotoxicity of Ruthenium(II) and Rhenium(I) Complexes of 2-Amino-4-phenylamino-6-(2-pyridyl)-1,3,5-triazine, Inorg. Chem., 46 (2007) 740-749.
[57] K.V. Kong, W.K. Leong, S.P. Ng, T.H. Nguyen, L.H. Lim, Osmium carbonyl clusters: a new class of apoptosis inducing agents, ChemMedChem, 3 (2008) 1269-1275.
[58] M. Hanif, M.V. Babak, C.G. Hartinger, Development of anticancer agents: wizardry with osmium, Drug Discovery Today, 19 (2014) 1640-1648.
[59] R. Crichton, The Importance of Iron for Biological Systems, in: Iron Metabolism, John Wiley & Sons, Ltd, 2009, pp. 17-58.
[60] N.C. Andrews, Forging a field: the golden age of iron biology, Blood, 112 (2008) 219-230.
[61] E. Nemeth, M.S. Tuttle, J. Powelson, M.B. Vaughn, A. Donovan, D.M. Ward, T. Ganz, J. Kaplan, Hepcidin Regulates Cellular Iron Efflux by Binding to Ferroportin and Inducing Its Internalization, Science, 306 (2004) 2090-2093.
[62] S.A. Shoichet, A.T. Bäumer, D. Stamenkovic, H. Sauer, A.F.H. Pfeiffer, C.R. Kahn, D. Müller-Wieland, C. Richter, M. Ristow, Frataxin promotes antioxidant defense in a thiol-dependent manner resulting in diminished malignant transformation in vitro, Hum. Mol. Genet., 11 (2002) 815-821.
[63] T.J. Schulz, R. Thierbach, A. Voigt, G. Drewes, B. Mietzner, P. Steinberg, A.F.H. Pfeiffer, M. Ristow, Induction of Oxidative Metabolism by Mitochondrial Frataxin Inhibits Cancer Growth: OTTO WARBURG REVISITED, J. Biol. Chem., 281 (2006) 977-981.
[64] R. Lill, B. Hoffmann, S. Molik, A.J. Pierik, N. Rietzschel, O. Stehling, M.A. Uzarska, H. Webert, C. Wilbrecht, U. Mühlenhoff, The role of mitochondria in cellular iron–sulfur protein biogenesis and iron metabolism, Biochimica et Biophysica Acta (BBA) - Molecular Cell Research, 1823 (2012) 1491-1508.
[65] W.B. Parker, Enzymology of Purine and Pyrimidine Antimetabolites Used in the Treatment of Cancer, Chem. Rev., 109 (2009) 2880-2893.

[66] G.A. Colditz, L.G. Branch, R.J. Lipnick, W.C. Willett, B. Rosner, B.M. Posner, C.H. Hennekens, Increased green and yellow vegetable intake and lowered cancer deaths in an elderly population, The American Journal of Clinical Nutrition, 41 (1985) 32-36.
[67] X. Wang, Y. Ouyang, J. Liu, M. Zhu, G. Zhao, W. Bao, F.B. Hu, Fruit and vegetable consumption and mortality from all causes, cardiovascular disease, and cancer: systematic review and dose-response meta-analysis of prospective cohort studies, BMJ, 349 (2014).
[68] Y. Choi, J.E. Lee, J.-M. Bae, Z.-M. Li, D.-H. Kim, M.-S. Lee, Y.-O. Ahn, M.-H. Shin, Vegetable Intake, but Not Fruit Intake, Is Associated with a Reduction in the Risk of Cancer Incidence and Mortality in Middle-Aged Korean Men, The Journal of Nutrition, 145 (2015) 1249-1255.
[69] Y. Zhang, P. Talalay, C.G. Cho, G.H. Posner, A major inducer of anticarcinogenic protective enzymes from broccoli: isolation and elucidation of structure, Proc. Natl. Acad. Sci. U. S. A., 89 (1992) 2399-2403.
[70] J.W. Fahey, Y. Zhang, P. Talalay, Broccoli sprouts: an exceptionally rich source of inducers of enzymes that protect against chemical carcinogens, Proc. Natl. Acad. Sci. U. S. A., 94 (1997) 10367-10372.
[71] G.H. Posner, C.G. Cho, J.V. Green, Y. Zhang, P. Talalay, Design and synthesis of bifunctional isothiocyanate analogs of sulforaphane: correlation between structure and potency as inducers of anticarcinogenic detoxication enzymes, J. Med. Chem., 37 (1994) 170-176.
[72] A.T. Dinkova-Kostova, W.D. Holtzclaw, R.N. Cole, K. Itoh, N. Wakabayashi, Y. Katoh, M. Yamamoto, P. Talalay, Direct evidence that sulfhydryl groups of Keap1 are the sensors regulating induction of phase 2 enzymes that protect against carcinogens and oxidants, Proc. Natl. Acad. Sci. U. S. A., 99 (2002) 11908-11913.
[73] Y.H. Ahn, Y. Hwang, H. Liu, X.J. Wang, Y. Zhang, K.K. Stephenson, T.N. Boronina, R.N. Cole, A.T. Dinkova-Kostova, P. Talalay, P.A. Cole, Electrophilic tuning of the chemoprotective natural product sulforaphane, Proc. Natl. Acad. Sci. U. S. A., 107 (2010) 9590-9595.
[74] P. Talalay, J.W. Fahey, Z.R. Healy, S.L. Wehage, A.L. Benedict, C. Min, A.T. Dinkova-Kostova, Sulforaphane mobilizes cellular defenses that protect skin against damage by UV radiation, Proc. Natl. Acad. Sci. U. S. A., 104 (2007) 17500-17505.
[75] L. Li, P. Rose, P.K. Moore, Hydrogen Sulfide and Cell Signaling, Annu. Rev. Pharmacol. Toxicol., 51 (2011) 169-187.
[76] B.D. Paul, S.H. Snyder, H2S signalling through protein sulfhydration and beyond, Nat. Rev. Mol. Cell Biol., 13 (2012) 499-507.
[77] K.D. Bloch, F. Ichinose, J.D. Roberts, Jr., W.M. Zapol, Inhaled NO as a therapeutic agent, Cardiovasc. Res., 75 (2007) 339-348.
[78] J.E. Keeble, P.K. Moore, Pharmacology and potential therapeutic applications of nitric oxide-releasing non-steroidal anti-inflammatory and related nitric oxide-donating drugs, Br. J. Pharmacol., 137 (2002) 295-310.
[79] T. Akaike, Role of free radicals in viral pathogenesis and mutation, Reviews in Medical Virology, 11 (2001) 87-101.
[80] R.O. Cannon, Role of nitric oxide in cardiovascular disease: focus on the endothelium, Clinical Chemistry, 44 (1998) 1809-1819.

[81] G. Favero, C. Paganelli, B. Buffoli, L.F. Rodella, R. Rezzani, Endothelium and Its Alterations in Cardiovascular Diseases: Life Style Intervention, BioMed Research International, 2014 (2014) 28.
[82] H.H.H.W. Schmidt, U. Walter, NO at work, Cell, 78 (1994) 919-925.
[83] C. Szabo, Hydrogen sulphide and its therapeutic potential, Nat Rev Drug Discov, 6 (2007) 917-935.
[84] J.L. Wallace, R. Wang, Hydrogen sulfide-based therapeutics: exploiting a unique but ubiquitous gasotransmitter, Nat Rev Drug Discov, 14 (2015) 329-345.
[85] W. Zhao, J. Zhang, Y. Lu, R. Wang, The vasorelaxant effect of H2S as a novel endogenous gaseous KATP channel opener, The EMBO Journal, 20 (2001) 6008-6016.
[86] K. Abe, H. Kimura, The possible role of hydrogen sulfide as an endogenous neuromodulator, The Journal of Neuroscience, 16 (1996) 1066-1071.
[87] R. Hosoki, N. Matsuki, H. Kimura, The Possible Role of Hydrogen Sulfide as an Endogenous Smooth Muscle Relaxant in Synergy with Nitric Oxide, Biochemical and biophysical research communications, 237 (1997) 527-531.
[88] S. Kubo, M. Kajiwara, A. Kawabata, Dual modulation of the tension of isolated gastric artery and gastric mucosal circulation by hydrogen sulfide in rats, Inflammopharmacol, 15 (2007) 288-292.
[89] M.Y. Ali, C.Y. Ping, Y.Y. Mok, L. Ling, M. Whiteman, M. Bhatia, P.K. Moore, Regulation of vascular nitric oxide in vitro and in vivo; a new role for endogenous hydrogen sulphide?, British journal of pharmacology, 149 (2006) 625-634.
[90] Y. Cheng, J.F. Ndisang, G. Tang, K. Cao, R. Wang, Hydrogen sulfide-induced relaxation of resistance mesenteric artery beds of rats, American Journal of Physiology - Heart and Circulatory Physiology, 287 (2004) H2316-H2323.
[91] B. Srilatha, P.G. Adaikan, P.K. Moore, Possible role for the novel gasotransmitter hydrogen sulphide in erectile dysfunction—a pilot study, European Journal of Pharmacology, 535 (2006) 280-282.
[92] R. d'Emmanuele di Villa Bianca, R. Sorrentino, P. Maffia, V. Mirone, C. Imbimbo, F. Fusco, R. De Palma, L.J. Ignarro, G. Cirino, Hydrogen sulfide as a mediator of human corpus cavernosum smooth-muscle relaxation, Proceedings of the National Academy of Sciences, 106 (2009) 4513-4518.
[93] N. Siebert, D. Cantré, C. Eipel, B. Vollmar, H2S contributes to the hepatic arterial buffer response and mediates vasorelaxation of the hepatic artery via activation of KATP channels, American Journal of Physiology - Gastrointestinal and Liver Physiology, 295 (2008) G1266-G1273.
[94] R. Motterlini, L.E. Otterbein, The therapeutic potential of carbon monoxide, Nat Rev Drug Discov, 9 (2010) 728-743.
[95] M. Bilban, A. Haschemi, B. Wegiel, B.Y. Chin, O. Wagner, L.E. Otterbein, Heme oxygenase and carbon monoxide initiate homeostatic signaling, J Mol Med (Berl), 86 (2008) 267-279.
[96] G.L. Bannenberg, H.L.A. Vieira, Therapeutic applications of the gaseous mediators carbon monoxide and hydrogen sulfide, Expert Opin. Ther. Pat., 19 (2009) 663-682.

[97] F.L. Thorp-Greenwood, An Introduction to Organometallic Complexes in Fluorescence Cell Imaging: Current Applications and Future Prospects, Organometallics, 31 (2012) 5686-5692.
[98] A.J. Amoroso, M.P. Coogan, J.E. Dunne, V. Fernandez-Moreira, J.B. Hess, A.J. Hayes, D. Lloyd, C. Millet, S.J.A. Pope, C. Williams, Rhenium fac tricarbonyl bisimine complexes: biologically useful fluorochromes for cell imaging applications, Chemical communications, (2007) 3066-3068.
[99] A. Coleman, C. Brennan, J.G. Vos, M.T. Pryce, Photophysical properties and applications of Re(I) and Re(I)–Ru(II) carbonyl polypyridyl complexes, Coordination Chemistry Reviews, 252 (2008) 2585-2595.
[100] V. Fernandez-Moreira, F.L. Thorp-Greenwood, M.P. Coogan, Application of d6 transition metal complexes in fluorescence cell imaging, Chemical communications, 46 (2010) 186-202.
[101] X. Wang, X. Wang, Z. Guo, Functionalization of Platinum Complexes for Biomedical Applications, Accounts of Chemical Research, 48 (2015) 2622-2631.
[102] V.W.-W. Yam, E.C.-C. Cheng, Highlights on the recent advances in gold chemistry-a photophysical perspective, Chemical Society Reviews, 37 (2008) 1806-1813.
[103] C.P. Bagowski, Y. You, H. Scheffler, D.H. Vlecken, D.J. Schmitz, I. Ott, Naphthalimide gold(i) phosphine complexes as anticancer metallodrugs, Dalton Transactions, (2009) 10799-10805.
[104] J.D. Finkelstein, J.J. Martin, Homocysteine, Int. J. Biochem. Cell Biol., 32 (2000) 385-389.
[105] M.T. Heafield, S. Fearn, G.B. Steventon, R.H. Waring, A.C. Williams, S.G. Sturman, Plasma cysteine and sulphate levels in patients with motor neurone, Parkinson's and Alzheimer's disease, Neurosci. Lett., 110 (1990) 216-220.
[106] D.W. Jacobsen, Homocysteine and vitamins in cardiovascular disease, Clin Chem, 44 (1998) 1833-1843.
[107] H. Refsum, P.M. Ueland, O. Nygard, S.E. Vollset, Homocysteine and cardiovascular disease, Annu. Rev. Med., 49 (1998) 31-62.
[108] T. Finkel, Oxidant signals and oxidative stress, Curr. Opin. Cell Biol., 15 (2003) 247-254.
[109] T. Finkel, N.J. Holbrook, Oxidants, oxidative stress and the biology of ageing, Nature, 408 (2000) 239-247.
[110] J.G. Ray, C.A. Laskin, Folic acid and homocyst(e)ine metabolic defects and the risk of placental abruption, pre-eclampsia and spontaneous pregnancy loss: A systematic review, Placenta, 20 (1999) 519-529.
[111] A.D. Smith, Homocysteine, B vitamins, and cognitive deficit in the elderly, Am. J. Clin. Nutr., 75 (2002) 785-786.
[112] G.L. Ellman, Tissue sulfhydryl groups, Arch. Biochem. Biophys., 82 (1959) 70-77.
[113] W. Chen, Y. Zhao, T. Seefeldt, X. Guan, Determination of thiols and disulfides via HPLC quantification of 5-thio-2-nitrobenzoic acid, J. Pharm. Biomed. Anal., 48 (2008) 1375-1380.
[114] C. Komuro, K. Ono, Y. Shibamoto, T. Nishidai, M. Takahashi, M. Abe, Rapid and simple method for quantitative determination of non-protein sulphydryls in mouse liver by reversed-phase high-performance liquid chromatography, J. Chromatogr., 338 (1985) 209-212.

[115] A.R. Elwaer, C.W. McLeod, K.C. Thompson, On-line separation and determination of bromate in drinking waters using flow injection ICP mass spectrometry, Anal. Chem., 72 (2000) 5725-5730.
[116] A. Zinellu, S. Sotgia, B. Scanu, M.F. Usai, A.G. Fois, V. Spada, A. Deledda, L. Deiana, P. Pirina, C. Carru, Simultaneous detection of N-acetyl-L-cysteine and physiological low molecular mass thiols in plasma by capillary electrophoresis, Amino Acids, 37 (2009) 395-400.
[117] M. Rafii, R. Elango, G. Courtney-Martin, J.D. House, L. Fisher, P.B. Pencharz, High-throughput and simultaneous measurement of homocysteine and cysteine in human plasma and urine by liquid chromatography-electrospray tandem mass spectrometry, Anal. Biochem., 371 (2007) 71-81.
[118] N. Burford, M.D. Eelman, D.E. Mahony, M. Morash, Definitive identification of cysteine and glutathione complexes of bismuth by mass spectrometry: assessing the biochemical fate of bismuth pharmaceutical agents, Chem Commun (Camb), (2003) 146-147.
[119] K. Amarnath, V. Amarnath, K. Amarnath, H.L. Valentine, W.M. Valentine, A specific HPLC-UV method for the determination of cysteine and related aminothiols in biological samples, Talanta, 60 (2003) 1229-1238.
[120] M. Wen, H. Liu, F. Zhang, Y. Zhu, D. Liu, Y. Tian, Q. Wu, Amorphous FeNiPt nanoparticles with tunable length for electrocatalysis and electrochemical determination of thiols, Chem Commun (Camb), (2009) 4530-4532.
[121] H.S. Jung, X. Chen, J.S. Kim, J. Yoon, Recent progress in luminescent and colorimetric chemosensors for detection of thiols, Chem. Soc. Rev., 42 (2013) 6019-6031.
[122] C. Yin, F. Huo, J. Zhang, R. Martinez-Manez, Y. Yang, H. Lv, S. Li, Thiol-addition reactions and their applications in thiol recognition, Chem. Soc. Rev., 42 (2013) 6032-6059.
[123] A.P. de Silva, H.Q. Gunaratne, T. Gunnlaugsson, A.J. Huxley, C.P. McCoy, J.T. Rademacher, T.E. Rice, Signaling Recognition Events with Fluorescent Sensors and Switches, Chem. Rev., 97 (1997) 1515-1566.
[124] X. Chen, T. Pradhan, F. Wang, J.S. Kim, J. Yoon, Fluorescent chemosensors based on spiroring-opening of xanthenes and related derivatives, Chem. Rev., 112 (2012) 1910-1956.
[125] Y. Yang, Q. Zhao, W. Feng, F. Li, Luminescent chemodosimeters for bioimaging, Chem. Rev., 113 (2013) 192-270.
[126] S. Sreejith, K.P. Divya, A. Ajayaghosh, A near-infrared squaraine dye as a latent ratiometric fluorophore for the detection of aminothiol content in blood plasma, Angew Chem Int Ed Engl, 47 (2008) 7883-7887.
[127] M.E. Moragues, R. Martinez-Manez, F. Sancenon, Chromogenic and fluorogenic chemosensors and reagents for anions. A comprehensive review of the year 2009, Chem. Soc. Rev., 40 (2011) 2593-2643.
[128] T.J. Tolbert, C.H. Wong, New methods for proteomic research: preparation of proteins with N-terminal cysteines for labeling and conjugation, Angew Chem Int Ed Engl, 41 (2002) 2171-2174.
[129] Z. Yao, X. Feng, C. Li, G. Shi, Conjugated polyelectrolyte as a colorimetric and fluorescent probe for the detection of glutathione, Chem Commun (Camb), (2009) 5886-5888.
[130] S. Ji, J. Yang, Q. Yang, S. Liu, M. Chen, J. Zhao, Tuning the intramolecular charge transfer of alkynylpyrenes: effect on photophysical

properties and its application in design of OFF-ON fluorescent thiol probes, J. Org. Chem., 74 (2009) 4855-4865.
[131] B. Tang, Y. Xing, P. Li, N. Zhang, F. Yu, G. Yang, A rhodamine-based fluorescent probe containing a Se-N bond for detecting thiols and its application in living cells, J. Am. Chem. Soc., 129 (2007) 11666-11667.
[132] H. Maeda, H. Matsuno, M. Ushida, K. Katayama, K. Saeki, N. Itoh, 2,4-Dinitrobenzenesulfonyl fluoresceins as fluorescent alternatives to Ellman's reagent in thiol-quantification enzyme assays, Angew Chem Int Ed Engl, 44 (2005) 2922-2925.
[133] B. Tang, L. Yin, X. Wang, Z. Chen, L. Tong, K. Xu, A fast-response, highly sensitive and specific organoselenium fluorescent probe for thiols and its application in bioimaging, Chem Commun (Camb), (2009) 5293-5295.
[134] M.M. Pires, J. Chmielewski, Fluorescence imaging of cellular glutathione using a latent rhodamine, Org. Lett., 10 (2008) 837-840.
[135] J. Bouffard, Y. Kim, T.M. Swager, R. Weissleder, S.A. Hilderbrand, A highly selective fluorescent probe for thiol bioimaging, Org. Lett., 10 (2008) 37-40.
[136] L. Nie, H. Ma, M. Sun, X. Li, M. Su, S. Liang, Direct chemiluminescence determination of cysteine in human serum using quinine-Ce(IV) system, Talanta, 59 (2003) 959-964.
[137] S. Wang, H. Ma, J. Li, X. Chen, Z. Bao, S. Sun, Direct determination of reduced glutathione in biological fluids by Ce(IV)-quinine chemiluminescence, Talanta, 70 (2006) 518-521.
[138] B. Rezaei, A. Mokhtari, A simple and rapid flow injection chemiluminescence determination of cysteine with Ru(phen)3(2+)-Ce(IV) system, Spectrochim Acta A Mol Biomol Spectrosc, 66 (2007) 359-363.
[139] J. Zhu, I. Dhimitruka, D. Pei, 5-(2-Aminoethyl)dithio-2-nitrobenzoate as a more base-stable alternative to Ellman's reagent, Org. Lett., 6 (2004) 3809-3812.
[140] P.K. Pullela, T. Chiku, M.J. Carvan, 3rd, D.S. Sem, Fluorescence-based detection of thiols in vitro and in vivo using dithiol probes, Anal. Biochem., 352 (2006) 265-273.
[141] A.M. Piggott, P. Karuso, Fluorometric assay for the determination of glutathione reductase activity, Anal. Chem., 79 (2007) 8769-8773.
[142] N. Shao, J.Y. Jin, S.M. Cheung, R.H. Yang, W.H. Chan, T. Mo, A spiropyran-based ensemble for visual recognition and quantification of cysteine and homocysteine at physiological levels, Angew Chem Int Ed Engl, 45 (2006) 4944-4948.
[143] H. Wang, W.S. Wang, H.S. Zhang, Spectrofluorimetic determination of cysteine based on the fluorescence inhibition of Cd(II)-8-hydroxyquinoline-5-sulphonic acid complex by cysteine, Talanta, 53 (2001) 1015-1019.
[144] Y. Fu, H. Li, W. Hu, D. Zhu, Fluorescence probes for thiol-containing amino acids and peptides in aqueous solution, Chem Commun (Camb), (2005) 3189-3191.
[145] X.F. Yang, P. Liu, L. Wang, M. Zhao, A chemosensing ensemble for the detection of cysteine based on the inner filter effect using a rhodamine B spirolactam, J Fluoresc, 18 (2008) 453-459.
[146] B. Han, J. Yuan, E. Wang, Sensitive and selective sensor for biothiols in the cell based on the recovered fluorescence of the CdTe quantum dots-Hg(II) system, Anal. Chem., 81 (2009) 5569-5573.

[147] S. Garrod, M.E. Bollard, A.W. Nicholls, S.C. Connor, J. Connelly, J.K. Nicholson, E. Holmes, Integrated Metabonomic Analysis of the Multiorgan Effects of Hydrazine Toxicity in the Rat, Chem. Res. Toxicol., 18 (2005) 115-122.
[148] J.-W. Mo, B. Ogorevc, X. Zhang, B. Pihlar, Cobalt and Copper Hexacyanoferrate Modified Carbon Fiber Microelectrode as an All-Solid Potentiometric Microsensor for Hydrazine, Electroanalysis, 12 (2000) 48-54.
[149] A. Serov, C. Kwak, Direct hydrazine fuel cells: A review, Applied Catalysis B: Environmental, 98 (2010) 1-9.
[150] S.S. Narayanan, F. Scholz, A Comparative Study of the Electrocatalytic Activities of Some Metal Hexacyanoferrates for the Oxidation of Hydrazine, Electroanalysis, 11 (1999) 465-469.
[151] U. Ragnarsson, Synthetic methodology for alkyl substituted hydrazines, Chemical Society Reviews, 30 (2001) 205-213.
[152] A. Safavi, A.A. Ensafi, Kinetic spectrophotometric determination of hydrazine, Anal. Chim. Acta, 300 (1995) 307-311.
[153] A.A. Ensafi, B. Naderi, Flow-Injection Spectrophotometric Determination of Hydrazine, Microchem. J., 56 (1997) 269-275.
[154] G.W. Watt, J.D. Chrisp, Spectrophotometric Method for Determination of Hydrazine, Anal. Chem., 24 (1952) 2006-2008.
[155] W. McBride, R. Henry, S. Skolnik, Potentiometric Analytical Methods for Hydrazino Compounds. Sydrazine Sulfate, Anal. Chem., 23 (1951) 890-893.
[156] J.R. Stetter, K.F. Blurton, A.M. Valentine, K.A. Tellefsen, The Electrochemical Oxidation of Hydrazine and Methylhydrazine on Gold: Application to Gas Monitoring, J. Electrochem. Soc., 125 (1978) 1804-1807.
[157] A. Safavi, M.A. Karimi, Flow injection chemiluminescence determination of hydrazine by oxidation with chlorinated isocyanurates, Talanta, 58 (2002) 785-792.
[158] D.P. Elder, D. Snodin, A. Teasdale, Control and analysis of hydrazine, hydrazides and hydrazones—Genotoxic impurities in active pharmaceutical ingredients (APIs) and drug products, J. Pharm. Biomed. Anal., 54 (2011) 900-910.
[159] D.-G. Cho, J.L. Sessler, Modern reaction-based indicator systems, Chem. Soc. Rev., 38 (2009) 1647-1662.
[160] G. Mohr, New chromogenic and fluorogenic reagents and sensors for neutral and ionic analytes based on covalent bond formation–a review of recent developments, Anal. Bioanal. Chem., 386 (2006) 1201-1214.
[161] C. Allardyce, P. Dyson, Medicinal Properties of Organometallic Compounds, in: G. Simonneaux (Ed.) Bioorganometallic Chemistry, Springer Berlin Heidelberg, 2006, pp. 177-210.
[162] A.F. Peacock, P.J. Sadler, Medicinal organometallic chemistry: designing metal arene complexes as anticancer agents, Chem.--Asian J., 3 (2008) 1890-1899.
[163] L.D. Dale, J.H. Tocher, T.M. Dyson, D.I. Edwards, D.A. Tocher, Studies on DNA damage and induction of SOS repair by novel multifunctional bioreducible compounds. II. A metronidazole adduct of a ruthenium-arene compound, Anticancer Drug Des, 7 (1992) 3-14.

[164] A. Houlton, R.M.G. Roberts, J. Silver, Studies on the anti-tumour activity of some iron sandwich compounds, J. Organomet. Chem., 418 (1991) 107-112.
[165] P. Koepf-Maier, H. Koepf, Non-platinum group metal antitumor agents. History, current status, and perspectives, Chem. Rev., 87 (1987) 1137-1152.
[166] E. Neuse, Macromolecular Ferrocene Compounds as Cancer Drug Models, J. Inorg. Organomet. Polym. Mater., 15 (2005) 3-31.
[167] D.R. van Staveren, N. Metzler-Nolte, Bioorganometallic Chemistry of Ferrocene, Chem. Rev., 104 (2004) 5931-5986.
[168] J.L. Hickey, R.A. Ruhayel, P.J. Barnard, M.V. Baker, S.J. Berners-Price, A. Filipovska, Mitochondria-targeted chemotherapeutics: the rational design of gold(I) N-heterocyclic carbene complexes that are selectively toxic to cancer cells and target protein selenols in preference to thiols, J. Am. Chem. Soc., 130 (2008) 12570-12571.
[169] I. Ott, On the medicinal chemistry of gold complexes as anticancer drugs, Coord. Chem. Rev., 253 (2009) 1670-1681.
[170] D.A. Medvetz, K.M. Hindi, M.J. Panzner, A.J. Ditto, Y.H. Yun, W.J. Youngs, Anticancer Activity of Ag(I) N-Heterocyclic Carbene Complexes Derived from 4,5-Dichloro-1H-Imidazole, Met.-Based Drugs, 2008 (2008).
[171] I. Ott, B. Kircher, R. Dembinski, R. Gust, Alkyne hexacarbonyl dicobalt complexes in medicinal chemistry and drug development, Expert Opin. Ther. Pat., 18 (2008) 327-337.
[172] I. Ott, K. Schmidt, B. Kircher, P. Schumacher, T. Wiglenda, R. Gust, Antitumor-active cobalt-alkyne complexes derived from acetylsalicylic acid: studies on the mode of drug action, J. Med. Chem., 48 (2005) 622-629.
[173] M.A. Neukamm, A. Pinto, N. Metzler-Nolte, Synthesis and cytotoxicity of a cobaltcarbonyl-alkyne enkephalin bioconjugate, Chemical Communications, (2008) 232-234.
[174] G. Gasser, M.A. Neukamm, A. Ewers, O. Brosch, T. Weyhermüller, N. Metzler-Nolte, Synthesis and Characterization of Dicobalthexacarbonyl-Alkyne Derivatives of Amino Acids, Peptides, and Peptide Nucleic Acid (PNA) Monomers, Inorg. Chem., 48 (2009) 3157-3166.
[175] J.C. Franke, M. Plotz, A. Prokop, C.C. Geilen, H.G. Schmalz, J. Eberle, New caspase-independent but ROS-dependent apoptosis pathways are targeted in melanoma cells by an iron-containing cytosine analogue, Biochem. Pharmacol., 79 (2010) 575-586.
[176] D. Schlawe, A. Majdalani, J. Velcicky, E. Hessler, T. Wieder, A. Prokop, H.G. Schmalz, Iron-containing nucleoside analogues with pronounced apoptosis-inducing activity, Angew Chem Int Ed Engl, 43 (2004) 1731-1734.
[177] S. Top, A. Vessieres, P. Pigeon, M.N. Rager, M. Huche, E. Salomon, C. Cabestaing, J. Vaissermann, G. Jaouen, Selective estrogen-receptor modulators (SERMs) in the cyclopentadienylrhenium tricarbonyl series: synthesis and biological behaviour, ChemBioChem, 5 (2004) 1104-1113.
[178] G. Jaouen, S. Top, A. Vessieres, G. Leclercq, M.J. McGlinchey, The first organometallic selective estrogen receptor modulators (SERMs) and their relevance to breast cancer, Curr. Med. Chem., 11 (2004) 2505-2517.
[179] L. Hewison, S.H. Crook, B.E. Mann, A.J.H.M. Meijer, H. Adams, P. Sawle, R.A. Motterlini, New Types of CO-Releasing Molecules (CO-RMs), Based on Iron Dithiocarbamate Complexes and [Fe(CO)3I(S2COEt)], Organometallics, 31 (2012) 5823-5834.

[180] H.W. Peindy N'Dongo, I. Ott, R. Gust, U. Schatzschneider, Microwave-assisted solid-phase synthesis, cellular uptake, and cytotoxicity studies of cymantrene–peptide bioconjugates, J. Organomet. Chem., 694 (2009) 823-827.
[181] J. Niesel, A. Pinto, H.W. Peindy N'Dongo, K. Merz, I. Ott, R. Gust, U. Schatzschneider, Photoinduced CO release, cellular uptake and cytotoxicity of a tris(pyrazolyl)methane (tpm) manganese tricarbonyl complex, Chem Commun (Camb), (2008) 1798-1800.
[182] I. Neundorf, J. Hoyer, K. Splith, R. Rennert, H.W. Peindy N'Dongo, U. Schatzschneider, Cymantrene conjugation modulates the intracellular distribution and induces high cytotoxicity of a cell-penetrating peptide, Chemical Communications, (2008) 5604-5606.
[183] W. Hu, K. Splith, I. Neundorf, K. Merz, U. Schatzschneider, Influence of the metal center and linker on the intracellular distribution and biological activity of organometal–peptide conjugates, JBIC Journal of Biological Inorganic Chemistry, 17 (2012) 175-185.
[184] K. Splith, W. Hu, U. Schatzschneider, R. Gust, I. Ott, L.A. Onambele, A. Prokop, I. Neundorf, Protease-Activatable Organometal−Peptide Bioconjugates with Enhanced Cytotoxicity on Cancer Cells, Bioconjugate Chem., 21 (2010) 1288-1296.
[185] K. Splith, I. Neundorf, W. Hu, H.W.P. N'Dongo, V. Vasylyeva, K. Merz, U. Schatzschneider, Influence of the metal complex-to-peptide linker on the synthesis and properties of bioactive CpMn(CO)3 peptide conjugates, Dalton Trans., 39 (2010) 2536-2545.
[186] T.E. Sloan, A. Wojcicki, Linkage isomerism in carbonyl-.pi.-cyclopentadienyl(thiocyanato)metal complexes, Inorg. Chem., 7 (1968) 1268-1273.
[187] B.M. Mattson, W.A.G. Graham, Mechanism of halide abstraction from .eta.5-cyclopentadienyl(dicarbonyl)iodoiron by silver tetrafluoroborate, Inorg. Chem., 20 (1981) 3186-3189.
[188] W.C. Claycomb, N.A. Lanson, Jr., B.S. Stallworth, D.B. Egeland, J.B. Delcarpio, A. Bahinski, N.J. Izzo, Jr., HL-1 cells: a cardiac muscle cell line that contracts and retains phenotypic characteristics of the adult cardiomyocyte, Proc. Natl. Acad. Sci. U. S. A., 95 (1998) 2979-2984.
[189] Y. Leverrier, A.J. Ridley, Apoptosis: caspases orchestrate the ROCK 'n' bleb, Nat. Cell Biol., 3 (2001) E91-93.
[190] M.L. Coleman, E.A. Sahai, M. Yeo, M. Bosch, A. Dewar, M.F. Olson, Membrane blebbing during apoptosis results from caspase-mediated activation of ROCK I, Nat. Cell Biol., 3 (2001) 339-345.
[191] J.C. Mills, N.L. Stone, J. Erhardt, R.N. Pittman, Apoptotic membrane blebbing is regulated by myosin light chain phosphorylation, J. Cell Biol., 140 (1998) 627-636.
[192] C. Lu, P. Li, R. Gallegos, V. Uttamsingh, C.Q. Xia, G.T. Miwa, S.K. Balani, L.S. Gan, Comparison of intrinsic clearance in liver microsomes and hepatocytes from rats and humans: evaluation of free fraction and uptake in hepatocytes, Drug Metab. Dispos., 34 (2006) 1600-1605.
[193] H. Liu, C. Sabus, G. Carter, C. Du, A. Avdeef, M. Tischler, In Vitro Permeability of Poorly Aqueous Soluble Compounds Using Different Solubilizers in the PAMPA Assay with Liquid Chromatography/Mass Spectrometry Detection, Pharm. Res., 20 (2003) 1820-1826.

[194] E.H. Kerns, L. Di, S. Petusky, M. Farris, R. Ley, P. Jupp, Combined application of parallel artificial membrane permeability assay and Caco-2 permeability assays in drug discovery, J. Pharm. Sci., 93 (2004) 1440-1453.
[195] A. Avdeef, S. Bendels, L. Di, B. Faller, M. Kansy, K. Sugano, Y. Yamauchi, PAMPA—critical factors for better predictions of absorption, J. Pharm. Sci., 96 (2007) 2893-2909.
[196] K. Taguchi, H. Motohashi, M. Yamamoto, Molecular mechanisms of the Keap1–Nrf2 pathway in stress response and cancer evolution, Genes Cells, 16 (2011) 123-140.
[197] T.S. Chong, P. Li, W.K. Leong, W.Y. Fan, TR-FTIR absorption spectroscopy of transition metal carbonyl radicals generated by photodissociation of metal–metal bonds, by halogen abstraction or by radical ligand substitution, J. Organomet. Chem., 690 (2005) 4132-4138.
[198] G.-Y. Liou, P. Storz, Reactive oxygen species in cancer, Free Radical Res., 44 (2010) 479-496.
[199] P.T. Schumacker, Reactive oxygen species in cancer cells: Live by the sword, die by the sword, Cancer Cell, 10 175-176.
[200] M. Valko, C.J. Rhodes, J. Moncol, M. Izakovic, M. Mazur, Free radicals, metals and antioxidants in oxidative stress-induced cancer, Chem.-Biol. Interact., 160 (2006) 1-40.
[201] D. Trachootham, J. Alexandre, P. Huang, Targeting cancer cells by ROS-mediated mechanisms: a radical therapeutic approach?, Nat Rev Drug Discov, 8 (2009) 579-591.
[202] D.G. Alway, K.W. Barnett, Photochemical isomerization of cyclopentadienylmetal complexes, J. Organomet. Chem., 99 (1975) C52-C54.
[203] I. Vermes, C. Haanen, H. Steffens-Nakken, C. Reutelingsperger, A novel assay for apoptosis. Flow cytometric detection of phosphatidylserine expression on early apoptotic cells using fluorescein labelled Annexin V, J. Immunol. Methods, 184 (1995) 39-51.
[204] M. Ullah, Sulforaphane (SFN): An Isothiocyanate in a Cancer Chemoprevention Paradigm, Medicines, 2 (2015) 141.
[205] R. WANG, Two's company, three's a crowd: can H2S be the third endogenous gaseous transmitter?, The FASEB Journal, 16 (2002) 1792-1798.
[206] C.A. Piantadosi, Biological Chemistry of Carbon Monoxide, Antioxid. Redox Signaling, 4 (2002) 259-270.
[207] A. Brydun, Y. Watari, Y. Yamamoto, K. Okuhara, H. Teragawa, F. Kono, K. Chayama, T. Oshima, R. Ozono, Reduced Expression of Heme Oxygenase-1 in Patients with Coronary Atherosclerosis, Hypertens Res, 30 (2007) 341-348.
[208] N. Yamada, M. Yamaya, S. Okinaga, K. Nakayama, K. Sekizawa, S. Shibahara, H. Sasaki, Microsatellite Polymorphism in the Heme Oxygenase-1 Gene Promoter Is Associated with Susceptibility to Emphysema, The American Journal of Human Genetics, 66 187-195.
[209] F.A.D.T.G. Wagener, E.J.M. Toonen, L. Wigman, J. Fransen, M.C.W. Creemers, T.R.D.J. Radstake, M.J.H. Coenen, P. Barrera, P.L.C.M. van Riel, F.G.M. Russel, HMOX1 promoter polymorphism modulates the relationship between disease activity and joint damage in rheumatoid arthritis, Arthritis & Rheumatism, 58 (2008) 3388-3393.
[210] F. Song, X. Li, M. Zhang, P. Yao, N. Yang, X. Sun, F.B. Hu, L. Liu, Association Between Heme Oxygenase-1 Gene Promoter Polymorphisms and

Type 2 Diabetes in a Chinese Population, American Journal of Epidemiology, 170 (2009) 747-756.
[211] A.F.N. Tavares, M. Teixeira, C.C. Romão, J.D. Seixas, L.S. Nobre, L.M. Saraiva, Reactive Oxygen Species Mediate Bactericidal Killing Elicited by Carbon Monoxide-releasing Molecules, Journal of Biological Chemistry, 286 (2011) 26708-26717.
[212] A.R. Marques, L. Kromer, D.J. Gallo, N. Penacho, S.S. Rodrigues, J.D. Seixas, G.J.L. Bernardes, P.M. Reis, S.L. Otterbein, R.A. Ruggieri, A.S.G. Gonçalves, A.M.L. Gonçalves, M.N.D. Matos, I. Bento, L.E. Otterbein, W.A. Blättler, C.C. Romão, Generation of Carbon Monoxide Releasing Molecules (CO-RMs) as Drug Candidates for the Treatment of Acute Liver Injury: Targeting of CO-RMs to the Liver, Organometallics, 31 (2012) 5810-5822.
[213] B.E. Mann, CO-Releasing Molecules: A Personal View, Organometallics, 31 (2012) 5728-5735.
[214] S. Romanski, H. Rücker, E. Stamellou, M. Guttentag, J.-M. Neudörfl, R. Alberto, S. Amslinger, B. Yard, H.-G. Schmalz, Iron Dienylphosphate Tricarbonyl Complexes as Water-Soluble Enzyme-Triggered CO-Releasing Molecules (ET-CORMs), Organometallics, 31 (2012) 5800-5809.
[215] U. Schatzschneider, PhotoCORMs: Light-triggered release of carbon monoxide from the coordination sphere of transition metal complexes for biological applications, Inorganica Chimica Acta, 374 (2011) 19-23.
[216] T.R. Johnson, B.E. Mann, J.E. Clark, R. Foresti, C.J. Green, R. Motterlini, Metal Carbonyls: A New Class of Pharmaceuticals?, Angewandte Chemie International Edition, 42 (2003) 3722-3729.
[217] W. Huber, R. Linder, J. Niesel, U. Schatzschneider, B. Spingler, P.C. Kunz, A Comparative Study of Tricarbonylmanganese Photoactivatable CO Releasing Molecules (PhotoCORMs) by Using the Myoglobin Assay and Time-Resolved IR Spectroscopy, European Journal of Inorganic Chemistry, 2012 (2012) 3140-3146.
[218] V.P.L. Velásquez, T.M.A. Jazzazi, A. Malassa, H. Görls, G. Gessner, S.H. Heinemann, M. Westerhausen, Derivatives of Photosensitive CORM-S1 – CO Complexes of Iron and Ruthenium with the (OC)2M(S–C–C–NH2)2 Fragment, European Journal of Inorganic Chemistry, 2012 (2012) 1072-1078.
[219] R. Kretschmer, G. Gessner, H. Görls, S.H. Heinemann, M. Westerhausen, Dicarbonyl-bis(cysteamine)iron(II): A light induced carbon monoxide releasing molecule based on iron (CORM-S1), Journal of inorganic biochemistry, 105 (2011) 6-9.
[220] G.A.N. Felton, C.A. Mebi, B.J. Petro, A.K. Vannucci, D.H. Evans, R.S. Glass, D.L. Lichtenberger, Review of electrochemical studies of complexes containing the Fe2S2 core characteristic of [FeFe]-hydrogenases including catalysis by these complexes of the reduction of acids to form dihydrogen, Journal of Organometallic Chemistry, 694 (2009) 2681-2699.
[221] C. Tard, C.J. Pickett, Structural and Functional Analogues of the Active Sites of the [Fe]-, [NiFe]-, and [FeFe]-Hydrogenases, Chemical reviews, 109 (2009) 2245-2274.
[222] R. Hosoki, N. Matsuki, H. Kimura, The possible role of hydrogen sulfide as an endogenous smooth muscle relaxant in synergy with nitric oxide, Biochem. Biophys. Res. Commun., 237 (1997) 527-531.
[223] H. Kimura, Hydrogen sulfide: from brain to gut, Antioxid Redox Signal, 12 (2010) 1111-1123.

[224] D. Boehning, S.H. Snyder, Novel neural modulators, Annu. Rev. Neurosci., 26 (2003) 105-131.
[225] A.F. Perna, D. Lanza, I. Sepe, I. Raiola, R. Capasso, N.G. De Santo, D. Ingrosso, Hydrogen sulfide, a toxic gas with cardiovascular properties in uremia: how harmful is it?, Blood Purif, 31 (2011) 102-106.
[226] C. Szabo, Roles of hydrogen sulfide in the pathogenesis of diabetes mellitus and its complications, Antioxid Redox Signal, 17 (2012) 68-80.
[227] N.O. Devarie-Baez, P.E. Bagdon, B. Peng, Y. Zhao, C.-M. Park, M. Xian, Light-Induced Hydrogen Sulfide Release from "Caged" gem-Dithiols, Org. Lett., 15 (2013) 2786-2789.
[228] X. Gu, Y.Z. Zhu, Therapeutic applications of organosulfur compounds as novel hydrogen sulfide donors and/or mediators, Expert Review of Clinical Pharmacology, 4 (2011) 123-133.
[229] A. Stein, S.M. Bailey, Redox biology of hydrogen sulfide: Implications for physiology, pathophysiology, and pharmacology, Redox Biology, 1 (2013) 32-39.
[230] G.L. Bannenberg, H.L. Vieira, Therapeutic applications of the gaseous mediators carbon monoxide and hydrogen sulfide, Expert Opin. Ther. Pat., 19 (2009) 663-682.
[231] X. Zhao, I.P. Georgakaki, M.L. Miller, R. Mejia-Rodriguez, C.-Y. Chiang, M.Y. Darensbourg, Catalysis of H2/D2 Scrambling and Other H/D Exchange Processes by [Fe]-Hydrogenase Model Complexes, Inorganic chemistry, 41 (2002) 3917-3928.
[232] S. McLean, B.E. Mann, R.K. Poole, Sulfite species enhance carbon monoxide release from CO-releasing molecules: Implications for the deoxymyoglobin assay of activity, Analytical biochemistry, 427 (2012) 36-40.
[233] R.D. Rimmer, H. Richter, P.C. Ford, A Photochemical Precursor for Carbon Monoxide Release in Aerated Aqueous Media, Inorganic chemistry, 49 (2010) 1180-1185.
[234] P.J. Medvecz, K.M. Nichols, Experimental Determination of Line Strengths for Selected Carbon Monoxide and Carbon Dioxide Absorption Lines at Temperatures between 295 and 1250 K, Applied Spectroscopy, 48 (1994) 1442-1450.
[235] K.W. Davies, D. Maivald, J.J. Grabowski, A photoacoustic calorimetric characterization of the reaction enthalpy and volume for the preparation of a reactive intermediate from CpMn(CO)3, Journal of Photochemistry and Photobiology A: Chemistry, 197 (2008) 335-341.
[236] E.J. Lyon, I.P. Georgakaki, J.H. Reibenspies, M.Y. Darensbourg, Coordination Sphere Flexibility of Active-Site Models for Fe-Only Hydrogenase: Studies in Intra- and Intermolecular Diatomic Ligand Exchange, Journal of the American Chemical Society, 123 (2001) 3268-3278.
[237] R.G.W. Gingerich, R.J. Angelici, Reactions of the SH- and S2- groups in W(CO)5(SH)- and .mu.-S[W(CO)5]22, J. Am. Chem. Soc., 101 (1979) 5604-5608.
[238] H. Hermann, F.W. Grevels, A. Henne, K. Schaffner, Flash photolysis with infrared detection. The photochemistry and secondary thermal reactions of M(CO)6 [M = Cr, Mo, and W], The Journal of Physical Chemistry, 86 (1982) 5151-5154.

[239] O.M. Suleimenov, R.E. Krupp, Solubility of hydrogen sulfide in pure water and in NaCl solutions, from 20 to 320°C and at saturation pressures, Geochim. Cosmochim. Acta, 58 (1994) 2433-2444.
[240] M.C. Baird, Seventeen-electron metal-centered radicals, Chem. Rev., 88 (1988) 1217-1227.
[241] C.H. Bamford, R. Denyer, Initiation of Free Radical Polymerization by Manganese Carbonyl and Carbon Tetrachloride, Nature, 217 (1968) 59-60.
[242] C.H. Bamford, S.U. Mullik, Photoinitiation of free-radical polymerization by transition metal carbonyls in systems without halides, Journal of the Chemical Society, Faraday Transactions 1: Physical Chemistry in Condensed Phases, 72 (1976) 368-375.
[243] M.S. Kharasch, E.V. Jensen, W.H. Urry, Addition of Carbon Tetrachloride and Chloroform to Olefins, Science, 102 (1945) 128.
[244] M.S. Kharasch, P.S. Skell, P. Fisher, Reactions of Atoms and Free Radicals in Solution. XII. The Addition of Bromo Esters to Olefins, J. Am. Chem. Soc., 70 (1948) 1055-1059.
[245] H.T. Poh, J.W. Kee, T.S. Chwee, W.Y. Fan, A persistent manganese carbonyl radical with infrared absorption and fluorescence modality, Journal of Organometallic Chemistry, 759 (2014) 11-14.
[246] P. Lau, H. Braunwarth, G. Huttner, D. Guenauer, K. Evertz, W. Imhof, C. Emmerich, L. Zsolnai, Oxidative transformation of [RCp(CO)2MnSR].bul. radicals into manganese inidene compounds [RCp(CO)2Mn]2SR+, Organometallics, 10 (1991) 3861-3873.
[247] B.C. Jacobson, B. Moy, G.A. Colditz, C.S. Fuchs, Postmenopausal hormone use and symptoms of gastroesophageal reflux, Arch Intern Med, 168 (2008) 1798-1804.
[248] F.X. Zhang, L. Han, L.B. Israel, J.G. Daras, M.M. Maye, N. K. Ly, C.-J. Zhong, Colorimetric detection of thiol-containing amino acids using gold nanoparticles, Analyst, 127 (2002) 462-465.
[249] S.D. Zelnick, D.R. Mattie, P.C. Stepaniak, Occupational Exposure to Hydrazines: Treatment of Acute Central Nervous System Toxicity, Aviation, Space, and Environmental Medicine, 74 (2003) 1285-1291.
[250] H. Bhutani, S. Singh, S. Vir, K.K. Bhutani, R. Kumar, A.K. Chakraborti, K.C. Jindal, LC and LC-MS study of stress decomposition behaviour of isoniazid and establishment of validated stability-indicating assay method, J. Pharm. Biomed. Anal., 43 (2007) 1213-1220.
[251] M. Sun, L. Bai, D.Q. Liu, A generic approach for the determination of trace hydrazine in drug substances using in situ derivatization-headspace GC–MS, J. Pharm. Biomed. Anal., 49 (2009) 529-533.
[252] J. Liu, W. Zhou, T. You, F. Li, E. Wang, S. Dong, Detection of Hydrazine, Methylhydrazine, and Isoniazid by Capillary Electrophoresis with a Palladium-Modified Microdisk Array Electrode, Anal. Chem., 68 (1996) 3350-3353.
[253] H. Eierdanz, A. Berndt, Is the Unpaired Electron in Radical Cations of Sterically Hindered Alkenes Localized or Delocalized?, Angewandte Chemie International Edition in English, 21 (1982) 690-691.
[254] D. Sellmann, J. Müller, Reaktionen an komplexgebundenen liganden: XXXVII. Stabilisierung von instabilen aminyl-radikalen durch komplexierung an übergangsmetalle; Synthese und reaktivität von CpMn(Co)2-komplexen mit amin- und aminyl-liganden, J. Organomet. Chem., 281 (1985) 249-262.

[255] J. Peters, M.W. George, J.J. Turner, Photochemistry of [CpMo(CO)3]2. Direct Detection and Kinetics of the Radical CpMo(CO)3 in n-Heptane Solution at Room Temperature by Fast Time-Resolved Infrared Spectroscopy, Organometallics, 14 (1995) 1503-1506.
[256] R.F. Ferrante, J.L. Wilkerson, W.R.M. Graham, W. Weltner, ESR spectra of the MnO, MnO2, MnO3, and MnO4 molecules at 4 °K, The Journal of Chemical Physics, 67 (1977) 5904-5913.

Appendices

Appendix A – NMR Spectra of Synthesized Compounds

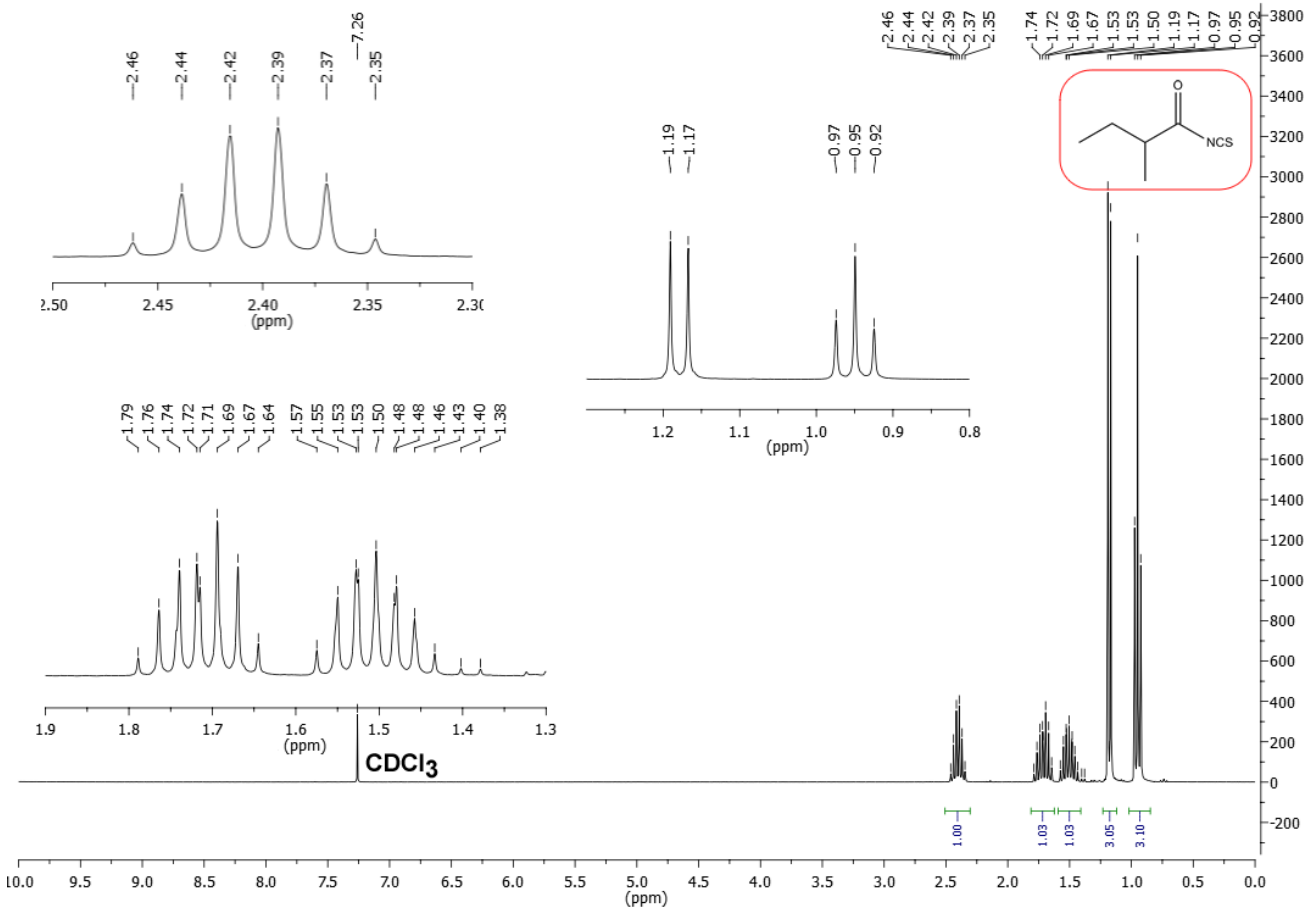

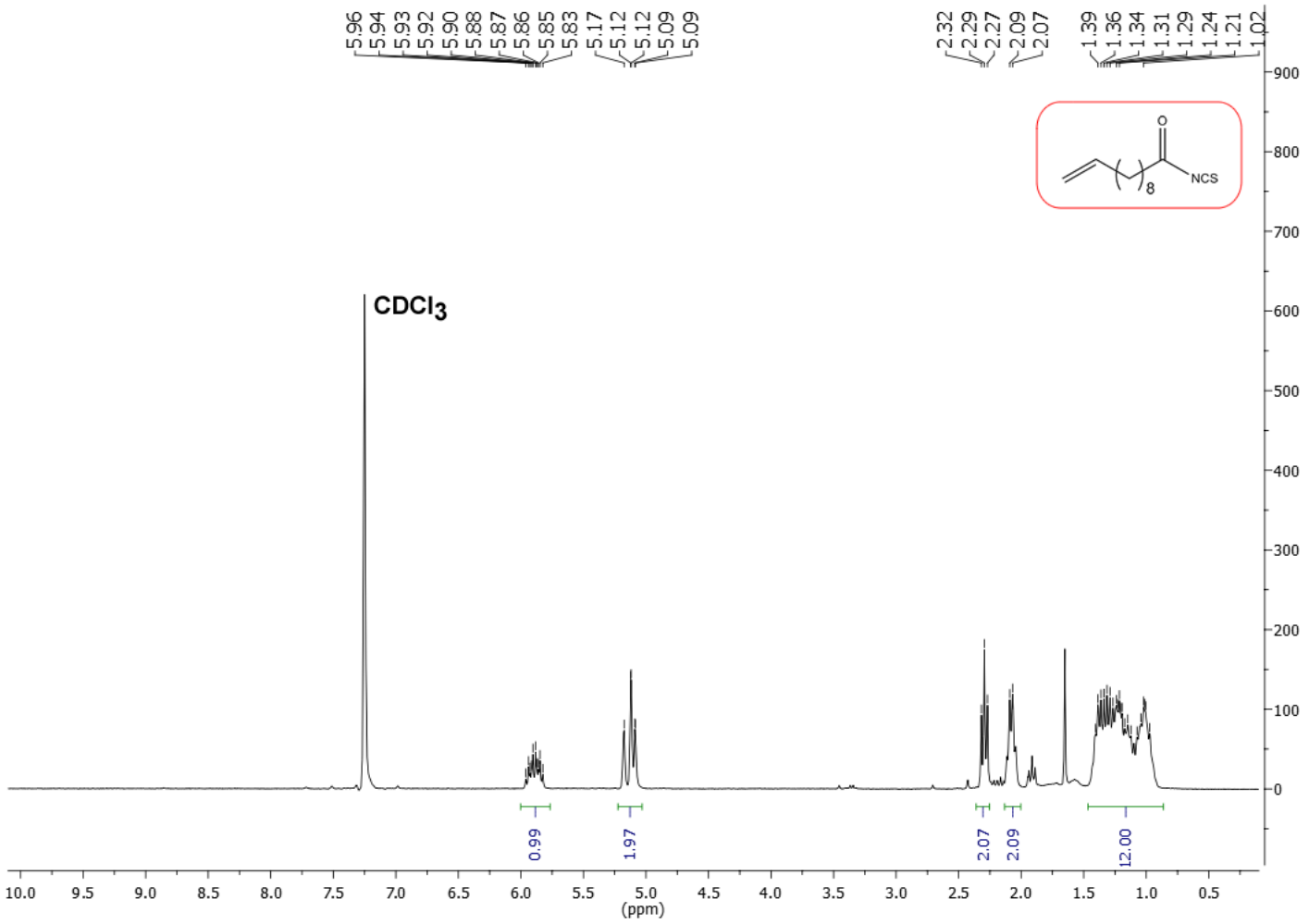
5.96
5.94
5.93
5.92
5.90
5.88
5.87
5.86
5.85
5.83
5.17
5.12
5.12
5.09
5.09
2.32
2.29
2.27
2.09
2.07
1.39
1.36
1.34
1.31
1.29
1.24
1.21
1.02
O
NCS
8
CDCl3
0.99
1.97
2.07
2.09
12.00
(ppm)

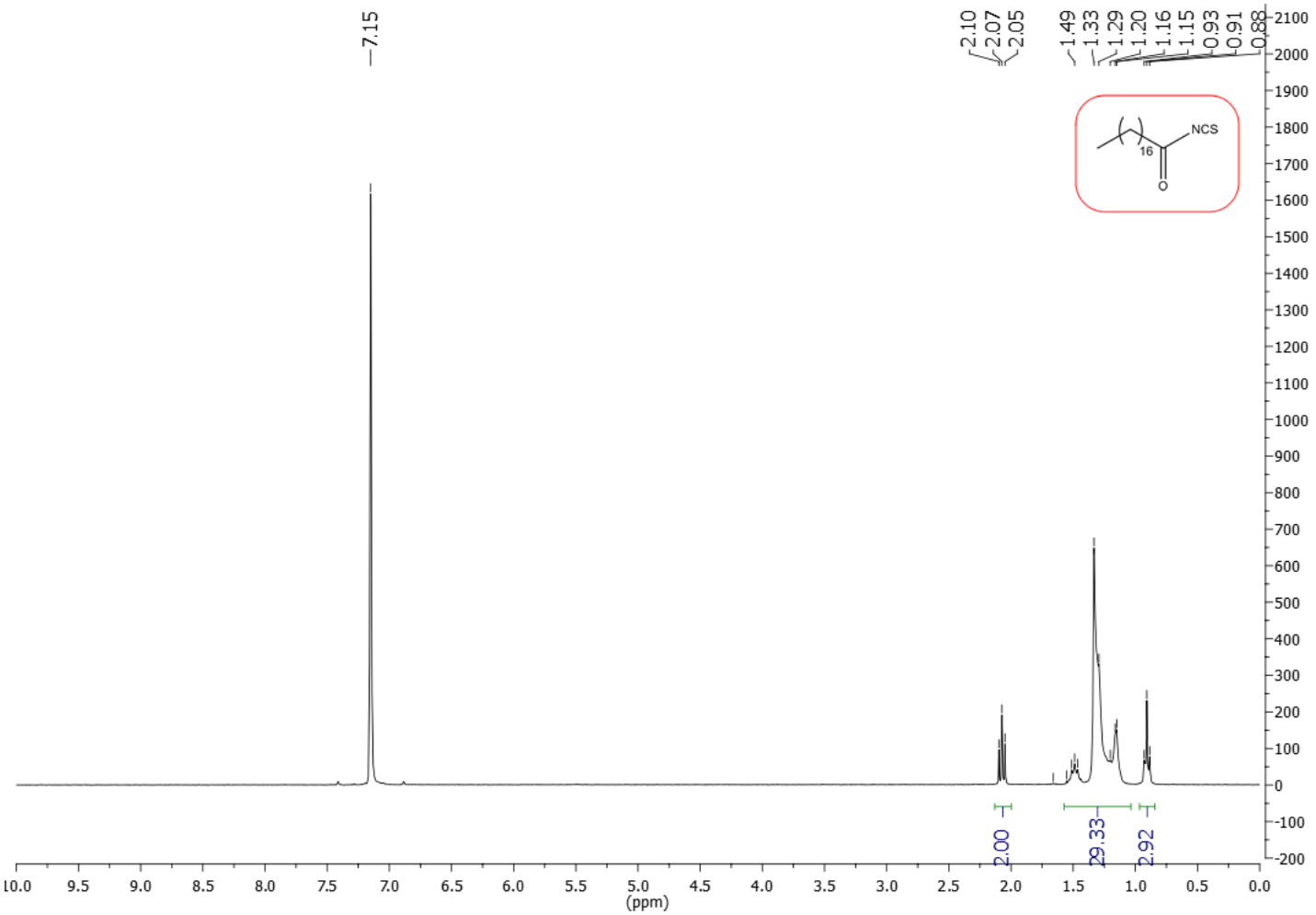
7.15
2.10
2.07
2.05
1.49
1.33
1.29
1.20
1.16
1.15
0.93
0.91
0.88
NCS
16
O
2.00
29.33
2.92
(ppm)

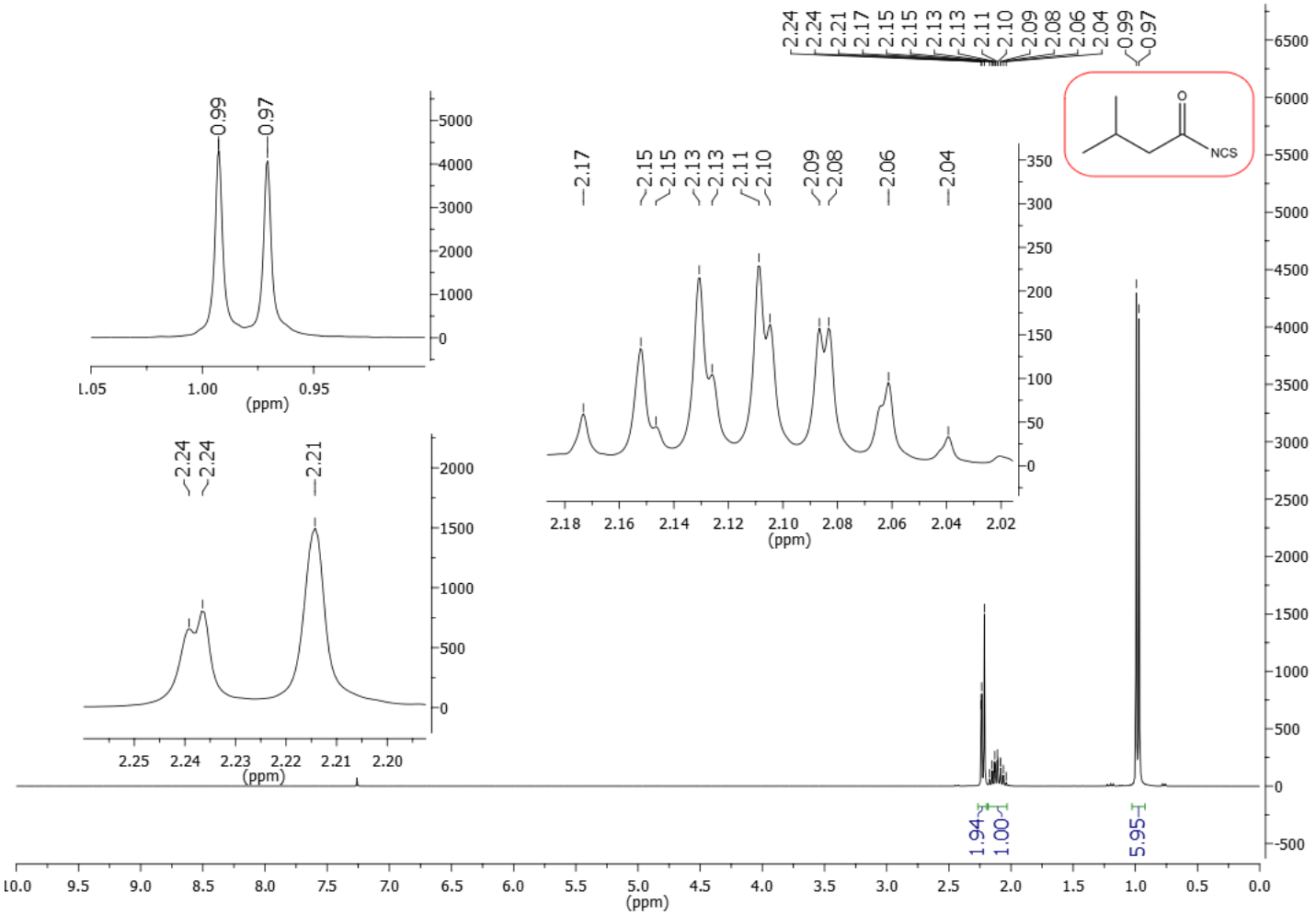
2.24
2.24
2.21
2.17
2.15
2.15
2.13
2.13
2.11
2.10
2.09
2.08
2.06
2.04
0.99
0.97
NCS
0.99
0.97
(ppm)
2.24
2.24
2.21
(ppm)
2.17
2.15
2.15
2.13
2.13
2.11
2.10
2.09
2.08
2.06
2.04
(ppm)
1.94
1.00
5.95
(ppm)

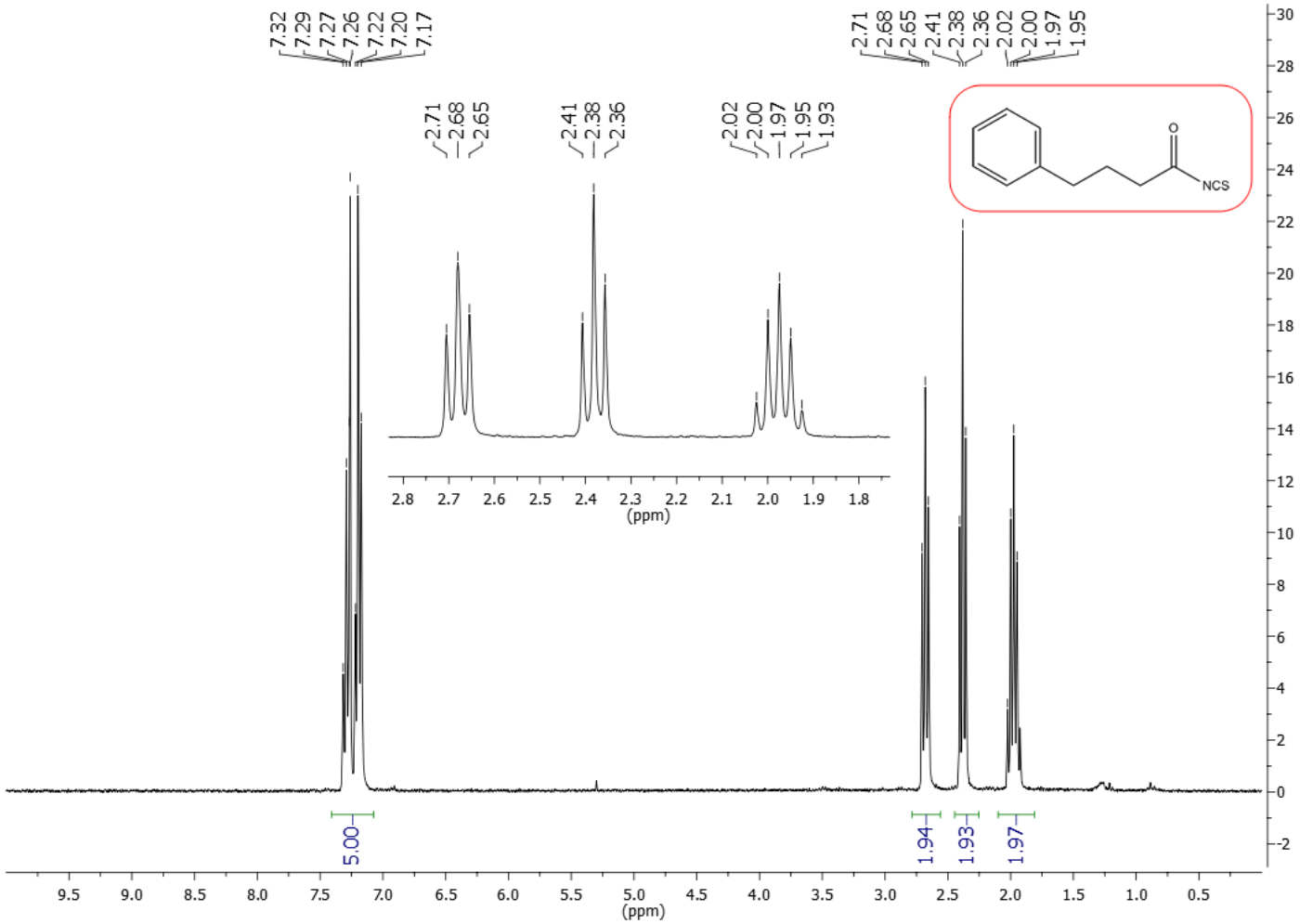
7.32
7.29
7.27
7.26
7.22
7.20
7.17
2.71
2.68
2.65
2.41
2.38
2.36
2.02
2.00
1.97
1.95
1.93
NCS
(ppm)
5.00
1.94
1.93
1.97
(ppm)

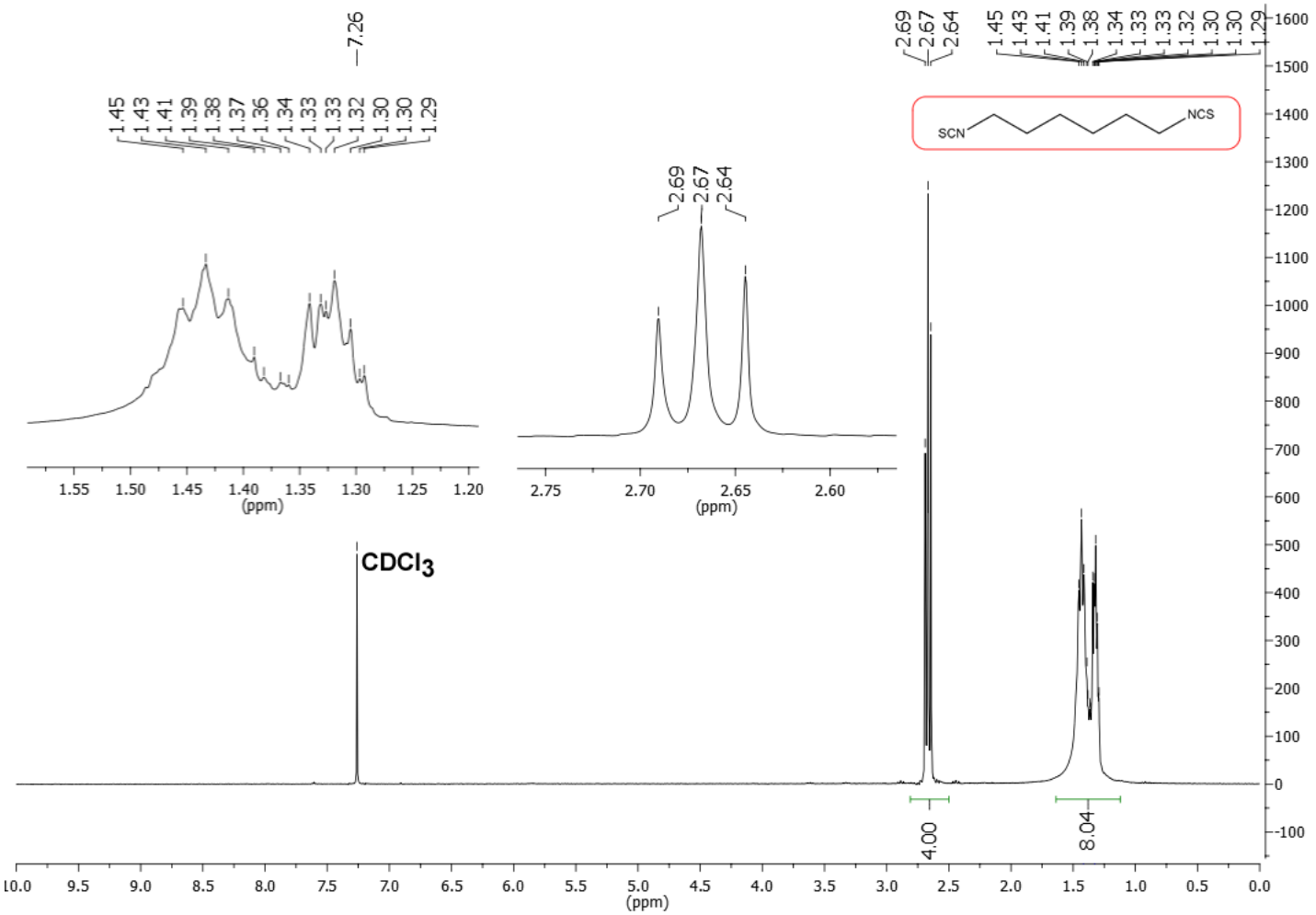
7.26
1.45
1.43
1.41
1.39
1.38
1.37
1.36
1.34
1.33
1.33
1.32
1.30
1.30
1.29
2.69
2.67
2.64
SCN
NCS
CDCl3
4.00
8.04
(ppm)

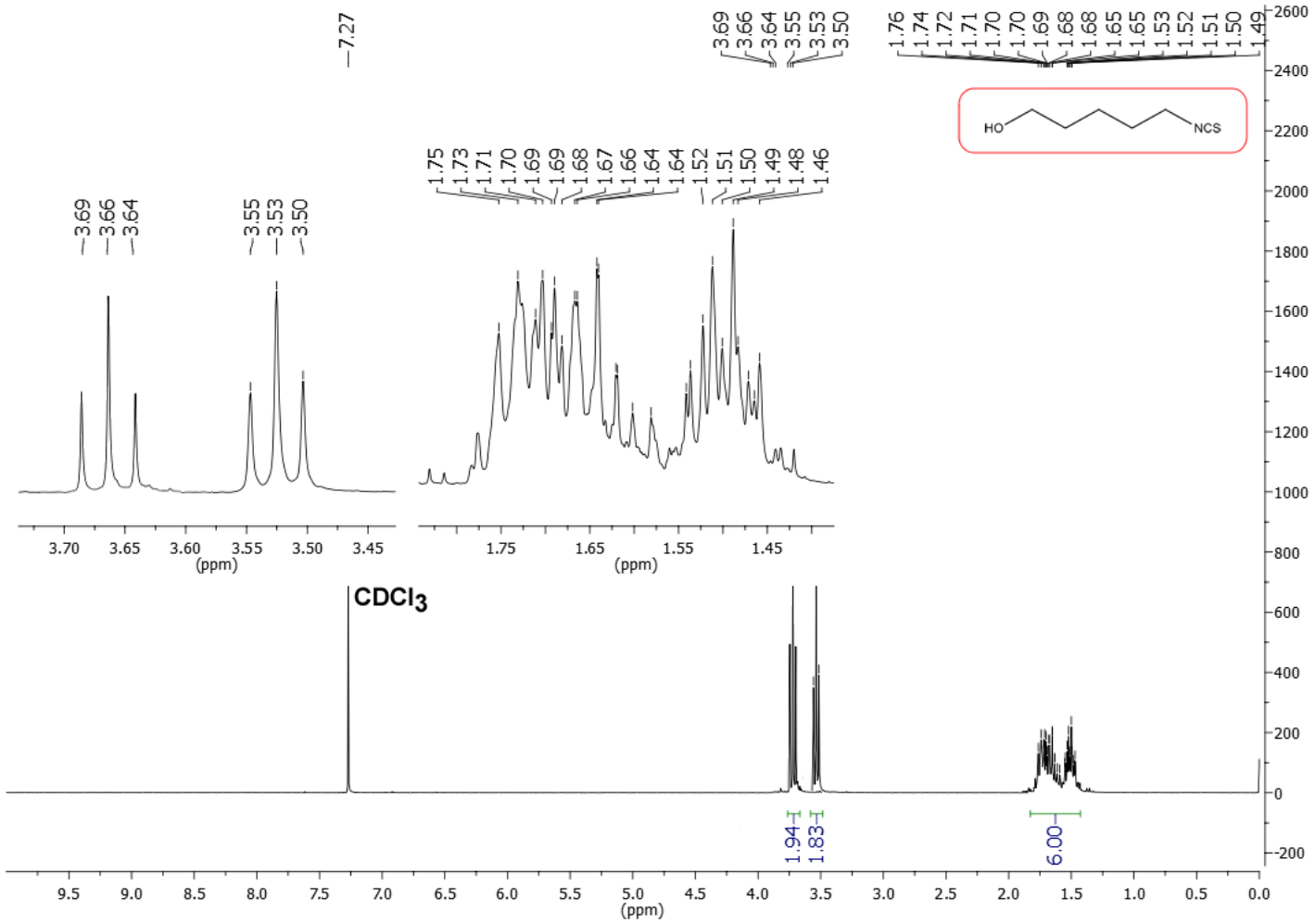
7.27
3.69
3.66
3.64
3.55
3.53
3.50
1.76
1.74
1.72
1.71
1.70
1.70
1.69
1.68
1.68
1.65
1.65
1.53
1.52
1.51
1.50
1.49
HO
NCS
1.75
1.73
1.71
1.70
1.69
1.69
1.68
1.67
1.66
1.64
1.64
1.52
1.51
1.50
1.49
1.48
1.46
3.70
3.65
3.60
3.55
3.50
3.45
(ppm)
1.75
1.65
1.55
1.45
(ppm)
CDCl3
1.94
1.83
6.00
9.5
9.0
8.5
8.0
7.5
7.0
6.5
6.0
5.5
5.0
4.5
4.0
3.5
3.0
2.5
2.0
1.5
1.0
0.5
0.0
(ppm)
2600
2400
2200
2000
1800
1600
1400
1200
1000
800
600
400
200
0
-200

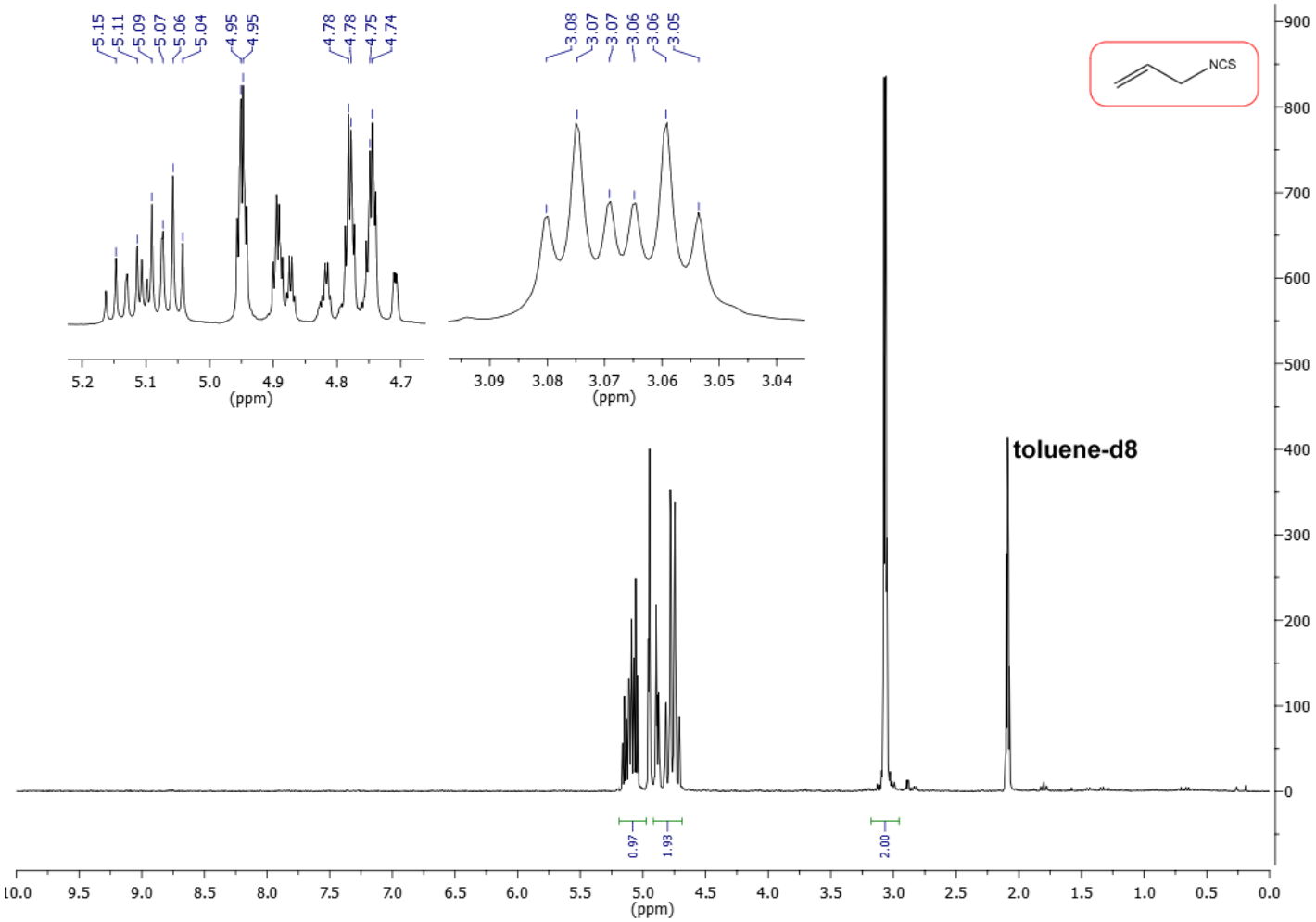
5.15
5.11
5.09
5.07
5.06
5.04
4.95
4.95
4.78
4.78
4.75
4.74
3.08
3.07
3.07
3.06
3.06
3.05
NCS
toluene-d8
0.97
1.93
2.00
(ppm)
(ppm)
(ppm)

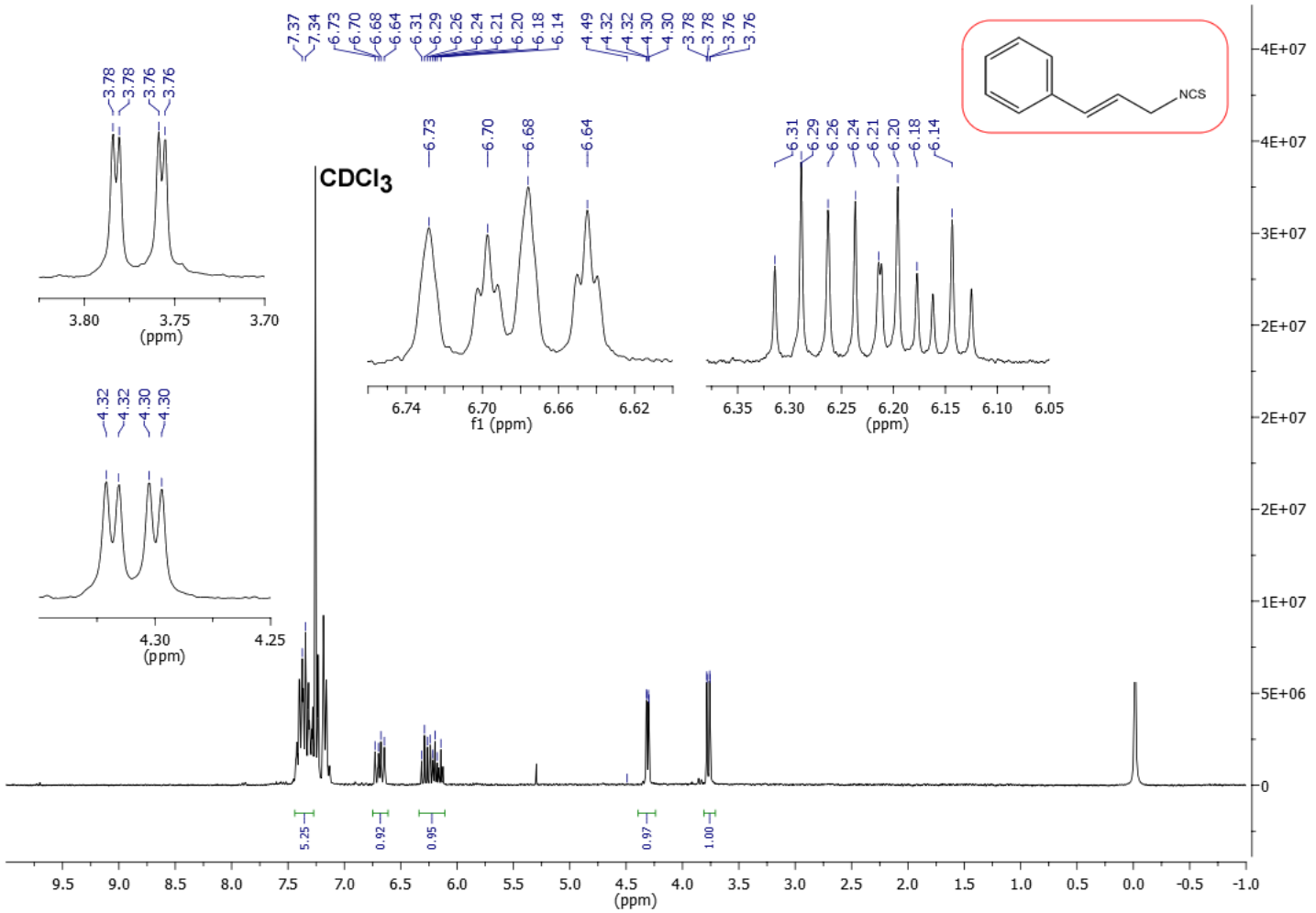
7.37
7.34
6.73
6.70
6.68
6.64
6.31
6.29
6.26
6.24
6.21
6.20
6.18
6.14
4.49
4.32
4.32
4.30
4.30
3.78
3.78
3.76
3.76
CDCl3
NCS
3.80
3.75
3.70
(ppm)
6.74
6.70
6.66
6.62
f1 (ppm)
6.35
6.30
6.25
6.20
6.15
6.10
6.05
(ppm)
4.32
4.32
4.30
4.30
4.30
4.25
(ppm)
5.25
0.92
0.95
0.97
1.00
9.5
9.0
8.5
8.0
7.5
7.0
6.5
6.0
5.5
5.0
4.5
4.0
3.5
3.0
2.5
2.0
1.5
1.0
0.5
0.0
-0.5
-1.0
(ppm)
4E+07
4E+07
3E+07
2E+07
2E+07
2E+07
1E+07
5E+06
0

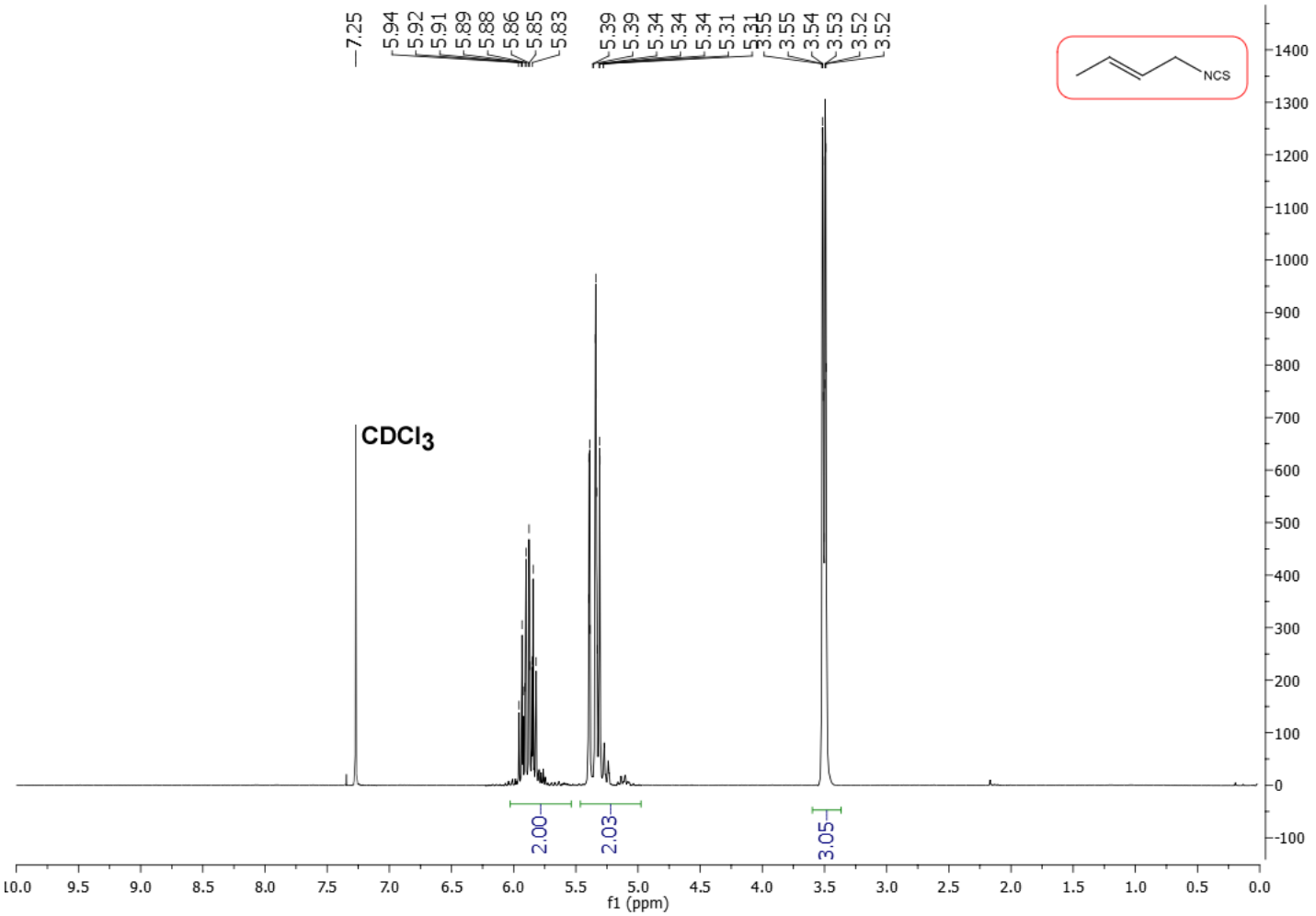
7.25
5.94
5.92
5.91
5.89
5.88
5.86
5.85
5.83
5.39
5.39
5.34
5.34
5.34
5.31
5.31
3.55
3.55
3.54
3.53
3.52
3.52
NCS
CDCl3
2.00
2.03
3.05
f1 (ppm)

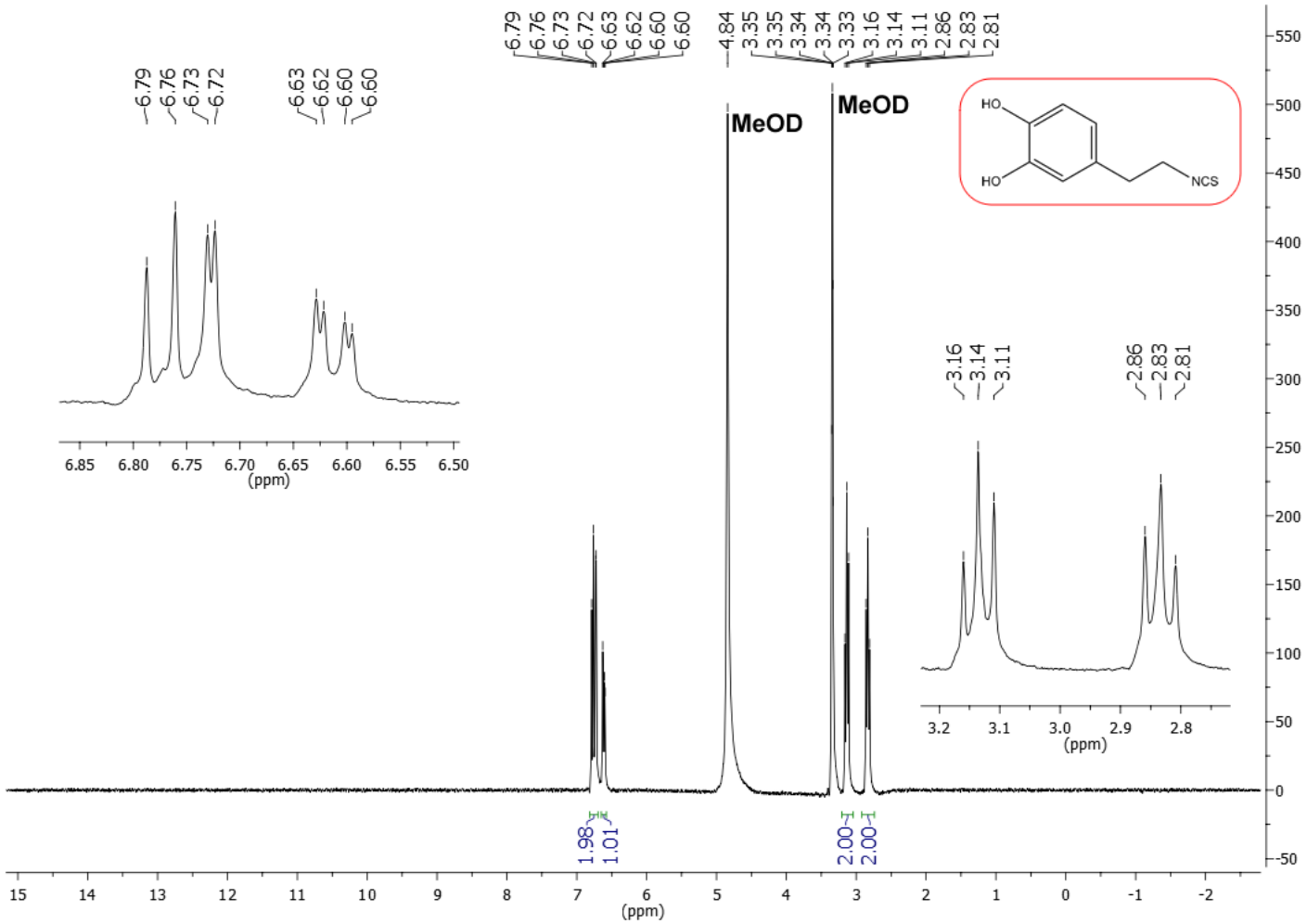
6.79
6.76
6.73
6.72
6.63
6.62
6.60
6.60
4.84
3.35
3.35
3.34
3.34
3.33
3.16
3.14
3.11
2.86
2.83
2.81
MeOD
MeOD
HO
HO
NCS
6.85 6.80 6.75 6.70 6.65 6.60 6.55 6.50
(ppm)
3.2 3.1 3.0 2.9 2.8
(ppm)
1.98
1.01
2.00
2.00
15 14 13 12 11 10 9 8 7 6 5 4 3 2 1 0 -1 -2
(ppm)
550 500 450 400 350 300 250 200 150 100 50 0 -50

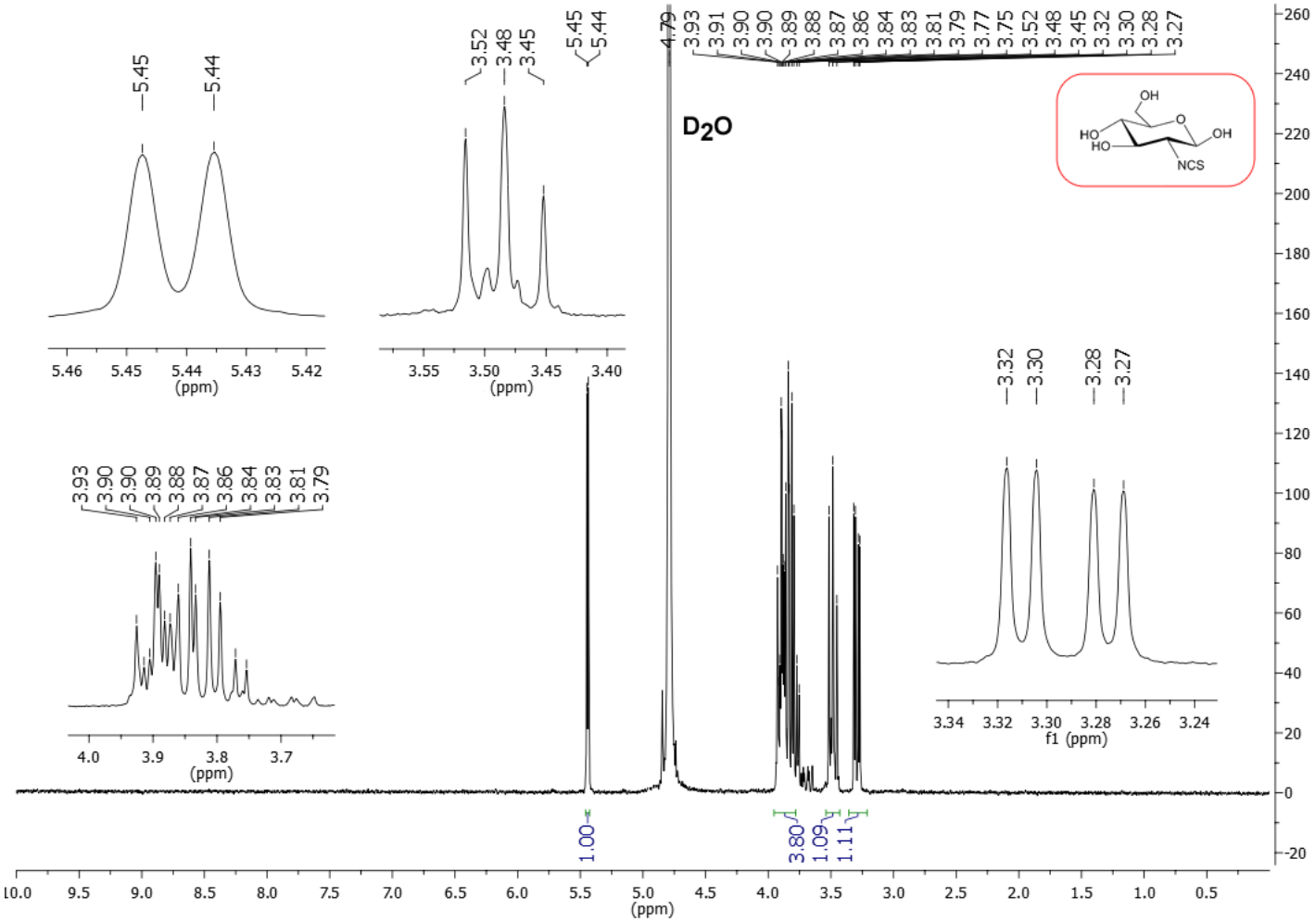
D2O
OH
HO
HO
O
OH
NCS
5.45
5.44
3.52
3.48
3.45
4.79
3.93
3.91
3.90
3.90
3.89
3.88
3.87
3.86
3.84
3.83
3.81
3.79
3.77
3.75
3.52
3.48
3.45
3.32
3.30
3.28
3.27
(ppm)
f1 (ppm)
1.00
3.80
1.09
1.11

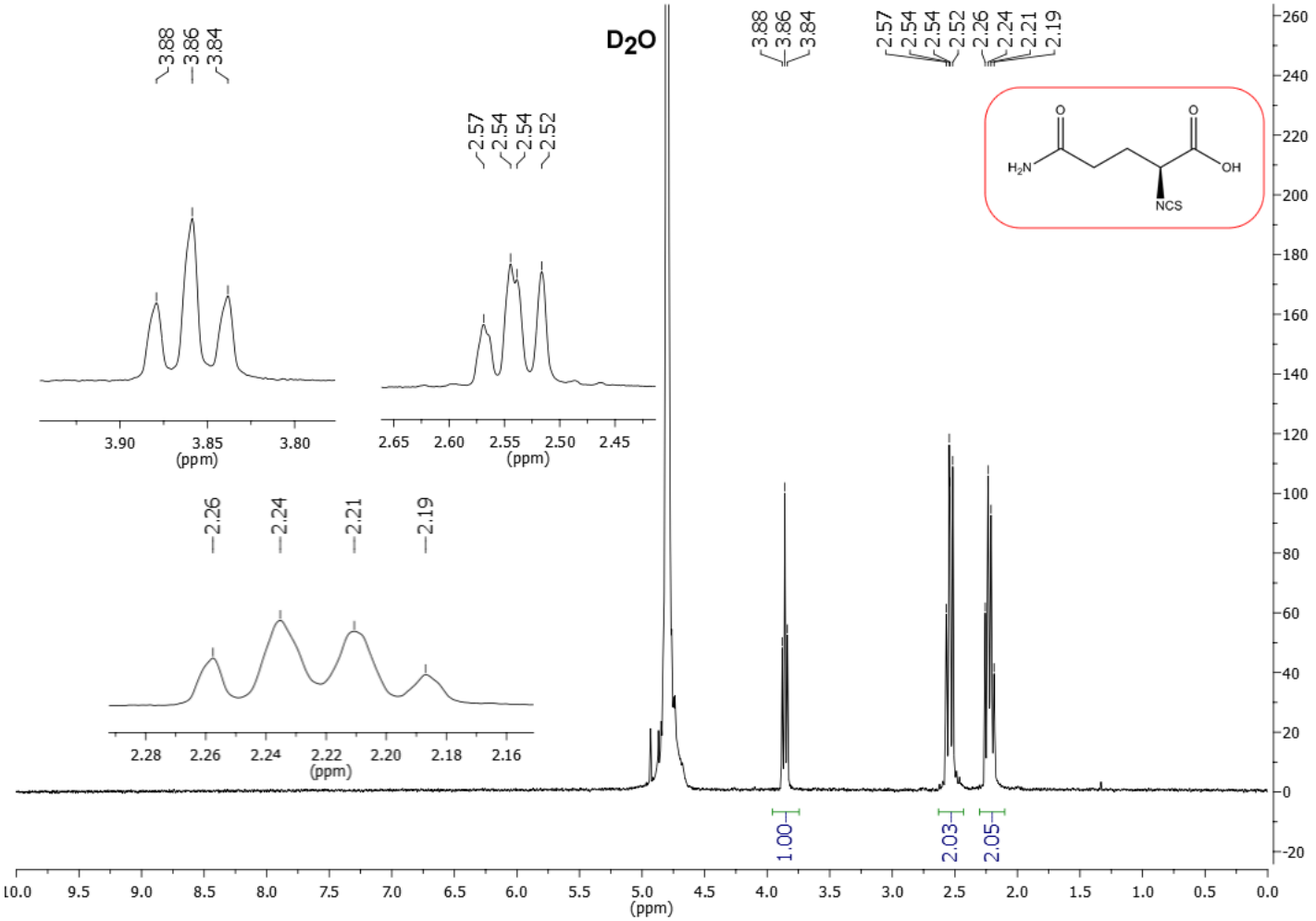
D2O
3.88
3.86
3.84
2.57
2.54
2.54
2.52
2.26
2.24
2.21
2.19
H2N
OH
NCS
1.00
2.03
2.05
(ppm)

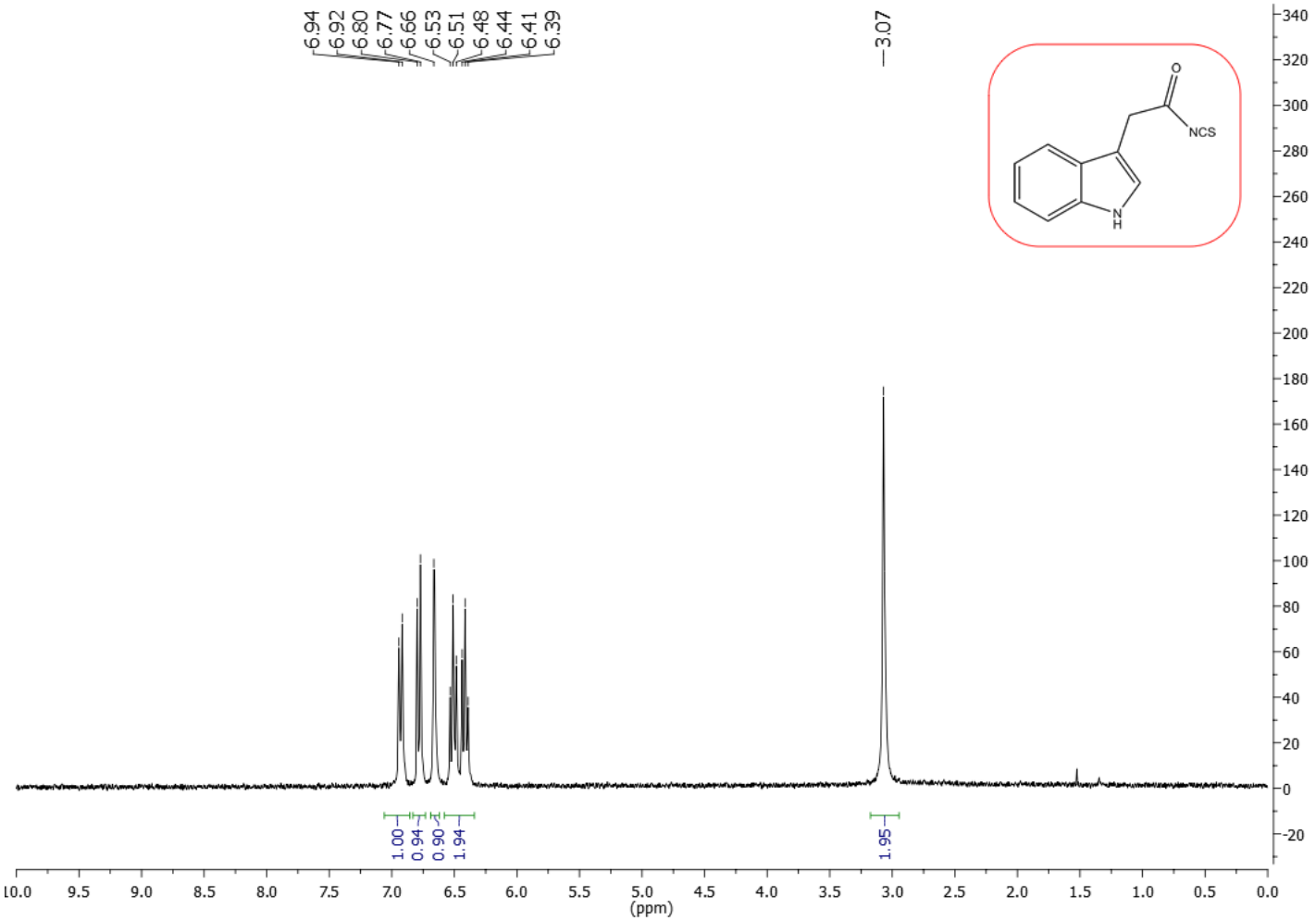
6.94
6.92
6.80
6.77
6.66
6.53
6.51
6.48
6.44
6.41
6.39
3.07
O
NCS
N
H
1.00
0.94
0.90
1.94
1.95
(ppm)

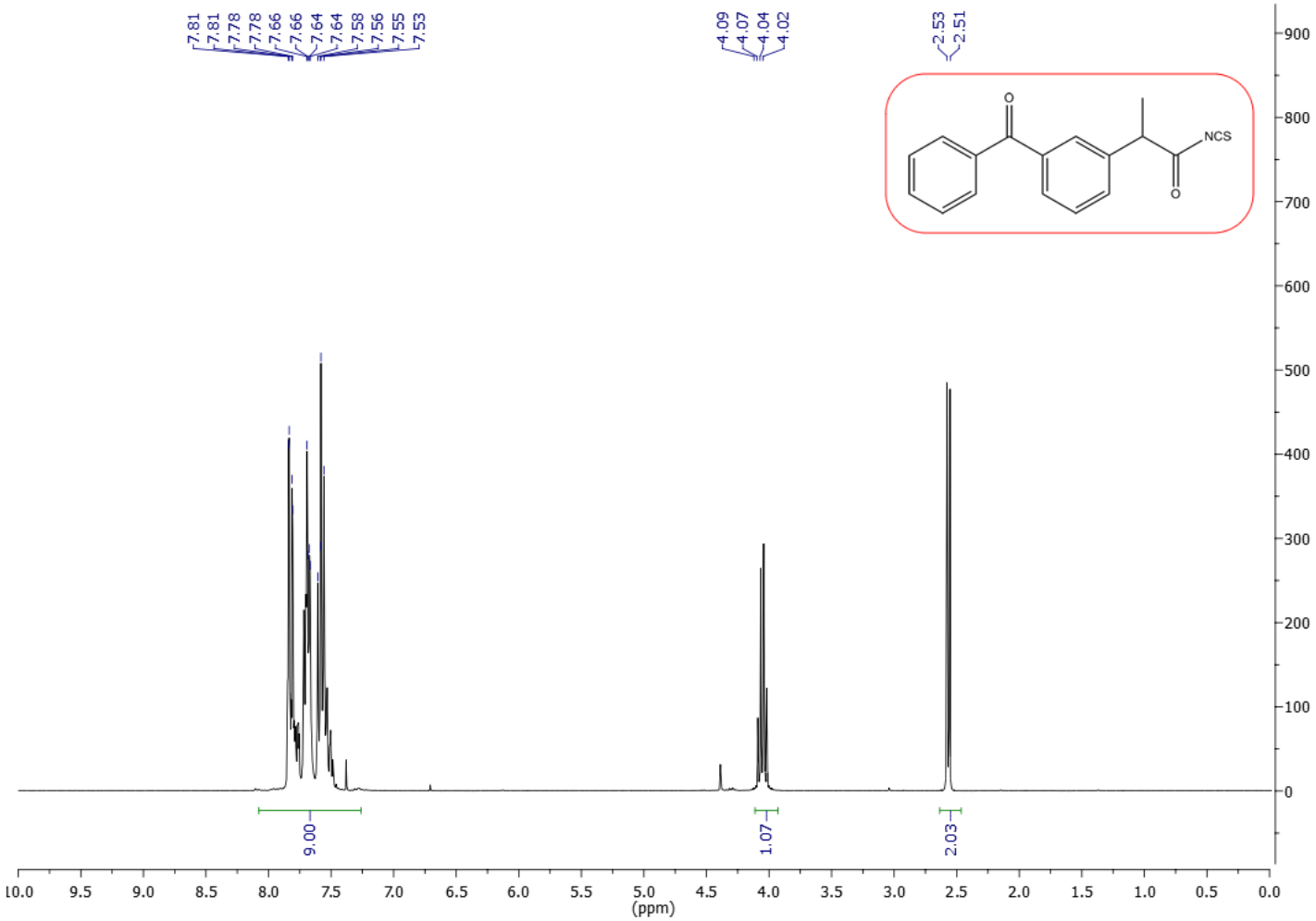
7.81
7.81
7.78
7.78
7.66
7.66
7.64
7.64
7.58
7.56
7.55
7.53
4.09
4.07
4.04
4.02
2.53
2.51
O
NCS
O
9.00
1.07
2.03
(ppm)

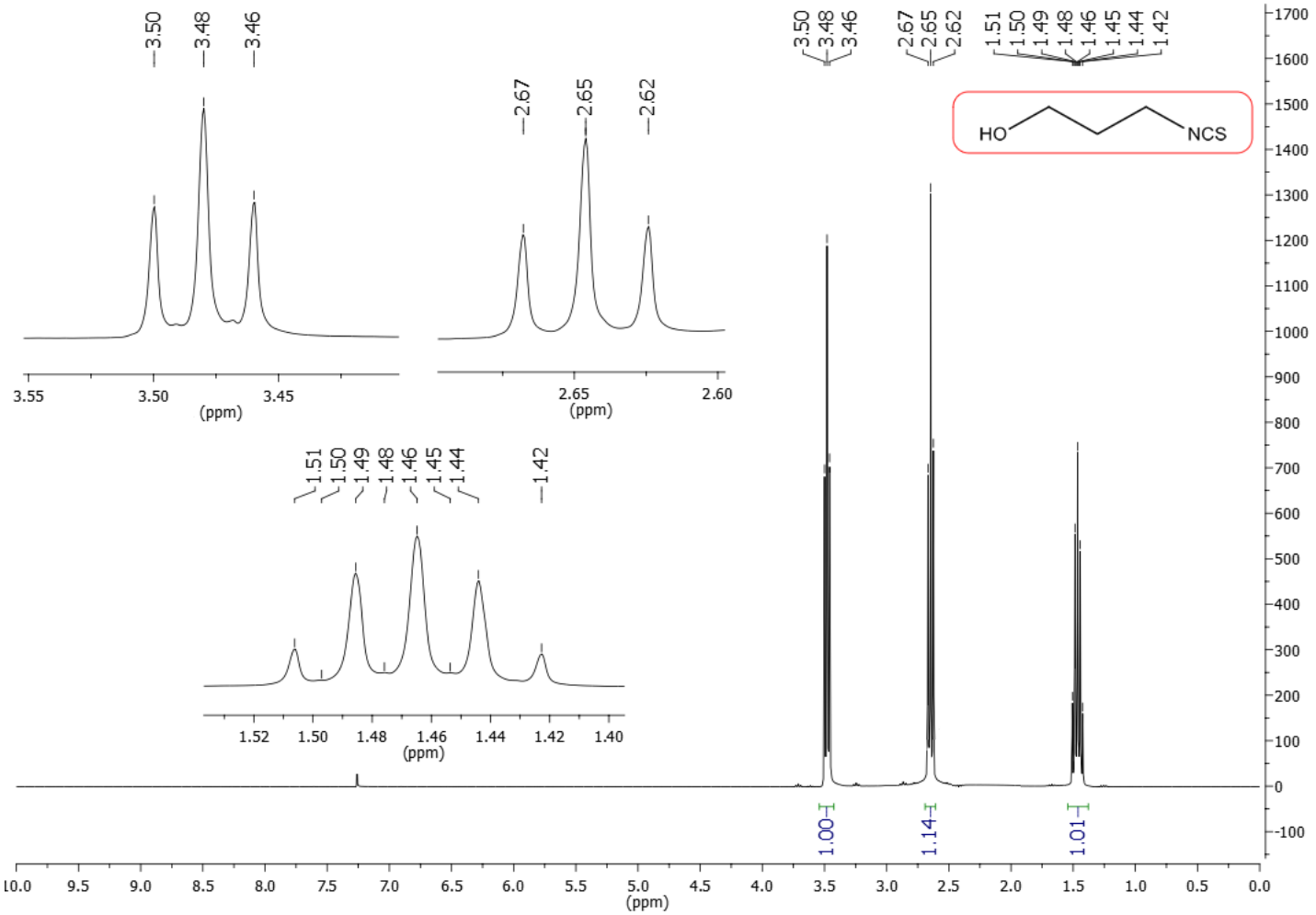
3.50
3.48
3.46
2.67
2.65
2.62
1.51
1.50
1.49
1.48
1.46
1.45
1.44
1.42
HO
NCS
1.00
1.14
1.01
(ppm)

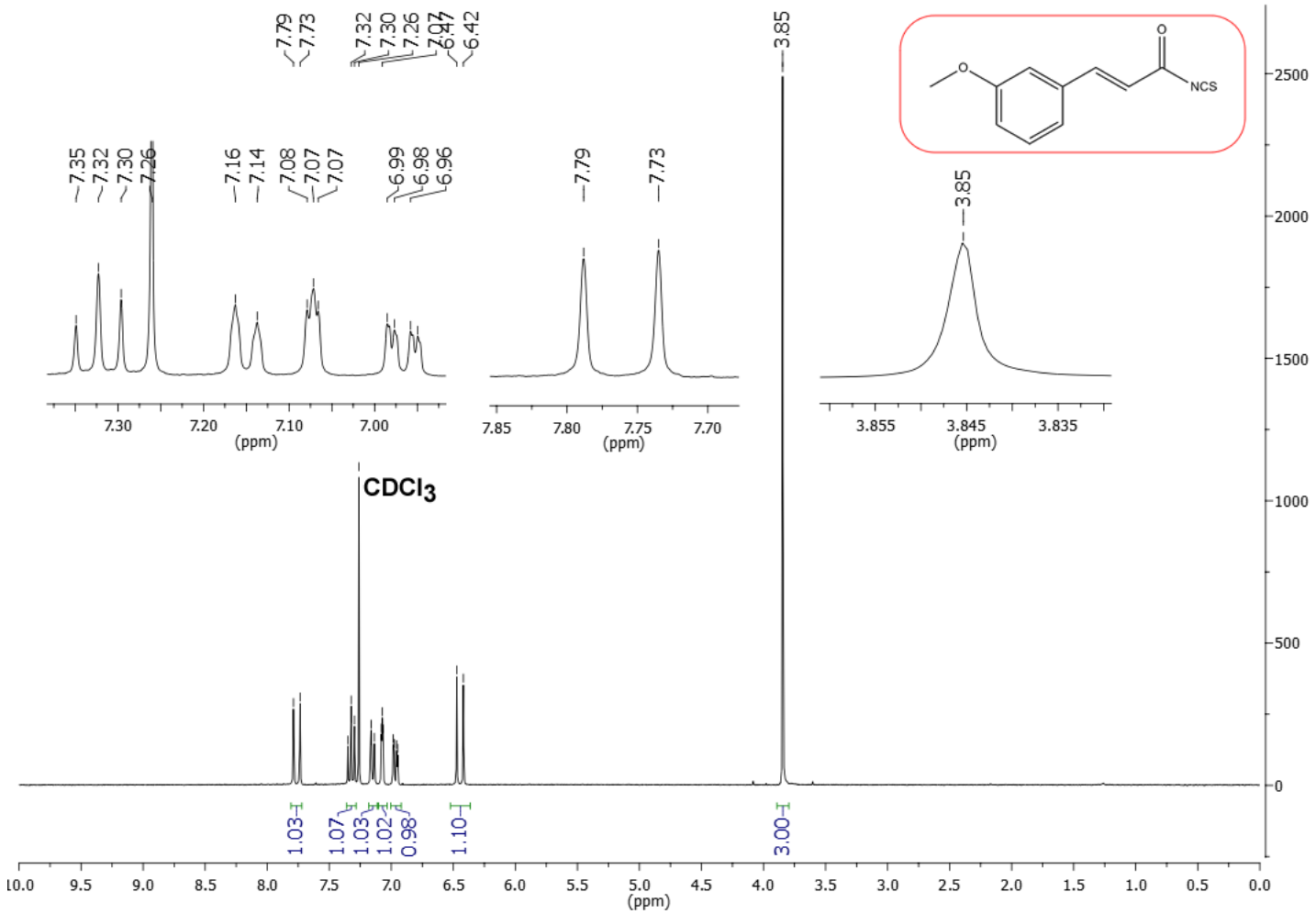
7.79
7.73
7.32
7.30
7.26
7.07
6.47
6.42
3.85
7.35
7.32
7.30
7.26
7.16
7.14
7.08
7.07
7.07
6.99
6.98
6.96
7.79
7.73
3.85
NCS
O
O
7.30
7.20
7.10
7.00
(ppm)
7.85
7.80
7.75
7.70
(ppm)
3.855
3.845
3.835
(ppm)
CDCl3
1.03
1.07
1.03
1.02
0.98
1.10
3.00
10.0
9.5
9.0
8.5
8.0
7.5
7.0
6.5
6.0
5.5
5.0
4.5
4.0
3.5
3.0
2.5
2.0
1.5
1.0
0.5
0.0
(ppm)
2500
2000
1500
1000
500
0

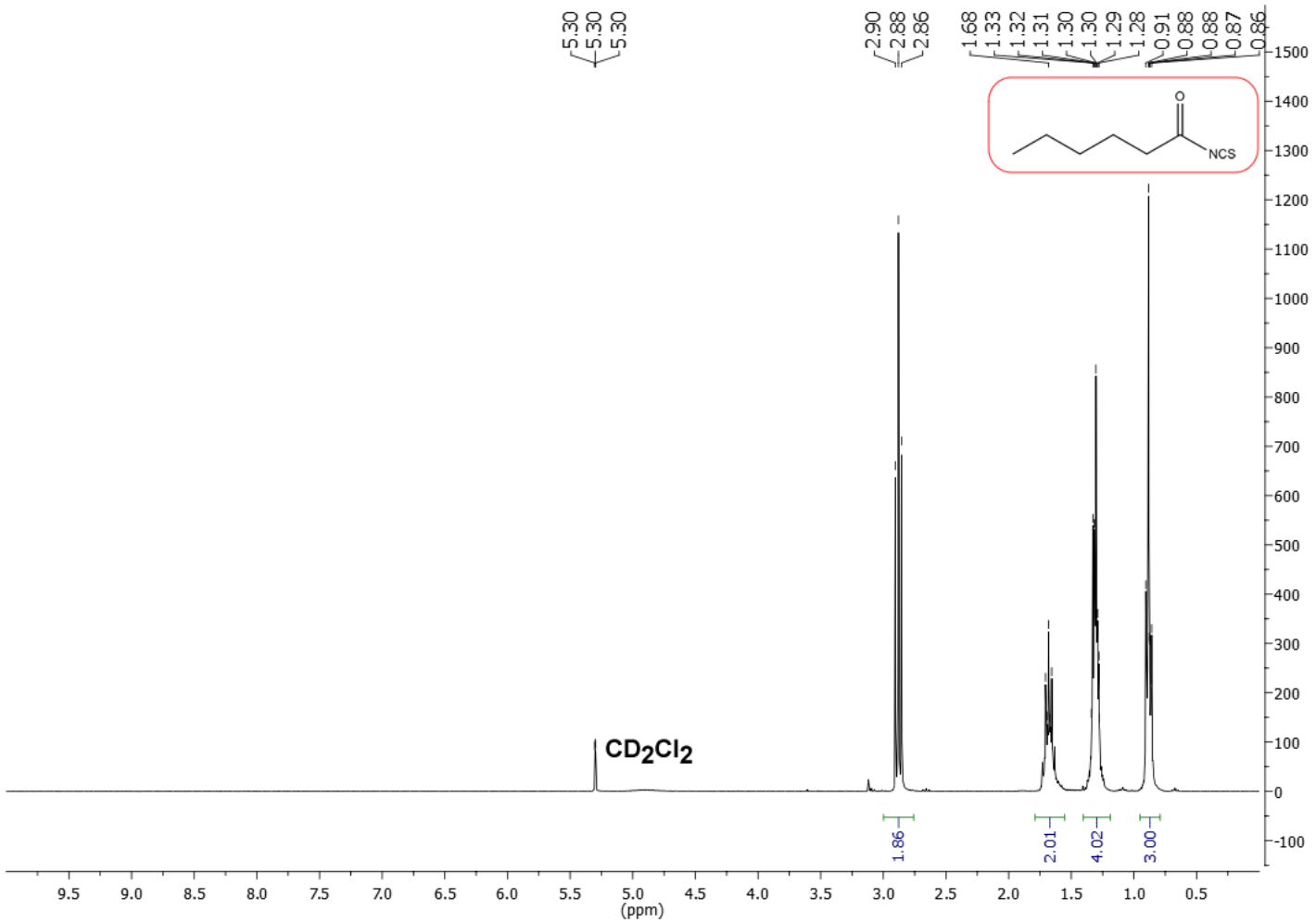
5.30
5.30
5.30
2.90
2.88
2.86
1.68
1.33
1.32
1.31
1.30
1.30
1.29
1.28
0.91
0.88
0.88
0.87
0.86
O
NCS
CD2Cl2
1.86
2.01
4.02
3.00
(ppm)

Appendix B - Dose Response Curves for Complexes 1 – 7

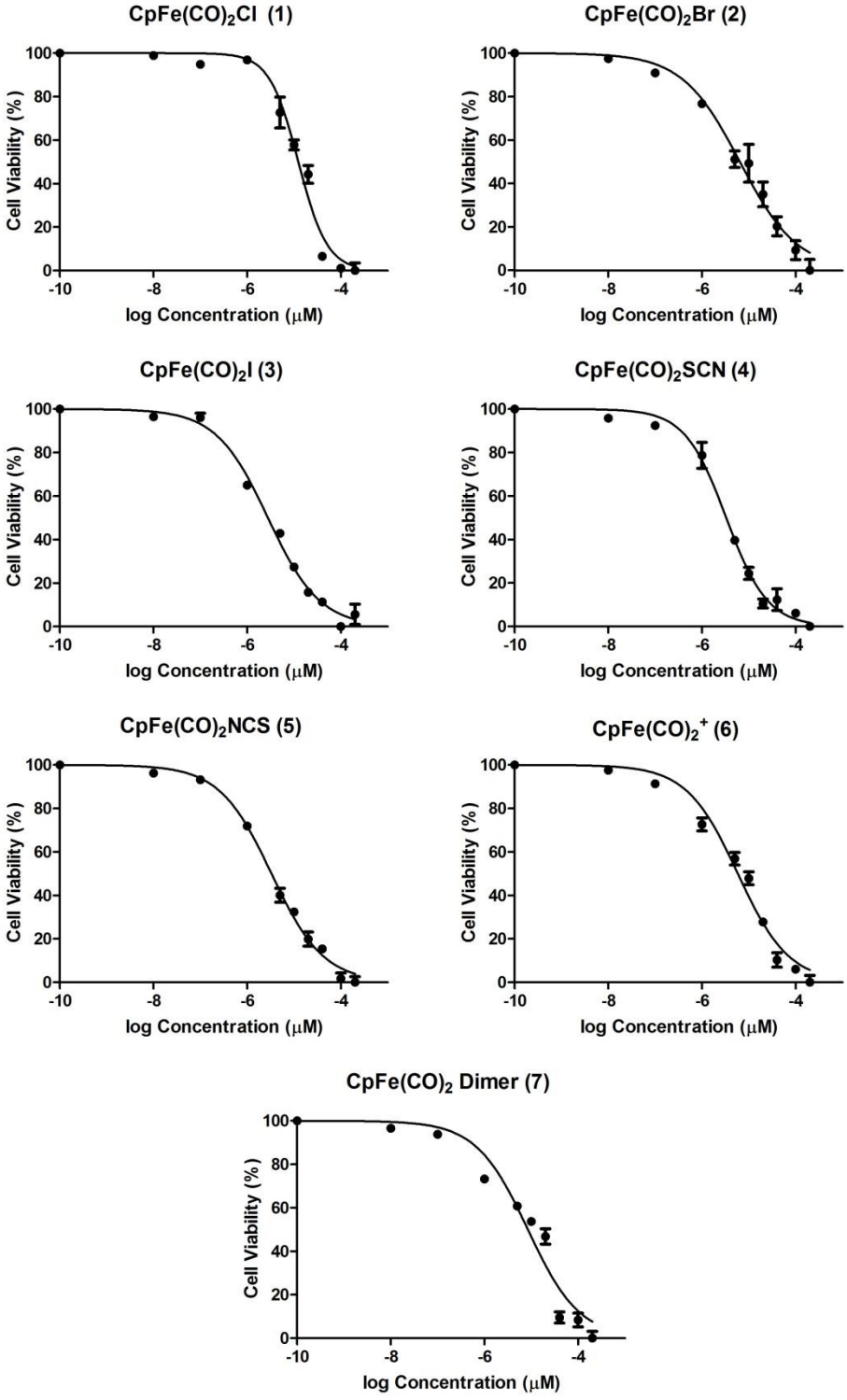

IC50 Plots. Dose response curve for the MDA-MB-231 cell line after separate treatment with complexes **1** – **7**.

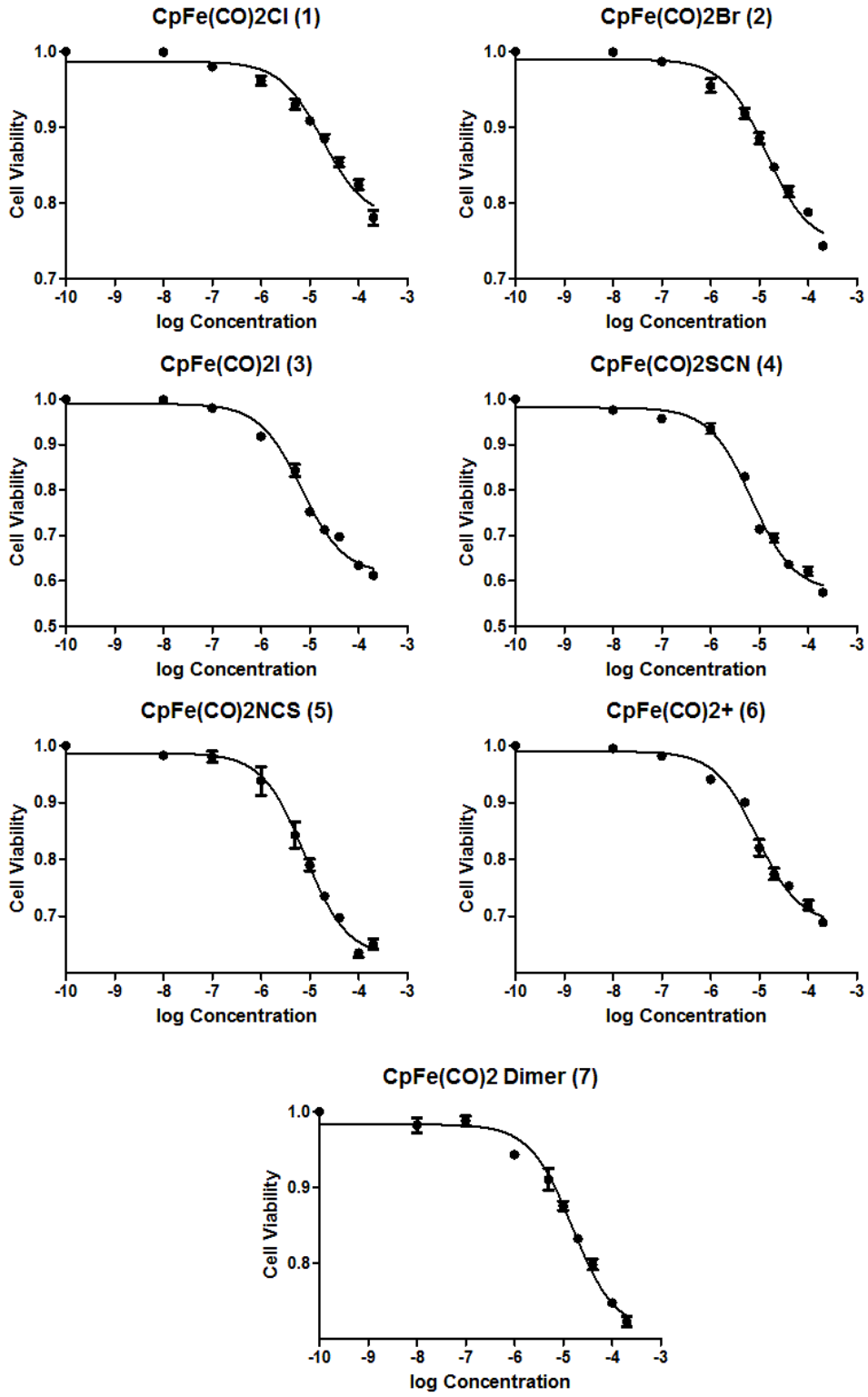

IC50 Plots. Dose response curve for the HeLa cell line after separate treatment with complexes **1** – **7**.

Appendix C – Confocal images

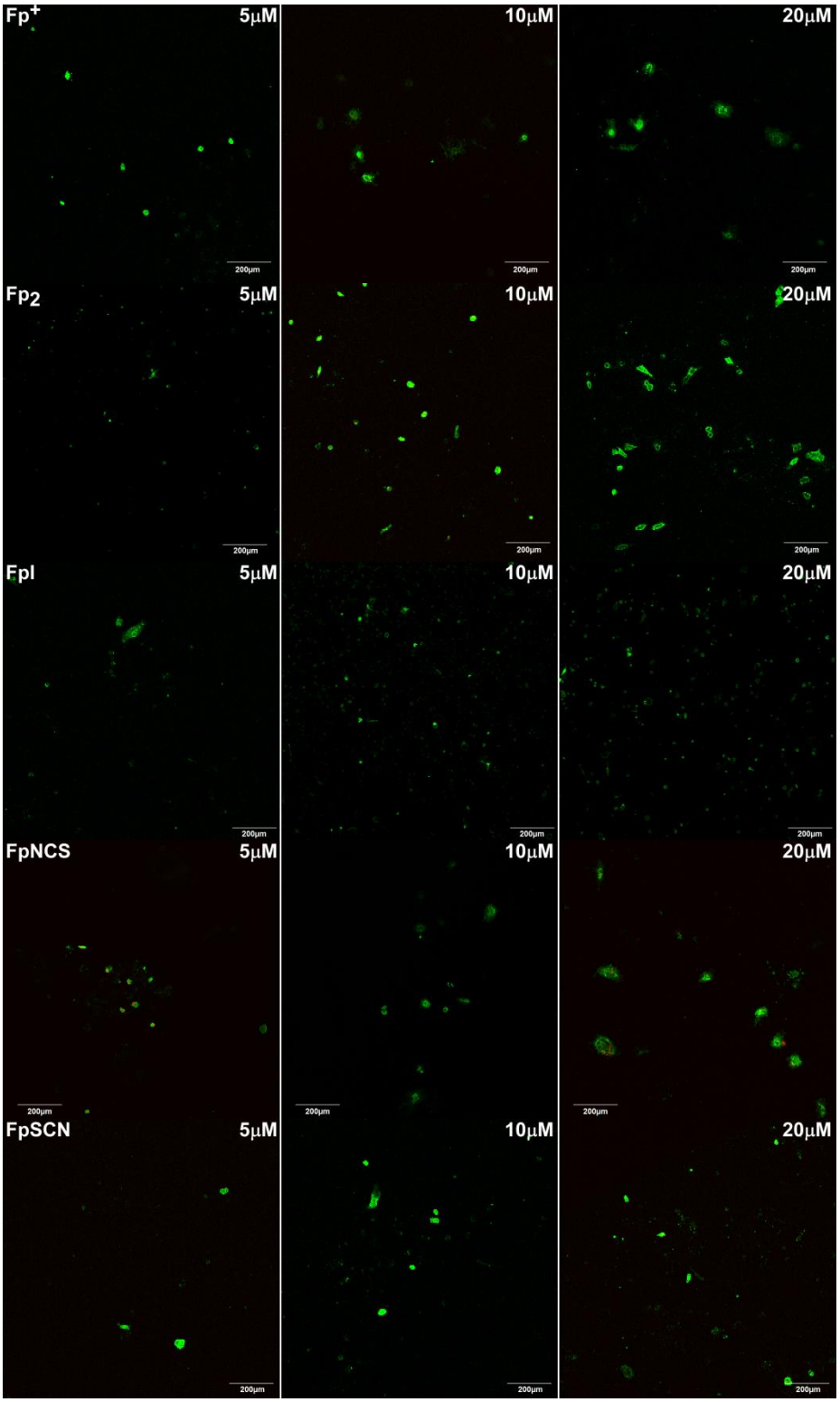

Confocal images of MDA-MB-231 cells after treatment with the respective iron complexes. The cells are stained with Annexin V and PI and the relative distributions of the AV^+/PI^- cells gives an indication of the cell viability after 24 hours incubation.

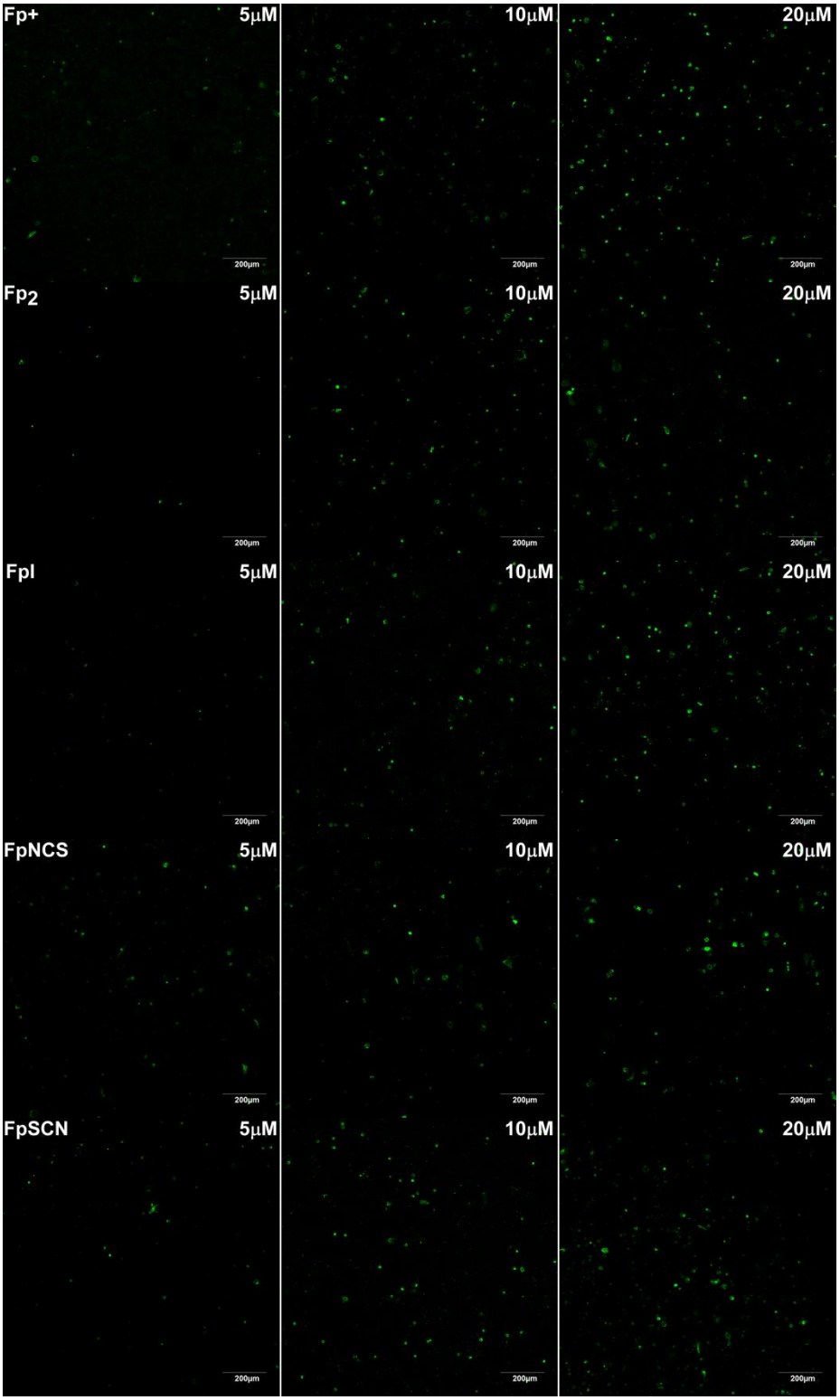

Confocal images of HeLa cells after treatment with the respective iron complexes. The cells are stained with Annexin V and PI and the relative distributions of the AV^{+}/PI^{-} cells gives an indication of the cell viability after 24 hours incubation.

Appendix D – Flow Cytometry Dot Plots

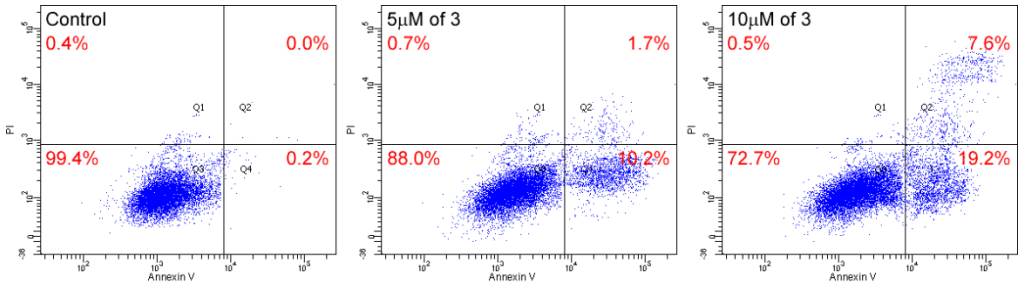

Flow Data of 3 with MDA-MB-231. Detection of early and late apoptotic MDA-MB-231 cells after staining with Annexin V-Alexa Fluor 488 and PI. Cells were incubated for 24 h with 0 (control), 5 and 10 μM solutions of **3** before staining.

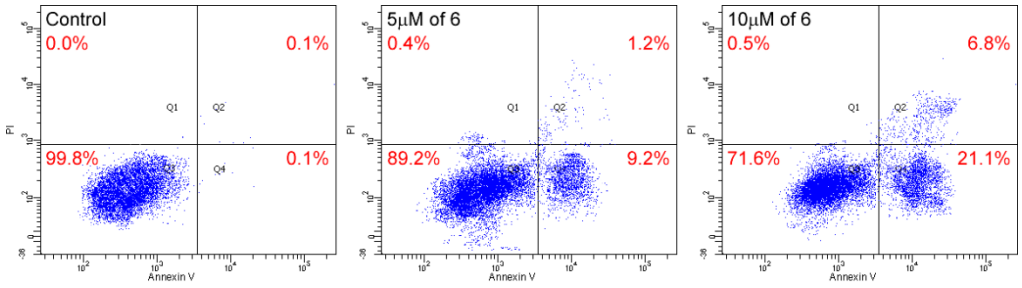

Flow Data of 6 with MDA-MB-231. Detection of early and late apoptotic MDA-MB-231 cells after staining with Annexin V-Alexa Fluor 488 and PI. Cells were incubated for 24 h with 0 (control), 5 and 10 μM solutions of **6** before staining.

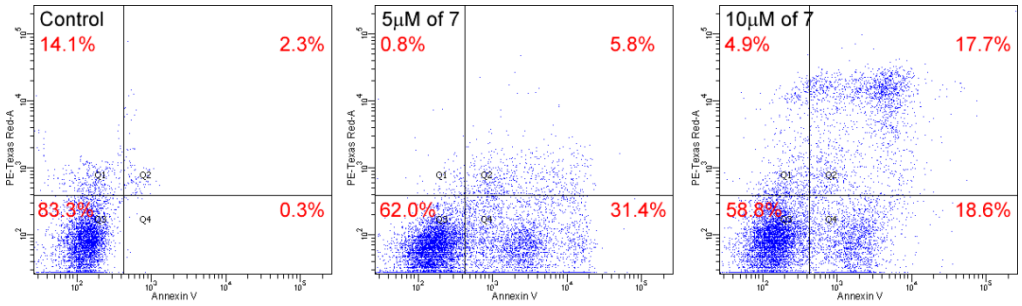

Flow Data of 7 with MDA-MB-231. Detection of early and late apoptotic MDA-MB-231 cells after staining with Annexin V-Alexa Fluor 488 and PI. Cells were incubated for 24 h with 0 (control), 5 and 10 μM solutions of **7** before staining.

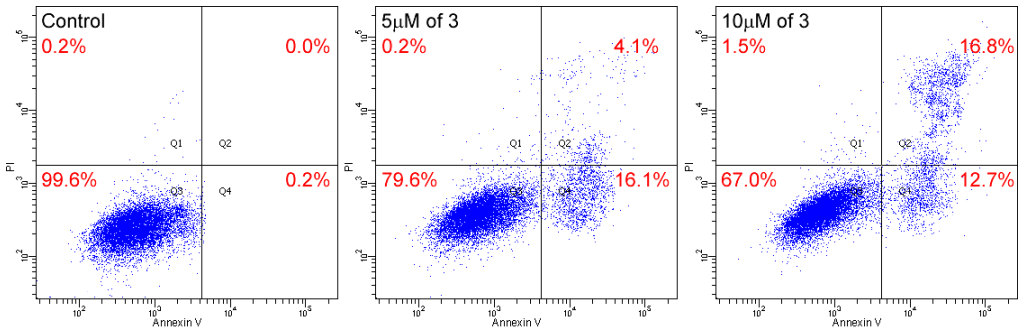

Flow Data of 3 with HeLa. Detection of early and late apoptotic HeLa cells after staining with Annexin V-Alexa Fluor 488 and PI. Cells were incubated for 24 h with 0 (control), 5 and 10 μM solutions of **3** before staining.

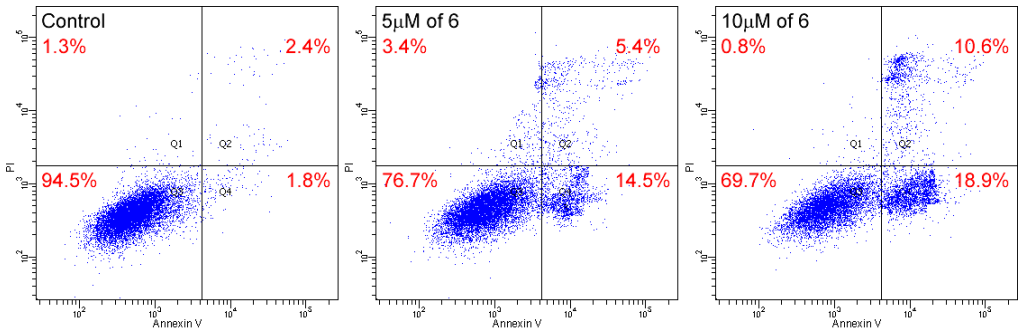

Flow Data of 6 with HeLa. Detection of early and late apoptotic HeLa cells after staining with Annexin V-Alexa Fluor 488 and PI. Cells were incubated for 24 h with 0 (control), 5 and 10 μM solutions of **6** before staining.

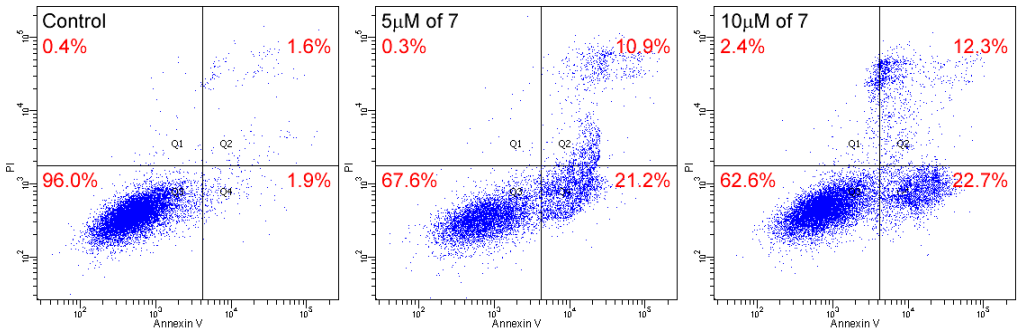

Flow Data of 7 with HeLa. Detection of early and late apoptotic HeLa cells after staining with Annexin V-Alexa Fluor 488 and PI. Cells were incubated for 24 h with 0 (control), 5 and 10 μM solutions of **7** before staining.

Appendix E - Mass Spectrometry Data for $M(CO)_5SH$ Complexes

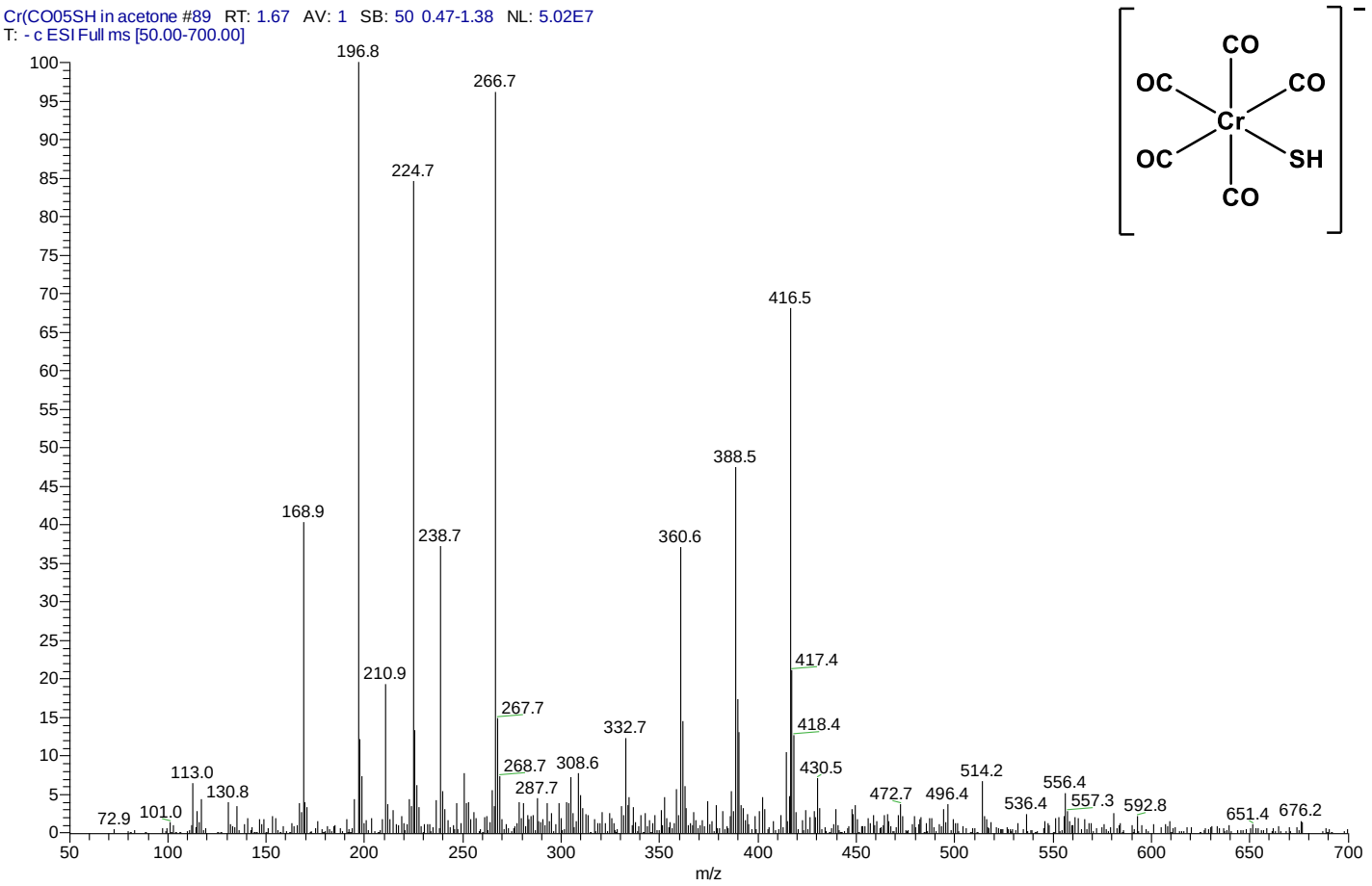

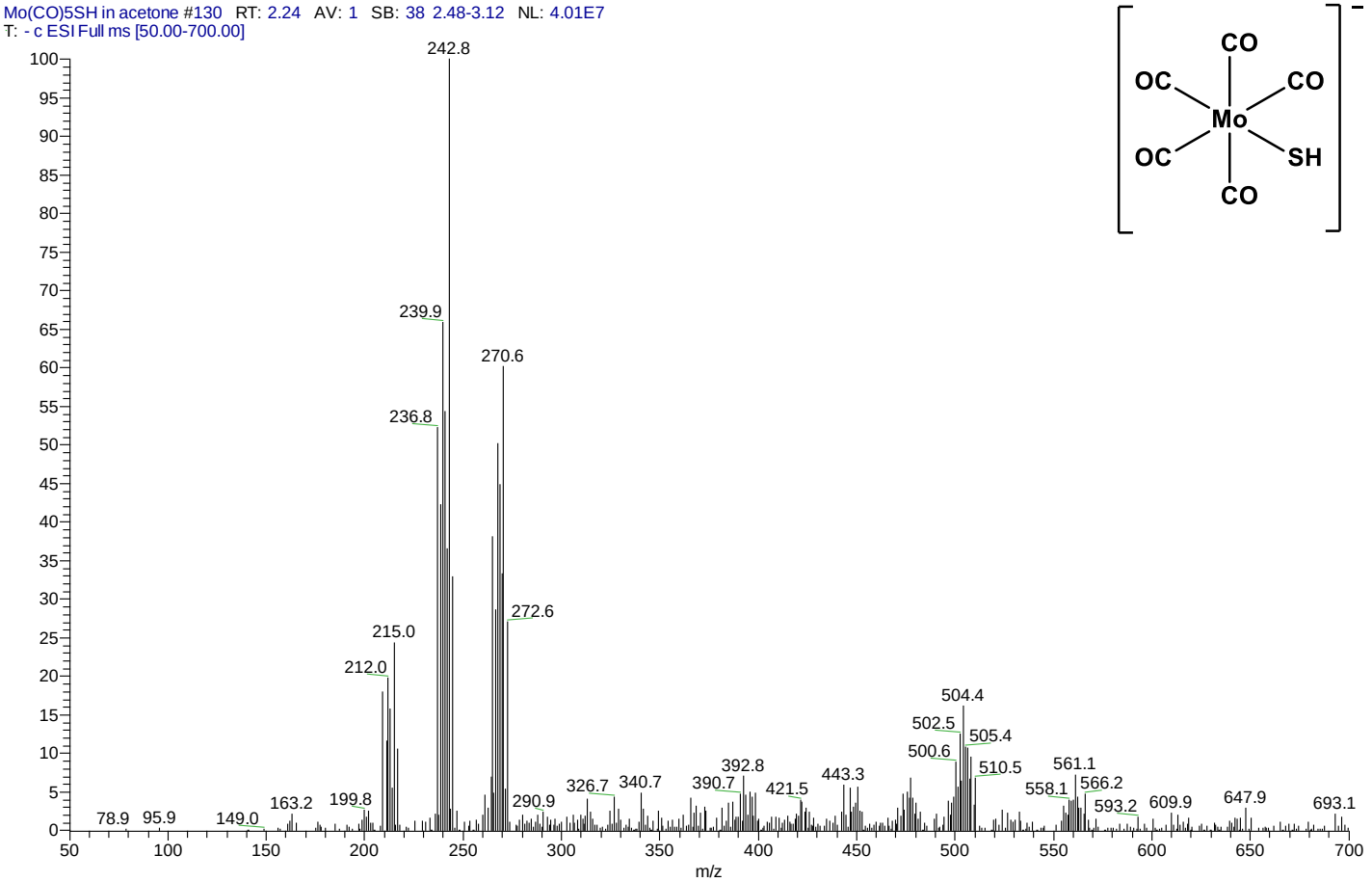
Mo(CO)5SH in acetone #130 RT: 2.24 AV: 1 SB: 38 2.48-3.12 NL: 4.01E7
T: - c ESI Full ms [50.00-700.00]
242.8
239.9
270.6
236.8
272.6
215.0
212.0
504.4
502.5
505.4
500.6
510.5
392.8
561.1
566.2
558.1
593.2
443.3
390.7
421.5
326.7
340.7
290.9
199.8
163.2
78.9
95.9
149.0
609.9
647.9
693.1
m/z
CO
OC
CO
Mo
OC
SH
CO

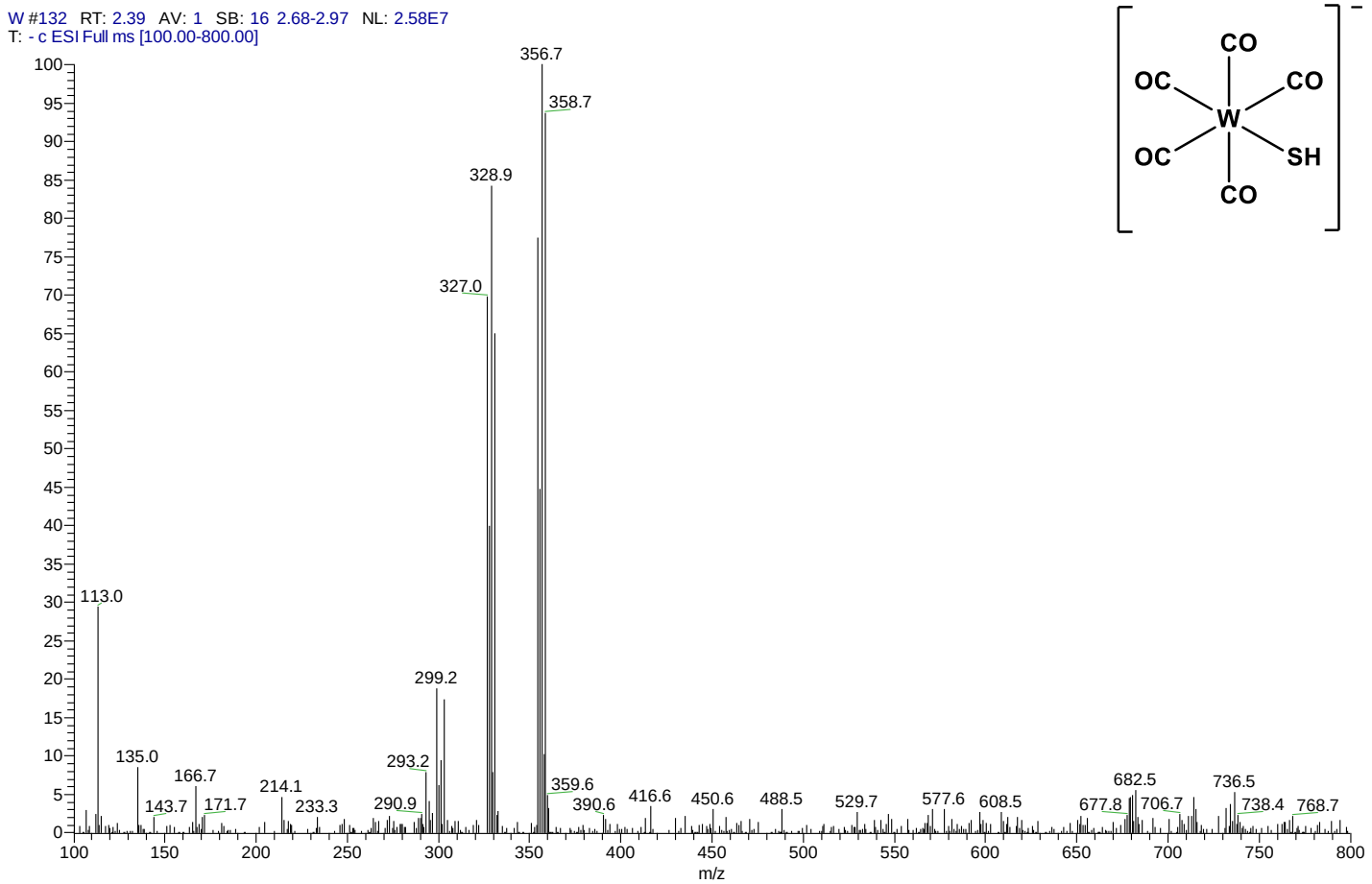
W #132 RT: 2.39 AV: 1 SB: 16 2.68-2.97 NL: 2.58E7
T: - c ESI Full ms [100.00-800.00]
356.7
358.7
328.9
327.0
113.0
299.2
135.0
293.2
166.7
214.1
359.6
143.7
171.7
233.3
290.9
390.6
416.6
450.6
488.5
529.7
577.6
608.5
682.5
736.5
677.8
706.7
738.4
768.7
m/z
CO
OC
CO
W
OC
SH
CO

Appendix F – Crystallographic Data

1. Triphenyl Isothiocyanate

Identification code	c141	
Empirical formula	C20 H15 N S	
Formula weight	301.39	
Temperature	100(2) K	
Wavelength	0.71073 Å	
Crystal system	Monoclinic	
Space group	P2(1)/n	
Unit cell dimensions	a = 9.1433(11) Å	α= 90°.
	b = 17.476(2) Å	β= 106.801(2)°.
	c = 10.1867(13) Å	γ = 90°.
Volume	1558.2(3) $Å^3$	
Z	4	
Density (calculated)	1.285 Mg/m^3	
Absorption coefficient	0.203 mm^{-1}	
F(000)	632	
Crystal size	0.60 x 0.34 x 0.20 mm^3	
Theta range for data collection	2.33 to 27.50°.	
Index ranges	-11<=h<=10, -19<=k<=22, -12<=l<=13	
Reflections collected	10898	
Independent reflections	3571 [R(int) = 0.0298]	
Completeness to theta = 27.50°	100.0 %	
Absorption correction	Semi-empirical from equivalents	
Max. and min. transmission	0.9605 and 0.8879	
Refinement method	Full-matrix least-squares on F^2	
Data / restraints / parameters	3571 / 0 / 199	
Goodness-of-fit on F^2	1.044	
Final R indices [I>2sigma(I)]	R1 = 0.0412, wR2 = 0.1114	
R indices (all data)	R1 = 0.0491, wR2 = 0.1171	
Largest diff. peak and hole	0.411 and -0.412 $e.Å^{-3}$	

Table 2. Atomic coordinates (x 10^4) and equivalent isotropic displacement parameters ($Å^2$ x 10^3) for C141. U(eq) is defined as one third of the trace of the orthogonalized U^{ij} tensor.

	x	y	z	U(eq)
S(1)	2480(1)	405(1)	7611(1)	41(1)
N(1)	4132(1)	1018(1)	6002(1)	19(1)
C(1)	4260(2)	1557(1)	4935(1)	16(1)
C(2)	3435(2)	2298(1)	5107(1)	16(1)
C(3)	3456(2)	2554(1)	6404(1)	19(1)
C(4)	2720(2)	3228(1)	6560(1)	22(1)
C(5)	1974(2)	3654(1)	5420(2)	22(1)
C(6)	1980(2)	3416(1)	4129(2)	24(1)
C(7)	2705(2)	2738(1)	3967(1)	21(1)
C(8)	5968(2)	1696(1)	5143(1)	17(1)
C(9)	6500(2)	2400(1)	4847(2)	22(1)
C(10)	8056(2)	2515(1)	5033(2)	28(1)
C(11)	9082(2)	1927(1)	5513(2)	30(1)
C(12)	8560(2)	1222(1)	5793(2)	31(1)
C(13)	7012(2)	1105(1)	5615(2)	24(1)
C(14)	3468(2)	1157(1)	3566(1)	16(1)
C(15)	4258(2)	926(1)	2666(1)	21(1)
C(16)	3495(2)	548(1)	1460(2)	26(1)
C(17)	1949(2)	405(1)	1146(2)	25(1)
C(18)	1152(2)	637(1)	2046(2)	26(1)
C(19)	1907(2)	1004(1)	3250(2)	23(1)
C(20)	3380(2)	767(1)	6654(1)	21(1)

Table 3. Bond lengths [Å] and angles [°] for C141.

S(1)-C(20)	1.5782(15)
N(1)-C(20)	1.1708(18)
N(1)-C(1)	1.4683(17)
C(1)-C(2)	1.5336(18)
C(1)-C(8)	1.5332(18)
C(1)-C(14)	1.5402(18)
C(2)-C(3)	1.3904(18)
C(2)-C(7)	1.3917(19)
C(3)-C(4)	1.3881(19)
C(3)-H(3)	0.9500
C(4)-C(5)	1.382(2)
C(4)-H(4)	0.9500
C(5)-C(6)	1.382(2)
C(5)-H(5)	0.9500
C(6)-C(7)	1.391(2)
C(6)-H(6)	0.9500
C(7)-H(7)	0.9500
C(8)-C(9)	1.3892(19)
C(8)-C(13)	1.3940(19)
C(9)-C(10)	1.394(2)
C(9)-H(9)	0.9500
C(10)-C(11)	1.382(2)
C(10)-H(10)	0.9500
C(11)-C(12)	1.381(2)
C(11)-H(11)	0.9500
C(12)-C(13)	1.389(2)
C(12)-H(12)	0.9500
C(13)-H(13)	0.9500
C(14)-C(15)	1.3812(19)
C(14)-C(19)	1.3949(19)
C(15)-C(16)	1.392(2)
C(15)-H(15)	0.9500
C(16)-C(17)	1.379(2)
C(16)-H(16)	0.9500
C(17)-C(18)	1.387(2)
C(17)-H(17)	0.9500

C(18)-C(19)	1.380(2)
C(18)-H(18)	0.9500
C(19)-H(19)	0.9500

C(20)-N(1)-C(1)	147.78(13)
N(1)-C(1)-C(2)	108.06(10)
N(1)-C(1)-C(8)	107.14(10)
C(2)-C(1)-C(8)	111.44(10)
N(1)-C(1)-C(14)	105.20(10)
C(2)-C(1)-C(14)	111.59(10)
C(8)-C(1)-C(14)	112.98(10)
C(3)-C(2)-C(7)	119.10(12)
C(3)-C(2)-C(1)	120.58(12)
C(7)-C(2)-C(1)	120.27(12)
C(4)-C(3)-C(2)	120.55(13)
C(4)-C(3)-H(3)	119.7
C(2)-C(3)-H(3)	119.7
C(5)-C(4)-C(3)	119.95(13)
C(5)-C(4)-H(4)	120.0
C(3)-C(4)-H(4)	120.0
C(6)-C(5)-C(4)	120.02(13)
C(6)-C(5)-H(5)	120.0
C(4)-C(5)-H(5)	120.0
C(5)-C(6)-C(7)	120.23(13)
C(5)-C(6)-H(6)	119.9
C(7)-C(6)-H(6)	119.9
C(6)-C(7)-C(2)	120.12(13)
C(6)-C(7)-H(7)	119.9
C(2)-C(7)-H(7)	119.9
C(9)-C(8)-C(13)	118.90(13)
C(9)-C(8)-C(1)	121.13(12)
C(13)-C(8)-C(1)	119.96(12)
C(8)-C(9)-C(10)	120.40(14)
C(8)-C(9)-H(9)	119.8
C(10)-C(9)-H(9)	119.8
C(11)-C(10)-C(9)	120.20(14)
C(11)-C(10)-H(10)	119.9
C(9)-C(10)-H(10)	119.9

C(12)-C(11)-C(10)	119.76(14)
C(12)-C(11)-H(11)	120.1
C(10)-C(11)-H(11)	120.1
C(11)-C(12)-C(13)	120.32(15)
C(11)-C(12)-H(12)	119.8
C(13)-C(12)-H(12)	119.8
C(12)-C(13)-C(8)	120.42(14)
C(12)-C(13)-H(13)	119.8
C(8)-C(13)-H(13)	119.8
C(15)-C(14)-C(19)	119.15(12)
C(15)-C(14)-C(1)	122.30(12)
C(19)-C(14)-C(1)	118.52(12)
C(14)-C(15)-C(16)	120.04(13)
C(14)-C(15)-H(15)	120.0
C(16)-C(15)-H(15)	120.0
C(17)-C(16)-C(15)	120.58(13)
C(17)-C(16)-H(16)	119.7
C(15)-C(16)-H(16)	119.7
C(16)-C(17)-C(18)	119.58(13)
C(16)-C(17)-H(17)	120.2
C(18)-C(17)-H(17)	120.2
C(19)-C(18)-C(17)	119.99(13)
C(19)-C(18)-H(18)	120.0
C(17)-C(18)-H(18)	120.0
C(18)-C(19)-C(14)	120.65(13)
C(18)-C(19)-H(19)	119.7
C(14)-C(19)-H(19)	119.7
N(1)-C(20)-S(1)	175.72(13)

Symmetry transformations used to generate equivalent atoms:

Table 4. Anisotropic displacement parameters ($Å^2$ x 10^3) for C141. The anisotropic displacement factor exponent takes the form: $-2\pi^2[h^2 a^{*2}U^{11} + ... + 2 h k a^* b^* U^{12}]$

	U^{11}	U^{22}	U^{33}	U^{23}	U^{13}	U^{12}
S(1)	28(1)	52(1)	48(1)	29(1)	20(1)	8(1)
N(1)	20(1)	19(1)	20(1)	2(1)	6(1)	1(1)
C(1)	17(1)	16(1)	16(1)	1(1)	6(1)	0(1)
C(2)	13(1)	18(1)	18(1)	-1(1)	5(1)	-1(1)
C(3)	18(1)	22(1)	17(1)	0(1)	4(1)	-1(1)
C(4)	23(1)	23(1)	21(1)	-5(1)	9(1)	-1(1)
C(5)	19(1)	18(1)	29(1)	-4(1)	6(1)	1(1)
C(6)	24(1)	21(1)	23(1)	1(1)	1(1)	2(1)
C(7)	24(1)	22(1)	16(1)	-2(1)	4(1)	1(1)
C(8)	16(1)	21(1)	14(1)	-4(1)	3(1)	-1(1)
C(9)	22(1)	23(1)	25(1)	-3(1)	9(1)	-1(1)
C(10)	26(1)	29(1)	32(1)	-9(1)	14(1)	-9(1)
C(11)	16(1)	45(1)	31(1)	-12(1)	8(1)	-5(1)
C(12)	19(1)	38(1)	33(1)	-1(1)	4(1)	5(1)
C(13)	19(1)	26(1)	26(1)	0(1)	4(1)	1(1)
C(14)	18(1)	14(1)	17(1)	0(1)	4(1)	0(1)
C(15)	16(1)	23(1)	23(1)	-3(1)	6(1)	-3(1)
C(16)	22(1)	32(1)	24(1)	-9(1)	10(1)	-3(1)
C(17)	22(1)	26(1)	23(1)	-8(1)	3(1)	-3(1)
C(18)	14(1)	29(1)	32(1)	-8(1)	4(1)	-3(1)
C(19)	18(1)	26(1)	27(1)	-7(1)	9(1)	-2(1)
C(20)	17(1)	20(1)	22(1)	4(1)	2(1)	4(1)

Table 5. Hydrogen coordinates (x 10^4) and isotropic displacement parameters ($Å^2$x 10 ^{3}) for C141.

	x	y	z	U(eq)
H(3)	3980	2266	7191	23
H(4)	2729	3396	7449	26
H(5)	1456	4111	5525	27
H(6)	1487	3716	3349	28
H(7)	2702	2574	3077	25
H(9)	5800	2806	4515	27
H(10)	8411	2999	4830	33
H(11)	10143	2008	5650	37
H(12)	9263	815	6109	37
H(13)	6663	619	5816	29
H(15)	5322	1025	2871	25
H(16)	4045	387	847	31
H(17)	1434	149	319	30
H(18)	85	543	1834	31
H(19)	1359	1155	3871	28

2. Hexanoyl Isothiocyanate

Table 1. Crystal data and structure refinement for C164.

Identification code	c164	
Empirical formula	C7 H14 N2 O S	
Formula weight	174.26	
Temperature	100(2) K	
Wavelength	0.71073 Å	
Crystal system	Triclinic	
Space group	P-1	
Unit cell dimensions	a = 5.001(9) Å	α= 83.64(3)°.
	b = 6.898(13) Å	β= 86.47(3)°.
	c = 13.48(3) Å	γ = 85.77(3)°.
Volume	460.2(15) $Å^3$	
Z	2	
Density (calculated)	1.257 Mg/m^3	
Absorption coefficient	0.301 mm^{-1}	
F(000)	188	
Crystal size	0.60 x 0.04 x 0.02 mm^3	
Theta range for data collection	2.98 to 25.00°.	
Index ranges	-5<=h<=5, -4<=k<=8, -15<=l<=15	
Reflections collected	2557	
Independent reflections	1593 [R(int) = 0.0487]	
Completeness to theta = 25.00°	99.2 %	
Absorption correction	Semi-empirical from equivalents	
Max. and min. transmission	0.9940 and 0.8400	
Refinement method	Full-matrix least-squares on F^2	
Data / restraints / parameters	1593 / 0 / 113	
Goodness-of-fit on F^2	1.066	
Final R indices [I>2sigma(I)]	R1 = 0.0726, wR2 = 0.1580	
R indices (all data)	R1 = 0.1188, wR2 = 0.1842	
Largest diff. peak and hole	0.439 and -0.333 $e.Å^{-3}$	

Table 2. Atomic coordinates (x 10^4) and equivalent isotropic displacement parameters ($Å^2$x 10^3) for C164. U(eq) is defined as one third of the trace of the orthogonalized U^{ij} tensor.

	x	y	z	U(eq)
S(1)	7034(3)	-2779(2)	-141(1)	26(1)
O(2)	10791(7)	-142(5)	2337(3)	29(1)
C(1)	8681(10)	-2036(8)	773(4)	23(1)
N(1)	10850(9)	-2952(7)	1131(4)	28(1)
N(2)	7720(9)	-367(7)	1179(4)	24(1)
C(3)	8787(11)	515(8)	1911(4)	26(1)
C(4)	7179(10)	2361(8)	2148(4)	27(1)
C(5)	8293(10)	3349(8)	2965(4)	26(1)
C(6)	6524(10)	5130(8)	3223(4)	28(1)
C(7)	7650(11)	6237(8)	3971(4)	31(1)
C(8)	5872(12)	7999(8)	4238(5)	39(2)

Table 3. Bond lengths [Å] and angles [°] for C164.

S(1)-C(1)	1.669(6)
O(2)-C(3)	1.219(6)
C(1)-N(1)	1.306(7)
C(1)-N(2)	1.372(7)
N(2)-C(3)	1.369(7)
C(3)-C(4)	1.510(8)
C(4)-C(5)	1.511(8)
C(5)-C(6)	1.520(8)
C(6)-C(7)	1.490(8)
C(7)-C(8)	1.515(8)
N(1)-C(1)-N(2)	117.4(5)
N(1)-C(1)-S(1)	123.8(5)
N(2)-C(1)-S(1)	118.7(4)
C(3)-N(2)-C(1)	128.1(5)
O(2)-C(3)-N(2)	123.6(5)
O(2)-C(3)-C(4)	123.7(5)
N(2)-C(3)-C(4)	112.7(5)
C(3)-C(4)-C(5)	113.8(5)
C(4)-C(5)-C(6)	112.0(4)
C(7)-C(6)-C(5)	113.9(5)
C(6)-C(7)-C(8)	113.9(5)

Symmetry transformations used to generate equivalent atoms:

Table 4. Anisotropic displacement parameters ($Å^2$ x 10^3) for C164. The anisotropic displacement factor exponent takes the form: $-2\pi^2[h^2 a^{*2}U^{11} + ... + 2 h k a^* b^* U^{12}]$

	U^{11}	U^{22}	U^{33}	U^{23}	U^{13}	U^{12}
S(1)	19(1)	20(1)	39(1)	-12(1)	-5(1)	5(1)
O(2)	22(2)	27(2)	41(2)	-7(2)	-10(2)	5(2)
C(1)	17(3)	21(3)	28(3)	1(2)	5(2)	-2(2)
N(1)	19(2)	24(3)	41(3)	-16(2)	-7(2)	9(2)
N(2)	18(2)	17(3)	38(3)	-10(2)	-5(2)	2(2)
C(3)	31(3)	18(3)	27(3)	-2(2)	9(3)	1(2)
C(4)	25(3)	21(3)	34(3)	-10(2)	1(2)	3(2)
C(5)	23(3)	22(3)	32(3)	-7(2)	1(2)	-3(2)
C(6)	19(3)	27(3)	37(3)	-5(3)	-3(2)	2(2)
C(7)	33(3)	25(3)	34(3)	-4(3)	-3(3)	-2(3)
C(8)	40(4)	29(4)	50(4)	-19(3)	-3(3)	5(3)

Table 5. Hydrogen coordinates (x 10^4) and isotropic displacement parameters ($Å^2$x 10 ^{3}) for C164.

	x	y	z	U(eq)
H(1N)	11850(90)	-2430(70)	1640(40)	17(13)
H(2N)	11500(120)	-3920(90)	840(40)	35(18)
H(1A)	6520(130)	160(100)	870(50)	50(20)
H(4A)	5314	2041	2353	32
H(4B)	7116	3291	1534	32
H(5A)	10113	3753	2746	31
H(5B)	8453	2404	3571	31
H(6A)	6247	6017	2604	33
H(6B)	4747	4702	3487	33
H(7A)	9417	6678	3704	37
H(7B)	7947	5345	4588	37
H(8A)	5715	8954	3646	58
H(8B)	6666	8595	4768	58
H(8C)	4087	7587	4473	58

Table 6. Hydrogen bonds for C164 [Å and °].

D-H...A	d(D-H)	d(H...A)	d(D...A)	<(DHA)
N(1)-H(1N)...O(2)	0.99(5)	1.95(5)	2.663(7)	127(4)
N(1)-H(2N)...S(1)#1	0.85(6)	2.60(7)	3.436(7)	171(5)
N(2)-H(1A)...S(1)#2	0.79(7)	2.60(7)	3.362(6)	162(7)

Symmetry transformations used to generate equivalent atoms:
#1 -x+2,-y-1,-z #2 -x+1,-y,-z

3. Cyclopentadienyl iron dicarbonyl thiocyanate

Table 1. Crystal data and structure refinement for C790.

Identification code	c790	
Empirical formula	C8 H5 Fe N O2 S	
Formula weight	235.04	
Temperature	100(2) K	
Wavelength	0.71073 Å	
Crystal system	Triclinic	
Space group	P-1	
Unit cell dimensions	a = 6.798(4) Å	α= 93.169(7)°.
	b = 7.024(4) Å	β= 95.036(7)°.
	c = 10.813(6) Å	γ = 118.514(7)°.
Volume	449.1(4) $Å^3$	
Z	2	
Density (calculated)	1.738 Mg/m^3	
Absorption coefficient	1.871 mm^{-1}	
F(000)	236	
Crystal size	0.40 x 0.26 x 0.10 mm^3	
Theta range for data collection	1.90 to 27.50°.	
Index ranges	-8<=h<=8, -9<=k<=9, -14<=l<=14	
Reflections collected	4151	
Independent reflections	2052 [R(int) = 0.0515]	
Completeness to theta = 27.50°	99.3 %	
Absorption correction	Semi-empirical from equivalents	
Max. and min. transmission	0.7457 and 0.5570	
Refinement method	Full-matrix least-squares on F^2	
Data / restraints / parameters	2052 / 0 / 118	
Goodness-of-fit on F^2	1.065	
Final R indices [I>2sigma(I)]	R1 = 0.0533, wR2 = 0.1200	
R indices (all data)	R1 = 0.0738, wR2 = 0.1469	
Largest diff. peak and hole	0.932 and -0.803 $e.Å^{-3}$	

Table 2. Atomic coordinates (x 10^4) and equivalent isotropic displacement parameters ($Å^2$ x 10^3) for C790. U(eq) is defined as one third of the trace of the orthogonalized U^{ij} tensor.

	x	y	z	U(eq)
Fe(1)	5305(1)	2275(1)	2345(1)	10(1)
S(1)	3906(2)	-1262(2)	1484(1)	17(1)
O(1)	1895(6)	898(6)	4058(3)	23(1)
O(2)	2515(7)	3033(7)	435(4)	28(1)
N(1)	3899(8)	-3427(8)	3640(4)	23(1)
C(1)	7645(8)	4815(8)	3658(5)	16(1)
C(2)	7870(9)	5491(9)	2433(5)	21(1)
C(3)	8446(8)	4115(9)	1697(5)	17(1)
C(4)	8586(9)	2631(9)	2479(5)	20(1)
C(5)	8068(8)	3019(8)	3681(5)	17(1)
C(6)	3916(8)	-2506(8)	2776(5)	15(1)
C(7)	3219(8)	1435(8)	3394(4)	13(1)
C(8)	3615(9)	2715(8)	1168(5)	17(1)

Table 3. Bond lengths [Å] and angles [°] for C790.

Fe(1)-C(8)	1.778(5)
Fe(1)-C(7)	1.789(5)
Fe(1)-C(2)	2.083(5)
Fe(1)-C(1)	2.084(5)
Fe(1)-C(5)	2.096(5)
Fe(1)-C(3)	2.109(5)
Fe(1)-C(4)	2.114(5)
Fe(1)-S(1)	2.2970(18)
S(1)-C(6)	1.690(5)
O(1)-C(7)	1.135(6)
O(2)-C(8)	1.146(6)
N(1)-C(6)	1.163(7)
C(1)-C(5)	1.422(7)
C(1)-C(2)	1.428(7)
C(1)-H(1)	1.0000
C(2)-C(3)	1.432(8)
C(2)-H(2)	1.0000
C(3)-C(4)	1.410(7)
C(3)-H(3)	1.0000
C(4)-C(5)	1.422(7)
C(4)-H(4)	1.0000
C(5)-H(5)	1.0000
C(8)-Fe(1)-C(7)	93.9(2)
C(8)-Fe(1)-C(2)	91.3(2)
C(7)-Fe(1)-C(2)	122.0(2)
C(8)-Fe(1)-C(1)	121.2(2)
C(7)-Fe(1)-C(1)	91.4(2)
C(2)-Fe(1)-C(1)	40.1(2)
C(8)-Fe(1)-C(5)	158.1(2)
C(7)-Fe(1)-C(5)	96.8(2)
C(2)-Fe(1)-C(5)	66.9(2)
C(1)-Fe(1)-C(5)	39.8(2)
C(8)-Fe(1)-C(3)	97.6(2)
C(7)-Fe(1)-C(3)	158.5(2)
C(2)-Fe(1)-C(3)	40.0(2)

C(1)-Fe(1)-C(3)	67.1(2)
C(5)-Fe(1)-C(3)	66.8(2)
C(8)-Fe(1)-C(4)	133.4(2)
C(7)-Fe(1)-C(4)	132.7(2)
C(2)-Fe(1)-C(4)	65.9(2)
C(1)-Fe(1)-C(4)	66.2(2)
C(5)-Fe(1)-C(4)	39.5(2)
C(3)-Fe(1)-C(4)	39.0(2)
C(8)-Fe(1)-S(1)	90.99(17)
C(7)-Fe(1)-S(1)	91.22(16)
C(2)-Fe(1)-S(1)	146.40(17)
C(1)-Fe(1)-S(1)	147.46(15)
C(5)-Fe(1)-S(1)	107.74(15)
C(3)-Fe(1)-S(1)	106.59(15)
C(4)-Fe(1)-S(1)	88.71(15)
C(6)-S(1)-Fe(1)	100.96(17)
C(5)-C(1)-C(2)	107.8(4)
C(5)-C(1)-Fe(1)	70.5(3)
C(2)-C(1)-Fe(1)	69.9(3)
C(5)-C(1)-H(1)	126.1
C(2)-C(1)-H(1)	126.1
Fe(1)-C(1)-H(1)	126.1
C(1)-C(2)-C(3)	108.3(5)
C(1)-C(2)-Fe(1)	70.0(3)
C(3)-C(2)-Fe(1)	71.0(3)
C(1)-C(2)-H(2)	125.8
C(3)-C(2)-H(2)	125.8
Fe(1)-C(2)-H(2)	125.8
C(4)-C(3)-C(2)	106.9(5)
C(4)-C(3)-Fe(1)	70.7(3)
C(2)-C(3)-Fe(1)	69.0(3)
C(4)-C(3)-H(3)	126.5
C(2)-C(3)-H(3)	126.5
Fe(1)-C(3)-H(3)	126.5
C(3)-C(4)-C(5)	109.5(5)
C(3)-C(4)-Fe(1)	70.3(3)
C(5)-C(4)-Fe(1)	69.6(3)
C(3)-C(4)-H(4)	125.2

C(5)-C(4)-H(4)	125.2
Fe(1)-C(4)-H(4)	125.2
C(4)-C(5)-C(1)	107.4(4)
C(4)-C(5)-Fe(1)	70.9(3)
C(1)-C(5)-Fe(1)	69.7(3)
C(4)-C(5)-H(5)	126.3
C(1)-C(5)-H(5)	126.3
Fe(1)-C(5)-H(5)	126.3
N(1)-C(6)-S(1)	177.7(5)
O(1)-C(7)-Fe(1)	179.9(5)
O(2)-C(8)-Fe(1)	178.1(5)

Symmetry transformations used to generate equivalent atoms:

Table 4. Anisotropic displacement parameters ($Å^2$ x 10^3) for C790. The anisotropic displacement factor exponent takes the form: $-2\pi^2[h^2 a^{*2}U^{11} + ... + 2 h k a^* b^* U^{12}]$

	U^{11}	U^{22}	U^{33}	U^{23}	U^{13}	U^{12}
Fe(1)	10(1)	11(1)	4(1)	1(1)	-1(1)	2(1)
S(1)	23(1)	13(1)	8(1)	-1(1)	-1(1)	3(1)
O(1)	21(2)	33(2)	12(2)	5(2)	8(2)	9(2)
O(2)	27(2)	47(3)	15(2)	13(2)	0(2)	20(2)
N(1)	26(3)	24(2)	18(2)	5(2)	2(2)	12(2)
C(1)	16(3)	11(2)	11(2)	-3(2)	0(2)	0(2)
C(2)	13(2)	15(3)	24(3)	7(2)	-3(2)	-1(2)
C(3)	9(2)	23(3)	9(2)	3(2)	1(2)	-1(2)
C(4)	15(3)	26(3)	14(2)	-1(2)	0(2)	6(2)
C(5)	10(2)	17(3)	17(3)	4(2)	-6(2)	2(2)
C(6)	16(2)	9(2)	16(3)	-2(2)	0(2)	5(2)
C(7)	16(3)	14(2)	4(2)	-1(2)	-3(2)	4(2)
C(8)	19(3)	14(2)	21(3)	7(2)	6(2)	9(2)

Table 5. Hydrogen coordinates (x 10^4) and isotropic displacement parameters ($Å^2$x 10^{-3}) for C790.

	x	y	z	U(eq)
H(1)	7290	5504	4377	19
H(2)	7692	6735	2145	25
H(3)	8733	4214	805	20
H(4)	8953	1459	2221	24
H(5)	8057	2213	4416	20

4. Cyclopentdienyl iron dicarbonyl isothiocyanate

Table 1. Crystal data and structure refinement for C532.

Identification code	c532	
Empirical formula	C8 H5 Fe N O2 S	
Formula weight	235.04	
Temperature	100(2) K	
Wavelength	0.71073 Å	
Crystal system	Monoclinic	
Space group	P2(1)/m	
Unit cell dimensions	a = 6.3240(10) Å	α= 90°.
	b = 8.9082(14) Å	β= 91.684(4)°.
	c = 7.8468(12) Å	γ = 90°.
Volume	441.86(12) $Å^3$	
Z	2	
Density (calculated)	1.767 Mg/m^3	
Absorption coefficient	1.902 mm^{-1}	
F(000)	236	
Crystal size	0.20 x 0.11 x 0.05 mm^3	
Theta range for data collection	2.60 to 27.50°.	
Index ranges	-7<=h<=8, -11<=k<=11, -9<=l<=10	
Reflections collected	3137	
Independent reflections	1075 [R(int) = 0.0322]	
Completeness to theta = 27.50°	99.1 %	
Absorption correction	Semi-empirical from equivalents	
Max. and min. transmission	0.9109 and 0.7022	
Refinement method	Full-matrix least-squares on F^2	
Data / restraints / parameters	1075 / 0 / 67	
Goodness-of-fit on F^2	1.236	
Final R indices [I>2sigma(I)]	R1 = 0.0310, wR2 = 0.0783	
R indices (all data)	R1 = 0.0405, wR2 = 0.1073	
Largest diff. peak and hole	0.647 and -0.688 $e.Å^{-3}$	

Table 2. Atomic coordinates (x 10^4) and equivalent isotropic displacement parameters ($Å^2$x 10^3) for C532. U(eq) is defined as one third of the trace of the orthogonalized U^{ij} tensor.

	x	y	z	U(eq)
Fe(1)	674(1)	2500	1677(1)	11(1)
S(1)	-3062(2)	2500	-3619(1)	19(1)
O(1)	-1864(3)	26(2)	3000(3)	22(1)
N(1)	-857(5)	2500	-481(4)	16(1)
C(1)	3507(6)	2500	301(5)	17(1)
C(2)	3410(4)	1206(3)	1345(4)	17(1)
C(3)	3288(4)	1702(3)	3076(4)	19(1)
C(4)	-916(4)	996(3)	2500(3)	16(1)
C(5)	-1746(6)	2500	-1793(5)	14(1)

Table 3. Bond lengths [Å] and angles [°] for C532.

Fe(1)-C(4)	1.806(3)
Fe(1)-C(4)#1	1.806(3)
Fe(1)-N(1)	1.925(4)
Fe(1)-C(3)#1	2.083(3)
Fe(1)-C(3)	2.083(3)
Fe(1)-C(2)#1	2.102(3)
Fe(1)-C(2)	2.102(3)
Fe(1)-C(1)	2.118(4)
S(1)-C(5)	1.636(4)
O(1)-C(4)	1.128(4)
N(1)-C(5)	1.159(5)
C(1)-C(2)#1	1.416(4)
C(1)-C(2)	1.416(4)
C(2)-C(3)	1.433(4)
C(3)-C(3)#1	1.422(6)
C(4)-Fe(1)-C(4)#1	95.80(17)
C(4)-Fe(1)-N(1)	92.50(11)
C(4)#1-Fe(1)-N(1)	92.50(11)
C(4)-Fe(1)-C(3)#1	120.42(12)
C(4)#1-Fe(1)-C(3)#1	89.99(12)
N(1)-Fe(1)-C(3)#1	146.56(11)
C(4)-Fe(1)-C(3)	89.99(12)
C(4)#1-Fe(1)-C(3)	120.42(12)
N(1)-Fe(1)-C(3)	146.56(11)
C(3)#1-Fe(1)-C(3)	39.91(16)
C(4)-Fe(1)-C(2)#1	156.97(12)
C(4)#1-Fe(1)-C(2)#1	96.10(12)
N(1)-Fe(1)-C(2)#1	106.59(11)
C(3)#1-Fe(1)-C(2)#1	40.05(11)
C(3)-Fe(1)-C(2)#1	66.98(11)
C(4)-Fe(1)-C(2)	96.10(12)
C(4)#1-Fe(1)-C(2)	156.97(12)
N(1)-Fe(1)-C(2)	106.59(11)
C(3)#1-Fe(1)-C(2)	66.98(11)
C(3)-Fe(1)-C(2)	40.05(11)

C(2)#1-Fe(1)-C(2)	66.53(15)
C(4)-Fe(1)-C(1)	132.08(9)
C(4)#1-Fe(1)-C(1)	132.08(9)
N(1)-Fe(1)-C(1)	87.88(15)
C(3)#1-Fe(1)-C(1)	66.33(13)
C(3)-Fe(1)-C(1)	66.33(13)
C(2)#1-Fe(1)-C(1)	39.22(9)
C(2)-Fe(1)-C(1)	39.22(9)
C(5)-N(1)-Fe(1)	178.9(3)
C(2)#1-C(1)-C(2)	109.0(4)
C(2)#1-C(1)-Fe(1)	69.75(18)
C(2)-C(1)-Fe(1)	69.75(18)
C(1)-C(2)-C(3)	107.5(3)
C(1)-C(2)-Fe(1)	71.03(19)
C(3)-C(2)-Fe(1)	69.27(15)
C(3)#1-C(3)-C(2)	107.97(17)
C(3)#1-C(3)-Fe(1)	70.05(8)
C(2)-C(3)-Fe(1)	70.68(16)
O(1)-C(4)-Fe(1)	177.9(2)
N(1)-C(5)-S(1)	178.5(4)

Symmetry transformations used to generate equivalent atoms:
#1 x,-y+1/2,z

Table 4. Anisotropic displacement parameters ($Å^2$ x 10^3) for C532. The anisotropic displacement factor exponent takes the form: $-2\pi^2[h^2 a^{*2}U^{11} + ... + 2 h k a^* b^* U^{12}]$

	U^{11}	U^{22}	U^{33}	U^{23}	U^{13}	U^{12}
Fe(1)	12(1)	11(1)	11(1)	0	0(1)	0
S(1)	26(1)	19(1)	13(1)	0	-5(1)	0
O(1)	23(1)	17(1)	26(1)	1(1)	5(1)	-5(1)
N(1)	16(2)	16(2)	16(2)	0	0(1)	0
C(1)	12(2)	19(2)	20(2)	0	4(2)	0
C(2)	10(1)	17(1)	24(1)	-2(1)	1(1)	2(1)
C(3)	12(1)	24(2)	19(1)	4(1)	-3(1)	1(1)
C(4)	16(1)	18(1)	14(1)	-2(1)	0(1)	4(1)
C(5)	14(2)	10(2)	17(2)	0	3(2)	0

Table 5. Hydrogen coordinates (x 10^4) and isotropic displacement parameters ($Å^2$x 10^{-3}) for C532.

	x	y	z	U(eq)
H(1)	3596	2500	-969	21
H(2)	3455	140	948	20
H(3)	3248	1042	4106	22